

Constraints on New Physics from Various Neutrino Experiments

Alexey Pronin

Dissertation submitted to the Faculty of the Virginia Polytechnic Institute and
State University in partial fulfillment of the requirements for the degree of

Doctor of Philosophy
in
Physics

Tatsu Takeuchi, Chair
Djordje Minic
Tetsuro Mizutani
Mark L. Pitt

April 9, 2008
Blacksburg, Virginia

Keywords: High Energy Physics, Elementary Particles, Neutrino, Physics beyond
the Standard Model

Constraints on New Physics from Various Neutrino Experiments

Alexey Pronin

(ABSTRACT)

In this thesis we consider a number of past, present, and future neutrino experiments designed to test physics beyond the Standard Model. First, we analyze potential new physics explanations of the NuTeV anomaly and check their compatibility with the most recent experimental data. The models we consider are: gauged $L_\mu - L_\tau$, gauged $B - 3L_\mu$, and $S_1, \vec{S}_3, V_1, \vec{V}_3$ leptoquarks. We find that only the triplet leptoquark models can explain NuTeV and be compatible with the data from other experiments at the same time, and only if the components of the triplet have different masses. Then, we analyze the prospects of discovery of heavy Majorana neutrinos (*neutrissimos*) suggested by the Okamura model at the LHC. We find that these particles, if produced, will live short enough to decay inside of the detector, while long enough to lead to a narrow peak in the invariant mass spectrum of the decay products. We estimate the typical masses of the neutrissimos to be in the TeV range. However, studies exist that have shown that if their masses are larger than about 150 GeV then the production cross-section is too small to lead to an observable event rate. Thus, we conclude that it will not be possible to detect the neutrissimo at the LHC unless its mass is smaller than about 150 GeV which corresponds to a very small region close to the edge of the parameter space of the Okamura model. Nevertheless, we argue that the signature of the neutrissimo may be detectable in other neutrino experiments which may be carried out in the future. As examples, we consider the NuSOnG experiment, which is a fixed target neutrino scattering experiment proposed at Fermilab, and a hypothetical long-baseline neutrino oscillation experiment in which the Fermilab NUMI beam is aimed at the Hyper-Kamiokande detector in Japan. In addition to the sensitivity to neutrissimos, we analyze the capabilities of these experiments to constraint the coupling constants and masses of new particles in various models of new physics suggested in the literature. The models we consider are: neutrissimo models, models with generation distinguishing Z 's such as topcolor assisted technicolor, models containing various types of leptoquarks, R-parity violating SUSY, and extended Higgs sector models. In several cases, we find that the limits thus obtained could be competitive with those expected from direct searches at the LHC. In the event that any of the particles discussed here are discovered at the LHC, then the observation, or non-observation, of these particles in the NuSOnG and Fermilab→Hyper-Kamiokande experiments could help in identifying what type of particle had been observed.

Acknowledgments

First of all, I would like to take this opportunity to express my enormous gratitude to my adviser, Dr. Tatsu Takeuchi, whose advising, professional guidance, and support were of tremendous help for me throughout all the years that I have been in graduate school at Virginia Tech. I learned a lot from him about many different aspects of Quantum Field Theory, Particle Physics, modern high energy physics experiments, and Statistics. I have been extremely lucky to have him as my adviser. He has a very interesting personality, very broad knowledge of the subject and most of all, he is a great teacher. I greatly appreciate his support and would love to keep our collaboration going even after my graduation.

I would also like to thank all my committee members: Dr. Lay Nam Chang, Dr. Djordje Minic, Dr. Tetsuro Mizutani, and Dr. Mark Pitt. Each of them have expressed tremendous help and support to my work on the PhD project. And I really appreciate the time and efforts they put in reading and commenting on this manuscript, and in writing uncountable number of recommendation letters on my behalf.

My special thanks to my wife Kseniya Pronina and my mother Tatiana Pronina for taking good care of our beautiful daughters, Aleona and Maria, and thus allowing me to concentrate on my research work. Without their help it would be absolutely impossible for me to work productively on my thesis.

I also owe many thanks to my collaborators: Dr. Mayumi Aoki, Dr. Gi-Chol Cho, Dr. Minako Honda, Yee Kao, Dr. Will Loinaz, and Dr. Naotoshi Okamura and to my fellows, former and current graduate students: Dr. Sandor Benczik, Dr. Mitra Shojania Feizabadi, Mike Kavic, and Dr. Saif Rayyan. It has been my pleasure to work with you and have you around!

Finally, I would like to thank Masafumi Kurachi, Sarira Sahu, Nguyen Phuoc Xuan, and Marek Zralek for helpful discussions.

This page left blank intentionally.

Contents

1	Introduction	1
1.1	Existing data	1
1.2	Soon to be available data	2
1.3	Future Experiments	3
1.4	Notation	4
2	The NuTeV anomaly and its explanations	5
2.1	The NuTeV anomaly	5
2.2	$L_\mu - L_\tau$ gauge boson	6
2.2.1	Z decay: $Z \rightarrow \mu^+ \mu^- X \rightarrow \mu^+ \mu^- \mu^+ \mu^-$	8
2.2.2	Precision measurements of Z couplings: $g_V^\tau - g_V^\mu$	9
2.2.3	Universality of the Z couplings: $Z \rightarrow e^+ e^-$ and $Z \rightarrow \mu^+ \mu^-$	10
2.2.4	Combined constraints	11
2.2.5	Constraining $Z - X$ mixing and radiative corrections simultaneously	12
2.2.6	W decay width	19
2.3	$B - 3L_\mu$ gauge boson	21
2.4	Leptoquark	22
2.4.1	Constraints on the Leptoquark Couplings and Masses	27
2.4.2	S_1 leptoquark	29
2.4.3	\vec{S}_3 leptoquark	30
2.4.4	V_1 leptoquark	32
2.4.5	\vec{V}_3 type leptoquark	33
3	Neutrissimo Models	37
3.1	Introduction.	37
3.2	The Parameter Space of the Okamura Model	39
3.3	The Lagrangian	41
3.4	Lifetimes	44
3.5	Results	45
3.6	Observability at the LHC	47
4	NuSOng	53
4.1	Introduction	53
4.1.1	Assumptions on $\nu_\mu e$ and $\bar{\nu}_\mu e$ ES	54
4.1.2	Assumptions on $\nu_\mu N$ and $\bar{\nu}_\mu N$ DIS	56

4.2	Constraints on New Physics Section	56
4.2.1	Oblique Correction Analysis	57
4.2.2	Non-Standard Interactions	58
4.2.3	Neutrissimos, Neutrino Mixing and Gauge Couplings	60
4.2.4	Sensitivity in the Case of Specific Theoretical Models	62
4.2.5	A New NuSONG Anomaly? $g_R^2 \neq (g_R^2)_{\text{SM}}$	74
5	Fermilab→Hyper-Kamiokande experiment	77
5.1	Introduction	77
5.2	Models with an extra Z' boson	79
5.2.1	Gauged $L_e - L_\mu$ and $L_e - L_\tau$	79
5.2.2	Gauged $B - (\alpha L_e + \beta L_\mu + \gamma L_\tau)$	81
5.2.3	Topcolor Assisted Technicolor	85
5.3	Generation Non-Diagonal Leptoquarks	89
5.3.1	S_1 and \vec{S}_3 leptoquarks	89
5.3.2	S_2 and \vec{S}_2 leptoquarks	91
5.3.3	V_2 and \vec{V}_2	92
5.3.4	V_1 and \vec{V}_3 leptoquarks	93
5.3.5	Constraints on the Leptoquark Couplings and Masses	95
5.4	SUSY Standard Model with R-parity Violation	99
5.4.1	$\hat{L}\hat{L}\hat{E}$ couplings	100
5.4.2	$\hat{L}\hat{Q}\hat{D}$ couplings	101
5.4.3	Constraints on the R-parity Violating Couplings and Squark/Slepton Masses	102
5.5	Extended Higgs Models	104
5.5.1	Singlet Higgs in the Zee and Babu-Zee Models	105
5.5.2	Triplet Higgs with $Y = +1$	106
6	Summary	109
6.1	NuTeV	109
6.2	Neutrissimo Lifetime	109
6.3	NuSONG	110
6.4	Fermilab→Hyper-Kamiokande	111
6.5	Future prospects	112
A	Ratios of the neutral to charged current events	113
B	Calculation of the W vertex corrections in the $L_\mu - L_\tau$ model	117
B.1	Matrix element	117
B.2	$\Delta\Gamma/\Gamma$	120
B.3	Calculation of the real part of F	123
B.4	Contribution from the renormalization of the wave functions	125
B.5	Putting all together	126
C	Minimum χ^2 fit in the $L_\mu - L_\tau$ model	129

D	Calculation of the neutrino lifetime	133
D.1	$N_i \rightarrow n_j + Z$	133
D.2	$N_i \rightarrow \ell_j^\mp + W^\pm$	135
D.3	$N_i \rightarrow n_j + h$	136
D.4	Integration over the phase space	137
E	Errors on the effective couplings in the NuSOnG analysis	141
	Bibliography	143

This page left blank intentionally.

List of Figures

2.1	Z_μ^m and X_μ^m exchange diagrams contributing to the $\nu_\mu(\bar{\nu}_\mu) - f$ scattering.	8
2.2	Upper and lower bounds on the M_X as a function of ρ_μ	10
2.3	Correction to the Z vertex due to the X exchange between the final state leptons.	11
2.4	Combining constraints on the $L_\mu - L_\tau$ model.	12
2.5	ρ_μ dependence on the M_X for the fitted value of δ_M	17
2.6	Constraints on the g_X and M_X of the $L_\mu - L_\tau$ model from the fit.	19
2.7	Constraints from the W branching ratios data.	20
2.8	$M_{S_3^-}$ dependence on $M_{S_3^0}$. $g_{3L}^{12} = 0.1$ – red line; $g_{3L}^{12} = 0.35$ – green dashed line; $g_{3L}^{12} = 0.65$ – blue dashed-dotted line.	32
2.9	$M_{V_3^-}$ dependence on $M_{V_3^0}$. $h_{3L}^{12} = 0.1$ – red line; $h_{3L}^{12} = 0.35$ – green dashed line; $h_{3L}^{12} = 0.65$ – blue dashed-dotted line.	34
3.1	The three complex numbers α , β and γ satisfying $\alpha + \beta + \gamma = 0$ form a close triangle. For each choice of the three lengths $ \alpha $, $ \beta $, and $ \gamma $, there are two possible orientations of the triangle (\odot and \otimes) which are related by complex conjugation (1st and 2nd columns). However, the \otimes case is equivalent to the \odot case with the lengths $ \beta $ and $ \gamma $ interchanged (2nd and 3rd columns).	40
3.2	The distances from any point inside an equilateral triangle of height three to its three sides add up to three. We can use these distances to specify $ \alpha ^2$, $ \beta ^2$, and $ \gamma ^2$. The triangle inequality is satisfied for points inside the unit circle which inscribes the triangle.	41
3.3	Contour lines and density plots for $\arg \beta$ (left) and $\arg \gamma$ (middle). The distances between two consecutive equipotential lines are $\Delta \arg \beta = \Delta \arg \gamma = 0.05\pi$. The color scheme is shown on the right.	42
3.4	The 2-body decay processes of the heavy neutrino N	44
3.5	(a), (b), (c) density and contour plots for masses M_1 , M_2 , and M_3 of the lightest N_1 , medium heavy N_2 and heaviest N_3 heavy neutrino respectively (TeV). The distances between two consecutive equipotential lines are $\Delta M_1 = 0.1$ TeV, $\Delta M_2 = \Delta M_3 = 0.05$ TeV; (d) the vicinity of the point where M_1 approaches zero ($r = 1$, $\theta = -\pi/2$); $\Delta M_1 = 0.025$ TeV; (e) mass color coding.	45
3.6	(a), (b), (c) density and contour plots for widths Γ_1 , Γ_2 , and Γ_3 of the lightest N_1 , medium heavy N_2 and heaviest N_3 heavy neutrino respectively (GeV). The distances between two consecutive equipotential lines are $\Delta \Gamma_1 = 1$ GeV, $\Delta \Gamma_2 = 2$ GeV, $\Delta \Gamma_3 = 3$ GeV; (d) the detailed picture of the central part of Γ_1 ; $\Delta \Gamma_1 = 1$ GeV; (e) width color coding.	46

3.7	(a), (b), (c) density and contour plots for lifetimes τ_1 , τ_2 , and τ_3 of the lightest N_1 , medium heavy N_2 and heaviest N_3 heavy neutrino respectively (10^{-26} sec). The distances between two consecutive equipotential lines are $\Delta\tau_1 = 1 \times 10^{-26}$ sec for $\tau_1 < 10 \times 10^{-26}$ sec and for $\tau_1 > 10 \times 10^{-26}$ sec equipotential lines corresponding to $\tau_1 = 20 \times 10^{-26}$, 40×10^{-26} and 200×10^{-26} sec are presented, $\Delta\tau_2 = 0.2 \times 10^{-26}$ sec, $\Delta\tau_3 = 0.1 \times 10^{-26}$ sec; (d) the detailed picture of the central part of τ_1 ; $\Delta\tau_1 = 10 \times 10^{-26}$ sec for $\tau_1 < 100 \times 10^{-26}$ sec and $\Delta\tau_1 = 100 \times 10^{-26}$ sec for $\tau_1 > 100 \times 10^{-26}$ sec; (e) lifetime color coding.	47
3.8	(a), (b), (c) density and contour plots for the widths-to-mass ratios of the lightest N_1 , medium heavy N_2 and heaviest N_3 heavy neutrinos respectively. The distances between two consecutive equipotential lines is 0.001 for all plots; (d) mass-to-width ratio color coding.	48
3.9	Feynman diagrams for $\Delta L = 2$ processes induced by a t-channel Majorana neutrino N in $q\bar{q}'$ collisions.	49
3.10	Feynman diagrams for $\Delta L = 2$ processes induced by an s-channel Majorana neutrino N in $q\bar{q}'$ collisions.	49
3.11	The value of the $S_{\mu\mu}$ parameter for the region of the parameter space where the mass of N_1 is smaller than 400 GeV.	50
4.1	The impact of NuSOng on the limits of S and T . The reference SM is $m_t = 170.9$ GeV, and $m_H = 115$ GeV. 1σ bands due to NuSOng observables are shown against the 90% contour from LEP/SLD. The central ellipses are the 68% and 90% confidence limit contours with NuSOng included.	57
4.2	Potential constraint on ϵ_e and ϵ_μ from NuSOng (see Eq. (4.33)). This is a two-dimensional projection of a 4 parameter fit with S , T , ϵ_e and ϵ_μ . The green ellipse is the 90% CL contour of a fit to all the charge current particle decay data + LEP/SLD.	61
4.3	Shifts in g_L^2 and g_R^2 due to leptoquarks. Horizontal lines indicate the projected 1σ limits of NuSOng.	74
4.4	Expected S - T plot if a 6σ deviation is seen in g_L^2 which is due to a non-zero gauge suppression parameter ϵ_μ . All four observables g_L^2 , g_R^2 , $\sigma(\nu_\mu e)$, and $\sigma(\bar{\nu}_\mu e)$ are shifted away from their SM values. Unfortunately, the expected errors in g_R^2 and $\sigma(\bar{\nu}_\mu e)$ are too large for this shift to be seen. Seeing the shift in $\sigma(\nu_\mu e)$ may also be difficult.	75
4.5	Expected S - T plot if a 6σ deviation is seen in g_L^2 which is due to a non-zero gauge suppression parameter ϵ_e . The $\nu_\mu N$ DIS observables g_L^2 and g_R^2 will be shifted away from their SM values, but not the $\nu_\mu e$ ES observables $\sigma(\nu_\mu e)$ and $\sigma(\bar{\nu}_\mu e)$. However, the expected error in g_R^2 is too large for this shift to be seen.	76
4.6	Expected S - T plot if a 6σ deviation is seen in g_L^2 which is due to triplet leptoquarks with large mass splitting. Only g_L^2 is shifted from its SM value.	76
5.1	Diagrams that contribute to neutrino oscillation matter effects in (a) the gauged $L_e - L_\mu$ model, and (b) the gauged $L_e - L_\tau$ model.	79
5.2	Diagrams that contribute to neutrino oscillation matter effects in (a) the gauged $X = B - \alpha L_e - \beta L_\mu - \gamma L_\tau$ model, $\ell = \{e, \mu, \tau\}$, $f = \{u, d, e\}$, and (b) topcolor assisted technicolor, $f = \{u_L, u_R, d_L, d_R, e_L, e_R\}$	82
5.3	$\xi_{Z'}$ dependence on the Z' mass for the special case $\alpha = \beta = 0$, $\gamma = 3$	84

5.4	Lower bounds on Z' mass.	85
5.5	ξ_{TT} dependence on the Z' mass in the top color assisted technicolor model.	88
5.6	Diagrams contributing to neutrino oscillation matter effects from the exchange of (a) S_1^0 or the isospin 0 component of \vec{S}_3 , and (b) the isospin -1 component of \vec{S}_3 . The EM charge $Q_{em} = I_3 + Y$ for S_1^0 and S_3^0 are $+\frac{1}{3}$, while that for S_3^- is $-\frac{2}{3}$	89
5.7	Diagrams contributing to neutrino oscillation matter effects from the exchange of (a) S_2^- , and (b) \tilde{S}_2^- . The EM charge $Q_{em} = I_3 + Y$ for S_2^- is $+\frac{2}{3}$, while that for \tilde{S}_2^- is $-\frac{1}{3}$	91
5.8	Diagrams contributing to neutrino oscillation matter effects from the exchange of (a) V_2^- , and (b) \tilde{V}_2^- . The EM charge $Q_{em} = I_3 + Y$ for V_2^- is $+\frac{1}{3}$, while that for \tilde{V}_2^- is $-\frac{2}{3}$	92
5.9	Diagrams contributing to neutrino oscillation matter effects from the exchange of (a) V_1^0 or the isospin 0 component of \vec{V}_3 , and (b) the isospin -1 component of \vec{V}_3 . The EM charges $Q_{em} = I_3 + Y$ for V_1^0 and V_3^0 are $+\frac{2}{3}$, while that for V_3^- is $-\frac{1}{3}$	94
5.10	ξ_{LQ} dependence on the leptoquark mass for $\sqrt{\Delta\lambda_{LQ}^2} = 0.5$. (a) S_1 ; (b) V_2, \tilde{V}_2 ; (c) \vec{S}_3 ; (d) S_2, \tilde{S}_2 ; (e) V_1 ; (f) \vec{V}_3	96
5.11	Lower bounds on the leptoquark masses. (a) S_1, S_2, \tilde{S}_2 ; (b) V_1, V_2, \tilde{V}_2 ; (c) \vec{S}_3 ; (d) \vec{V}_3	97
5.12	LLE interactions that contribute to neutrino oscillation matter effects..	100
5.13	LQD interactions that contribute to neutrino oscillation matter effects..	101
5.14	Dependence of $\xi_{\tilde{\mu},\tilde{d},h}$ on the smuon, sdown, and h^\pm masses for $\sqrt{\delta\lambda_{\tilde{\mu},\tilde{d},h}^2} = 0.5$ in the (a) $\hat{L}\hat{L}\hat{E}$ R-parity violating interaction; (b) $\hat{L}\hat{Q}\hat{D}$ R-parity violating interaction; and (c) the Zee/Babu-Zee models.	102
5.15	Lower bounds on (a) the smuon mass in the $\hat{L}\hat{L}\hat{E}$ R-parity violating interaction model, (b) the sdown mass in the $\hat{L}\hat{Q}\hat{D}$ R-parity violating interaction model, and (c) the h^\pm mass in the Zee/Babu-Zee models, respectively.	103
5.16	Diagrams which generate the Majorana masses and mixings of the neutrino in the (a) Zee [75] and (b) Babu-Zee [76] models.	105
5.17	Contribution to neutrino oscillation matter effects from a singly-charged Higgs in the Zee, Babu-Zee, and $Y = 1$ Triplet Higgs models.	106
B.1	Correction to the W vertex due to the X exchange between the final state leptons.	118
B.2	The tree level W vertex.	121
B.3	The X contribution to the self-energy.	125

This page left blank intentionally.

List of Tables

2.1	The values of $\delta\rho$, δ_V , and δ_M extracted from the χ^2 fit.	15
2.2	Results on the effective coupling constants for leptons	16
2.3	Quantum numbers of scalar and vector leptoquarks with $SU(3)_C \times SU(2)_L \times U(1)_Y$ invariant couplings to quark-lepton pairs ($Q_{\text{em}} = I_3 + Y$).	24
2.4	Direct search limits on the Leptoquark mass from the Tevatron. ^(a) β is the assumed branching fraction $B(LQ \rightarrow q\ell) = 1 - B(LQ \rightarrow q\nu)$, and ^(b) λ is the Yukawa coupling of the Leptoquark with the quark-lepton pair. ^(c) Combined bound with the pair production data.	27
2.5	The quark-muon interactions induced by leptoquark exchange, the bounds from CDF [36], and the bounds from the measurement of R_π . Only the couplings that also contribute to NuTeV are listed. Analysis of the Tevatron Run II data is expected to improve the CDF bound by a factor of four.	28
2.6	The 95% CL lower bound on the compositeness scale from CDF [36]. Results from D0 [37] do not provide limits for cases where the muons couple to only u or d , but we expect the bounds to be in the range $4 \sim 7$ TeV.	28
4.1	Correlation among the fit parameters in a fit to charged current decay and LEP/SLD data.	62
4.2	Correlation among the fit parameters in a fit to charge current decay, LEP/SLD, and possible NuSOnG data.	62
4.3	Potential bounds on the R-parity violating LLE (top) and LQD (bottom) couplings from NuSOnG, assuming that only one coupling is non-zero at a time for each set. All squark and slepton masses are set to 100 GeV. To obtain limits for different masses, rescale by $(\frac{M}{100\text{GeV}})$. Current bounds are from Ref. [78].	66
4.4	Potential and existing 95% bounds on the leptoquark couplings squared when the leptoquark masses are set to 100 GeV. To obtain the limits for different leptoquark masses, multiply by $(M_{LQ}/100\text{ GeV})^2$. Existing bounds on the S_1 , \tilde{S}_3 , V_1 , and \tilde{V}_3 couplings from $R_\pi = B(\pi \rightarrow e\nu)/B(\pi \rightarrow \mu\nu)$ are also shown.	74
4.5	The values of $M_{LQ}/ \lambda_{LQ}^{12} $ required for the leptoquarks S_2 , \tilde{S}_2 , V_2 , \tilde{V}_2 to shift the value of g_R^2 by $\pm 3\sigma$ and $\pm 6\sigma$. For comparison, the 2σ lower bound from NuTeV is also listed, though the reanalysis could change the bounds significantly. The NuTeV bounds are asymmetric for positive and negative shifts in g_R^2 due to the fact that the NuTeV central value is about 0.6σ above the SM value.	75

5.1	The 95% confidence level lower bounds on the compositeness scale Λ^\pm (TeV) from leptonic LEP/LEP2 data. Dividing by $\sqrt{4\pi}$ converts these limits to those on $(M_{Z'}/g_{z'})$.	81
5.2	Current and possible lower bounds on the Z' mass in gauged $B - \alpha L_3 - \beta L_\mu - \gamma L_\tau$ models.	84
5.3	Charge assignments of the ordinary fermions. The $U(1)$ charges are equal to the SM hypercharges normalized to $Q_{em} = I_3 + Y$.	86
5.4	Constraints on the leptoquark couplings with all the leptoquark masses set to 100 GeV. To obtain the bounds for a different leptoquark mass M_{LQ} , simply rescale these numbers with the factor $(M_{LQ}/100 \text{ GeV})^2$.	95
5.5	Direct search limits on the Leptoquark mass from the Tevatron. ^(a) β is the assumed branching fraction $B(LQ \rightarrow q\ell) = 1 - B(LQ \rightarrow q\nu)$, and ^(b) λ is the Yukawa coupling of the Leptoquark with the quark-lepton pair. ^(c) Combined bound with the pair production data.	96
5.6	The quark-muon interactions induced by leptoquark exchange, and the bounds from CDF [36] compared with potential bounds from neutrino oscillations. Only the couplings that also contribute to neutrino oscillation are listed. Analysis of the Tevatron Run II data is expected to improve the CDF bound by a factor of two.	99
5.7	The 95% CL lower bound on the compositeness scale from CDF [36]. Results from D0 [37] do not provide limits for cases where the muons couple to only u or d , but we expect the bounds to be in the range $4 \sim 7$ TeV.	99
5.8	Current 2σ bounds on R-parity violating couplings from Ref. [78]. These bounds assume that each coupling is non-zero only one at a time.	104
6.1	The result of our survey. The potential bound from the Fermilab→Hyper-Kamiokande experiment is compared with existing bounds, and the expected bounds from the LHC. If the existing bound is already stronger, no comparison with the LHC bound is made. *The leptoquark bound will be competitive with the LHC, provided that $\sqrt{ C_{LQ} \delta\lambda_{LQ}^2 } = O(1)$.	111

Chapter 1

Introduction

The Standard Model (SM) of elementary particles embodies our current knowledge of elementary particles and their interactions. It has been very successful in explaining experimental data for more than thirty years. Apart from the discovery of non-zero neutrino masses in the late 90's, no significant deviations from the SM predictions have been found so far. However, there are many reasons to believe that the SM is not the ultimate theory of Nature because it does not provide answers to many important questions. For instance, the SM does not tell us what flavor is and why Nature contains three different generations of quarks and leptons, why there is mixing between different flavors and what causes the mixing, why neutrino masses and mixing angles demonstrate significant deviations from the pattern observed in the quark sector, what the origin of the matter-antimatter asymmetry of the Universe is, etc. The situation is two-fold: on the one hand, one has a theory whose agreement with experiment is simply amazing and beats all world records; on the other hand, without experimental hints, it is not clear where one should look for physics beyond the SM. In this thesis I will present my view on this matter and show a number of examples illustrating how one can interpret the outcomes of various experiments in terms of new physics and how one can constrain possible new physics scenarios using experimental data. I will consider the constraints on different models of new physics derived from 1) the existing data (NuTeV, LEP, Tevatron), 2) potential constraints from the data which *will* soon be available (LHC), and 3) potential constraints from the data which *could* become available in the future (NuSOng, Fermilab→HyperK). In this introduction, I briefly review each of these cases and point the reader to the parts of the thesis containing more detailed explanation and discussion.

1.1 Existing data

The question of great importance is: What type of new physics should one expect? Many proposals, such as SUSY, Technicolor, Extra Dimensions models, take the naturalness problem as a starting point and suggest their own solution to this problem in terms of new physics. However, there are no well-defined criteria of naturalness and it is often just a matter of opinion which theory is natural and which is not. Moreover, none of these proposals are based on experimental data. This is why, in my opinion, a better place to look for possible new physics may be the few *known* experimental anomalies, that is, experimental data which do not quite agree with the SM. The examples of such anomalies are:

1. The Neutrinos at the Tevatron (NuTeV) [1] experiment at Fermilab has measured the ratio of neutral to charged current events in muon (anti)neutrino-nucleon scattering. It has found that this ratio is smaller than the SM prediction. In particular, the value of the parameter g_L^2 (to be introduced in Chapter 2) measured in the NuTeV experiment is 3σ below its SM value. This disagreement is often referred to as the NuTeV anomaly. Although, the NuTeV result is controversial and currently in the process of being reanalyzed it still remains a distinct possibility that the observed disagreement with the SM value of g_L^2 is due to the presence of new physics. In Chapter 2 we give a number of examples of models of new physics suggested in the literature to explain the NuTeV result.
2. The invisible widths of the Z , measured at the CERN collider LEP and the SLAC Linear Collider [2] is also known to be 2σ below the SM prediction.
3. In addition to that, the branching fractions of W , $B(W \rightarrow e\bar{\nu}_e)$, $B(W \rightarrow \mu\bar{\nu}_\mu)$, $B(W \rightarrow \tau\bar{\nu}_\tau)$, measured at CERN [3], were found to be different from each other, whereas according to the SM they all must be the same. In particular, the ratios $B(W \rightarrow \tau\bar{\nu}_\tau)/B(W \rightarrow e\bar{\nu}_e)$ and $B(W \rightarrow \tau\bar{\nu}_\tau)/B(W \rightarrow \mu\bar{\nu}_\mu)$ differ from unity by more than 2σ . The branching fractions of W into electrons and muons perfectly agree. It should be pointed out, though, that this LEP2 result disagrees with low energy data on lepton universality extracted from π , μ , and τ decays [4], making it difficult to interpret.

It is interesting to note that all the experiments in this list involve neutrino interactions. This suggests that if any of these anomalies are genuine and due to the existence of new physics, then their explanations could reveal the mechanism responsible for the generation of the masses and mixing angles in the neutrino as well as in the quark sector. Thus, it is very important to know which models are capable of explaining these anomalies, how viable they are in light of the most recent experimental data, and whether the new physics proposed by these models can be seen at the LHC or in some other experiments. Thus, in Chapter 2 we present a list of possible explanations of the NuTeV anomaly in terms of various new physics scenarios suggested in the literature. The list includes gauged $L_\mu - L_\tau$, gauged $B - 3L_\mu$, and various types of leptoquarks. Then we will consider constraints on these models coming from the existing experiments (LEP, Tevatron, etc.).

1.2 Soon to be available data

Although many possible extensions of the SM have been suggested during the past decades, all of them are fine-tuned to reproduce the SM predictions at the energy scales accessible in modern particle physics experiments. To confirm the existence of physics beyond the SM and, moreover, to see which one of the suggested models of new physics, if any, is correct, one has to explore higher energy scales. Fortunately, the Large Hadronic Collider (LHC) built exactly for this purpose is coming online in 2008. The LHC will probe the energy scale at which the SM is expected either to fail and reveal some features of a more fundamental theory of Nature or to demonstrate the SM features which have not yet been observed experimentally such as the existence of Higgs particles. In either case, I believe that it is going to be a great time for both theoretical and experimental high energy physics.

In order to illustrate how we can use the LHC data to constrain possible new physics scenario, we consider an example of so-called *neutrissimo* models [5] which was suggested in the literature to

explain the NuTeV anomaly. The explanation relies on the observation that both the NuTeV result and the decay rate of the Z are smaller than the SM prediction. This suggests that the coupling of the neutrino to the Z is suppressed with respect to the SM. It was argued in Ref. [6] that such suppression can occur naturally in models in which the right handed neutrinos are added to the SM content if we judiciously choose the form of the mass texture and allow mixing between different generations. Ref. [5] shows an explicit example, called the Okamura model, which demonstrates how this idea can be implemented in practice. Such a model contains both light and heavy Majorana neutrino mass eigenstates obtained by diagonalization of the mass texture. The typical masses of the heavy Majorana states, called neutrissimos, are of order a few TeV in this model. The basic idea is that there was simply not enough energy to produce the neutrissimos in the NuTeV experiment and it led to the suppression of the Z -neutrino couplings.

If neutrissimos exist then, having their masses in the TeV range, they could be produced at the LHC. The question is: Will we be able to detect them or not? We address this question in Chapter 3 of the thesis which also contains more detailed description of the neutrissimo models. The consideration given in Chapter 3 is based on our work presented in Ref. [7].

1.3 Future Experiments

Evidence for neutrissimos can also be searched for in other experiments including those which may be performed in the future. For example, a new experiment called NuSOng (Neutrino Scattering on Glass) is being planned at Fermilab. (See our recent paper [8].) If approved, it will check the NuTeV result, repeating the measurements of the muon (anti)neutrino-nucleon scattering with event statistics two orders of magnitude higher than that of NuTeV. As a result, NuSOng is projected to halve the experimental error on g_L^2 (to be introduced in Chapter 2) as compared to NuTeV. In addition, the NuSOng experiment will also measure the muon neutrino-electron scattering cross section to an accuracy of 0.7% using inverse muon beta decay to normalize the neutrino flux. Different explanations of the NuTeV result will affect the neutrino-electron scattering differently, so NuSOng can, in principle, distinguish among them. The consideration of this possibility is given in the beginning of Chapter 4.

In chapter 5 we consider a Long Baseline neutrino oscillation experiment (LBL) which could be carried out in the future. The LBL neutrino oscillation experiments are also sensitive to the physics beyond the SM through matter effects and will be complementary to the LHC. The consideration given in chapter 5 is based on our work presented in Ref. [9], in which we consider a hypothetical experiment in which a muon neutrino beam prepared at Fermilab is sent to the planned Hyper-Kamiokande detector in Japan. It was shown in the first paper of Ref. [10] that such an experiment is capable of constraining neutral current universality violation to better than 1 percent after 5 years of data taking. We analyzed how various physics beyond the SM can modify the matter effects in this experiment. We considered models with generation distinguishing Z 's such as topcolor assisted technicolor, models containing various types of leptoquarks, R-parity violating SUSY, and extended Higgs sector models.

1.4 Notation

In this section we summarize the notation which we extensively use in the first and the third chapters of this thesis.

The exchange of the Z boson between the neutrino ν and fermion $f \neq \nu$ leads to the effective interaction

$$\begin{aligned} \mathcal{L} &= -\sqrt{2}G_F \left[\bar{\nu}\gamma_\mu(g_V^\nu - g_A^\nu\gamma_5)\nu \right] \left[\bar{f}\gamma^\mu(g_V^f - g_A^f\gamma_5)f \right] \\ &= -\sqrt{2}G_F \left[g_L^\nu \bar{\nu}\gamma_\mu(1 - \gamma_5)\nu + g_R^\nu \bar{\nu}\gamma_\mu(1 + \gamma_5)\nu \right] \\ &\quad \times \left[g_L^f \bar{f}\gamma^\mu(1 - \gamma_5)f + g_R^f \bar{f}\gamma^\mu(1 + \gamma_5)f \right], \end{aligned} \quad (1.1)$$

where the Standard Model values of the couplings are:

$$\begin{aligned} g_L^\nu &= \sqrt{\rho} \left(+\frac{1}{2} \right), \\ g_R^\nu &= 0, \\ g_L^f &= \sqrt{\rho} \left(I_3^f - Q^f \sin^2 \theta_W \right), \\ g_R^f &= \sqrt{\rho} \left(-Q^f \sin^2 \theta_W \right), \end{aligned} \quad (1.2)$$

or equivalently,

$$\begin{aligned} g_V^\nu &= g_L^\nu + g_R^\nu = \sqrt{\rho} \left(+\frac{1}{2} \right), \\ g_A^\nu &= g_L^\nu - g_R^\nu = \sqrt{\rho} \left(+\frac{1}{2} \right), \\ g_V^f &= g_L^f + g_R^f = \sqrt{\rho} \left(I_3^f - 2Q^f \sin^2 \theta_W \right), \\ g_A^f &= g_L^f - g_R^f = \sqrt{\rho} \left(I_3^f \right). \end{aligned} \quad (1.3)$$

Here, I_3^f and Q^f are the weak isospin and electromagnetic charge of fermion f , respectively. At tree level in the SM, the ρ -parameter is one. If we assume that $g_R^\nu = 0$ even in the presence of new physics, then Eq. (1.1) can be written as

$$\begin{aligned} \mathcal{L} &= -\sqrt{2}G_F \left[\bar{\nu}\gamma_\mu P_L \nu \right] \left[g_V^{\nu f} \bar{f}\gamma^\mu f - g_A^{\nu f} \bar{f}\gamma^\mu \gamma_5 f \right] \\ &= -2\sqrt{2}G_F \left[\bar{\nu}\gamma_\mu P_L \nu \right] \left[g_L^{\nu f} \bar{f}\gamma^\mu P_L f + g_R^{\nu f} \bar{f}\gamma^\mu P_R f \right], \end{aligned} \quad (1.4)$$

where

$$\begin{aligned} g_V^{\nu f} &= 2g_L^\nu g_V^f = \rho \left(I_3^f - 2Q^f \sin^2 \theta_W \right), \\ g_A^{\nu f} &= 2g_L^\nu g_A^f = \rho \left(I_3^f \right), \\ g_L^{\nu f} &= 2g_L^\nu g_L^f = \rho \left(I_3^f - Q^f \sin^2 \theta_W \right), \\ g_R^{\nu f} &= 2g_L^\nu g_R^f = \rho \left(-Q^f \sin^2 \theta_W \right). \end{aligned} \quad (1.5)$$

Chapter 2

The NuTeV anomaly and its explanations

In this chapter we give an example of an existing experiment the result of which disagrees with the SM. We discuss various interpretations of this disagreement in terms of new physics scenarios which have been suggested in the literature and analyze the viability of these interpretations in light of the most recent experimental data.

2.1 The NuTeV anomaly

The Neutrinos at the Tevatron (NuTeV) experiment [1] has measured the ratios of the neutral to charged current events in muon (anti-)neutrino-nucleon scattering. For the isoscalar target¹ used in the experiment these ratios are related to the left- and right-handed coupling of the Z -boson to quarks as follows.

$$R_\nu = \frac{\sigma(\nu_\mu N \rightarrow \nu_\mu X)}{\sigma(\nu_\mu N \rightarrow \mu^- X)} = g_L^2 + r g_R^2, \quad (2.1)$$

$$R_{\bar{\nu}} = \frac{\sigma(\bar{\nu}_\mu N \rightarrow \bar{\nu}_\mu X)}{\sigma(\bar{\nu}_\mu N \rightarrow \mu^+ X)} = g_L^2 + \frac{g_R^2}{r}, \quad (2.2)$$

where

$$r \equiv \frac{\sigma(\bar{\nu}_\mu N \rightarrow \mu^+ X)}{\sigma(\nu_\mu N \rightarrow \mu^- X)} \sim \frac{1}{2}. \quad (2.3)$$

The parameters g_L^2 and g_R^2 are

$$g_L^2 = (g_L^{\nu u})^2 + (g_L^{\nu d})^2, \quad (2.4)$$

$$g_R^2 = (g_R^{\nu u})^2 + (g_R^{\nu d})^2. \quad (2.5)$$

A somewhat simplified derivation of Eqs. (2.1)-(2.2) is given in Appendix A. See Ref. [11] for a more thorough discussion.

¹The isoscalar target¹ means that the target contains equal amount of the protons and neutrons or, alternatively, u and d quarks.

NuTeV has determined the parameters g_L^2 and g_R^2 to be

$$g_L^2 = 0.30005 \pm 0.00137, \quad (2.6)$$

$$g_R^2 = 0.03076 \pm 0.00110. \quad (2.7)$$

The SM prediction of these parameters based on a global fit to non-NuTeV data given in Ref. [1] is

$$(g_L^2)_{\text{SM}} = 0.3042, \quad (2.8)$$

$$(g_R^2)_{\text{SM}} = 0.0301 \quad (2.9)$$

which differs from the NuTeV result by 3σ in g_L^2 . This disagreement is often referred to as ‘the NuTeV anomaly’. In principal, it is possible to fit the SM to the NuTeV result but in this case the preferred range of the Higgs mass is $m_H > 660$ GeV (90% CL) [12] which is well above the value of $m_H \sim 90$ GeV preferred by the non-NuTeV global fit [13].

Although the NuTeV result remains controversial and is currently in the process of being reanalyzed, several reasonable explanations of this result have been suggested in the literature. First of all, we must consider the explanations of NuTeV which lies within the SM framework. This mainly includes theoretical uncertainties due to Quantum Chromodynamics (QCD) effects which might be comparable to or larger than the quoted experimental uncertainty of the NuTeV result. For instance, several groups are evaluating uncertainties coming from next-to-leading (NLO) QCD corrections [14], NLO electroweak corrections [15], and parton distribution functions (especially as involves assumptions about sea-quark asymmetries) [16]. These uncertainties are found to be large and could potentially be responsible for the entire NuTeV anomaly and their actual impact on the result of NuTeV awaits a reanalysis of the NuTeV data.

On the other hand, it still remains a distinct possibility that the NuTeV anomaly is genuine and its explanation lies in physics beyond the SM. Several possible explanation of the NuTeV anomaly in terms of new physics have been suggested in the literature [17, 6]. This includes models with gauged $L_\mu - L_\tau$, gauged $B - 3L_\mu$, S_1 , \vec{S}_3 , V_1 , \vec{V}_3 leptoquarks, and TeV scale heavy Majorana neutrinos. However, it is important to realize that all these explanations of NuTeV were suggested several years ago. Now we have more experimental data available to us and thus have to update the experimental constraints on these models and reanalyze their compatibility with the NuTeV result. Thus, in this chapter we present a list of models capable of explaining NuTeV and reanalyze the viability of these explanations of NuTeV in light of the most recent experimental data.

2.2 $L_\mu - L_\tau$ gauge boson

The NuTeV anomaly [1] can be partially explained if one accepts the existence of the new gauge symmetry $L_\mu - L_\tau$ [18, 19, 20], where L_μ and L_τ are the muon and tau lepton numbers respectively. The model in which this idea can be realized was presented by Ma and Roy in Ref. [21]. This model postulates the existence of the anomaly-free gauge symmetry $U(1)_X$. The gauge boson X associated with this symmetry couples to $(\nu_\mu, \mu)_L$, μ_R with charge +1 and to $(\nu_\tau, \tau)_L$, τ_R with charge -1, but not to any other fermion. The model also postulates the existence of the usual Standard Model (SM) Higgs doublet $\Phi = (\phi^+, \phi^0)$ with charge 0 and two additional Higgs doublets $\eta_{1,2} = (\eta_{1,2}^+, \eta_{1,2}^0)$ with charges ± 1 under $U(1)_X$. After spontaneous symmetry breaking the fields

Φ , $\eta_{1,2}$ get VEV's: $v_0 \equiv \langle \phi^0 \rangle$, $v_{1,2} \equiv \langle \eta_{1,2}^0 \rangle$. This generates mixing between the new X boson and the usual SM Z boson leading to the mass term of the form:

$$\mathcal{L}_{ZX} = \frac{1}{2} (Z_\mu, X_\mu) \cdot \mathcal{M}_{ZX}^2 \cdot \begin{pmatrix} Z^\mu \\ X^\mu \end{pmatrix}, \quad (2.10)$$

where

$$\mathcal{M}_{ZX}^2 \equiv \begin{bmatrix} 2g_X^2(v_1^2 + v_2^2) & g_X g_Z(v_1^2 - v_2^2) \\ g_X g_Z(v_1^2 - v_2^2) & (g_Z^2/2)(v_0^2 + v_1^2 + v_2^2) \end{bmatrix}. \quad (2.11)$$

g_X is the X boson gauge coupling constant and $g_Z = \sqrt{g^2 + g'^2} = g/c_W$ at tree level. (g and g' are the usual SM gauge couplings and $c_W = \cos \theta_W$.)

Under the assumption that $v_1 \simeq v_2$, so that the $X - Z$ mixing is small, the mass matrix given by Eq. (2.11) has the following eigenvalues:

$$M_Z^2 \simeq \frac{1}{2} g_Z^2 (v_0^2 + 2v_1^2), \quad M_X^2 \simeq 4g_X^2 v_1^2, \quad (2.12)$$

and the $X - Z$ mixing angle is given by

$$\sin \theta \simeq \frac{g_X g_Z (v_1^2 - v_2^2)}{M_X^2 - M_Z^2}. \quad (2.13)$$

This means that the interaction eigenstates (Z_μ, X_μ) are related to the mass eigenstates (Z_μ^m, X_μ^m) through the following formulas:

$$\begin{aligned} Z_\mu &= \cos \theta \cdot Z_\mu^m + \sin \theta \cdot X_\mu^m, \\ X_\mu &= -\sin \theta \cdot Z_\mu^m + \cos \theta \cdot X_\mu^m. \end{aligned} \quad (2.14)$$

In the SM the low energy effective interactions of ν_μ and $\bar{\nu}_\mu$ with quarks and electrons can be described by the effective Lagrangian of the form

$$\mathcal{L}_{\text{eff}}^{\text{SM}} = -\frac{g_Z^2}{M_Z^2} \cdot \frac{1}{4} \cdot \left[\bar{\nu}_\mu \gamma^\mu \left(g_V^\nu - g_A^\nu \gamma_5 \right) \nu_\mu \right] \cdot \left[\bar{f} \gamma_\mu \left(g_V^f - g_A^f \gamma_5 \right) f \right], \quad (2.15)$$

where $f = \{u, d, e\}$ and

$$g_Z^2 = 4\sqrt{2}G_\mu M_Z^2. \quad (2.16)$$

The $X - Z$ mixing modifies the effective interaction Eq. (2.15) since now one needs to take into account the Z_μ^m and X_μ^m exchange diagrams shown in Fig. 2.1. As a result, the effective strength of this interaction changes from g_Z^2/M_Z^2 to

$$\begin{aligned} & g_Z^2 \left(\frac{\cos^2 \theta}{M_Z^2} + \frac{\sin^2 \theta}{M_X^2} \right) - 2g_X g_Z \sin \theta \cos \theta \left(\frac{1}{M_Z^2} - \frac{1}{M_X^2} \right) \\ & \simeq \frac{g_Z^2}{M_Z^2} \left[1 + \frac{2g_X}{g_Z} \left(\frac{M_Z^2}{M_X^2} - 1 \right) \sin \theta \right] \equiv \frac{g_Z^2}{M_Z^2} \rho_\mu. \end{aligned} \quad (2.17)$$

The first term on the top line of Eq.(2.17) corresponds to the diagrams shown in Figs. 2.1a and 2.1b while the last term represents contributions of the diagrams in Figs. 2.1c and 2.1d.

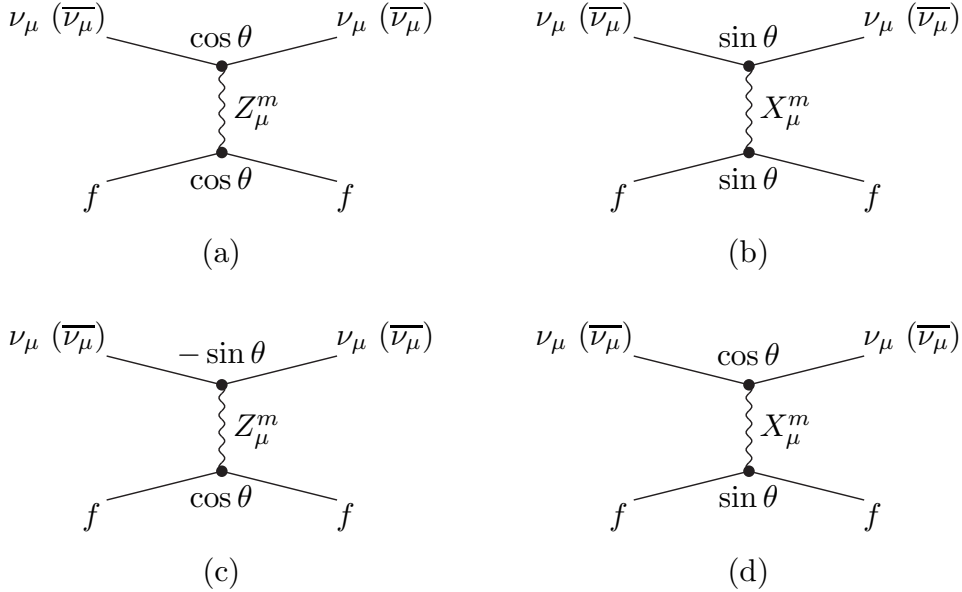


Figure 2.1: Z_μ^m and X_μ^m exchange diagrams contributing to the $\nu_\mu(\bar{\nu}_\mu) - f$ scattering.

Note that the form of the expression for the effective strength in Eq. (2.17) does not depend on the details of the Higgs sector of the model. The only assumption we made in deriving this expression is the existence of mixing between Z and X given by Eq. (2.14).

In sections 2.2.1 through 2.2.4 we reproduce the analysis by Ma and Roy [21, 22], updating those parts affected by new data. In section 2.2.5 we improve the analysis of Ma and Roy [21, 22] by considering the effects of mixing and the Z vertex corrections simultaneously. Finally, in section 2.2.6 we consider the constraints on the X mass and coupling coming from the most recent W decay data [3].

2.2.1 Z decay: $Z \rightarrow \mu^+ \mu^- X \rightarrow \mu^+ \mu^- \mu^+ \mu^-$

If the X boson exists then it can be searched for in the products of the Z decay. The Z can decay into μ^+ , μ^- , and X with consecutive decay of the latter into muon-antimuon pair. Thus, LEP I data on Z decay into the four-muon final state [23] establish a lower bound on M_X as a function of g_X . In addition to that, Eq. (2.12) implies

$$g_X^2 = \frac{M_X^2}{\frac{4M_Z^2}{g_Z^2} - 2v_0^2}. \quad (2.18)$$

Therefore

$$g_X > \frac{g_Z M_X}{2M_Z}. \quad (2.19)$$

These essentially rule out $M_X < 60$ GeV. For details see the paper by Ma and Roy [21, 22].

2.2.2 Precision measurements of Z couplings: $g_V^\tau - g_V^\mu$

Another constraint on the $L_\mu - L_\tau$ model comes from the precision measurement of Z couplings [25]. The presence of the $Z - X$ mixing modifies the way the Z interacts with the leptons of the second and third generations. The effective couplings relevant for further consideration are

$$e : \quad g_V^e = \sqrt{\rho} \left(-\frac{1}{2} + 2 \sin^2 \theta_W \right), \quad (2.20)$$

$$\mu : \quad g_V^\mu = \sqrt{\rho} \left(-\frac{1}{2} + 2 \sin^2 \theta_W \right) - 2 \left(\frac{g_X}{g_Z} \right) \sin \theta, \quad (2.21)$$

$$\tau : \quad g_V^\tau = \sqrt{\rho} \left(-\frac{1}{2} + 2 \sin^2 \theta_W \right) + 2 \left(\frac{g_X}{g_Z} \right) \sin \theta. \quad (2.22)$$

Ref. [26] reports the following values for g_V^e , g_V^μ and g_V^τ

$$g_V^e = -0.03816 \pm 0.00047, \quad (2.23)$$

$$g_V^\mu = -0.0367 \pm 0.0023, \quad (2.24)$$

$$g_V^\tau = -0.0366 \pm 0.0010. \quad (2.25)$$

Adding errors in quadrature, one obtains

$$g_V^\tau - g_V^\mu = 4(g_X/g_Z) \sin \theta = 0.0001 \pm 0.0025 \quad (2.26)$$

$$2 \cdot (g_V^\tau - g_V^e) = 4(g_X/g_Z) \sin \theta = 2 \cdot (0.00157 \pm 0.00111). \quad (2.27)$$

The 2σ bound on this combination is

$$-A_{\min} \leq 4(g_X/g_Z) \sin \theta \leq A_{\max}, \quad (2.28)$$

where $A_{\max} \equiv .0051$ and $A_{\min} \equiv .0012$. The upper bound A_{\max} is derived from Eq. (2.26) and the lower bound A_{\min} from Eq. (2.27) above.

On the other hand, Eq. (2.17) implies that

$$4(g_X/g_Z) \sin \theta = 2(\rho_\mu - 1) \left(\frac{M_X^2}{M_Z^2 - M_X^2} \right). \quad (2.29)$$

In order to explain the NuTeV anomaly one needs to have $\rho_\mu < 1$ to suppress the number of the neutral current events. Thus, combining Eqs. (2.28) and (2.29) one can obtain bounds on the M_X as a function of ρ_μ . The result is the following.

1. $M_X > M_Z$.

- If $\rho_\mu > 1 - \frac{A_{\max}}{2} \simeq 0.9974$ then there exists the lower bound given by

$$M_X > \frac{M_Z}{\sqrt{1 - \frac{2(1 - \rho_\mu)}{A_{\max}}}}; \quad (2.30)$$

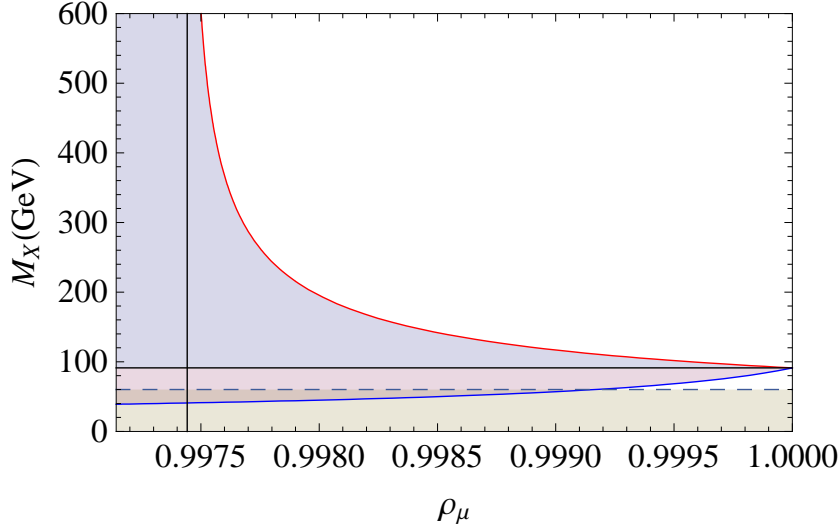


Figure 2.2: Upper and lower bounds on the M_X as a function of ρ_μ .

- If $\rho_\mu < 0.9974$ it is not possible to satisfy the LEP constraint with positive M_X^2 in this case.

2. $M_X < M_Z$. Then the upper bound is given by

$$M_X < \frac{M_Z}{\sqrt{1 + \frac{2(1 - \rho_\mu)}{A_{\min}}}}. \quad (2.31)$$

To illustrate this result we choose $\rho_\mu = 0.9976$, the value used by Ma and Roy in Ref. [21] to reduce the disagreement between the NuTeV results and theoretical predictions to 1.6σ level. Then using Eq's (2.30) and (2.31) one obtains the following 2σ bounds on M_X :

$$M_X < 42 \text{ GeV} \quad \text{or} \quad M_X > 367 \text{ GeV}. \quad (2.32)$$

As we already mentioned above, the result of the NuTeV experiment is controversial and in the process of being reanalyzed. Thus, we do not want to commit ourselves to some particular value for ρ_μ . Fig. 2.2 shows the upper (red curve) and the lower (blue curve) bounds on M_X as functions of ρ_μ . As ρ approaches unity these curves converge to the same value of $M_X = M_Z$. The vertical black line corresponds to $\rho_\mu = 0.9974$. The horizontal dashed line represents the 60 GeV lower bound from the searches of Z decay into $\mu^+\mu^-X$ (see Sec. 2.2.1). The regions between the red and blue curves, and below the 60 GeV line are excluded.

2.2.3 Universality of the Z couplings: $Z \rightarrow e^+e^-$ and $Z \rightarrow \mu^+\mu^-$

In the presence of the X boson the universality of the Z boson coupling to e^+e^- , $\mu^+\mu^-$, and $\tau^+\tau^-$ would be violated since the latter ones couple to X and have an extra one-loop radiative correction to the vertex diagram, $\Delta\Gamma$. The corresponding process is shown in Fig. 2.3. This extra correction

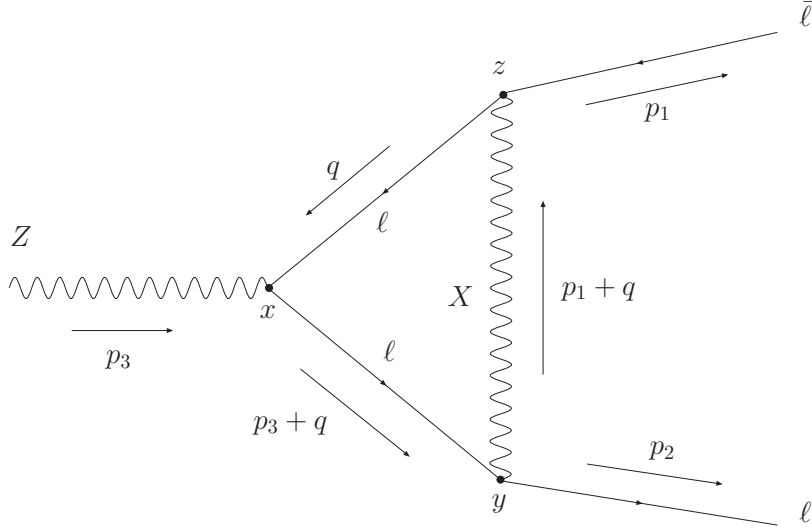


Figure 2.3: Correction to the Z vertex due to the X exchange between the final state leptons.

can be found in [24, 22]² and the result is

$$\begin{aligned} \frac{\Delta\Gamma}{\Gamma} = & - \frac{g_X^2}{4\pi^2} \left\{ \frac{7}{4} + \delta + \left(\delta + \frac{3}{2} \right) \ln \delta \right. \\ & \left. + (1 + \delta)^2 \left[\text{Li}_2 \left(\frac{\delta}{1 + \delta} \right) + \frac{1}{2} \ln^2 \left(\frac{\delta}{1 + \delta} \right) - \frac{\pi^2}{6} \right] \right\}, \end{aligned} \quad (2.33)$$

where $\delta \equiv M_X^2/M_Z^2$, and

$$\text{Li}_2(x) \equiv - \int_0^x \frac{dt}{t} \ln(1 - t) \quad (2.34)$$

is the Spence function. The measured Z partial widths are [25]

$$\Gamma_e = 83.91 \pm 0.12, \quad \Gamma_\mu = 83.99 \pm 0.18. \quad (2.35)$$

This implies that

$$\frac{\Delta\Gamma}{\Gamma} = 0.0009 \pm 0.0026. \quad (2.36)$$

1.96 σ bound on this ratio (corresponding to 95% CL) is

$$\Delta\Gamma/\Gamma < 0.006. \quad (2.37)$$

2.2.4 Combined constraints

Now we are in the position to construct the combined constraints on the possible values of g_X and M_X in the $L_\mu - L_\tau$ model. In order to do that we need to choose some particular value for ρ_μ and

²Formula for the $\Delta\Gamma/\Gamma$ in Ref. [22] contains a typo.

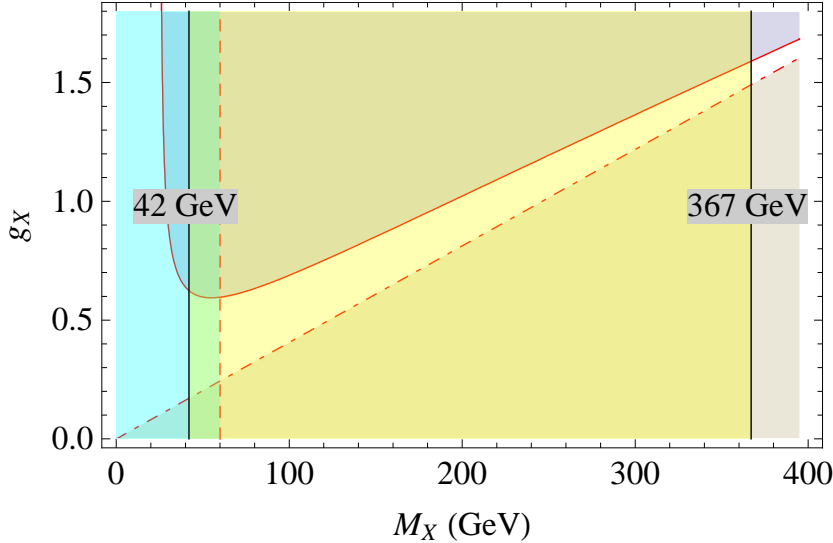


Figure 2.4: Combining constraints on the $L_\mu - L_\tau$ model.

plot together all constraints obtained so far. We take $\rho_\mu = 0.9976$, the value used by Ma and Roy in Ref. [21]. The resulting combined plot is shown in Fig. 2.4.

The dash-dotted red line corresponds to the bound given by the inequality Eq. (2.19). It excludes the gray region below this line. Two vertical solid black lines represent the bounds on the X boson mass given by Eq. (2.32). The yellow region between this two lines is not compatible with the results of the precision measurements of the Z vector couplings. Solid red line is the upper bound on g_X coming from the universality of the Z coupling to the e^+e^- and $\mu^+\mu^-$. It is obtained by combining the results of Eq's (2.33) and (2.37). The purple region above this curve is excluded. Finally, the vertical dashed red line represents the LEP-I constraint on the mass and coupling of the X boson from $Z \rightarrow \mu\mu X$ decay presented in Sec. 2.2.1. The values of M_X smaller than this bound (blue region) are not compatible with the LEP-I measurements. We see that for the chosen value of ρ_μ the 42 GeV constraint from the precision measurements of the Z vector couplings lies below the LEP-I constraint. On the other hand, Fig. 2.2 shows that it would lie above the the LEP-I constraint for the values of ρ_μ larger than 0.9992 which is indistinguishable from unity in the NuTeV experiment.

Combining these constraints together we see that the only allowed region of the parameter space is the one shown in white. The X boson mass in this region is greater than 367 GeV and the corresponding values of the coupling constant g_X are greater than one. This means that the theory approaches the non-perturbative region and the one loop analysis becomes less and less reliable. One should point it out that such large values of the coupling constant can lead to the dangerous effects for the model in question. For example, such a large coupling could lead to forming a stable bound state of μ^+ and μ^- which has not been observed experimentally.

2.2.5 Constraining $Z - X$ mixing and radiative corrections simultaneously

The analysis of the previous sections was essentially the repetition and update of the analysis performed by Ma and Roy in Ref. [21, 22]. Ma and Roy derive the constraints on the masses and couplings of the X boson using two sets of experimental data:

- the measurements of the Z effective couplings to leptons, and
- the measurements of the Z partial decay widths to charged lepton pairs.

We point out that there are some problems with Ma and Roy's analysis. First of all, the two sets of measurements are not completely independent since the measurements of the Z partial widths were used to find the value of the Z effective couplings to leptons. And second, Ma and Roy do not consider all corrections simultaneously. They derive constraints on the X mass using the measurements of the Z effective couplings and considering corrections coming from $Z - X$ mixing. Then they derive constraints on the possible values of the X mass and coupling using the measurements of the Z partial decay widths and considering the radiative corrections to the Z vertex due to the X exchange. Thus, in each case they only consider *one effect at a time*. But, in principal, we can have *both effects at the same time*: the radiative corrections to the Z vertex due to the X exchange affects the values of the Z effective couplings to leptons and $Z - X$ mixing affects the values of the Z partial decay widths to charged leptons. Thus, in this section we improve the analysis by considering both of these effects simultaneously.

But before we proceed, let us figure out the shift of the vectorial and axial effective couplings of the mu and tau leptons to the Z and clean up typos in some formulas of Ma and Roy's paper [21].

Neutrinos

For the electron neutrino case the effective couplings $g_V^{\nu_e}$ and $g_A^{\nu_e}$ remain the same as in the SM.

$$g_V^{\nu_e} = g_A^{\nu_e} = \sqrt{\rho} \cdot I_3^{\nu_e} = \sqrt{\rho} \left(+\frac{1}{2} \right). \quad (2.38)$$

For the muon neutrino case³ the SM Lagrangian is

$$\mathcal{L}_{SM} = g_Z \cdot g_L^{\nu_\mu} \cdot (\bar{\nu}_\mu \gamma^\alpha P_L \nu_\mu) \cdot Z_\alpha = \frac{g_Z}{2} \cdot [g_V^{\nu_\mu} \cdot (\bar{\nu}_\mu \gamma^\alpha \nu_\mu) - g_A^{\nu_\mu} \cdot (\bar{\nu}_\mu \gamma^\alpha \gamma^5 \nu_\mu)] \cdot Z_\alpha. \quad (2.39)$$

In this case $g_V^{\nu_\mu} = g_A^{\nu_\mu} = g_L^{\nu_\mu}$.

The X couples to the muon neutrino and the interaction Lagrangian is⁴:

$$\mathcal{L}_X = g_X \cdot (\bar{\nu}_\mu \gamma^\alpha \nu_\mu) \cdot X_\alpha. \quad (2.40)$$

Now, we should take into account that X is a linear combination of the Z and Z' (mass eigenstates⁵):

$$X_\alpha = -\sin \theta \cdot Z_\alpha + \cos \theta \cdot Z'_\alpha. \quad (2.41)$$

Using Eqs. (2.40) and (2.41) we find that the additional with respect to the SM interaction Lagrangian is

$$\delta \mathcal{L} = -g_X \sin \theta \cdot (\bar{\nu}_\mu \gamma^\alpha \nu_\mu) = \frac{g_Z}{2} \cdot \left(-2 \frac{g_X}{g_Z} \sin \theta \right) \cdot (\bar{\nu}_\mu \gamma^\alpha \nu_\mu) \cdot Z_\alpha. \quad (2.42)$$

³In the tau neutrino case the consideration is exactly the same. The only difference is in the overall sign of the shift due to $Z - X$ mixing.

⁴We assume that right handed neutrinos do not exist. In our notation ν_μ is the purely left-handed muon neutrino.

⁵Strictly speaking Z is also a mixture of mass eigenstates but it is irrelevant for what follows.

We rewrite this equation as

$$\delta\mathcal{L} = \frac{g_Z}{2} \cdot \left(-2\frac{g_X}{g_Z} \sin\theta \right) \cdot (\bar{\nu}_\mu \gamma^\alpha P_L \nu_\mu) \cdot Z_\alpha = \frac{g_Z}{2} \cdot \left(-\frac{g_X}{g_Z} \sin\theta \right) \cdot [(\bar{\nu}_\mu \gamma^\alpha \nu_\mu) - (\bar{\nu}_\mu \gamma^\alpha \gamma^5 \nu_\mu)] \cdot Z_\alpha. \quad (2.43)$$

Then both $g_V^{\nu\mu}$ and $g_A^{\nu\mu}$ of the SM are shifted by the same amount⁶

$$\delta g_V^{\nu\mu} = \delta g_A^{\nu\mu} = -\frac{g_X}{g_Z} \sin\theta, \quad (2.44)$$

which differs by a factor of 1/2 from the value obtained by Ma and Roy in [21].

Charged leptons

For the purpose of completeness let us also figure out the shift of the vectorial and axial couplings to the Z due to $Z - X$ mixing for charged leptons. For electrons the effective couplings g_V^e and g_A^e remain the same as in the SM. Namely,

$$g_V^e = \sqrt{\rho} \left(-\frac{1}{2} + 2\sin^2\theta_W \right), \quad g_A^e = \sqrt{\rho} \left(-\frac{1}{2} \right). \quad (2.45)$$

For muons⁷ the SM Lagrangian is

$$\mathcal{L}_{SM} = g_Z \cdot [g_L^\mu \cdot (\bar{\mu} \gamma^\alpha P_L \mu) + g_R^\mu \cdot (\bar{\mu} \gamma^\alpha P_R \mu)] \cdot Z_\alpha = \frac{g_Z}{2} \cdot [g_V^\mu \cdot (\bar{\mu} \gamma^\alpha \mu) - g_A^\mu \cdot (\bar{\mu} \gamma^\alpha \gamma^5 \mu)] \cdot Z_\alpha, \quad (2.46)$$

where $g_V^\mu = g_L^\mu + g_R^\mu$ and $g_A^\mu = g_L^\mu - g_R^\mu$.

The X -muon interaction Lagrangian is:

$$\mathcal{L}_X = g_X \cdot (\bar{\mu} \gamma^\alpha \mu) \cdot X_\alpha. \quad (2.47)$$

Taking into account the mixing given by Eq. (2.7) we obtain

$$\delta\mathcal{L} = -g_X \sin\theta \cdot (\bar{\mu} \gamma^\alpha \mu) \cdot Z_\alpha = \frac{g_Z}{2} \cdot \left(-2\frac{g_X}{g_Z} \sin\theta \right) \cdot (\bar{\mu} \gamma^\alpha \mu) \cdot Z_\alpha. \quad (2.48)$$

So, comparing Eqs. (2.46) and (2.48), we observe that the $Z - X$ mixing generates a shift of the vectorial effective coupling and does not change the value of the axial effective coupling:

$$\delta g_V^\mu = -2\frac{g_X}{g_Z} \sin\theta, \quad \delta g_A^\mu = 0, \quad (2.49)$$

which is in agreement with the result obtained by Ma and Roy in Ref. [21].

Fit results

Thus, we see that the presence of the $Z - X$ mixing and the radiative correction to the Z vertex due to X exchange between the external leptons modify the way the Z interacts with the leptons

⁶Note that for the purely left-handed muon neutrino $\delta g_A^{\nu\mu}$ and $\delta g_V^{\nu\mu}$ must be equal to each other.

⁷In the tau lepton case the consideration is exactly the same. The only difference is in the overall sign of the shift due to $Z - X$ mixing.

Parameter	Central value	Standard deviation
δs^2	-0.0006962	0.002140
$\delta\rho$	0.0007324	0.0010725
δ_M	-0.0007420	0.0009443
δ_V	-0.0008905	0.0006408

Table 2.1: The values of $\delta\rho$, δ_V , and δ_M extracted from the χ^2 fit.

of the second and third generations. Effective couplings become

$$e : \quad g_V^e = \sqrt{\rho} \left(-\frac{1}{2} + 2 \sin^2 \theta_W \right), \quad g_A^e = \sqrt{\rho} \left(-\frac{1}{2} \right), \quad (2.50)$$

$$\mu : \quad g_V^\mu = \sqrt{\rho} \left(-\frac{1}{2} + 2 \sin^2 \theta_W \right) (1 + \delta_V) + \delta_M, \quad g_A^\mu = \sqrt{\rho} \left(-\frac{1}{2} \right) (1 + \delta_V), \quad (2.51)$$

$$\tau : \quad g_V^\tau = \sqrt{\rho} \left(-\frac{1}{2} + 2 \sin^2 \theta_W \right) (1 + \delta_V) - \delta_M, \quad g_A^\tau = \sqrt{\rho} \left(-\frac{1}{2} \right) (1 + \delta_V) \quad (2.52)$$

for charged leptons and

$$\nu_e : \quad g_V^{\nu_e} = \sqrt{\rho} \left(+\frac{1}{2} \right), \quad g_A^{\nu_e} = \sqrt{\rho} \left(+\frac{1}{2} \right), \quad (2.53)$$

$$\nu_\mu : \quad g_V^{\nu_\mu} = \sqrt{\rho} \cdot \frac{1}{2} (1 + \delta_V) + \frac{\delta_M}{2}, \quad g_A^{\nu_\mu} = \sqrt{\rho} \cdot \frac{1}{2} (1 + \delta_V) + \frac{\delta_M}{2}, \quad (2.54)$$

$$\nu_\tau : \quad g_V^{\nu_\tau} = \sqrt{\rho} \cdot \frac{1}{2} (1 + \delta_V) - \frac{\delta_M}{2}, \quad g_A^{\nu_\tau} = \sqrt{\rho} \cdot \frac{1}{2} (1 + \delta_V) - \frac{\delta_M}{2} \quad (2.55)$$

for neutrinos. δ_V and δ_M are the vertex and mixing corrections, respectively, in the $L_\mu - L_\tau$ model. Their values are found to be:

$$\begin{aligned} \delta_V = & -\frac{g_X^2}{8\pi^2} \left\{ \frac{7}{4} + \delta + \left(\delta + \frac{3}{2} \right) \ln \delta \right. \\ & \left. + (1 + \delta)^2 \left[\text{Li}_2 \left(\frac{\delta}{1 + \delta} \right) + \frac{1}{2} \ln^2 \left(\frac{\delta}{1 + \delta} \right) - \frac{\pi^2}{6} \right] \right\}, \end{aligned} \quad (2.56)$$

$$\delta_M = -2 \left(\frac{g_X}{g_Z} \right) \sin \theta, \quad (2.57)$$

where $\delta \equiv M_X^2/M_Z^2$ and the Spence function $\text{Li}_2(x)$ is given by Eq. (2.34).

The measured by LEP values of the effective couplings of leptons to the Z are listed in Table 2.2. To do the fit to the SM values we have to take into account radiative corrections other than that included in δ_V . There are two types of radiative correction we must consider: the SM corrections, and the extra corrections appearing in the $L_\mu - L_\tau$ model. The SM corrections shift the value of the ρ parameter from unity and change the value of the $\sin^2 \theta_W$ from its tree level value. We calculate these corrections using ZFITTER [27].

j	Parameter	Average	Correlations							
			g_A^ν	g_A^e	g_A^μ	g_A^τ	g_V^e	g_V^μ	g_V^τ	
1	$g_A^\nu \equiv g_V^\nu$	$+0.5003 \pm 0.0012$	1.00							
2	g_A^e	-0.50111 ± 0.00035	-0.75	1.00						
3	g_A^μ	-0.50120 ± 0.00054	0.39	-0.13	1.00					
4	g_A^τ	-0.50204 ± 0.00064	0.37	-0.12	0.35	1.00				
5	g_V^e	-0.03816 ± 0.00047	-0.10	0.01	-0.01	-0.03	1.00			
6	g_V^μ	-0.0367 ± 0.0023	0.02	0.00	-0.30	0.01	-0.10	1.00		
7	g_V^τ	-0.0366 ± 0.0010	0.02	-0.01	0.01	-0.07	-0.02	0.01	1.00	
		i	1	2	3	4	5	6	7	

Table 2.2: Results on the effective coupling constants for leptons [26].

The $L_\mu - L_\tau$ model contains at least two extra Higgs fields. These extra fields contribute to the Z vacuum polarization and this also affects the values of ρ and $\sin^2 \theta_W$. We will call these extra corrections specific to the $L_\mu - L_\tau$ model $\delta\rho$ and δs^2 respectively. In addition to that we also have extra corrections due to mixing, δ_M , and the extra vertex corrections, δ_V .

Using the data of Table 2.2 we can fit the parameters δs^2 , $\delta\rho$, δ_V , and δ_M to the observed values of $g_{V,A}^f$ ($f = \{\nu, e, \mu, \tau\}$). The results of the χ^2 fit⁸ are listed in Table 2.1.

Now we can use the fitted values of δ_M and δ_V to improve the analysis of Ma and Roy given in Ref. [21]

Constraints from δ_M

From Eqs. (2.29) and (2.57) we see that the parameter δ_M is equal to

$$\delta_M = -(1 - \rho_\mu) \cdot \frac{M_X^2}{M_X^2 - M_Z^2}. \quad (2.58)$$

This means that

$$\rho_\mu = 1 + \delta_M \left[1 - \left(\frac{M_Z}{M_X} \right)^2 \right]. \quad (2.59)$$

Fig. 2.5 shows how ρ_μ depends on the M_X where we used the value of δ_M from the fit.

Allowing 2σ deviation of the δ_M from its central value we obtain

$$-A_{\min} \leq -\frac{M_X^2}{M_X^2 - M_Z^2} \leq A_{\max} \quad (2.60)$$

where

$$A_{\min} = -\frac{\bar{\delta}_M - 2\sigma_{\delta_M}}{1 - \rho_\mu}, \quad (2.61)$$

$$A_{\max} = \frac{\bar{\delta}_M + 2\sigma_{\delta_M}}{1 - \rho_\mu}. \quad (2.62)$$

⁸For the details on how we made this fit see Appendix C.

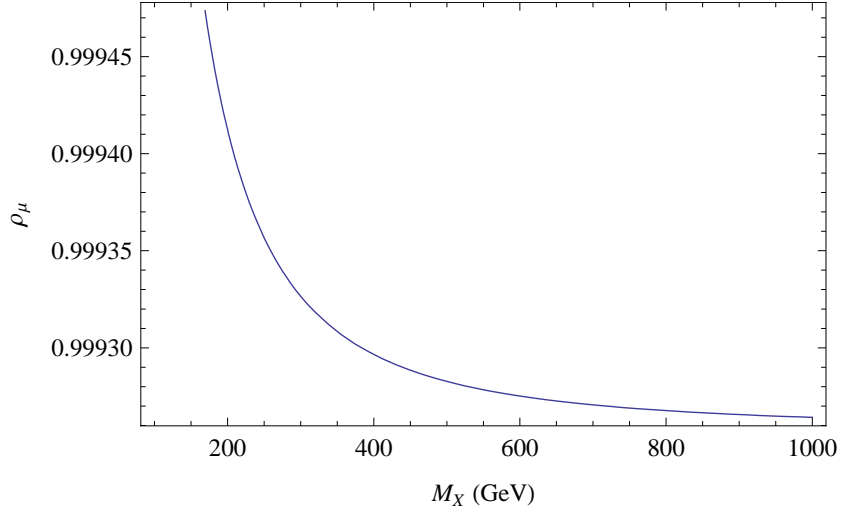


Figure 2.5: ρ_μ dependence on the M_X for the fitted value of δ_M .

Here $\bar{\delta}_M$ and σ_{δ_M} are the central value and the standard deviation of the δ_M , respectively. Their values are given in Table 2.1.

In order to find the constraints on the allowed values of M_X we need to consider two cases: $M_X > M_Z$ and $M_X < M_Z$.

1. If $M_X > M_Z$ then $-M_X^2/(M_X^2 - M_Z^2)$ is always negative. So, the inequality with A_{\max} is always satisfied. The inequality with A_{\min} gives

$$A_{\min} \geq \frac{M_X^2}{M_X^2 - M_Z^2}. \quad (2.63)$$

We observe that the left-hand side is smaller than one while the right-hand side is always greater than one for the case in question. So, this inequality cannot be satisfied. Therefore, this model cannot explain NuTeV if $M_X > M_Z$.

2. If $M_X < M_Z$ then Eq. (2.60) becomes

$$-A_{\min} \leq \frac{M_X^2}{M_Z^2 - M_X^2} \leq A_{\max}. \quad (2.64)$$

The $M_X^2/(M_Z^2 - M_X^2)$ is always positive. Therefore the inequality with A_{\min} is trivially satisfied. The inequality with A_{\max} can be solved for M_X . The result is

$$M_X < \frac{M_Z}{\sqrt{1 + \frac{1}{A_{\max}}}}. \quad (2.65)$$

Now, let us determine what value of ρ_μ ⁹ we need to bring the NuTeV result within one σ agreement with the SM predictions. The value of the g_L^2 measured by NuTeV is

$$(g_L^2)_{\text{NuTeV}} = 0.30005 \pm 0.00137. \quad (2.66)$$

⁹See Eq. (2.17)

The SM prediction is

$$(g_L^2)_{\text{SM}} = 0.3042. \quad (2.67)$$

Therefore, the value of ρ_μ we need is

$$\rho_\mu = \sqrt{\frac{0.30005 + 0.00137}{0.3042}} \approx 0.9954. \quad (2.68)$$

If we now plug this value of ρ_μ into Eq. (2.65) we obtain the following upper bound on the values of the X mass:

$$M_X < 40.8 \text{ GeV}. \quad (2.69)$$

This upper bound is obviously smaller than the 60 GeV lower bound on the X mass obtained in section 2.2.1. Thus we see that the $L_\mu - L_\tau$ model cannot explain the entire NuTeV anomaly without conflicting with the LEP data.

It was argued by Ma and Roy in Ref. [21] that the $L_\mu - L_\tau$ model can explain at least a part of the NuTeV anomaly and bring the disagreement between the SM prediction and the measured value of the g_L^2 at the 1.6σ level. We can try to do the same thing using the data we obtained from the fit. The value of ρ_μ needed to bring the NuTeV result within 1.6σ agreement with the SM predictions is

$$\rho_\mu = \sqrt{\frac{0.30005 + 1.6 \cdot 0.00137}{0.3042}} \approx 0.9968. \quad (2.70)$$

With this value of ρ_μ the upper bound on the X mass moves up a little bit and becomes

$$M_X < 46.7 \text{ GeV} \quad (2.71)$$

which is still smaller than the 60 GeV lower bound on the X mass obtained in section 2.2.1. Thus, we see that the $L_\mu - L_\tau$ model is not a viable candidate for explaining the NuTeV anomaly even partially because such an explanation conflicts with the LEP data.

Constraints from δ_V

Now, let us consider constraints on g_X and M_X from the fitted value of δ_V .

$$\delta_V = -\frac{g_X^2}{8\pi^2} \cdot f(M_X), \quad (2.72)$$

where

$$f(M_X) = \frac{7}{4} + \delta + \left(\delta + \frac{3}{2}\right) \ln \delta + (1 + \delta)^2 \left[\text{Li}_2\left(\frac{\delta}{1 + \delta}\right) + \frac{1}{2} \ln^2\left(\frac{\delta}{1 + \delta}\right) - \frac{\pi^2}{6} \right] \quad (2.73)$$

as can be seen from Eq. (2.56). $\delta \equiv M_X^2/M_Z^2$ as before. Allowing 2σ deviation from the central value of the δ_V we obtain

$$-A_{\min} \leq -\frac{g_X^2}{8\pi^2} \cdot f(M_X) \leq A_{\max}, \quad (2.74)$$

where

$$A_{\min} = -(-0.0008905 - 2 \cdot 0.0006408) = 0.002172, \quad (2.75)$$

$$A_{\max} = -0.0008905 + 2 \cdot 0.0006408 = 0.0003911. \quad (2.76)$$

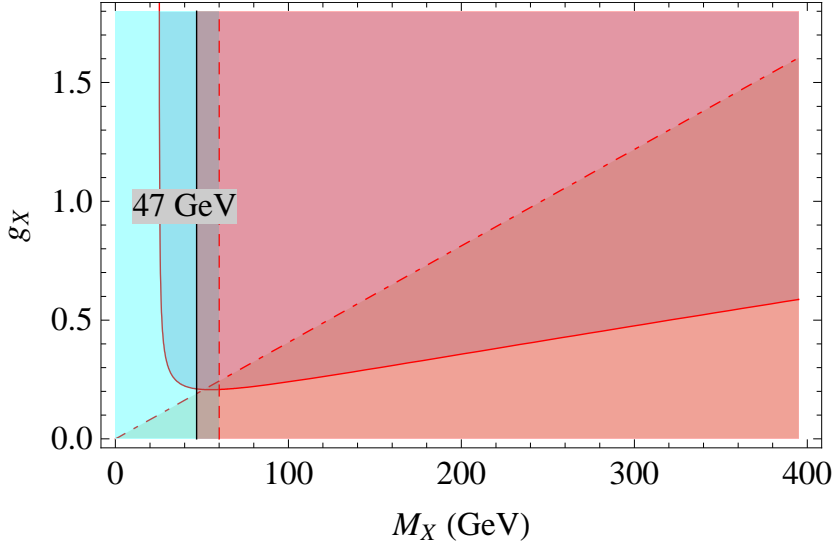


Figure 2.6: Constraints on the g_X and M_X of the $L_\mu - L_\tau$ model from the fit.

$f(M_X)$ is negative for sufficiently large M_X . Therefore, we only have to consider the inequality with A_{\max} . It implies that

$$g_X \leq \sqrt{\frac{8\pi^2 A_{\max}}{-f(M_X)}}. \quad (2.77)$$

Combined constraints

The combined constraints are plotted in Fig. 2.6. The figure also include constraints obtained in Section 2.2.1. The ruled out regions are shown in different colors.

The dash-dotted red line corresponds to the bound given by the inequality Eq. (2.19). The region below this line is excluded. The vertical solid black line represents the bounds on the X boson mass given by Eq. (2.71). The region to the left of this line (red) is excluded by the result of the fit to the SM observables. Solid red line is the upper bound on g_X coming from the result of the fit for the parameter δ_V and given by Eq. (2.77). The region above this curve is excluded. Finally, the vertical dashed red line represents the 60 GeV LEP-I constraint on the mass and coupling of the X boson from $Z \rightarrow \mu\mu X$ decay discussed in Sec. 2.2.1. The values of M_X smaller than this bound (blue region) are not compatible with the LEP-I measurements.

We observe from the figure that it does not contain any white (allowed) region at all. Thus, we conclude that the fit to the SM observables completely rules out the possibility that the $L_\mu - L_\tau$ model can explain NuTeV and at the same time be compatible with the results of the precision measurements.

2.2.6 W decay width

Another independent set of constraints on the $L_\mu - L_\tau$ model comes from the preliminary measurements of the W partial width. Ref. [3] reports the following results for the branching ratios of W

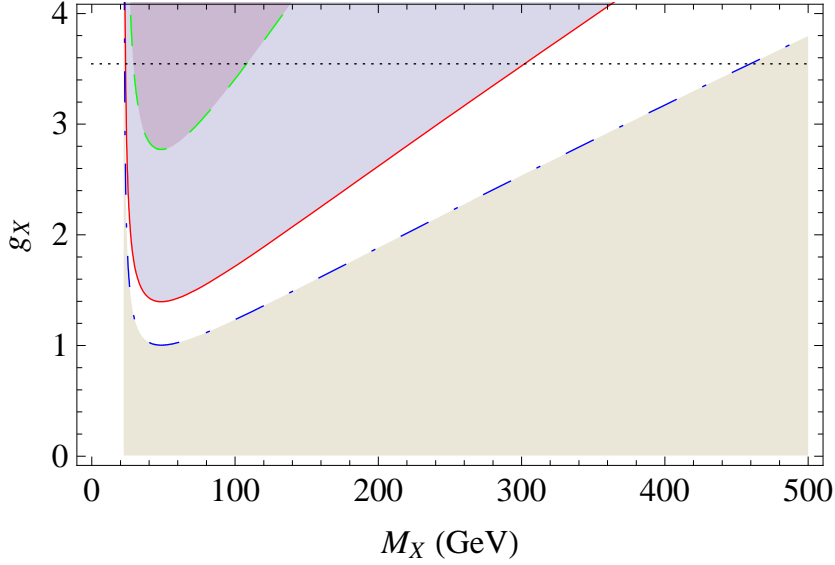


Figure 2.7: Constraints from the W branching ratios data.

into leptons of different flavor:

$$B(W \rightarrow \mu\bar{\nu}_\mu)/B(W \rightarrow e\bar{\nu}_e) = 0.994 \pm 0.020, \quad (2.78)$$

$$B(W \rightarrow \tau\bar{\nu}_\tau)/B(W \rightarrow e\bar{\nu}_e) = 1.074 \pm 0.029, \quad (2.79)$$

$$B(W \rightarrow \tau\bar{\nu}_\tau)/B(W \rightarrow \mu\bar{\nu}_\mu) = 1.080 \pm 0.028. \quad (2.80)$$

It is not difficult to express the ratio $\Delta\Gamma/\Gamma$ in terms of the branching ratios given above. In the $L_\mu - L_\tau$ model both μ and τ channel give extra corrections to the W decay vertex. So, we can write

$$\frac{\Delta\Gamma}{\Gamma} = B(W \rightarrow \mu\bar{\nu}_\mu)/B(W \rightarrow e\bar{\nu}_e) - 1 = -0.006 \pm 0.020, \quad (2.81)$$

$$\frac{\Delta\Gamma}{\Gamma} = B(W \rightarrow \tau\bar{\nu}_\tau)/B(W \rightarrow e\bar{\nu}_e) - 1 = +0.074 \pm 0.029. \quad (2.82)$$

The first equation above implies the following 95% CL (1.96σ) upper bound on the possible values of $\Delta\Gamma/\Gamma$

$$\frac{\Delta\Gamma}{\Gamma} \leq 0.033. \quad (2.83)$$

The second equation above implies both upper and lower 95% CL bounds on the possible values of $\Delta\Gamma/\Gamma$ given by

$$0.017 \leq \frac{\Delta\Gamma}{\Gamma} \leq 0.131. \quad (2.84)$$

The analytic expression for the $\Delta\Gamma/\Gamma$ ratio is given by essentially the same formula as for the Z decay case Eq. (2.33) in which M_Z is replaced with the W mass M_W . We derive this formula in Appendix B. The constraints given by Eqs. (2.83) and (2.84) are presented graphically in Fig. 2.7. The red solid line represents the upper bound given by Eq. (2.83). The dashed green line corresponds to the upper and the dash-dotted blue line to the lower bounds of Eq. (2.84). The

excluded regions are shown in different colors. The only allowed region of the parameter space is the white region between the solid red and the dash-dotted blue line. One observes that the values of the coupling constant in this region are larger than one and approaches the perturbative bound of $\alpha_X (\equiv g_X^2/4\pi) = 1$ or $g_X = \sqrt{4\pi}$ (the dotted black horizontal line) as the value of the M_X increases.

In addition to that, in the $L_\mu - L_\tau$ model both μ and τ contributes equally to the W decay vertex. This implies that in this model the branching ratios in the numerator and the denominator of Eq. (2.80) must be equal to each other and their ratio must be equal to unity. But it is not compatible with the experimental data. In fact, if one takes the W decay data seriously, this possibility is ruled out at more than 99% CL ($2.58\sigma = 0.072$) as can be easily seen from the right hand side of Eq. (2.80).

So, we conclude that the W decay data also greatly disfavor this model.

2.3 $B - 3L_\mu$ gauge boson

We next consider the gauged $B - 3L_\mu$ model, where B is the baryon number and L_μ is the muon number. The gauge boson of this model couples to the quarks of all generations and to leptons of the second generation. To satisfy the anomaly cancellation condition we must also add an extra right-handed neutrino to the particle content of the SM.

It was suggested by Davidson et al. in Ref. [17] to use the $B - 3L_\mu$ gauge boson as a possible explanation of the NuTeV anomaly. Thus, in this section we analyze how the existence of such a particle would affect the NuTeV result.

The SM effective Lagrangian describing the 4-Fermi neutral current interaction between muon neutrino and quarks has the form¹⁰:

$$\mathcal{L}_{\text{SM}} = -2\sqrt{2} \cdot G_F \cdot [g_L^{\nu u} \cdot (\bar{u}_L \gamma^\alpha u_L) + g_R^{\nu u} \cdot (\bar{u}_R \gamma^\alpha u_R) + g_L^{\nu d} \cdot (\bar{d}_L \gamma^\alpha d_L) + g_R^{\nu d} \cdot (\bar{d}_R \gamma^\alpha d_R)] \cdot (\bar{\nu}_\mu \gamma_\alpha \nu_\mu). \quad (2.85)$$

In the framework of the $B - 3L_\mu$ model one generates an additional contribution to the effective Lagrangian (2.85) given by¹¹

$$\begin{aligned} \mathcal{L}_{B-3L_\mu} &= -\frac{g_{Z'}^2}{M_{Z'}^2} \cdot \frac{1}{3} \cdot (-3) \cdot (\bar{u} \gamma^\alpha u + \bar{d} \gamma^\alpha d) \cdot (\bar{\nu}_\mu \gamma_\alpha \nu_\mu) \\ &= \frac{g_{Z'}^2}{M_{Z'}^2} \cdot (\bar{u}_L \gamma^\alpha u_L + \bar{u}_R \gamma^\alpha u_R + \bar{d}_L \gamma^\alpha d_L + \bar{d}_R \gamma^\alpha d_R) \cdot (\bar{\nu}_\mu \gamma_\alpha \nu_\mu). \end{aligned} \quad (2.86)$$

Adding (2.85) and (2.86) together one obtains

$$\begin{aligned} \mathcal{L}_{\text{SM}} + \mathcal{L}_{B-3L_\mu} &= -2\sqrt{2} \cdot G_F \cdot [\tilde{g}_L^{\nu u} \cdot (\bar{u}_L \gamma^\alpha u_L) + \tilde{g}_R^{\nu u} \cdot (\bar{u}_R \gamma^\alpha u_R) \\ &\quad + \tilde{g}_L^{\nu d} \cdot (\bar{d}_L \gamma^\alpha d_L) + \tilde{g}_R^{\nu d} \cdot (\bar{d}_R \gamma^\alpha d_R)] \cdot (\bar{\nu}_\mu \gamma_\alpha \nu_\mu), \end{aligned} \quad (2.87)$$

where $\tilde{g}_P^{\nu q} \equiv g_P^{\nu q} - \delta g$, $P = \{L, R\}$, $q = \{u, d\}$ and

$$\delta g \equiv \frac{g_{Z'}^2}{M_{Z'}^2} \cdot (2\sqrt{2} \cdot G_F)^{-1}. \quad (2.88)$$

¹⁰see for instance the expression on the bottom of p. 2 in the paper by Davidson et al. [17]

¹¹see for example a similar Eq. (33) in [9]

Squaring $\tilde{g}_L^{\nu u}$ and $\tilde{g}_L^{\nu d}$ gives

$$(\tilde{g}_L^{\nu u})^2 = (g_L^{\nu u})^2 - 2g_L^{\nu u}\delta g + \delta g^2, \quad (2.89)$$

$$(\tilde{g}_L^{\nu d})^2 = (g_L^{\nu d})^2 - 2g_L^{\nu d}\delta g + \delta g^2. \quad (2.90)$$

The NuTeV experiment measured the following quantity:

$$(\tilde{g}_L)^2 = (\tilde{g}_L^{\nu u})^2 + (\tilde{g}_L^{\nu d})^2 = g_L^2 - \delta g(2g_L^{\nu u} + 2g_L^{\nu d} - 2\delta g) = g_L^2 + \Delta, \quad (2.91)$$

where

$$\Delta \equiv -\delta g(2g_L^{\nu u} + 2g_L^{\nu d} - 2\delta g). \quad (2.92)$$

Plugging $g_L^{\nu u} = \rho \left(\frac{1}{2} - \frac{2}{3}s_W^2\right)$ and $g_L^{\nu d} = \rho \left(-\frac{1}{2} + \frac{1}{3}s_W^2\right)$ into the expression above yields

$$\Delta = -\delta g \cdot \left(1 - \frac{4}{3}s_W^2 - 1 + \frac{2}{3}s_W^2 - 2\delta g\right) = \delta g \cdot \left(2\delta g + \frac{2}{3}s_W^2\right), \quad (2.93)$$

where we set $\rho = 1$. Thus, one observes that in the model with the $B - 3L_\mu$ gauge boson the SM value g_L^2 is shifted by the positive value of Δ making \tilde{g}_L^2 bigger than g_L^2 . But the NuTeV experiment saw the opposite: the measured value

$$(\tilde{g}_L^2)_{\text{NuTeV}} = 0.30005 \pm 0.00137 \quad (2.94)$$

was *smaller* than the SM prediction of

$$(g_L^2)_{\text{SM}} = 0.3042. \quad (2.95)$$

Thus, we conclude that the claim made by Davidson et al. in Ref. [17] that the $B - 3L_\mu$ gauge boson can explain the NuTeV anomaly is wrong.

2.4 Leptoquark

Leptoquarks are particles carrying both baryon number B , and lepton number L . They occur in various extensions of the SM such as Grand Unification Theories (GUT's) or Extended Technicolor (ETC). In GUT models, the quarks and leptons are placed in the same multiplet of the GUT group. The massive gauge bosons which correspond to the broken generators of the GUT group which change quarks into leptons, and vice versa, are vector leptoquarks. In ETC models, the technicolor interaction will bind the techniquarks and the technileptons into scalar or vector bound states. These leptoquark states couple to the ordinary quarks and leptons through ETC interactions.

The interactions of leptoquarks with ordinary matter can be described in a model-independent fashion by an effective low-energy Lagrangian as discussed in Ref. [28]. Assuming the fermionic content of the SM, the most general dimensionless $SU(3)_C \times SU(2)_L \times U(1)_Y$ invariant couplings of scalar and vector leptoquarks satisfying baryon and lepton number conservation is given by:

$$\mathcal{L} = \mathcal{L}_{F=2} + \mathcal{L}_{F=0}, \quad (2.96)$$

where

$$\begin{aligned}
\mathcal{L}_{F=2} = & \left[g_{1L} \bar{q}_L^c i\tau_2 \ell_L + g_{1R} \bar{u}_R^c e_R \right] S_1 + \tilde{g}_{1R} \left[\bar{d}_R^c e_R \right] \tilde{S}_1 \\
& + g_{3L} \left[\bar{q}_L^c i\tau_2 \vec{\tau} \ell_L \right] \vec{S}_3 \\
& + \left[g_{2L} \bar{d}_R^c \gamma^\mu \ell_L + g_{2R} \bar{q}_L^c \gamma^\mu e_R \right] V_{2\mu} + \tilde{g}_{2L} \left[\bar{u}_R^c \gamma^\mu \ell_L \right] \tilde{V}_{2\mu} + h.c. , \tag{2.97}
\end{aligned}$$

$$\begin{aligned}
\mathcal{L}_{F=0} = & \left[h_{2L} \bar{u}_R \ell_L + h_{2R} \bar{q}_L i\tau_2 e_R \right] S_2 + \tilde{h}_{2L} \left[\bar{d}_R \ell_L \right] \tilde{S}_2 \\
& + \left[h_{1L} \bar{q}_L \gamma^\mu \ell_L + h_{1R} \bar{d}_R \gamma^\mu e_R \right] V_{1\mu} + \tilde{h}_{1R} \left[\bar{u}_R \gamma^\mu e_R \right] \tilde{V}_{1\mu} \\
& + h_{3L} \left[\bar{q}_L \vec{\tau} \gamma^\mu \ell_L \right] \vec{V}_{3\mu} + h.c. \tag{2.98}
\end{aligned}$$

Here, the scalar and vector leptoquark fields are denoted by S and V , respectively, their subscripts indicating the dimension of their $SU(2)_L$ representation. The same index is attached to their respective coupling constants, the g 's and h 's, with the extra subscript L or R indicating the chirality of the lepton involved in the interaction. For simplicity, color, weak isospin, and generation indices have been suppressed. The leptoquarks $S_1, \tilde{S}_1, \vec{S}_3, V_2, \tilde{V}_2$ carry fermion number $F = 3B + L = -2$, while the leptoquarks $S_2, \tilde{S}_2, V_1, \tilde{V}_1, \vec{V}_3$ have $F = 0$.

Rewriting the fermion doublets and the leptoquark multiplets in terms of the individual component fields, Eqs. (2.97) and (2.98) are expanded as follows:

$$\begin{aligned}
\mathcal{L}_{F=2} = & \left[g_{1L} (\bar{u}_L^c e_L - \bar{d}_L^c \nu_L) + g_{1R} (\bar{u}_R^c e_R) \right] S_1^0 + \tilde{g}_{1R} \left[\bar{d}_R^c e_R \right] \tilde{S}_1^0 \\
& + \left[g_{2L} (\bar{d}_R^c \gamma^\mu e_L) + g_{2R} (\bar{d}_R^c \gamma^\mu e_R) \right] V_{2\mu}^+ + \left[g_{2L} (\bar{d}_R^c \gamma^\mu \nu_L) + g_{2R} (\bar{u}_L^c \gamma^\mu e_R) \right] V_{2\mu}^- \\
& + \tilde{g}_{2L} \left[(\bar{u}_R^c \gamma^\mu e_L) \tilde{V}_{2\mu}^+ + (\bar{u}_R^c \gamma^\mu \nu_L) \tilde{V}_{2\mu}^- \right] \\
& + g_{3L} \left[-\sqrt{2} (\bar{d}_L^c e_L) S_3^+ - (\bar{u}_L^c e_L + \bar{d}_L^c \nu_L) S_3^0 + \sqrt{2} (\bar{u}_L^c \nu_L) S_3^- \right] + h.c. , \tag{2.99}
\end{aligned}$$

$$\begin{aligned}
\mathcal{L}_{F=0} = & \left[h_{2L} (\bar{u}_R e_L) + h_{2R} (\bar{u}_L e_R) \right] S_2^+ + \left[h_{2L} (\bar{u}_R \nu_L) - h_{2R} (\bar{d}_L e_R) \right] S_2^- \\
& + \tilde{h}_{2L} \left[(\bar{d}_R e_L) \tilde{S}_2^+ + (\bar{d}_R \nu_L) \tilde{S}_2^- \right] \\
& + \left[h_{1L} (\bar{u}_L \gamma^\mu \nu_L + \bar{d}_L \gamma^\mu e_L) + h_{1R} (\bar{d}_R \gamma^\mu e_R) \right] V_{1\mu}^0 + \tilde{h}_{1R} \left[\bar{u}_R \gamma^\mu e_R \right] \tilde{V}_{1\mu}^0 \\
& + h_{3L} \left[\sqrt{2} (\bar{u}_L \gamma^\mu e_L) V_{3\mu}^+ + (\bar{u}_L \gamma^\mu \nu_L - \bar{d}_L \gamma^\mu e_L) V_{3\mu}^0 + \sqrt{2} (\bar{d}_L \gamma^\mu \nu_L) V_{3\mu}^- \right] + h.c. \tag{2.100}
\end{aligned}$$

Superscripts indicate the weak isospin of each field, not the electromagnetic charge. For fields with subscript 1, the superscript 0 is redundant and may be dropped. The quantum numbers and couplings of the various leptoquarks fields are summarized in Table 2.3. Note that the scalar \tilde{S}_1 and the vector $\tilde{V}_{1\mu}$ do not couple to the neutrinos, so they are irrelevant to our discussion and will not be considered further. The isospin plus components of the remaining leptoquarks, namely $S_2^+, \tilde{S}_2^+, S_3^+, V_{2\mu}^+, \tilde{V}_{2\mu}^+$, and $V_{3\mu}^+$, do not couple to the neutrinos either, but we will keep them in our Lagrangian since their coupling constants are common with the other components that do couple, and are important in understanding how the couplings are constrained by neutrinoless experiments.

Leptoquark	Spin	F	$SU(3)_C$	I_3	Y	Q_{em}	Allowed Couplings
S_1	S_1^0	0	$\bar{3}$	0	$\frac{1}{3}$	$\frac{1}{3}$	$g_{1L}(\bar{u}_L^c e_L - \bar{d}_L^c \nu_L), g_{1R}(\bar{u}_R^c e_R)$
\tilde{S}_1	\tilde{S}_1^0	0	$\bar{3}$	0	$\frac{4}{3}$	$\frac{4}{3}$	$\tilde{g}_{1R}(\bar{d}_R^c e_R)$
$V_{2\mu}$	$V_{2\mu}^+$ $V_{2\mu}^-$	1	$\bar{3}$	$+\frac{1}{2}$ $-\frac{1}{2}$	$\frac{2}{6}$	$\frac{2}{3}$ $\frac{1}{3}$	$g_{2L}(\bar{d}_R^c \gamma^\mu e_L), g_{2R}(\bar{d}_L^c \gamma^\mu e_R)$ $g_{2L}(\bar{d}_R^c \gamma^\mu \nu_L), g_{2R}(\bar{u}_L^c \gamma^\mu e_R)$
$\tilde{V}_{2\mu}$	$\tilde{V}_{2\mu}^+$ $\tilde{V}_{2\mu}^-$	1	$\bar{3}$	$+\frac{1}{2}$ $-\frac{1}{2}$	$-\frac{1}{6}$	$\frac{1}{3}$ $-\frac{2}{3}$	$\tilde{g}_{2L}(\bar{u}_R^c \gamma^\mu e_L)$ $\tilde{g}_{2L}(\bar{u}_R^c \gamma^\mu \nu_L)$
\tilde{S}_3	S_3^+ S_3^0 S_3^-	0	$\bar{3}$	+1 0 -1	$\frac{1}{3}$	$\frac{4}{3}$ $\frac{1}{3}$ $-\frac{2}{3}$	$-\sqrt{2}g_{3L}(\bar{d}_L^c e_L)$ $-g_{3L}(\bar{u}_L^c e_L + \bar{d}_L^c \nu_L)$ $\sqrt{2}g_{3L}(\bar{u}_L^c \nu_L)$
S_2	S_2^+ S_2^-	0	3	$+\frac{1}{2}$ $-\frac{1}{2}$	$\frac{7}{6}$	$\frac{5}{3}$ $\frac{2}{3}$	$h_{2L}(\bar{u}_R e_L), h_{2R}(\bar{u}_L e_R)$ $h_{2L}(\bar{u}_R \nu_L), -h_{2R}(\bar{d}_L e_R)$
\tilde{S}_2	\tilde{S}_2^+ \tilde{S}_2^-	0	3	$+\frac{1}{2}$ $-\frac{1}{2}$	$\frac{1}{6}$	$\frac{2}{3}$ $-\frac{1}{3}$	$\tilde{h}_{2L}(\bar{d}_R e_L)$ $\tilde{h}_{2L}(\bar{d}_R \nu_L)$
$V_{1\mu}$	$V_{1\mu}^0$	1	3	0	$\frac{2}{3}$	$\frac{2}{3}$	$h_{1L}(\bar{u}_L \gamma^\mu \nu_L + \bar{d}_L \gamma^\mu e_L), h_{1R}(\bar{d}_R \gamma^\mu e_R)$
$\tilde{V}_{1\mu}$	$\tilde{V}_{1\mu}^0$	1	3	0	$\frac{5}{3}$	$\frac{5}{3}$	$\tilde{h}_{1R}(\bar{u}_R \gamma^\mu e_R)$
$\tilde{V}_{3\mu}$	$V_{3\mu}^+$ $V_{3\mu}^0$ $V_{3\mu}^-$	1	3	+1 0 -1	$\frac{2}{3}$	$\frac{5}{3}$ $\frac{2}{3}$ $-\frac{1}{3}$	$\sqrt{2}h_{3L}(\bar{u}_L \gamma^\mu e_L)$ $h_{3L}(\bar{u}_L \gamma^\mu \nu_L - \bar{d}_L \gamma^\mu e_L)$ $\sqrt{2}h_{3L}(\bar{d}_L \gamma^\mu \nu_L)$

Table 2.3: Quantum numbers of scalar and vector leptoquarks with $SU(3)_C \times SU(2)_L \times U(1)_Y$ invariant couplings to quark-lepton pairs ($Q_{em} = I_3 + Y$).

Since the leptoquarks must distinguish among different generation fermions to contribute to quark-muon (anti-)neutrino scattering we generalize their interactions by allowing the coupling constants to depend on the generations of the quarks and leptons that couple to each leptoquark:

$$\begin{aligned}
\mathcal{L}_{F=2} = & \left[g_{1L}^{ij}(\bar{u}_{iL}^c e_{jL} - \bar{d}_{iL}^c \nu_{jL}) + g_{1R}^{ij}(\bar{u}_{iR}^c e_{jR}) \right] S_1^0 \\
& + \left[g_{2L}^{ij}(\bar{d}_{iR}^c \gamma^\mu e_{jL}) + g_{2R}^{ij}(\bar{d}_{iL}^c \gamma^\mu e_{jR}) \right] V_{2\mu}^+ + \left[g_{2L}^{ij}(\bar{d}_{iR}^c \gamma^\mu \nu_{jL}) + g_{2R}^{ij}(\bar{u}_{iL}^c \gamma^\mu e_{jR}) \right] V_{2\mu}^- \\
& + \tilde{g}_{2L}^{ij} \left[(\bar{u}_{iR}^c \gamma^\mu e_{jL}) \tilde{V}_{2\mu}^+ + (\bar{u}_{iR}^c \gamma^\mu \nu_{jL}) \tilde{V}_{2\mu}^- \right] \\
& + g_{3L}^{ij} \left[-\sqrt{2}(\bar{d}_{iL}^c e_{jL}) S_3^+ - (\bar{u}_{iL}^c e_{jL} + \bar{d}_{iL}^c \nu_{jL}) S_3^0 + \sqrt{2}(\bar{u}_{iL}^c \nu_{jL}) S_3^- \right] + h.c. , \quad (2.101)
\end{aligned}$$

$$\begin{aligned}
\mathcal{L}_{F=0} = & \left[h_{2L}^{ij}(\bar{u}_{iR} e_{jL}) + h_{2R}^{ij}(\bar{u}_{iL} e_{jR}) \right] S_2^+ + \left[h_{2L}^{ij}(\bar{u}_{iR} \nu_{jL}) - h_{2R}^{ij}(\bar{d}_{iL} e_{jR}) \right] S_2^- \\
& + \tilde{h}_{2L}^{ij} \left[(\bar{d}_{iR} e_{jL}) \tilde{S}_2^+ + (\bar{d}_{iR} \nu_{jL}) \tilde{S}_2^- \right] \\
& + \left[h_{1L}^{ij}(\bar{u}_{iL} \gamma^\mu \nu_{jL} + \bar{d}_{iL} \gamma^\mu e_{jL}) + h_{1R}^{ij}(\bar{d}_{iR} \gamma^\mu e_{jR}) \right] V_{1\mu}^0 \\
& + h_{3L}^{ij} \left[\sqrt{2}(\bar{u}_{iL} \gamma^\mu e_{jL}) V_{3\mu}^+ + (\bar{u}_{iL} \gamma^\mu \nu_{jL} - \bar{d}_{iL} \gamma^\mu e_{jL}) V_{3\mu}^0 + \sqrt{2}(\bar{d}_{iL} \gamma^\mu \nu_{jL}) V_{3\mu}^- \right] + h.c. \quad (2.102)
\end{aligned}$$

Here, i is the quark generation number, and j is the lepton generation number. Summation over repeated indices is assumed. The interactions that contribute to quark-muon (anti-)neutrino scattering are those with indices $(ij) = (12)$.

It is often assumed in the literature that generation non-diagonal couplings are absent to account for the non-observation of flavor changing neutral currents and lepton flavor violation. However, the constraints from such rare processes are always on *products of different (ij)-couplings* and not on the *individual* non-diagonal couplings by themselves. For instance, non-observation of the decay $K_L \rightarrow \bar{e}\mu$ constrains the product of (12) and (21) couplings, but not the (12) and (21) couplings separately, which allows one of them to be sizable if the other is small. Constraints on the individual (12) and (13) couplings actually come from precision measurements of *flavor conserving* processes, such as $R_\pi = \Gamma(\pi \rightarrow \mu\nu_\mu)/\Gamma(\pi \rightarrow e\nu_e)$ which constrains the square of the (12) coupling, and those constraints are not yet that strong [29, 30].

In order to affect the result of the NuTeV experiment the leptoquark must couple to the (anti-)neutrino of the second generation and the first generation quarks. The main result of the NuTeV experiment was that the measured value of the parameter g_L^2 disagreed with the SM prediction. Thus, we are most interested in the leptoquarks which couple to the left-handed u and d quarks because the presence of such interaction will obviously affect the value of g_L^2 .

We follow the notation given in Ref. [9]. There are four types of leptoquarks which couple to the muon (anti-)neutrino and the left-handed u and d quarks. They are:

1. S_1 leptoquark. It has spin 0, $I_3 = 0$, $Y = 1/3$, and $Q_{\text{em}} = 1/3$ ($Q_{\text{em}} = I_3 + Y$). The corresponding Lagrangian has the form:

$$\mathcal{L} = [g_{1L}^{12} \cdot (\bar{u}_L^c \mu_L - \bar{d}_L^c \nu_\mu) + g_{1R}^{12} \cdot (\bar{u}_R^c \mu_R)] \cdot S_1 + \text{h.c.} \quad (2.103)$$

2. \vec{S}_3 leptoquark. It has spin 0, $I_3 = \{+1, 0, -1\}$, $Y = 1/3$, and $Q_{\text{em}} = \{4/3, 1/3, -2/3\}$. The Lagrangian has the form:

$$\mathcal{L} = g_{3L}^{12} \cdot \left[-\sqrt{2} \cdot (\bar{d}_L^c \mu_L) \cdot S_3^+ - (\bar{u}_L^c \mu_L + \bar{d}_L^c \nu_\mu) \cdot S_3^0 + \sqrt{2} \cdot (\bar{u}_L^c \nu_\mu) \cdot S_3^- \right] + \text{h.c.} \quad (2.104)$$

3. V_1 leptoquark. It has spin 1, $I_3 = 0$, $Y = 2/3$, and $Q_{\text{em}} = 2/3$. The Lagrangian is

$$\mathcal{L} = [h_{1L}^{12} \cdot (\bar{u}_L \gamma^\alpha \nu_\mu + \bar{d}_L \gamma^\alpha \mu_L) + h_{1R}^{12} \cdot (\bar{d}_R \gamma^\alpha \mu_R)] \cdot V_{1\alpha} + \text{h.c.} \quad (2.105)$$

4. \vec{V}_3 leptoquark. It has spin 1, $I_3 = \{+1, 0, -1\}$, $Y = 2/3$, and $Q_{\text{em}} = \{5/3, 2/3, -1/3\}$. The Lagrangian is

$$\mathcal{L} = h_{3L}^{12} \cdot \left[\sqrt{2} \cdot (\bar{u}_L \gamma^\alpha \mu_L) \cdot V_{3\alpha}^+ + (\bar{u}_L \gamma^\alpha \nu_\mu - \bar{d}_L \gamma^\alpha \mu_L) \cdot V_{3\alpha}^0 + \sqrt{2} \cdot (\bar{d}_L \gamma^\alpha \nu_\mu) \cdot V_{3\alpha}^- \right] + \text{h.c.} \quad (2.106)$$

The ν_μ -quark effective Lagrangian of the SM at tree level is

$$\begin{aligned} \mathcal{L}_{\text{SM}} = & -2\sqrt{2}G_F \cdot [(\bar{\nu}_\mu \gamma^\alpha \mu_L)(\bar{d}_L \gamma_\alpha u_L) + \text{h.c.}] \\ & -2\sqrt{2}G_F \cdot [g_L^{\nu u}(\bar{u}_L \gamma^\alpha u_L) + g_R^{\nu u}(\bar{u}_R \gamma^\alpha u_R) + g_L^{\nu d}(\bar{d}_L \gamma^\alpha d_L) + g_R^{\nu d}(\bar{d}_R \gamma^\alpha d_R)] (\bar{\nu}_\mu \gamma_\alpha \nu_\mu). \end{aligned} \quad (2.107)$$

The leptoquarks listed above induce extra contributions to both neutral and charged current parts of the SM effective Lagrangian¹²:

$$\mathcal{L}_{\text{eff}}^{(n)} = -2\sqrt{2}G_F \cdot [\varepsilon_{\mu\mu}^{dL} \cdot (\bar{\nu}_\mu \gamma^\alpha \nu_\mu)(\bar{d}\gamma_\alpha P_L d) + \varepsilon_{\mu\mu}^{uL} \cdot (\bar{\nu}_\mu \gamma^\alpha \nu_\mu)(\bar{u}\gamma_\alpha P_L u)], \quad (2.108)$$

$$\mathcal{L}_{\text{eff}}^{(c)} = -2\sqrt{2}G_F \cdot \varepsilon_c \cdot (\bar{\mu}\gamma^\alpha P_L \nu_\mu)(\bar{u}\gamma_\alpha P_L d) + \text{h.c.}, \quad (2.109)$$

where $\varepsilon_{\mu\mu}^{dL}$, $\varepsilon_{\mu\mu}^{uL}$, and ε_c are the effective couplings whose values depend on the type of leptoquark.

In the presence of $\mathcal{L}_{\text{eff}}^{(n)}$ the parameters $g_L^{\nu d, u}$ change: $g_L^{\nu d, u} \rightarrow \tilde{g}_L^{\nu d, u} = g_L^{\nu d, u} + \varepsilon_{\mu\mu}^{d, uL}$. By definition $g_L^2 = (g_L^{\nu u})^2 + (g_L^{\nu d})^2$. Therefore, in the leading order the change of the g_L^2 due to the leptoquark contribution to the neutral current part of the effective SM Lagrangian is

$$(\delta g_L^2)^{(n)} = 2(g_L^{\nu d} \varepsilon_{\mu\mu}^{dL} + g_L^{\nu u} \varepsilon_{\mu\mu}^{uL}). \quad (2.110)$$

Now, let us find the change of the g_L^2 due to the leptoquark contribution to the charged current part. The following ratio was measured in the NuTeV experiment:

$$R_\nu = \frac{\sigma(\nu N \rightarrow \nu X)}{\sigma(\nu N \rightarrow \mu X)} = g_L^2 + r g_R^2. \quad (2.111)$$

In the presence of $\mathcal{L}_{\text{eff}}^{(c)}$ the denominator of the expression above gets reduced by the factor of $(1 + \varepsilon_c)^2$. This means that

$$\frac{(g_L^2)_{\text{SM}} + r(g_R^2)_{\text{SM}}}{(1 + \varepsilon_c)^2} = (g_L^2)_{\text{NuTeV}} + r(g_R^2)_{\text{NuTeV}}. \quad (2.112)$$

Since $(1 + \varepsilon_c)^{-2} \approx 1 - 2\varepsilon_c$, one gets $(g_L^2)_{\text{NuTeV}} = (g_L^2)_{\text{SM}} - 2g_L^2 \varepsilon_c$. Therefore, the change of the g_L^2 due to the leptoquark contribution to the charged current part of the effective SM Lagrangian is

$$(\delta g_L^2)^{(c)} = -2g_L^2 \varepsilon_c. \quad (2.113)$$

Similarly, the change of the g_R^2 due to the leptoquark contribution to the charged current part of the effective SM Lagrangian is

$$(\delta g_R^2)^{(c)} = -2g_R^2 \varepsilon_c. \quad (2.114)$$

Note that for the leptoquarks we are considering $g_R^{\nu d}$ and $g_R^{\nu u}$ will not be affected simply because the muon neutrino does not couple to right-handed quarks as can be seen from Eq's (2.103-2.106). Therefore, g_R^2 will only be shifted by the amount given by Eq. (2.114).

Combining Eq's (2.110) and (2.113) we find that the total change of the g_L^2 is

$$\delta g_L^2 = 2(g_L^{\nu d} \varepsilon_{\mu\mu}^{dL} + g_L^{\nu u} \varepsilon_{\mu\mu}^{uL} - g_L^2 \varepsilon_c). \quad (2.115)$$

We want to emphasize that the g_L^2 in the expression above is the SM value of this parameter.

¹² Using the terminology and logic of Ref. [17] we are only considering left-handed 'vector' operators. In the presence of leptoquarks, 'scalar' and 'tensor' operators can also be generated. 'Tensor' operators can in principle explain NuTeV by increasing the value of the charged current. However, they always appear in pairs with the 'scalar' operators so that the effective couplings of these two types of operators have the same orders of magnitude. It was found in Ref [17] (pp. 14-15) that 1) the scalar operator itself cannot explain NuTeV because the value of the coupling required for that is inconsistent with the measurement of R_π , and 2) if some 'tensor' operator has the value of the effective coupling needed to explain NuTeV then the corresponding 'scalar' operator overcontributes to the value of R_π . Thus, we exclude 'tensor' and 'scalar' operators from the scope of our consideration.

Process	(ij)	LQ	Assumptions	95% CL bound	Reference
$p\bar{p} \rightarrow LQ \bar{L}\bar{Q} X \rightarrow (j\nu)(j\nu)X$	(**)	S	$\beta = 0^{(a)}$	117 GeV	CDF [31]
$p\bar{p} \rightarrow LQ \bar{L}\bar{Q} X \rightarrow (j\nu)(j\nu)X$	(**)	S	$\beta = 0$	135 GeV	D0 [32]
$p\bar{p} \rightarrow LQ \bar{L}\bar{Q} X \rightarrow (j\mu)(j\mu)X$	(*2)	S	$\beta = 0.5$	208 GeV	CDF [33]
$p\bar{p} \rightarrow LQ \bar{L}\bar{Q} X \rightarrow (j\mu)(j\nu)X$	(*2)	S	$\beta = 0.5$	204 GeV	D0 [34]
$p\bar{p} \rightarrow LQ \mu X \rightarrow (j\mu)\mu X$	(*2)	S	$\beta = 0.5, \lambda = 1^{(b)}$	226 GeV ^(c)	D0 [35]

Table 2.4: Direct search limits on the Leptoquark mass from the Tevatron. ^(a) β is the assumed branching fraction $B(LQ \rightarrow q\ell) = 1 - B(LQ \rightarrow q\nu)$, and ^(b) λ is the Yukawa coupling of the Leptoquark with the quark-lepton pair. ^(c)Combined bound with the pair production data.

2.4.1 Constraints on the Leptoquark Couplings and Masses

Limits on leptoquark masses from direct searches at the Tevatron are listed in Table 2.4. Bounds from LEP and LEP II are weaker due to their smaller center of mass energies. Since the NuTeV experiment is only sensitive to leptoquarks with $(ij) = (12)$ coupling, we only quote limits which apply to leptoquarks with *only* this particular coupling, that is, leptoquarks that decay into a first generation quark, and a second generation lepton. Though it is usually stated in collider analyses that leptoquarks are assumed to decay into a quark-lepton pair of one particular generation, it is often the case that the jets coming from the quarks are not flavor tagged. Analyses that look for the leptoquark in the quark-neutrino decay channel are of course blind to the flavor of the neutrino. Therefore, the bounds listed apply to leptoquarks with generation non-diagonal couplings also.

As can be seen from Table 2.4, the mass bounds from the Tevatron are typically around 200 GeV and are mostly independent of the leptoquark-quark-lepton coupling λ . This independence is due to the dominance of the strong interaction processes, $q\bar{q}$ annihilation and gluon fusion, in the leptoquark pair-production cross sections, and the fact that heavy leptoquarks decay without a displaced vertex even for very small values of λ : the decay widths of scalar and vector leptoquarks with leptoquark-quark-lepton coupling λ are given by $\lambda^2 M_{LQ}/16\pi$ and $\lambda^2 M_{LQ}/24\pi$, respectively, which correspond to lifetimes of $O(10^{-21})$ seconds for $M_{LQ} = O(10^2)$ GeV, and $\lambda = O(10^{-2})$.

Bounds on leptoquarks with $(ij) = (12)$ couplings can also be obtained from bounds on contact interactions of the form

$$\mathcal{L} = \pm \frac{4\pi}{(\Lambda_{q\mu}^\pm)^2} (\bar{q}\gamma^\mu P_X q) (\bar{\mu}\gamma_\mu P_L \mu) , \quad (2.116)$$

where $X = L$ or R , and $q = u$ or d . For instance, at energies much lower than the leptoquark mass, the exchange of the S_1 leptoquark leads to the interaction [9]

$$\mathcal{L}_{S_1} = + \frac{|g_{1L}^{12}|^2}{2M_{S_1}^2} (\bar{u}\gamma^\mu P_L u) (\bar{\mu}\gamma_\mu P_L \mu) . \quad (2.117)$$

The remaining cases are listed in Table 2.5. The 95% CL lower bounds on the $\Lambda_{q\ell}^\pm$'s from CDF can be found in Ref. [36]¹³, and the cases relevant to our discussion are listed in Table 2.6. These bounds translate into bounds on the leptoquark masses and couplings listed in the third column of Table 2.5.

¹³See also discussion in Ref. [9].

LQ	Induced Interaction	CDF 95% CL [36]	Bounds from R_π
S_1	$+\frac{ g_{1L}^{12} ^2}{2M_{S_1}^2} (\bar{u}\gamma^\mu P_L u) (\bar{\mu}\gamma_\mu P_L \mu)$	$\frac{ g_{1L}^{12} ^2}{M_{S_1}^2} \leq 2.2 \text{ TeV}^{-2}$	$\frac{ g_{1L}^{12} ^2}{M_{S_1}^2} \leq 0.37 \text{ TeV}^{-2}$
\vec{S}_3	$+\frac{ g_{3L}^{12} ^2}{2M_{S_3}^2} (\bar{u}\gamma^\mu P_L u + 2\bar{d}\gamma^\mu P_L d) (\bar{\mu}\gamma_\mu P_L \mu)$	—	$\frac{ g_{3L}^{12} ^2}{M_{S_3}^2} \leq 0.08 \text{ TeV}^{-2}$
V_1	$-\frac{ h_{1L}^{12} ^2}{M_{V_1}^2} (\bar{d}\gamma^\mu P_L d) (\bar{\mu}\gamma_\mu P_L \mu)$	$\frac{ h_{1L}^{12} ^2}{M_{V_1}^2} \leq 4.3 \text{ TeV}^{-2}$	$\frac{ h_{1L}^{12} ^2}{M_{V_1}^2} \leq 0.18 \text{ TeV}^{-2}$
\vec{V}_3	$-\frac{ h_{3L}^{12} ^2}{M_{V_3}^2} (2\bar{u}\gamma^\mu P_L u + \bar{d}\gamma^\mu P_L d) (\bar{\mu}\gamma_\mu P_L \mu)$	—	$\frac{ h_{3L}^{12} ^2}{M_{V_3}^2} \leq 0.04 \text{ TeV}^{-2}$

Table 2.5: The quark-muon interactions induced by leptoquark exchange, the bounds from CDF [36], and the bounds from the measurement of R_π . Only the couplings that also contribute to NuTeV are listed. Analysis of the Tevatron Run II data is expected to improve the CDF bound by a factor of four.

$(q\mu)$ chirality	$\Lambda_{u\mu}^+$ (TeV)	$\Lambda_{u\mu}^-$ (TeV)	$\Lambda_{d\mu}^+$ (TeV)	$\Lambda_{d\mu}^-$ (TeV)
(LL)	3.4	4.1	2.3	1.7

Table 2.6: The 95% CL lower bound on the compositeness scale from CDF [36]. Results from D0 [37] do not provide limits for cases where the muons couple to only u or d , but we expect the bounds to be in the range $4 \sim 7$ TeV.

The presence of $\mathcal{L}_{\text{eff}}^{(c)}$ given by Eq. (2.109) changes the value of R_π as follows [38, 39, 29].

$$R_\pi \equiv \frac{B(\pi \rightarrow e\bar{\nu}_e)}{B(\pi \rightarrow \mu\bar{\nu}_\mu)} = R_\pi^{\text{SM}} \cdot (1 - 2\varepsilon_c) , \quad (2.118)$$

where R_π^{SM} is the SM value of this ratio¹⁴. This provides us with another important source of constraints on the possible values of the squared coupling-to-mass ratios for the leptoquarks. These constraints were considered in Ref. [29, 30]¹⁵. However, the theoretical and experimental values of R_π have been improved over the last years. Thus, we update the analysis. The theoretical value of the R_π is [40]

$$R_\pi^{\text{th}} = (1.2354 \pm 0.0002) \times 10^{-4}. \quad (2.119)$$

The experimental value of the R_π is [25]

$$R_\pi^{\text{exp}} = (1.230 \pm 0.004) \times 10^{-4}. \quad (2.120)$$

Now, it is not difficult to obtain the 2σ constraints on the possible values of the squared coupling-to-mass ratios for the different types of leptoquark. We make use of Eqs. (2.130), (2.140), (2.152), (2.155) given below which relate these ratios to the values of ε_c for each particular type of leptoquark. The bounds obtained in such a way are summarized in the last column of Table 2.5.

Comparing the last two columns of Table 2.5 we observe that the CDF bounds are significantly weaker than those derived from the R_π measurement. However, it should be noted that the results of Ref. [36] are from Tevatron Run I, and we can expect the Run II results to improve these bounds. Indeed, Ref. [37] from D0 analyzes the Run II data for contact interactions of the form

$$\mathcal{L} = \pm \frac{4\pi}{(\Lambda^\pm)^2} (\bar{u}\gamma^\mu P_X u + \bar{d}\gamma^\mu P_X d) (\bar{\mu}\gamma_\mu P_L \mu) , \quad X = L \text{ or } R , \quad (2.121)$$

¹⁴Here we make an assumption that there exists only one type of leptoquark contributing to the value of R_π and ignore possible ‘scalar’ and ‘tensor’ operators in the effective Lagrangian as discussed in footnote 12.

¹⁵See also the part discussing leptoquarks in Ref. [17].

and places 95% CL lower bounds on the Λ^\pm 's in the 4 ~ 7 TeV range. While these are not exactly the interactions induced by leptoquarks, we can nevertheless expect that the bounds on the $\Lambda_{q\mu}^\pm$'s will be in a similar range, and thereby conclude that the Run II data will roughly double the lower bounds from Run I. This means that the Run II bounds on the squared coupling-to-mass ratios for different types of leptoquarks will be about four times smaller than those of Run I shown in the third column of Table 2.5. If this estimates are correct then even the Run II Tevatron bounds are going to be weaker than bounds derived from the R_π measurements. Thus, in the further analysis we will concentrate our attention on the latter.

2.4.2 S_1 leptoquark

The relevant terms of the Lagrangian are

$$\mathcal{L} = g_{1L}^{12} \cdot (\bar{u}_L^c \mu_L - \bar{d}_L^c \nu_\mu) \cdot S_1 + \text{h.c.} \quad (2.122)$$

One can construct the effective Lagrangian correcting the neutral current part of the effective SM Lagrangian by considering the process $\nu_\mu, d_L \rightarrow S_1 \rightarrow \nu_\mu, d_L$. The matrix element associated with it is

$$iM = (-i)^2 |g_{1L}^{12}|^2 \cdot \langle \nu_\mu, d | (\bar{d}^c P_L \nu_\mu) \cdot \frac{i}{-M_{S_1}^2} \cdot (\bar{\nu}_\mu P_R d^c) | \nu_\mu, d \rangle. \quad (2.123)$$

Using Fierz rearrangement

$$(\bar{\nu}_\mu P_R d^c)(\bar{d}^c P_L \nu_\mu) = -\frac{1}{2} (\bar{\nu}_\mu \gamma^\alpha P_L \nu_\mu) (\bar{d}^c \gamma_\alpha P_R d^c) = \frac{1}{2} (\bar{\nu}_\mu \gamma^\alpha P_L \nu_\mu) (\bar{d} \gamma_\alpha P_L d) \quad (2.124)$$

we obtain

$$iM = i \frac{|g_{1L}^{12}|^2}{2M_{S_1}^2} \langle \nu_\mu | \bar{\nu}_\mu \gamma^\alpha \nu_\mu | \nu_\mu \rangle \langle d | \bar{d} \gamma_\alpha P_L d | d \rangle. \quad (2.125)$$

Therefore, the effective Lagrangian we are looking for is

$$\mathcal{L}_{\text{eff}}^{(n,d)} = \frac{|g_{1L}^{12}|^2}{2M_{S_1}^2} (\bar{\nu}_\mu \gamma^\alpha \nu_\mu) (\bar{d} \gamma_\alpha P_L d). \quad (2.126)$$

Thus,

$$\varepsilon_{\mu\mu}^{dL} = -\frac{1}{2\sqrt{2}G_F} \cdot \frac{|g_{1L}^{12}|^2}{2M_{S_1}^2}, \quad \varepsilon_{\mu\mu}^{uL} = 0. \quad (2.127)$$

Similarly, one can calculate the leptoquark correction to the charged current part of the effective SM Lagrangian by considering the process $\nu_\mu, d_L \rightarrow S_1 \rightarrow \mu, u_L$.

$$iM = -i \frac{|g_{1L}^{12}|^2}{2M_{S_1}^2} \langle \mu | \bar{\mu} \gamma^\alpha P_L \nu_\mu | \nu_\mu \rangle \langle u | \bar{u} \gamma_\alpha P_L d | d \rangle. \quad (2.128)$$

The effective Lagrangian is

$$\mathcal{L}_{\text{eff}}^{(c)} = -\frac{|g_{1L}^{12}|^2}{2M_{S_1}^2} (\bar{\mu} \gamma^\alpha P_L \nu_\mu) (\bar{u} \gamma_\alpha P_L d) + \text{h.c.} \quad (2.129)$$

The h.c. term comes from the inverse process $\mu, u_L \rightarrow S_1 \rightarrow \nu_\mu, d_L$. Eq. (2.129) implies that

$$\varepsilon_c = \frac{1}{2\sqrt{2}G_F} \cdot \frac{|g_{1L}^{12}|^2}{2M_{S_1}^2} = -\varepsilon_{\mu\mu}^{dL}. \quad (2.130)$$

Thus, using the result given by Eq. (2.115) one obtains that the total change of the g_L^2 in the presence of the S_1 leptoquark is

$$\delta g_L^2 = 2[g_L^{\nu d} \varepsilon_{\mu\mu}^{dL} - g_L^2 \varepsilon_c] = -2\varepsilon_c (g_L^{\nu d} + g_L^2). \quad (2.131)$$

Numerically, $g_L^{\nu d} = \rho \left(-\frac{1}{2} + \frac{1}{3}s_w^2\right)$, $s_w^2 = 0.23113$, $g_L^2 = 0.3042$. Therefore, setting $\rho = 1$, the tree level value, we obtain

$$\delta g_L^2 \approx +0.24 \cdot \varepsilon_c \geq 0, \quad (2.132)$$

because $\varepsilon_c \geq 0$ according to Eq. (2.130). Thus, we see that the S_1 leptoquark cannot explain the NuTeV anomaly because it generates the shift of g_L^2 which is positive rather than negative.

2.4.3 \vec{S}_3 leptoquark

The relevant terms of the Lagrangian are

$$\mathcal{L} = g_{3L}^{12} \cdot \left[-(\bar{u}_L^c \mu_L + \bar{d}_L^c \nu_\mu) \cdot S_3^0 + \sqrt{2} (\bar{u}_L^c \nu_\mu) \cdot S_3^- \right] + \text{h.c.} \quad (2.133)$$

Corrections to the neutral current part of the effective SM are generated through two different processes. They are

1. The processes $\nu_\mu, d_L \rightarrow S_3^0 \rightarrow \nu_\mu, d_L$. The matrix element associated with these processes is

$$iM = (-i)^2 |g_{3L}^{12}|^2 \cdot \langle \nu_\mu, d | (\bar{d}^c P_L \nu_\mu) \cdot \frac{i}{-M_{S_3^0}^2} \cdot (\bar{\nu}_\mu P_R d^c) | \nu_\mu, d \rangle. \quad (2.134)$$

Therefore, the corresponding effective Lagrangian is

$$\mathcal{L}_{\text{eff}}^{(n,d)} = \frac{|g_{3L}^{12}|^2}{2M_{S_3^0}^2} (\bar{\nu}_\mu \gamma^\alpha \nu_\mu) (\bar{d} \gamma_\alpha P_L d). \quad (2.135)$$

Thus,

$$\varepsilon_{\mu\mu}^{dL} = -\frac{1}{2\sqrt{2}G_F} \cdot \frac{|g_{3L}^{12}|^2}{2M_{S_3^0}^2}. \quad (2.136)$$

2. The processes $\nu_\mu, u_L \rightarrow S_3^- \rightarrow \nu_\mu, u_L$. Similarly to the previous case

$$\mathcal{L}_{\text{eff}}^{(n,u)} = \frac{|g_{3L}^{12}|^2}{M_{S_3^-}^2} (\bar{\nu}_\mu \gamma^\alpha \nu_\mu) (\bar{u} \gamma_\alpha P_L u). \quad (2.137)$$

Thus,

$$\varepsilon_{\mu\mu}^{uL} = -\frac{1}{2\sqrt{2}G_F} \cdot \frac{|g_{3L}^{12}|^2}{M_{S_3^-}^2}. \quad (2.138)$$

The correction to the charged current part of the effective SM Lagrangian can be calculated by considering the process $\nu_\mu, d_L \rightarrow S_1 \rightarrow \mu, u_L$. It is clear that in this case

$$\mathcal{L}_{\text{eff}}^{(c)} = \frac{|g_{3L}^{12}|^2}{2M_{S_3^0}^2} (\bar{\mu}\gamma^\alpha P_L \nu_\mu) (\bar{u}\gamma_\alpha P_L d) + \text{h.c.} \quad (2.139)$$

This implies that

$$\varepsilon_c = -\frac{1}{2\sqrt{2}G_F} \cdot \frac{|g_{3L}^{12}|^2}{2M_{S_3^0}^2} = \varepsilon_{\mu\mu}^{dL}. \quad (2.140)$$

In order to find the total shift of the g_L^2 , let us consider two cases:

1. ‘Degenerate’ case: assume that the masses of all three components of the triplet are the same. In this case $\varepsilon_{\mu\mu}^{uL} = 2\varepsilon_{\mu\mu}^{dL} = 2\varepsilon_c$. The total shift of the g_L^2 is

$$\begin{aligned} \delta g_L^2 &= 2(-\varepsilon_c)(-g_L^{\nu d} - 2g_L^{\nu u} + g_L^2) = 2(-\varepsilon_c)\left(-1 + \frac{4}{3}s_W^2 + \frac{1}{2} - \frac{1}{3}s_W^2 + g_L^2\right) \\ &= 2(-\varepsilon_c)\left(-\frac{1}{2} + s_W^2 + g_L^2\right) = 2(-\varepsilon_c)(-0.5 + 0.23113 + 0.3042) \approx +0.07 \cdot (-\varepsilon_c) \geq 0, \end{aligned} \quad (2.141)$$

because $\varepsilon_c \leq 0$ according to Eq. (2.140), and we set $\rho = 1$. Thus, we see that the degenerate \vec{S}_3 leptoquark cannot explain the NuTeV anomaly because it generates the shift of g_L^2 which is positive rather than negative.

2. ‘Non-degenerate’ case: assume that the masses of the components of the triplet are non-degenerate. In this case $\varepsilon_{\mu\mu}^{dL} = \varepsilon_c$ but $\varepsilon_{\mu\mu}^{uL}$ is an independent parameter. In order to explain NuTeV we need

$$\delta g_L^2 = (g_L^2)_{\text{NuTeV}} - (g_L^2)_{\text{SM}} = 2[\varepsilon_{\mu\mu}^{uL} g_L^{\nu u} + \varepsilon_c(g_L^{\nu d} - g_L^2)]. \quad (2.142)$$

Therefore

$$\delta g_L^2 = -\frac{|g_{3L}^{12}|^2}{2\sqrt{2}G_F} \cdot \left(\frac{2g_L^{\nu u}}{M_{S_3^-}^2} + \frac{g_L^{\nu d} - g_L^2}{M_{S_3^0}^2} \right). \quad (2.143)$$

This means that

$$\frac{2g_L^{\nu u}}{M_{S_3^-}^2} = \frac{g_L^2 - g_L^{\nu d}}{M_{S_3^0}^2} - 2\sqrt{2}G_F \frac{\delta g_L^2}{|g_{3L}^{12}|^2} \quad (2.144)$$

or

$$M_{S_3^-} = \sqrt{2g_L^{\nu u}} \cdot \left(\frac{g_L^2 - g_L^{\nu d}}{M_{S_3^0}^2} - 2\sqrt{2}G_F \frac{\delta g_L^2}{|g_{3L}^{12}|^2} \right)^{-1/2}. \quad (2.145)$$

We see that for a given $M_{S_3^0}$ and negative δg_L^2 there always exists the mass $M_{S_3^-}$ such that Eq. (2.143) is satisfied. Thus, the \vec{S}_3 leptoquark can in principle explain the NuTeV anomaly. The shift of the g_R^2 is given by Eq. (2.114):

$$(\delta g_R^2) = -2g_R^2 \varepsilon_c \quad (2.146)$$

where ε_c is determined by Eq. (2.140).

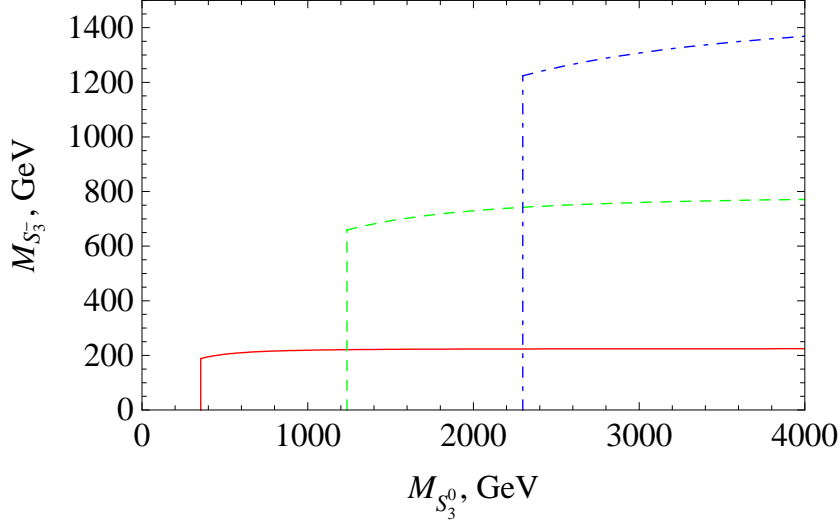


Figure 2.8: $M_{S_3^-}$ dependence on $M_{S_3^0}$. $g_{3L}^{12} = 0.1$ – red line; $g_{3L}^{12} = 0.35$ – green dashed line; $g_{3L}^{12} = 0.65$ – blue dashed-dotted line.

Fig. 2.8 illustrates the result above for

$$(g_L^2)_{\text{NuTeV}} = 0.30005, \quad (2.147)$$

the central values of the NuTeV result cited in [1]¹⁶, and $(g_L^2)_{\text{SM}} = 0.3042$. The graph shows how the mass of the S_3^- component of the triplet required to explain NuTeV depends on the mass of the S_3^0 component for three different choices of coupling. The vertical cutoffs are due to the lower bound on the mass of the S_3^0 component derived from the bound on the squared coupling-to-mass ratio given in the last column of Table 2.5.

2.4.4 V_1 leptoquark

The relevant interactions are

$$\mathcal{L} = h_{1L}^{12} \cdot (\bar{u}_L \gamma^\alpha \nu_\mu + \bar{d}_L \gamma^\alpha \mu_L) \cdot V_{1\alpha} + \text{h.c.} \quad (2.148)$$

The correction to the neutral current part of the effective SM Lagrangian is generated by the process $\nu_\mu, u_L \rightarrow \nu_\mu, u_L$ proceeding through the exchange of V_1 in the t -channel. The matrix element associated with it is

$$iM = (i)^2 |h_{1L}^{12}|^2 \cdot \langle \nu_\mu, u | (\bar{u} \gamma^\alpha P_L \nu_\mu) \cdot \frac{-i g_{\alpha\beta}}{-M_{V_1}^2} \cdot (\bar{\nu}_\mu \gamma^\beta P_L u) | \nu_\mu, u \rangle. \quad (2.149)$$

Using Fierz rearrangement

$$(\bar{\nu}_\mu \gamma^\alpha P_L u) \cdot (\bar{u} \gamma_\alpha P_L \nu_\mu) = + (\bar{\nu}_\mu \gamma^\alpha P_L \nu_\mu) \cdot (\bar{u} \gamma_\alpha P_L u) \quad (2.150)$$

we obtain

$$\mathcal{L}_{\text{eff}}^{(n,u)} = - \frac{|h_{1L}^{12}|^2}{M_{V_1}^2} (\bar{\nu}_\mu \gamma^\alpha \nu_\mu) (\bar{u} \gamma_\alpha P_L u). \quad (2.151)$$

¹⁶The NuTeV data are in the process of being reanalyzed. Thus this number can change in the future.

Thus,

$$\varepsilon_{\mu\mu}^{uL} = \frac{1}{2\sqrt{2}G_F} \cdot \frac{|h_{1L}^{12}|^2}{M_{V_1}^2}, \quad \varepsilon_{\mu\mu}^{dL} = 0. \quad (2.152)$$

The calculations of the correction to the charged current part of the effective SM Lagrangian are exactly the same and $\varepsilon_c = \varepsilon_{\mu\mu}^{uL}$. Thus, using the result given by Eq. (2.115) one obtains that the total change of the g_L^2 in the presence of the V_1 leptoquark is

$$\delta g_L^2 = 2[g_L^{\nu u} \varepsilon_{\mu\mu}^{uL} - g_L^2 \varepsilon_c] = 2\varepsilon_c (g_L^{\nu u} - g_L^2) = 2\varepsilon_c \left(\frac{1}{2} - \frac{2}{3}s_W^2 - 0.3042 \right) \approx 0.08 \cdot \varepsilon_c \geq 0, \quad (2.153)$$

where, again, we set $\rho = 1$. Thus, we see that the V_1 leptoquark cannot explain the NuTeV anomaly because it generates the shift of g_L^2 which is positive rather than negative.

2.4.5 \vec{V}_3 type leptoquark

The relevant terms of the Lagrangian are

$$\mathcal{L} = h_{3L}^{12} \cdot \left[(\bar{u}_L \gamma^\alpha \nu_\mu - \bar{d}_L \gamma^\alpha \mu_L) \cdot V_{3\alpha}^0 + \sqrt{2} (\bar{d}_L \gamma^\alpha \nu_\mu) \cdot V_{3\alpha}^- \right] + \text{h.c.} \quad (2.154)$$

This case is completely analogous to the case of V_1 leptoquark. The $\varepsilon_{\mu\mu}^{dL}$, $\varepsilon_{\mu\mu}^{uL}$, and ε_c are

$$\varepsilon_{\mu\mu}^{uL} = -\varepsilon_c = \frac{1}{2\sqrt{2}G_F} \cdot \frac{|h_{3L}^{12}|^2}{M_{V_3^0}^2}, \quad (2.155)$$

$$\varepsilon_{\mu\mu}^{dL} = \frac{1}{2\sqrt{2}G_F} \cdot \frac{2|h_{3L}^{12}|^2}{M_{V_3^-}^2}. \quad (2.156)$$

In order to find the total shift of the g_L^2 , let us consider two cases:

1. ‘Degenerate’ case: assume that the masses of all three components of the triplet are the same. In this case $\varepsilon_{\mu\mu}^{uL} = \varepsilon_{\mu\mu}^{dL}/2 = -\varepsilon_c$. The total shift of the g_L^2 is

$$\delta g_L^2 = 2(-\varepsilon_c)(2g_L^{\nu d} + g_L^{\nu u} + g_L^2) = 2(-\varepsilon_c) \left(\frac{1}{2} - \frac{2}{3}s_W^2 - 1 + \frac{2}{3}s_W^2 + g_L^2 \right) \approx -0.4 \cdot (-\varepsilon_c) \leq 0, \quad (2.157)$$

because $\varepsilon_c \leq 0$ according to Eq. (2.155). Thus, we see that the presence of the degenerate \vec{V}_3 leptoquark makes g_L^2 smaller which is exactly what was observed in the NuTeV experiment. Unfortunately, the value of ε_c needed to explain NuTeV conflicts with the measurements of R_π . Indeed, according to the bound shown in last column of Table 2.5 and Eq. (2.155), the value of the $(-\varepsilon_c)$ is limited from above as

$$-\varepsilon_c < \frac{1}{2\sqrt{2}G_F} \cdot 0.04 \cdot (1000)^{-2} \text{ GeV}^{-2} \approx 0.001. \quad (2.158)$$

This means that the value of g_L^2 can at most be reduced by $-0.4 \times 0.001 = -4 \times 10^{-4}$ while in order to explain NuTeV we need to make the value of this parameter smaller by

$$(g_L^2)_{\text{NuTeV}} - (g_L^2)_{\text{SM}} = 0.30005 - 0.3042 \approx -4 \cdot 10^{-3} \quad (2.159)$$

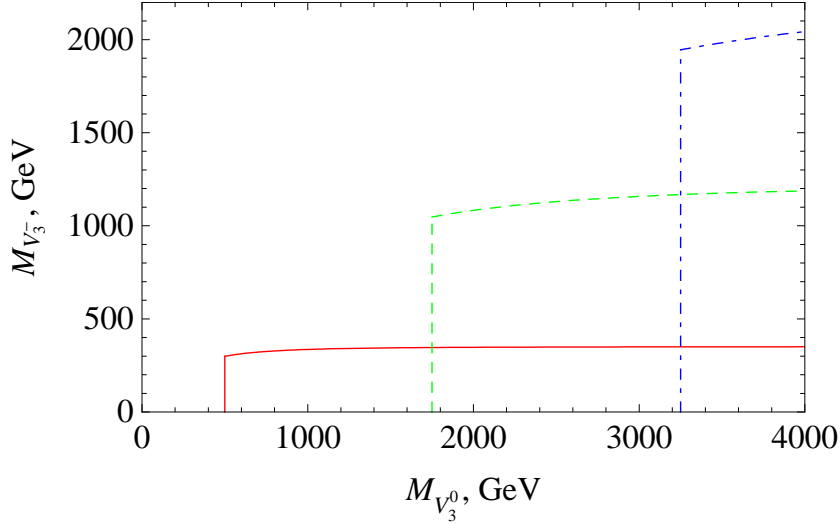


Figure 2.9: $M_{V_3^-}$ dependence on $M_{V_3^0}$. $h_{3L}^{12} = 0.1$ – red line; $h_{3L}^{12} = 0.35$ – green dashed line; $h_{3L}^{12} = 0.65$ – blue dashed-dotted line.

which is ten times bigger. Thus, we conclude that the \vec{V}_3 triplet leptoquark which components are mass degenerate can only explain a tiny fraction of the NuTeV anomaly.

2. ‘Non-degenerate’ case: assume that the masses of the components of the triplet are non-degenerate. In this case $\varepsilon_{\mu\mu}^{uL} = -\varepsilon_c$ but $\varepsilon_{\mu\mu}^{dL}$ is an independent parameter. In order to explain NuTeV we need

$$\delta g_L^2 = 2[\varepsilon_{\mu\mu}^{dL} g_L^{\nu d} + (-\varepsilon_c)(g_L^{\nu u} + g_L^2)] = 2 \cdot \frac{|h_{3L}^{12}|^2}{2\sqrt{2}G_F} \cdot \left(\frac{2g_L^{\nu d}}{M_{V_3^-}^2} + \frac{g_L^{\nu u} + g_L^2}{M_{V_3^0}^2} \right). \quad (2.160)$$

This means that

$$\frac{2g_L^{\nu d}}{M_{V_3^-}^2} = \sqrt{2}G_F \frac{\delta g_L^2}{|h_{3L}^{12}|^2} - \frac{g_L^2 + g_L^{\nu u}}{M_{V_3^0}^2} \quad (2.161)$$

or

$$M_{V_3^-} = \sqrt{-2g_L^{\nu d}} \cdot \left(\frac{g_L^2 + g_L^{\nu u}}{M_{V_3^0}^2} - \sqrt{2}G_F \frac{\delta g_L^2}{|h_{3L}^{12}|^2} \right)^{-1/2}. \quad (2.162)$$

We see that for a given $M_{V_3^0}$ and negative δg_L^2 there always exists the mass $M_{V_3^-}$ such that the Eq. (2.143) is satisfied. Thus, the \vec{V}_3 leptoquark can in principle explain the NuTeV anomaly. Fig. 2.9 illustrates the result above for the value of $(g_L^2)_{\text{NuTeV}}$ given by Eq. (2.147). The graph shows how the mass of the V_3^- component of the triplet required to explain NuTeV depends on the mass of the V_3^0 component for three different choices of coupling. The vertical cutoffs are due to the lower bound on the mass of the V_3^0 component which is derived from the bound on the squared coupling-to-mass ratio given in the last column of Table 2.5.

In the both ‘degenerate’ and ‘non-degenerate’ cases the shift of the g_R^2 is equal to

$$(\delta g_R^2) = -2g_R^2 \varepsilon_c \quad (2.163)$$

where ε_c is determined by Eq. (2.155).

This page left blank intentionally.

Chapter 3

Neutrissimo Models

In this chapter we give an example of what we can learn about new physics from the experimental data soon to be available to us. We consider a special class of models containing TeV scale heavy Majorana neutrinos mixing with the regular SM neutrinos and analyze whether or not it will be possible to detect these heavy Majorana neutrinos at the LHC.

3.1 Introduction.

Several models of neutrino mass have been suggested in the literature in which the neutrinos acquire masses through a seesaw [43] type mass texture, but the Majorana masses of the right-handed neutrinos are at the TeV scale instead of the GUT scale of $\sim 10^{16}$ GeV [5, 44, 45, 46, 47]. The smallness of the neutrino masses in those models is achieved either by the reduction of the rank of the mass matrix through a judicious choice of mass texture [5, 44], or by the suppression of the Dirac masses through an extended Higgs sector [45, 46, 47].

In such models, the heavy, mostly-right-handed mass eigenstates typically have masses of a few TeV, placing them within reach of the CERN Large Hadron Collider (LHC) or future e^+e^- linear colliders. If created, the particles will decay into a light neutrino+Higgs through the Yukawa interaction responsible for the Dirac masses, or into a light neutrino+ Z or a charged lepton+ W through the small admixture of the left-handed neutrino state. This last decay mode is particularly interesting since the decay products can be all visible. Of course, whether such a decay, and thus the particle, can be observed at colliders or not depends on whether the lifetime of the particle is short enough for it to decay inside the detector, and if that is the case, whether the width is small enough so that a narrow peak is discernible in the invariant mass of its decay products.

In this chapter, we calculate the lifetimes of the heavy, mostly-right-handed states of the model proposed by Okamura et al. in Ref. [5]. The original motivation of the model was to explain the NuTeV anomaly [1, 17], one possible solution of which requires largish mixing ($\theta^2 \sim 0.003$) between the light and heavy ($\gg M_Z$) neutrino states [6]. Denoting the left- and right-handed neutrino states

by ν and ξ , respectively, the Okamura texture is given by

$$\begin{bmatrix} \overline{\nu}_1^c & \overline{\nu}_2^c & \overline{\nu}_3^c & \overline{\xi}_1 & \overline{\xi}_2 & \overline{\xi}_3 \end{bmatrix} \begin{bmatrix} 0 & 0 & 0 & \alpha m & \beta m & \gamma m \\ 0 & 0 & 0 & \alpha m & \beta m & \gamma m \\ 0 & 0 & 0 & \alpha m & \beta m & \gamma m \\ \alpha m & \alpha m & \alpha m & \alpha M & 0 & 0 \\ \beta m & \beta m & \beta m & 0 & \beta M & 0 \\ \gamma m & \gamma m & \gamma m & 0 & 0 & \gamma M \end{bmatrix} \begin{bmatrix} \nu_1 \\ \nu_2 \\ \nu_3 \\ \xi_1^c \\ \xi_2^c \\ \xi_3^c \end{bmatrix}, \quad (3.1)$$

where the dimensionless parameters α , β , and γ are in general complex and assumed to satisfy the relation

$$\alpha + \beta + \gamma = 0. \quad (3.2)$$

This condition reduces the rank of the above mass matrix to three, leading automatically to three massless neutrino states. Though the actual light, mostly left-handed neutrino states in nature are not completely massless, this model suffices as a first approximation. We fix the normalization of the three complex parameters α , β , and γ to

$$|\alpha|^2 + |\beta|^2 + |\gamma|^2 = 3. \quad (3.3)$$

The dimensionful parameters m and M can be taken to be real and they set the scale of the Dirac and Majorana masses, respectively. The solution to the NuTeV anomaly requires their ratio to be [1, 5]

$$\frac{m}{M} \sim 0.03. \quad (3.4)$$

If the gauge singlet states ξ_i ($i = 1, 2, 3$) couple to other particles only through the Yukawa interactions which generate the Dirac submatrix of Eq. (3.1), then any permutation of the three complex parameters α , β and γ leads to the exact same model since we will have the freedom to relabel the three gauge singlet states without affecting any physics. In those cases, there exist a $3! = 6$ fold redundancy in the parameter space spanned by α , β , and γ . This will be assumed in the following.

If we set $M = 0$ in Eq. (3.1), we obtain

$$\begin{bmatrix} 0 & 0 & 0 & \alpha m & \beta m & \gamma m \\ 0 & 0 & 0 & \alpha m & \beta m & \gamma m \\ 0 & 0 & 0 & \alpha m & \beta m & \gamma m \\ \alpha m & \alpha m & \alpha m & 0 & 0 & 0 \\ \beta m & \beta m & \beta m & 0 & 0 & 0 \\ \gamma m & \gamma m & \gamma m & 0 & 0 & 0 \end{bmatrix} \quad (3.5)$$

which is manifestly rank 2. The non-zero eigenvalues of this matrix are¹

$$\pm m \sqrt{3(|\alpha|^2 + |\beta|^2 + |\gamma|^2)} = \pm 3m. \quad (3.6)$$

Therefore, this mass texture leads to four massless and two massive Majorana fermions. Pairing up the Majorana fermions with the same mass and opposite CP, we can reduce the set to one massive and two massless Dirac fermions [48]. If we assume that the up-type quarks share the same Dirac mass texture as the neutrinos, as would be the case in the Pati-Salam model [49], we obtain one

¹A factor of $\sqrt{3}$ is missing from Eq. (65) of Ref. [5].

massive quark which can be identified with the t , and two massless quarks which can be identified with the u and the c . To produce the t quark mass, we need

$$m \sim 60 \text{ GeV} , \quad (3.7)$$

which together with Eq. (3.4) implies

$$M \sim 2 \text{ TeV} . \quad (3.8)$$

Fixing m and M to these values, the parameter space of the Okamura model is given by the values of α , β , and γ which satisfy Eqs. (3.2) and (3.3).

In the following, we introduce a convenient graphical representation of the parameter space for the Okamura model, and calculate the masses and lifetimes of the three heavy mass eigenstates over it. We find that except for the vicinity of three isolated points at the ‘edge’ of the parameter space, the three masses are always in the TeV range, and the lifetimes are typically in the range of 10^{-26} to 10^{-24} seconds. In terms of the widths, these correspond to the range of $0.7 \sim 70$ GeV, which are fairly narrow compared to the masses.

3.2 The Parameter Space of the Okamura Model

We begin by noting that for the three complex parameters α , β , and γ to sum to zero, Eq. (3.2), they must form a closed triangle when summed tip-to-tail as vectors in the complex plane. Without loss of generality, we can set the phase of α to zero. This can always be achieved by changing the overall phase of α , β and γ , and does not affect any physical result. Therefore, the triangle formed by α , β , and γ can be assumed to have its base along the positive real axis. We define the ‘orientation’ of this triangle as the direction of the vectorial cross product $\alpha \times \beta$. If the orientation of the triangle is \odot (out of the complex plane), then β is in the upper complex plane while γ is in the lower complex plane. If the orientation of the triangle is \otimes (into the complex plane), then β is in the lower complex plane while γ is in the upper complex plane (see Fig. 3.1). Then, it is easy to see that specifying the lengths of the three sides $|\alpha|$, $|\beta|$, and $|\gamma|$, and the orientation of the triangle is equivalent to specifying the three complex numbers α , β , and γ .

Furthermore, we need not consider both orientations since the two cases can be transformed into each other by a simple interchange of the lengths of β and γ , and a relabeling of the singlet neutrino fields. As discussed previously, this does not affect any physical result either. Therefore, we will always take the triangle to be in the \odot orientation. This choice also reduces the redundancy of the parameter space from $3! = 6$ to 3 since we have used up the freedom to interchange β and γ to fix the orientation.

This consideration shows that specifying the three lengths $|\alpha|$, $|\beta|$, and $|\gamma|$ suffices to uniquely determine the Okamura texture, with cyclic permutations of the three lengths leading to the same model. (This residual redundancy comes from our freedom to choose which of the three lengths to call $|\alpha|$.) The question then, is, how can we specify those three lengths so they satisfy the normalization condition Eq. (3.3), and also the triangle inequalities:

$$|\beta| + |\gamma| \geq |\alpha| , \quad |\alpha| + |\beta| \geq |\gamma| , \quad |\alpha| + |\gamma| \geq |\beta| , \quad (3.9)$$

so they form a closed triangle? To this end, we utilize the fact that the sum of distances from any point inside a triangle to its three sides is constant: any point inside an equilateral triangle

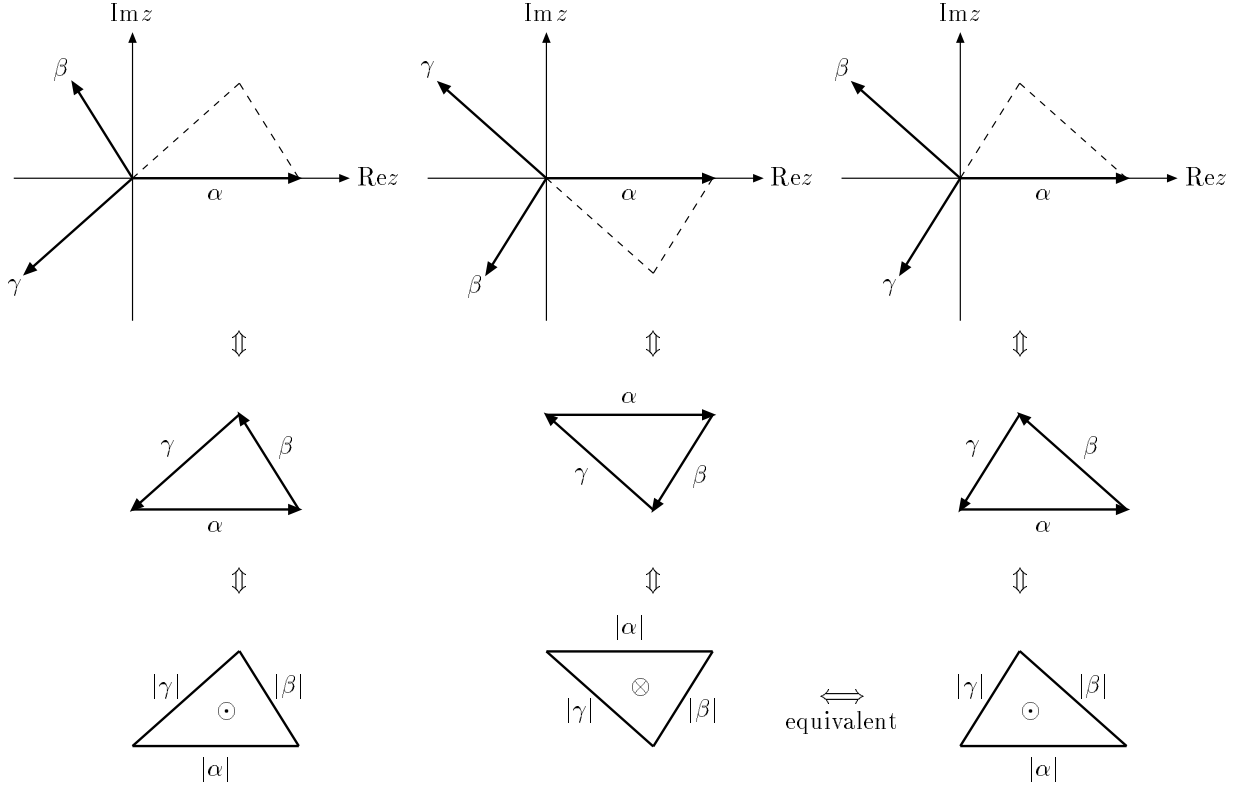


Figure 3.1: The three complex numbers α , β and γ satisfying $\alpha + \beta + \gamma = 0$ form a close triangle. For each choice of the three lengths $|\alpha|$, $|\beta|$, and $|\gamma|$, there are two possible orientations of the triangle (\odot and \otimes) which are related by complex conjugation (1st and 2nd columns). However, the \otimes case is equivalent to the \odot case with the lengths $|\beta|$ and $|\gamma|$ interchanged (2nd and 3rd columns).

of height three will have distances to the three sides which add up to three. If we identify these distances with $|\alpha|^2$, $|\beta|^2$, and $|\gamma|^2$, we can use the position of the point to specify the three lengths. Requiring the square-roots of these distances to satisfy the triangle inequality constrains the point to be inside a unit circle which inscribes the triangle. Therefore, for every point inside the unit circle, we can associate a corresponding parameter set for the Okamura texture (see Fig. 3.2).

If we specify the position of a point inside the unit circle with its polar coordinate (r, θ) , where $0 \leq r \leq 1$, $\theta \in [-\pi, \pi)$, the corresponding values of $|\alpha|$, $|\beta|$, and $|\gamma|$ are:

$$|\alpha| = \sqrt{1 + r \sin \theta}, \quad |\beta| = \sqrt{1 + r \sin \left(\theta - \frac{2\pi}{3} \right)}, \quad |\gamma| = \sqrt{1 + r \sin \left(\theta + \frac{2\pi}{3} \right)}. \quad (3.10)$$

The phases of the three numbers are:

$$\begin{aligned} \arg \alpha &= 0, \\ \arg \beta &= \pi - \cos^{-1} \frac{1/2 + r \sin(\theta - \pi/3)}{\sqrt{[1 + r \sin \theta][1 + r \sin(\theta - 2\pi/3)]}}, \\ \arg \gamma &= -\pi + \cos^{-1} \frac{1/2 + r \sin(\theta + \pi/3)}{\sqrt{[1 + r \sin \theta][1 + r \sin(\theta + 2\pi/3)]}}. \end{aligned} \quad (3.11)$$

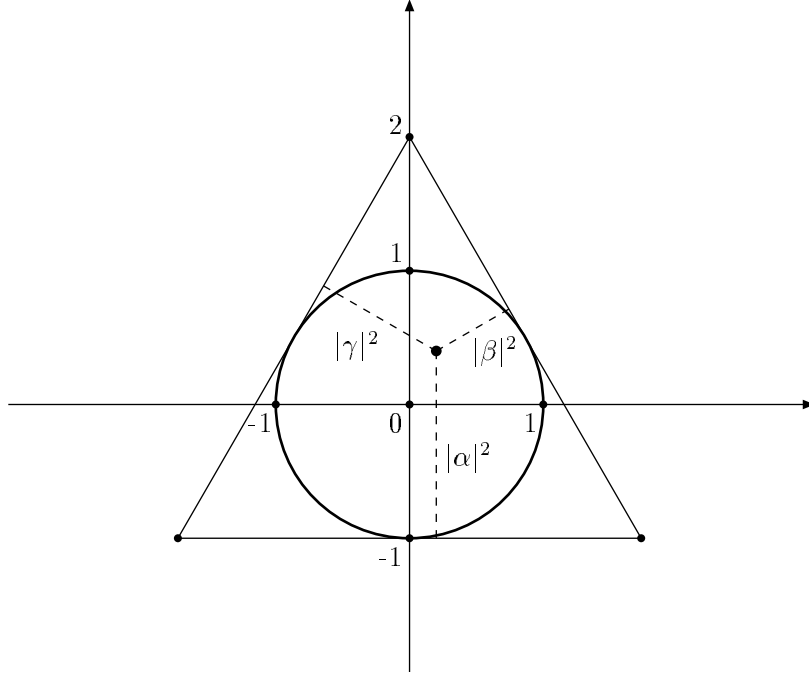


Figure 3.2: The distances from any point inside an equilateral triangle of height three to its three sides add up to three. We can use these distances to specify $|\alpha|^2$, $|\beta|^2$, and $|\gamma|^2$. The triangle inequality is satisfied for points inside the unit circle which inscribes the triangle.

In Fig. 3.3, we plot the dependence of $\arg \beta$ and $\arg \gamma$ on the position of the point inside the unit circle.

A cyclic permutation of α , β , and γ which leaves the physics invariant up to an overall phase corresponds to the transformation $\theta \rightarrow \theta + 2\pi/3$ (120° rotations). This means that we expect the same symmetry to be present in the mass spectrum and the values of heavy neutrino decay widths and lifetimes. This can be used as a useful check of our calculations.

3.3 The Lagrangian

To calculate the lifetimes of the heavy neutral states, we must first specify their interactions. We denote the left-handed charged lepton fields with ℓ , and the left- and right-handed neutrino fields with ν and ξ , respectively:

$$\ell = \begin{bmatrix} \ell_1 \\ \ell_2 \\ \ell_3 \end{bmatrix}, \quad \nu = \begin{bmatrix} \nu_1 \\ \nu_2 \\ \nu_3 \end{bmatrix}, \quad \xi = \begin{bmatrix} \xi_1 \\ \xi_2 \\ \xi_3 \end{bmatrix}. \quad (3.12)$$

The right-handed neutrino fields, ξ_i ($i = 1, 2, 3$), are gauge singlets. The components of the Higgs doublet are denoted

$$H = \begin{bmatrix} \phi^+ \\ \phi_0 \end{bmatrix}. \quad (3.13)$$

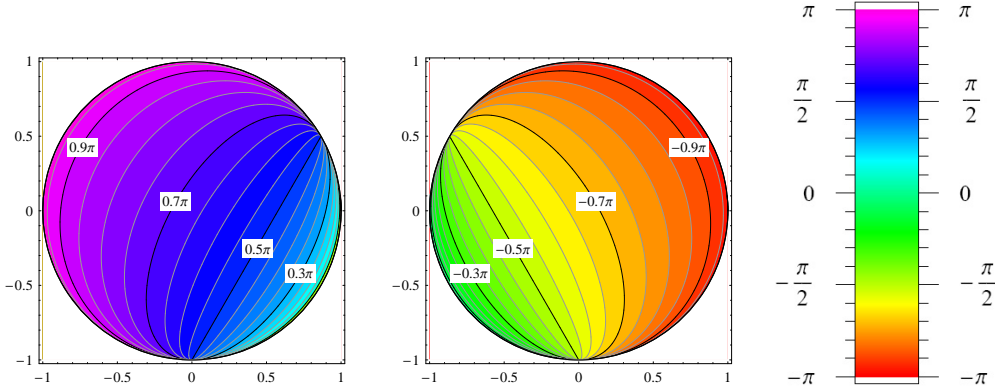


Figure 3.3: Contour lines and density plots for $\arg \beta$ (left) and $\arg \gamma$ (middle). The distances between two consecutive equipotential lines are $\Delta \arg \beta = \Delta \arg \gamma = 0.05\pi$. The color scheme is shown on the right.

Then, the Lagrangian which governs the interaction of the neutrinos is

$$\mathcal{L} = \mathcal{L}_{W,Z} + \mathcal{L}_H + \mathcal{L}_M , \quad (3.14)$$

where

$$\begin{aligned} \mathcal{L}_{W,Z} &= \frac{g}{\sqrt{2}} (\bar{\ell} \gamma^\mu \nu) W_\mu^- + \frac{g}{\sqrt{2}} (\bar{\nu} \gamma^\mu \ell) W_\mu^+ + \frac{g}{2 \cos \theta_W} (\bar{\nu} \gamma^\mu \nu) Z_\mu , \\ \mathcal{L}_H &= -\bar{\xi} \lambda (\phi^0 \nu - \phi^+ \ell) + h.c. , \\ \mathcal{L}_M &= -\frac{1}{2} \bar{\xi} \mathcal{M} \xi^c + h.c. . \end{aligned} \quad (3.15)$$

We neglect the Yukawa interactions which give rise to the charged lepton masses: the charged leptons are treated as massless as well as the light neutrino states. In the Okamura model, the Yukawa matrix λ and the Majorana mass matrix \mathcal{M} are given by

$$\lambda = \frac{\sqrt{2}m}{v} \begin{bmatrix} \alpha & \alpha & \alpha \\ \beta & \beta & \beta \\ \gamma & \gamma & \gamma \end{bmatrix} , \quad \mathcal{M} = M \begin{bmatrix} \alpha & 0 & 0 \\ 0 & \beta & 0 \\ 0 & 0 & \gamma \end{bmatrix} . \quad (3.16)$$

After the neutral Higgs develops a VEV,

$$\langle \phi^0 \rangle = \langle \phi^{0*} \rangle = \frac{v}{\sqrt{2}} , \quad (3.17)$$

the Yukawa matrix λ leads to the Dirac mass matrix of the neutrinos:

$$\mathcal{D} = \frac{v}{\sqrt{2}} \lambda = m \begin{bmatrix} \alpha & \alpha & \alpha \\ \beta & \beta & \beta \\ \gamma & \gamma & \gamma \end{bmatrix} . \quad (3.18)$$

The Goldstone bosons are absorbed into the W and the Z , $\phi^0 \rightarrow 1/\sqrt{2}(h + v)$ as usual, and the resulting Lagrangian is:

$$\mathcal{L} = \frac{g}{\sqrt{2}} (\bar{\ell} \gamma^\mu \nu) W_\mu^- + \frac{g}{\sqrt{2}} (\bar{\nu} \gamma^\mu \ell) W_\mu^+ + \frac{g}{2 \cos \theta_W} (\bar{\nu} \gamma^\mu \nu) Z_\mu$$

$$-\bar{\xi} \mathcal{D} \nu - \frac{1}{\sqrt{2}} (\bar{\xi} \lambda \nu) h - \frac{1}{2} \bar{\xi} \mathcal{M} \xi^c + h.c. \quad (3.19)$$

The neutrino mass terms can be written as

$$\begin{aligned} & \bar{\xi} \mathcal{D} \nu + \frac{1}{2} \bar{\xi} \mathcal{M} \xi^c + h.c. \\ &= \frac{1}{2} (\bar{\xi} \mathcal{D} \nu + \bar{\nu}^c \mathcal{D}^T \xi^c + \bar{\xi} \mathcal{M} \xi^c) + h.c. \\ &= \frac{1}{2} \begin{bmatrix} \bar{\nu}^c & \bar{\xi} \end{bmatrix} \begin{bmatrix} 0 & \mathcal{D}^T \\ \mathcal{D} & \mathcal{M} \end{bmatrix} \begin{bmatrix} \nu \\ \xi^c \end{bmatrix} + h.c. \end{aligned} \quad (3.20)$$

This mass matrix is diagonalized with a unitary transformation involving the ν and ξ^c fields:

$$\begin{bmatrix} \nu \\ \xi^c \end{bmatrix} = U \begin{bmatrix} \eta \\ \chi \end{bmatrix}, \quad (3.21)$$

so that

$$\begin{bmatrix} \bar{\nu}^c & \bar{\xi} \end{bmatrix} \begin{bmatrix} 0 & \mathcal{D}^T \\ \mathcal{D} & \mathcal{M} \end{bmatrix} \begin{bmatrix} \nu \\ \xi^c \end{bmatrix} = \begin{bmatrix} \bar{\eta}^c & \bar{\chi}^c \end{bmatrix} U^T \begin{bmatrix} 0 & \mathcal{D}^T \\ \mathcal{D} & \mathcal{M} \end{bmatrix} U \begin{bmatrix} \eta \\ \chi \end{bmatrix} = \begin{bmatrix} \bar{\eta}^c & \bar{\chi}^c \end{bmatrix} M_{\text{diag}} \begin{bmatrix} \eta \\ \chi \end{bmatrix}, \quad (3.22)$$

with $M_{\text{diag}} = \text{diag}(0, 0, 0, M_1, M_2, M_3)$. The η and χ fields are the left-handed mass eigenfields with η being the light (massless) states, and χ being the heavy states. Decomposing the 6×6 matrix U into four 3×3 matrices as

$$U = \begin{bmatrix} U_{\nu\eta} & U_{\nu\chi} \\ U_{\xi\eta} & U_{\xi\chi} \end{bmatrix}, \quad (3.23)$$

we can write

$$\begin{aligned} \nu &= U_{\nu\eta} \eta + U_{\nu\chi} \chi, \\ \xi &= U_{\xi\eta}^* \eta^c + U_{\xi\chi}^* \chi^c, \end{aligned} \quad (3.24)$$

(Because the η fields are exactly massless and degenerate in our model, the matrices $U_{\nu\eta}$ and $U_{\xi\eta}$ are not uniquely determined. However, this does not affect our final results. Note also, that though U is unitary, its four 3×3 submatrices are non-unitary in general.) The relevant interaction terms in the Lagrangian involving the χ fields are then:

$$\begin{aligned} \frac{g}{2 \cos \theta_W} (\bar{\nu} \gamma^\mu \nu) Z_\mu &\rightarrow \frac{g}{2 \cos \theta_W} \left[\bar{\eta} (U_{\nu\eta}^\dagger U_{\nu\chi}) \gamma^\mu \chi + \bar{\chi} (U_{\nu\chi}^\dagger U_{\nu\eta}) \gamma^\mu \eta \right] Z_\mu, \\ \frac{g}{\sqrt{2}} (\bar{\ell} \gamma^\mu \nu) W_\mu^- &\rightarrow \frac{g}{\sqrt{2}} (\bar{\ell} U_{\nu\chi} \gamma^\mu \chi) W_\mu^-, \\ \frac{1}{\sqrt{2}} (\bar{\xi} \lambda \nu) h &\rightarrow \frac{1}{\sqrt{2}} \left[\bar{\eta}^c (U_{\xi\eta}^T \lambda U_{\nu\chi}) \chi + \bar{\chi}^c (U_{\xi\chi}^T \lambda U_{\nu\eta}) \eta \right] h, \end{aligned} \quad (3.25)$$

plus the Hermitian conjugates of the later two lines. Introducing the Majorana fields

$$n = \eta + \eta^c, \quad N = \chi + \chi^c, \quad (3.26)$$

(note that these fields do not have definite lepton number) we can write

$$\eta = P_L n, \quad \eta^c = P_R n, \quad \chi = P_L N, \quad \chi^c = P_R N, \quad (3.27)$$

and the relevant interaction Lagrangian in terms of these fields becomes

$$\begin{aligned} \mathcal{L} = & \frac{g}{2 \cos \theta_W} \left[\bar{n} (A \gamma^\mu P_L - A^* \gamma^\mu P_R) N \right] Z_\mu \\ & + \frac{g}{\sqrt{2}} (\bar{\ell} B \gamma^\mu P_L N) W_\mu^- - \frac{g}{\sqrt{2}} (\bar{\ell}^c B^* \gamma^\mu P_R N) W_\mu^+ \\ & - \bar{n} (C h P_L + C^* \tilde{h} P_R) N, \end{aligned} \quad (3.28)$$

where

$$A \equiv U_{\nu\eta}^\dagger U_{\nu\chi}, \quad B \equiv U_{\nu\chi}, \quad C \equiv \frac{1}{\sqrt{2}} (U_{\nu\eta}^T \lambda^T U_{\xi\chi} + U_{\xi\eta}^T \lambda U_{\nu\chi}). \quad (3.29)$$

We have used the generic relations [50]

$$\bar{\psi}_1 O P_{R,L} \psi_2 = \bar{\psi}_2^c O^T P_{R,L} \psi_1^c, \quad \bar{\psi}_1 O \gamma^\mu P_{R,L} \psi_2 = -\bar{\psi}_2^c O^T \gamma^\mu P_{L,R} \psi_1^c, \quad (3.30)$$

(O is a matrix which carries flavor indices only), and the fact that $n^c = n$ and $N^c = N$ by construction, to rearrange the terms in Eq. (3.28) in such a way that all the N -fields stand at the rightmost position of each term to facilitate the extraction of the N -decay matrix elements.

3.4 Lifetimes

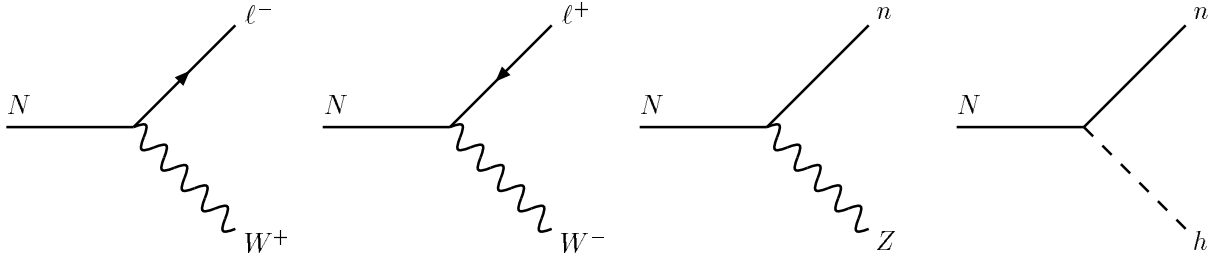


Figure 3.4: The 2-body decay processes of the heavy neutrino N .

From Eq. (3.28), we can immediately derive the amplitudes for the two-body decay processes of the heavy neutrinos, N_i ($i = 1, 2, 3$), shown in Fig. 3.4. If the N_i were lighter than the W , Z , or h , then we will need to consider three-body decay processes mediated by these particles, but it turns out that except for small neighborhoods around isolated points in the parameter space of the model, they are always heavier. It therefore suffices to consider only the two-body decay modes.

Now, straightforward calculations allow us to write down the partial decay widths for each channel of decay (the indices i and j below run from 1 to 3):

$$\begin{aligned} \Gamma(N_i \rightarrow n_j Z) &= \frac{\sqrt{2} G_F |A^{ji}|^2}{16\pi} M_i^3 \left(1 - \frac{M_Z^2}{M_i^2}\right)^2 \left(1 + 2 \frac{M_Z^2}{M_i^2}\right), \\ \Gamma(N_i \rightarrow \ell_j^+ W^-) = \Gamma(N_i \rightarrow \ell_j^- W^+) &= \frac{\sqrt{2} G_F |B^{ji}|^2}{16\pi} M_i^3 \left(1 - \frac{M_W^2}{M_i^2}\right)^2 \left(1 + 2 \frac{M_W^2}{M_i^2}\right), \end{aligned}$$

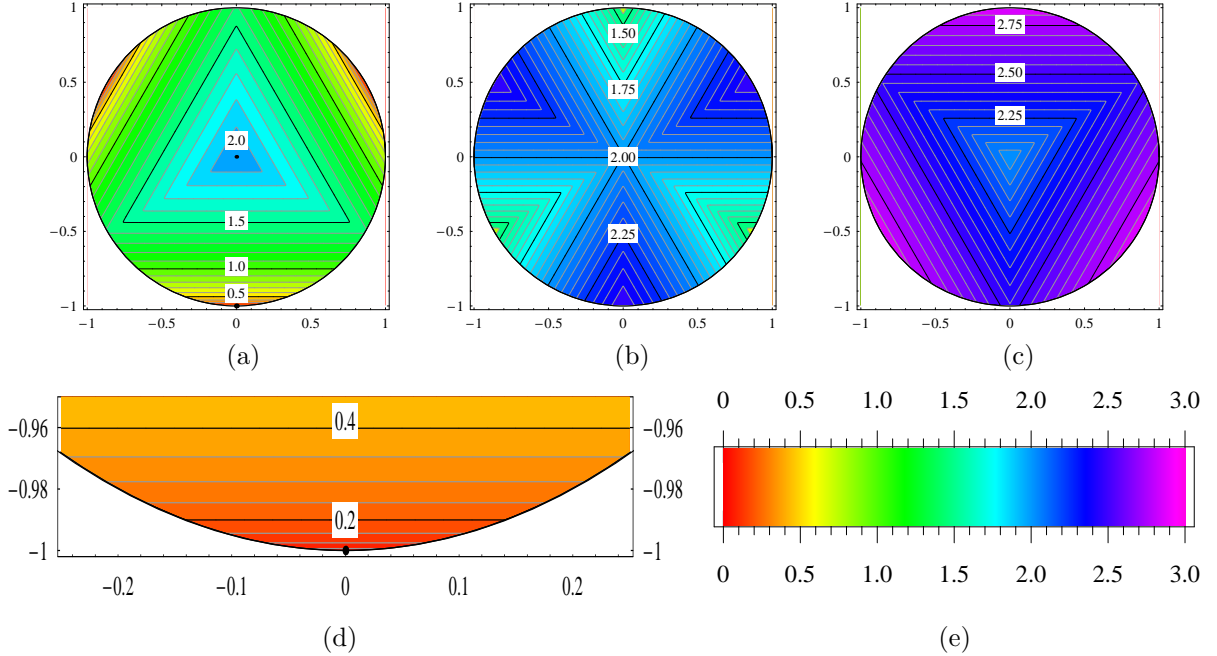


Figure 3.5: (a), (b), (c) density and contour plots for masses M_1 , M_2 , and M_3 of the lightest N_1 , medium heavy N_2 and heaviest N_3 heavy neutrino respectively (TeV). The distances between two consecutive equipotential lines are $\Delta M_1 = 0.1$ TeV, $\Delta M_2 = \Delta M_3 = 0.05$ TeV; (d) the vicinity of the point where M_1 approaches zero ($r = 1$, $\theta = -\pi/2$); $\Delta M_1 = 0.025$ TeV; (e) mass color coding.

$$\Gamma(N_i \rightarrow n_j h) = \frac{|C^{ji}|^2}{16\pi} M_i \left(1 - \frac{m_h^2}{M_i^2}\right)^2, \quad (3.31)$$

where M_Z , M_W , and m_h are the masses of the Z boson, W boson, and Higgs, respectively. The first two lines can be compared with the results of Djouadi in Ref. [51]. We give a detailed derivation of these formulas in Appendix D.

At first sight, these expressions may seem to imply that the $N \rightarrow nh$ channel is suppressed with respect to the other two since its partial width grows linearly with the mass M_i , while for the $N \rightarrow nZ$ and $N \rightarrow \ell W$ channels the widths grow as M_i^3 . However, the interactions of the heavy Majorana neutrino N with the gauge bosons are suppressed because only a small fraction of N is the left-handed neutrino ν . Since most of N is the right-handed neutrino ξ , no such suppression exists for its interaction with the Higgs h . Numerically, it turns out that all three channels of decay must be taken into account.

3.5 Results

Now we have everything at hand to calculate the lifetimes of the heavy neutrinos in the Okamura model. The parameter space of the model is represented by the interior of a unit circle as discussed in section 3.2. For each point inside the unit circle, we can calculate the Okamura texture using Eqs. (3.1), (3.7), (3.8), (3.10), and (3.11), diagonalize it to obtain the masses and mixings [52], and calculate the decay widths and lifetimes of the heavy neutrinos using Eq. (3.31). As the Higgs

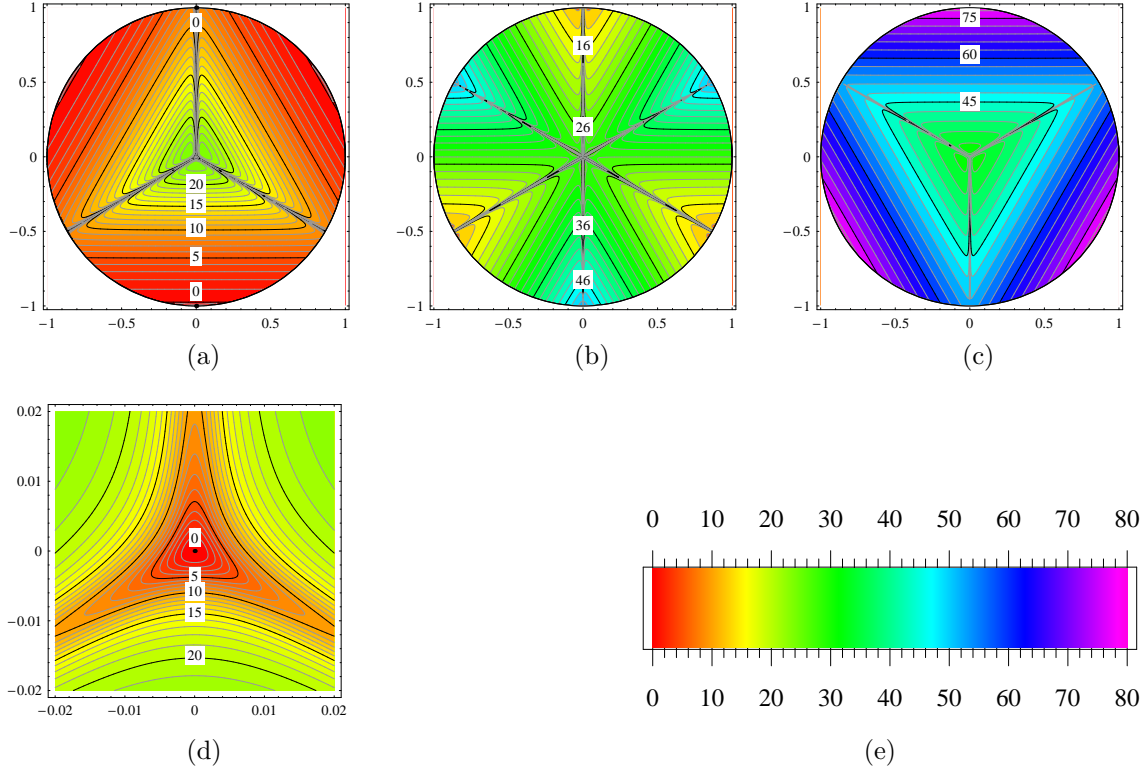


Figure 3.6: (a), (b), (c) density and contour plots for widths Γ_1 , Γ_2 , and Γ_3 of the lightest N_1 , medium heavy N_2 and heaviest N_3 heavy neutrino respectively (GeV). The distances between two consecutive equipotential lines are $\Delta\Gamma_1 = 1$ GeV, $\Delta\Gamma_2 = 2$ GeV, $\Delta\Gamma_3 = 3$ GeV; (d) the detailed picture of the central part of Γ_1 ; $\Delta\Gamma_1 = 1$ GeV; (e) width color coding.

mass, we take $m_H = 200$ GeV. (The choice of the Higgs mass has little effect on our result as long as $m_H \ll M_i$.)

The resulting contour and density plots for masses, decay widths, and lifetimes of the heavy neutrinos N_1 , N_2 and N_3 are presented in Figs. 3.5–3.7. First, note that the graphs are symmetric under rotations by multiples of $2\pi/3$ as anticipated in section 3.2. Next, from Fig. 3.5, we can easily see that the values of the heavy neutrino masses are larger than the W , Z , or Higgs thresholds for most of the parameter space, justifying our use of two-body decay amplitudes. The mass of N_1 becomes smaller than these thresholds only in the vicinity of three isolated points at $r = 1$, $\theta = -\pi/2 + 2\pi k/3$ ($k = 0, 1, 2$), as illustrated in Fig. 3.5d. As was shown in Ref. [5], at these three points one of the N -fields is completely massless while the other two have degenerate mass. The lightest N particle is completely stable at these points with zero decay width and infinite lifetime. However, the existence of such a light (less than W and Z thresholds) N particle is already ruled out experimentally by L3 [53] so we need not consider these points further.

It was also shown in Ref. [5] that at the center of the circle one heavy neutrino completely decouples from the light neutrino states (and therefore from the rest of the Standard Model particles) while the other two heavy states have degenerate masses. This decoupling can be seen in Fig. 3.6d and Fig. 3.7d where at the center of the circle the decay width of the lightest heavy neutrino is zero and the lifetime is infinite. A similar decoupling occurs at the points where $r = 1$

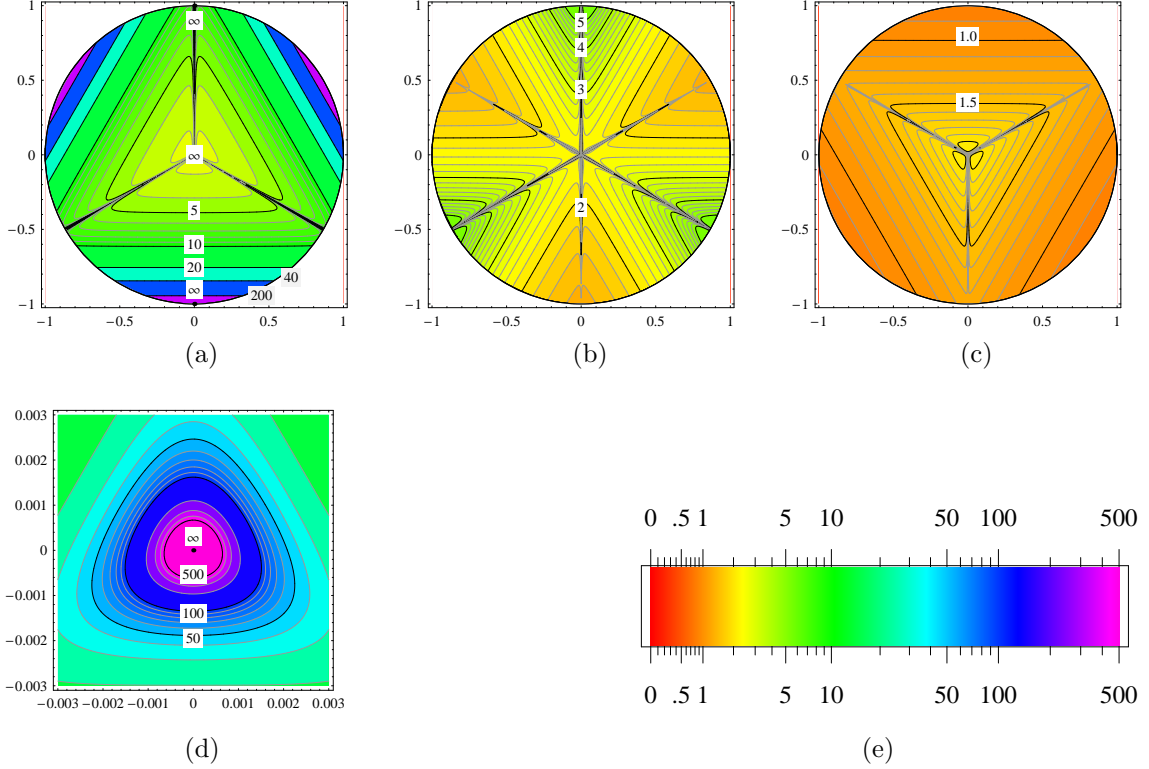


Figure 3.7: (a), (b), (c) density and contour plots for lifetimes τ_1 , τ_2 , and τ_3 of the lightest N_1 , medium heavy N_2 and heaviest N_3 heavy neutrino respectively (10^{-26} sec). The distances between two consecutive equipotential lines are $\Delta\tau_1 = 1 \times 10^{-26}$ sec for $\tau_1 < 10 \times 10^{-26}$ sec and for $\tau_1 > 10 \times 10^{-26}$ sec equipotential lines corresponding to $\tau_1 = 20 \times 10^{-26}$, 40×10^{-26} and 200×10^{-26} sec are presented, $\Delta\tau_2 = 0.2 \times 10^{-26}$ sec, $\Delta\tau_3 = 0.1 \times 10^{-26}$ sec; (d) the detailed picture of the central part of τ_1 ; $\Delta\tau_1 = 10 \times 10^{-26}$ sec for $\tau_1 < 100 \times 10^{-26}$ sec and $\Delta\tau_1 = 100 \times 10^{-26}$ sec for $\tau_1 > 100 \times 10^{-26}$ sec; (e) lifetime color coding.

and $\theta = -5\pi/6 + 2\pi k/3$, $k = 0, 1, 2$.

Except for the vicinity of these points, the lifetimes of the N particles are typically in the range of 10^{-26} to 10^{-24} seconds (see Fig. 3.7). Assuming that the particles are non-relativistic, the maximum distance they can travel from their production points before decay is in the range of 10^{-17} to 10^{-15} meters. If produced at colliders, they will decay inside the detector. On the other hand, the width-to-mass ratios of the particles are in the range of 0.1 to 3 percent as shown in Fig. 3.8. Therefore, the invariant mass spectrum of the decay products can be expected to show a very narrow peak.

3.6 Observability at the LHC

In this section we consider the prospects of discovery of the heavy Majorana neutrinos at the LHC. This question has attracted ever-increasing attention over the past decades and was extensively discussed in the literature by many authors [54, 56, 57, 58, 59, 60]. The unambiguous proof of the existence of a Majorana neutrino would be an observation of a lepton number violating process.

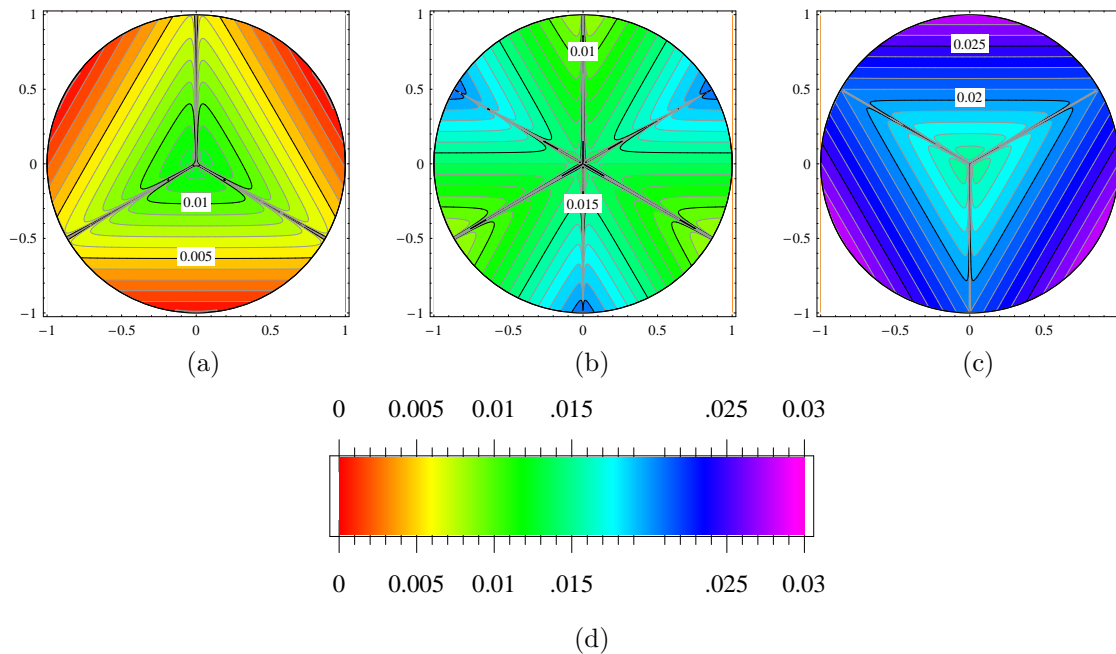


Figure 3.8: (a), (b), (c) density and contour plots for the widths-to-mass ratios of the lightest N_1 , medium heavy N_2 and heaviest N_3 heavy neutrinos respectively. The distances between two consecutive equipotential lines is 0.001 for all plots; (d) mass-to-width ratio color coding.

For example, in Ref. [54], Dicus, Karatas, and Roy consider the production of like-sign electrons, a lepton number violating process, as the signature of the heavy mostly-right-handed Majorana neutrino N : this can occur through the t - and u -channel exchange of N between two like-sign W 's radiated from the protons as shown in Fig. 3.9). Dicus, Karatas, and Roy estimated the cross-section of this process to be in the range of 0.01 to 0.03 fb for the neutrissimo mass from 150 to 2000 GeV. This corresponds to the event rate of 1 to 3 events per year for the LHC luminosity of $100 \text{ fb}^{-1}/\text{year}$. They used the following value of the mixing matrix element defined by Eq. (3.29):

$$|B_{11}|^2 = 0.043. \quad (3.32)$$

The typical value of $|B_{11}|^2$ calculated for the Okamura model is around 0.001 and it stays practically constant for the entire parameter space. We observe that this value is more than one order of magnitude smaller than that given by Eq. (3.32). This means that the corresponding cross-section and event rate for the Okamura model are more than two orders of magnitude smaller than that obtained by Dicus, Karatas, and Roy. The number of expected events at the LHC is extremely small, of order 10^{-2} per year, which makes it impossible to discover the neutrissimo at the LHC through this process. Thus, though we have found that the heavy neutral particles in the Okamura model have lifetimes in the range that allows for their observation at colliders, the analysis by Dicus, Karatas, and Roy suggests that they are impossible to observe at the LHC through the process we just considered.

In principle, the neutrissimo can be looked for in another process at the LHC. For instance, it can be produced in resonance through the process shown in Fig. 3.10 if it is kinematically accessible, i.e. if the neutrissimo mass is smaller than \sqrt{s} . The resonant production will have a substantially

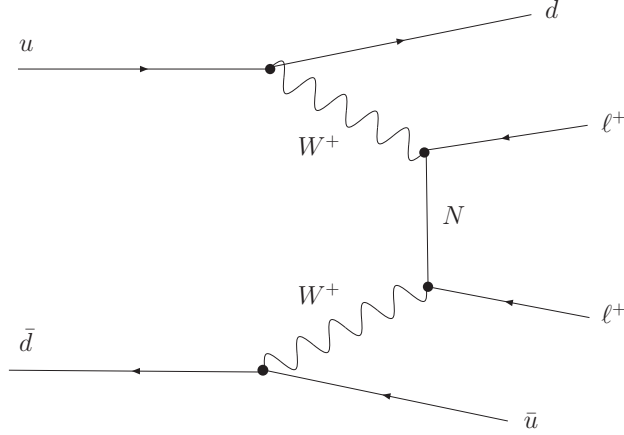


Figure 3.9: Feynman diagrams for $\Delta L = 2$ processes induced by a t-channel Majorana neutrino N in $q\bar{q}'$ collisions.

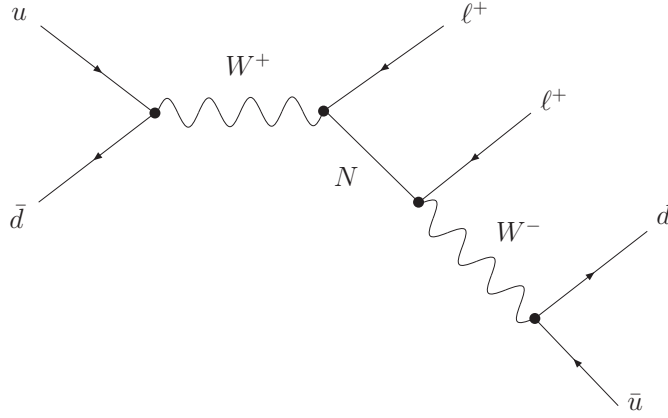


Figure 3.10: Feynman diagrams for $\Delta L = 2$ processes induced by an s-channel Majorana neutrino N in $q\bar{q}'$ collisions.

enhanced event rate [56, 57, 58, 59, 60]. In addition, it was suggested by Han and Zhang in Ref. [59] to look for like-sign dimuons $\mu^\pm\mu^\pm$, easier for detection than electrons in hadronic collisions, as the best signature for a heavy Majorana neutrino at both Tevatron and LHC energies. The final state W boson decays hadronically and there is no neutrino involved in the final state. This allows for the unambiguous identification of $\Delta L = 2$ processes. Han and Zhang approximate the signal cross-section as

$$\sigma(p\bar{p} \rightarrow \mu^\pm\mu^\pm W^\pm) \approx \sigma(p\bar{p} \rightarrow \mu^\pm N)B(N \rightarrow \mu^\pm W^\pm) \equiv S_{\mu\mu}\sigma_0, \quad (3.33)$$

where $S_{\mu\mu}$ is the “effective mixing parameter” of N with muons, defined in our notation as

$$S_{\mu\mu} = \frac{|B_{21}|^4}{\sum_{i=1}^3 |B_{i1}|^2}, \quad (3.34)$$

and σ_0 is a “bare cross-section”, essentially independent of the mixing parameters when the heavy neutrino decay width is narrow.

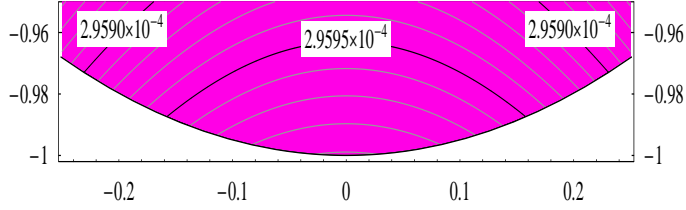


Figure 3.11: The value of the $S_{\mu\mu}$ parameter for the region of the parameter space where the mass of N_1 is smaller than 400 GeV.

Figs. 4a and 4b in the paper by Han and Zhang [59] illustrate the result they obtain. Fig. 4a shows the bare cross-section σ_0 as a function of the neutrino mass and Fig. 4b shows the graph corresponding to the 2σ upper bound that the LHC will be able to place on the values of the parameter $S_{\mu\mu}$ and neutrino mass. The region of the $(S_{\mu\mu}, m_N)$ parameter space² above the bound will be excluded if the LHC does not find the neutrinos.

If we fix the value of $S_{\mu\mu}$ then from Fig. 4b of Han and Zhang's paper we can obtain the value of mass that saturates the bound and using Fig. 4a we can find the value of the bare cross-section σ_0 that corresponds to this mass. Then, using Eq. (3.33) we can calculate the cross-section of the process corresponding to the chosen value of mixing and the value of the mass saturating the bound. Multiplying this cross-section by an integrated luminosity of the LHC we can convert it to the expected number of events. Han and Zhang find that for the integrated luminosity of $100 \text{ fb}^{-1}/\text{year}$ the heavy Majorana neutrino mass range with significant detection sensitivity, that is, the expected number of events if at least $1 \sim 10$ events per year, is from 10 to 400 GeV. Our Fig. 3.5 shows that only the N_1 neutrino has a region of the parameter space corresponding to such a low value of mass. This region is shown in Fig. 3.5d. Thus, we only consider N_1 contribution in Eq. (3.34).

In order to apply the result of Han and Zhang to the Okamura model, we need to know the value of the effective mixing parameter $S_{\mu\mu}$ in this model. Fig. 3.11 shows the density plot for the value of $S_{\mu\mu}$ in the Okamura model. We see that $S_{\mu\mu}$ stays practically constant in the region of interest and has the value of about 2×10^{-4} . Fig. 4b from Han and Zhang's paper shows that for this value of the effective mixing parameter the LHC will only be able to constrain the mass of the N_1 to about 150 GeV level. Thus, we conclude that it will not be possible to detect the neutrino of the Okamura model at the LHC unless its mass is smaller than about 150 GeV. Such a small value of mass corresponds to a very small region close to the edge of the parameter space of the Okamura model.

This result might seem to be discouraging but we want to point out that the neutrinos can be looked for in other experiments. In addition to the searches at hadronic colliders, we can also search for the neutrino in the e^-p scattering, e^+e^- annihilation processes, and $e^-\gamma$ collisions. For a recent review see Ref. [60]. Another place where we can look for the signatures of the neutrinos is the high statistics neutrino experiments which provide us with a unique opportunity to probe the neutrino sector of the SM at a high level of precision. In the next chapter we give an example of such an experiment, called NuSONG.

Finally, if the gauge group is extended to $SU(2)_L \times SU(2)_R \times U(1)_{B-L}$, then the N 's can be

² m_N stands for the neutrino mass as in the Han and Zhang's paper.

copiously produced through the W_R and Z' , as discussed in Refs. [62, 63, 64]. The question of whether the Okamura texture can be embedded into such a gauge structure will be left to future work.

This page left blank intentionally.

Chapter 4

NuSO_nG

In this chapter we give an example of an experiment which can be carried out in the future and discuss what we can learn about possible extensions of the SM which this experiment will be able to probe.

4.1 Introduction

NuSO_nG (Neutrino Scattering On Glass) is a fixed target muon neutrino scattering experiment which is currently being planned at the Fermi National Acceleration Laboratory [55, 8]. If approved, it will repeat the NuTeV measurements of the quark-muon (anti-)neutrino scattering to acquire two orders of magnitude improved statistics and, as a result, NuSO_nG is projected to halve the experimental error on g_L^2 and g_R^2 as compared to NuTeV. NuSO_nG will also measure the muon neutrino-electron elastic scattering (ES) cross section $\sigma(\nu_\mu + e^- \rightarrow \nu_\mu + e^-)$ to an accuracy of 0.7% using inverse muon beta decay (IMB) $\sigma(\nu_\mu + e^- \rightarrow \nu_e + \mu^-)$ to normalize the neutrino flux.

NuSO_nG will be sensitive to new physics that modifies neutrino-quark and neutrino-electron scattering. In this chapter, we analyze this possibility. First, we explain our assumptions about NuSO_nG. Then we parametrize possible new physics scenarios in terms of Non-Standard Interactions (NSI) of the neutrinos and investigate the bounds that the NuSO_nG experiment will be capable of imposing on the parameters of NSI. In another type of new physics scenario which NuSO_nG will be able to probe, the neutrinos mix with gauge sterile states. This mixing occurs naturally in the neutrissimo models discussed in Chapter 3 and it leads to a suppression of the neutrino-gauge coupling. Thus we also derive NuSO_nG bounds on neutrino mixing parameters in this type of new physics scenario. Finally, we consider a list of concrete models that NuSO_nG will be able to constrain and derive the NuSO_nG bounds on mass-to-coupling ratios in these models. The list of models we consider includes generation distinguishing Z' models, extended Higgs models, R -parity violating SUSY and generation non-diagonal leptoquarks¹.

¹We want to point out that our analysis of the NuSO_nG capabilities is still on-going and we might be able to say more in the future.

4.1.1 Assumptions on $\nu_\mu e$ and $\bar{\nu}_\mu e$ ES

NuSOng expects about 75k $\nu_\mu e$ ES events, and about 7k $\bar{\nu}_\mu e$ ES events. The statistical errors in each are therefore

$$\frac{1}{\sqrt{75000}} = 0.4\%, \quad \frac{1}{\sqrt{7000}} = 1.2\%. \quad (4.1)$$

Preliminary Monte Carlo studies suggest that the systematic error of the measurement will be about 0.6% [8]. Adding this error to the above in quadrature, we find

$$\begin{aligned} \sqrt{(0.004)^2 + (0.006)^2} &= 0.007, \\ \sqrt{(0.012)^2 + (0.006)^2} &= 0.013. \end{aligned} \quad (4.2)$$

So we are going to assume that NuSOng will measure $\sigma(\nu_\mu e)$ to a precision of 0.7%, and $\sigma(\bar{\nu}_\mu e)$ to 1.3%. That is:

$$\begin{aligned} \epsilon_{\nu e} &\equiv \frac{\Delta\sigma_{\nu e}}{\sigma_{\nu e}} = \pm 0.007, \\ \epsilon_{\bar{\nu} e} &\equiv \frac{\Delta\sigma_{\bar{\nu} e}}{\sigma_{\bar{\nu} e}} = \pm 0.013. \end{aligned} \quad (4.3)$$

We will neglect any correlations between the two (though part of the systematic errors are probably correlated). For the sake of comparison with New Physics models, it is convenient to recast this into limits on the coupling constants. This requires some preparation:

The differential cross sections are given by:

$$\begin{aligned} d\sigma(\nu_\mu e) &= \frac{G_F^2 m_e E_\nu}{2\pi} \left[(g_V^{\nu e} + g_A^{\nu e})^2 \frac{dT}{E_\nu} + (g_V^{\nu e} - g_A^{\nu e})^2 \left(1 - \frac{T}{E_\nu}\right)^2 \frac{dT}{E_\nu} \right] \\ &= \frac{2G_F^2 m_e E_\nu}{\pi} \left[(g_L^{\nu e})^2 \frac{dT}{E_\nu} + (g_R^{\nu e})^2 \left(1 - \frac{T}{E_\nu}\right)^2 \frac{dT}{E_\nu} \right], \\ d\sigma(\bar{\nu}_\mu e) &= \frac{G_F^2 m_e E_\nu}{2\pi} \left[(g_V^{\nu e} - g_A^{\nu e})^2 \frac{dT}{E_\nu} + (g_V^{\nu e} + g_A^{\nu e})^2 \left(1 - \frac{T}{E_\nu}\right)^2 \frac{dT}{E_\nu} \right] \\ &= \frac{2G_F^2 m_e E_\nu}{\pi} \left[(g_R^{\nu e})^2 \frac{dT}{E_\nu} + (g_L^{\nu e})^2 \left(1 - \frac{T}{E_\nu}\right)^2 \frac{dT}{E_\nu} \right], \end{aligned} \quad (4.4)$$

where T is the kinetic energy of the recoil electron and E_ν is the neutrino energy. If we introduce the variable $y = T/E_\nu$, then

$$\begin{aligned} \frac{d\sigma(\nu_\mu e)}{dy} &= \frac{G_F^2 m_e E_\nu}{2\pi} \left[(g_V^{\nu e} + g_A^{\nu e})^2 + (g_V^{\nu e} - g_A^{\nu e})^2 (1 - y)^2 \right] \\ &= \frac{2G_F^2 m_e E_\nu}{\pi} \left[(g_L^{\nu e})^2 + (g_R^{\nu e})^2 (1 - y)^2 \right], \\ \frac{d\sigma(\bar{\nu}_\mu e)}{dy} &= \frac{G_F^2 m_e E_\nu}{2\pi} \left[(g_V^{\nu e} - g_A^{\nu e})^2 + (g_V^{\nu e} + g_A^{\nu e})^2 (1 - y)^2 \right] \\ &= \frac{2G_F^2 m_e E_\nu}{\pi} \left[(g_R^{\nu e})^2 + (g_L^{\nu e})^2 (1 - y)^2 \right]. \end{aligned} \quad (4.5)$$

Integrating over the region $0 \leq y \leq 1$, we obtain the total cross sections which are

$$\begin{aligned}\sigma(\nu_\mu e) &= \frac{G_F^2 m_e E_\nu}{2\pi} \left[(g_V^{\nu e} + g_A^{\nu e})^2 + \frac{1}{3} (g_V^{\nu e} - g_A^{\nu e})^2 \right] = \frac{2G_F^2 m_e E_\nu}{\pi} \left[(g_L^{\nu e})^2 + \frac{1}{3} (g_R^{\nu e})^2 \right], \\ \sigma(\bar{\nu}_\mu e) &= \frac{G_F^2 m_e E_\nu}{2\pi} \left[\frac{1}{3} (g_V^{\nu e} + g_A^{\nu e})^2 + (g_V^{\nu e} - g_A^{\nu e})^2 \right] = \frac{2G_F^2 m_e E_\nu}{\pi} \left[(g_R^{\nu e})^2 + \frac{1}{3} (g_L^{\nu e})^2 \right].\end{aligned}\quad (4.6)$$

Note that

$$\begin{aligned}(g_V^{\nu e} + g_A^{\nu e})^2 &= (2g_L^{\nu e})^2 = \rho^2 (-1 + 2\sin^2 \theta_W)^2 = \rho^2 (1 - 4\sin^2 \theta_W + 4\sin^4 \theta_W), \\ (g_V^{\nu e} - g_A^{\nu e})^2 &= (2g_R^{\nu e})^2 = \rho^2 (2\sin^2 \theta_W)^2 = \rho^2 (4\sin^4 \theta_W).\end{aligned}\quad (4.7)$$

Therefore,

$$\begin{aligned}\sigma(\nu_\mu e) &= \frac{G_F^2 m_e E_\nu}{2\pi} \rho^2 \left[1 - 4\sin^2 \theta_W + \frac{16}{3} \sin^4 \theta_W \right], \\ \sigma(\bar{\nu}_\mu e) &= \frac{G_F^2 m_e E_\nu}{2\pi} \frac{\rho^2}{3} \left[1 - 4\sin^2 \theta_W + 16\sin^4 \theta_W \right],\end{aligned}\quad (4.8)$$

and

$$R_e = \frac{\sigma(\nu_\mu e)}{\sigma(\bar{\nu}_\mu e)} = 3 \frac{1 - 4\sin^2 \theta_W + \frac{16}{3} \sin^4 \theta_W}{1 - 4\sin^2 \theta_W + 16\sin^4 \theta_W}.\quad (4.9)$$

From Eq. (4.6), we can see that if both total cross sections $\sigma(\nu_\mu e)$ and $\sigma(\bar{\nu}_\mu e)$ are measured, we can constrain the pair $(g_V^{\nu e}, g_A^{\nu e})$, or equivalently, the pair $(g_L^{\nu e}, g_R^{\nu e})$. On the other hand, from Eq. (4.5), we can see that if the neutrino beam were mono-energetic, measuring the T dependence of the neutrino cross section alone will allow us to disentangle $g_L^{\nu e}$ and $g_R^{\nu e}$ without the anti-neutrino cross section. This is the strategy proposed in Ref. [65] to measure the NSI (Non-Standard Interactions) of the electron-neutrino using the ${}^7\text{Be}$ Solar neutrinos and the Borexino detector. In the case of NuSONG, the ν_μ beam is not mono-energetic, so the differential cross section will be a convolution of the ν_μ energy spectrum and Eq. (4.5).

In Appendix E we explain how measurements of $\sigma(\nu_\mu e)$ and $\sigma(\bar{\nu}_\mu e)$ translate into constraints on $g_V^{\nu e}$ and $g_A^{\nu e}$. For $\epsilon_{\nu e} = 0.007$ and $\epsilon_{\bar{\nu} e} = 0.013$, we find

$$\begin{aligned}\Delta g_V^{\nu e} &= 0.0036, \\ \Delta g_A^{\nu e} &= 0.0019, \\ \text{Corr}(g_V^{\nu e}, g_A^{\nu e}) &= -0.57,\end{aligned}\quad (4.10)$$

where we have used $\rho = 1$, $\sin^2 \theta_W = 0.2315$ as inputs. For comparison, the World Average according to the PDG [25] (dominated by CHARM II) is:

$$\begin{aligned}g_V^{\nu e} &= -0.040 \pm 0.015, \\ g_A^{\nu e} &= -0.507 \pm 0.014, \\ \text{Corr}(g_V^{\nu e}, g_A^{\nu e}) &= -0.05.\end{aligned}\quad (4.11)$$

So the errors are expected to improve dramatically.

4.1.2 Assumptions on $\nu_\mu N$ and $\bar{\nu}_\mu N$ DIS

The ratios of charged-current to neutral current cross sections in neutrino Deep Inelastic Scattering (DIS) are derived in Appendix A and given by

$$\begin{aligned} R^\nu &= \frac{\sigma_{NC}^\nu}{\sigma_{CC}^\nu} = g_L^2 + r g_R^2, \\ R^{\bar{\nu}} &= \frac{\sigma_{NC}^{\bar{\nu}}}{\sigma_{CC}^{\bar{\nu}}} = g_L^2 + \frac{1}{r} g_R^2, \\ r &= \frac{\sigma_{CC}^{\bar{\nu}}}{\sigma_{CC}^\nu}, \end{aligned} \tag{4.12}$$

where

$$\begin{aligned} g_L^2 &= (g_L^{\nu u})^2 + (g_L^{\nu d})^2 = (2g_L^\nu g_L^u)^2 + (2g_L^\nu g_L^d)^2 = \rho^2 \left(\frac{1}{2} - \sin^2 \theta_W + \frac{5}{9} \sin^4 \theta_W \right), \\ g_R^2 &= (g_R^{\nu u})^2 + (g_R^{\nu d})^2 = (2g_L^\nu g_R^u)^2 + (2g_L^\nu g_R^d)^2 = \rho^2 \left(\frac{5}{9} \sin^4 \theta_W \right). \end{aligned} \tag{4.13}$$

The NuTeV result in terms of g_L^2 and g_R^2 was

$$\begin{aligned} g_L^2 &= 0.30005 \pm 0.00137, \\ g_R^2 &= 0.03076 \pm 0.00110, \\ \text{Corr}(g_L^2, g_R^2) &= -0.017. \end{aligned} \tag{4.14}$$

The World average according to the PDG is

$$\begin{aligned} g_L^2 &= 0.3004 \pm 0.0012, \\ g_R^2 &= 0.0311 \pm 0.0010, \\ \text{Corr}(g_L^2, g_R^2) &= -0.11. \end{aligned} \tag{4.15}$$

We will assume that NuSOng will be able to halve the errors on NuTeV:

$$\begin{aligned} \Delta g_L^2 &= 0.0007, \\ \Delta g_R^2 &= 0.0006, \end{aligned} \tag{4.16}$$

with negligible correlation (since the correlation in NuTeV was only -0.017).

4.2 Constraints on New Physics Section

Here, we consider the constraints on new physics that will be placed by NuSOng if it agrees with the SM.

If new particles are heavier than the center of mass energy of NuSOng they cannot be produced at resonance in neutrino-quark or neutrino-electron collisions. Nevertheless, these new particles can shift the values of observables from SM predictions through radiative corrections. The precise measurements of these observables can either constrain the parameter space of new physics models contributing to the shifts or detect new physics at mass scales well above the energies of the colliding particles. In this way the precision neutrino scattering measurements at NuSOng will

place TeV-scale indirect constraints on many models of new physics, or perhaps detect new physics by measuring deviations from SM predictions. The new physics effects can be parametrized by a small number of effective operators. The parameters of these operators can be fit to NuSOnG data. Although the particular set of the effective operators we use depends on our assumptions about new physics, this approach gives a parameterization of new physics which is largely model-independent.

We first parameterize new physics using the oblique parameters ST , which is appropriate when the important effects of new physics appear in vacuum polarizations of gauge bosons. We next assume new physics effects manifest as higher-dimensional operators made of SM fermion fields. We separately consider the possibility that the gauge couplings to neutrinos are modified. Realistic models usually introduce several new operators with relations among the coefficients; we consider several examples.

4.2.1 Oblique Correction Analysis

For models of new physics in which the dominant loop corrections are vacuum polarization corrections to the $SU(2)_L \times U(1)_Y$ gauge boson propagators (“oblique” corrections), the STU [66, 67] parameterization provides a convenient framework in which to describe the effects of new physics on precision electroweak data. Differences between the predictions of a new physics model and those of a reference Standard Model (with a specified Higgs boson and top quark mass) can be expressed as nonzero values of the oblique correction parameters S , T and U . T and U are sensitive to new physics that violates isospin, while S is sensitive to isospin-conserving physics. Predictions of a Standard Model with Higgs or top masses different from the reference Standard Model may also be subsumed into shifts in S and T . (The U parameter is often omitted in the fit because only W mass depends on this parameter, so including both W mass and the U parameter in the fit does not affect the limits on S and T .) Within a specific model of new physics the shift on the ST plot away from the SM will be calculable [68].

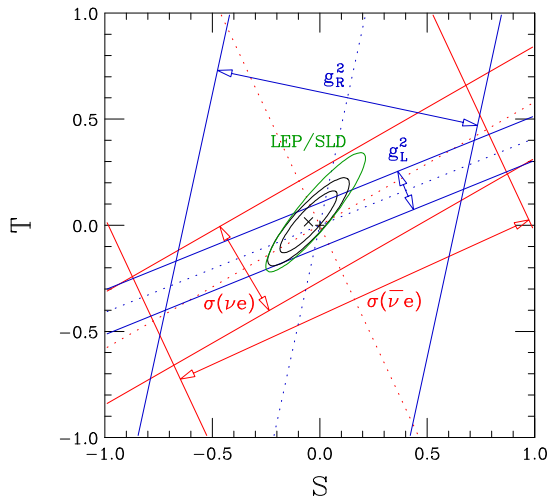


Figure 4.1: The impact of NuSOnG on the limits of S and T . The reference SM is $m_t = 170.9$ GeV, and $m_H = 115$ GeV. 1σ bands due to NuSOnG observables are shown against the 90% contour from LEP/SLD. The central ellipses are the 68% and 90% confidence limit contours with NuSOnG included.

The constraints on S and T from the full set of precision electroweak data strongly restrict the models of new physics which are viable. The strongest constraints are from LEP/SLD, which give a current bound of

$$\begin{aligned} S &= -0.02 \pm 0.11, \\ T &= +0.06 \pm 0.13, \\ \text{Corr}(S, T) &= 0.91. \end{aligned} \tag{4.17}$$

The ES and DIS measurements from NuSOng provide four distinct and complementary probes of S and T , as shown in Fig. 4.1. If the target precision is achieved, and assuming the NuSOng agree with SM predictions, NuSOng will further reduce the errors on S and T from the LEP/SLD values to

$$\begin{aligned} S &= -0.05 \pm 0.09, \\ T &= +0.02 \pm 0.10, \\ \text{Corr}(S, T) &= 0.87. \end{aligned} \tag{4.18}$$

The $\sim 25\%$ reduction in the errors is primarily due to the improved measurement of g_L^2 .

4.2.2 Non-Standard Interactions

NuSOng will probe new physics that modifies neutrino-quark and neutrino-electron scattering. If the masses associated to the new degrees of freedom are much larger than the center of mass energy ($s = 2m_e E_{\text{beam}} \lesssim 0.5 \text{ GeV}^2$) then modifications to these processes are well-described by higher-dimensional effective operators. In the context of neutrino reactions, these operators are also referred to as non-standard interactions (NSI's). In a model-independent effective Lagrangian approach these effective operators are added to the SM effective Lagrangian with arbitrary coefficients. Expressions for experimental observables can be computed using the new effective Lagrangian, and the arbitrary coefficients can then be constrained by fitting to data. Typically, bounds on the magnitude of the coefficients are obtained using only one or a few of the available effective operators. This approach simplifies the analysis and gives an indication of the scale of constraints, although we must be mindful of relationships among different operators that will be imposed by specific assumptions regarding the underlying physics.

To assess the sensitivity of NuSOng to “heavy” new physics in neutral current processes, we introduce the following effective Lagrangian for neutrino-fermion interactions [69, 70, 71]:

$$\begin{aligned} \mathcal{L}_{\text{NSI}} &= -\sqrt{2}G_F \left[\bar{\nu}_\alpha \gamma_\sigma P_L \nu_\beta \right] \left[\varepsilon_{\alpha\beta}^{fV} \bar{f} \gamma^\sigma f - \varepsilon_{\alpha\beta}^{fA} \bar{f} \gamma^\sigma \gamma_5 f \right] \\ &= -2\sqrt{2}G_F \left[\bar{\nu}_\alpha \gamma_\sigma P_L \nu_\beta \right] \left[\varepsilon_{\alpha\beta}^{fL} \bar{f} \gamma^\sigma P_L f + \varepsilon_{\alpha\beta}^{fR} \bar{f} \gamma^\sigma P_R f \right]. \end{aligned} \tag{4.19}$$

where $\alpha, \beta = e, \mu, \tau$ and L, R represent left-chiral and right-chiral fermion fields. If $\alpha \neq \beta$, then the $\alpha \leftrightarrow \beta$ terms must be Hermitian conjugates of each other, *i.e.* $\varepsilon_{\beta\alpha} = \varepsilon_{\alpha\beta}^*$. NuSOng is sensitive to the $\beta = \mu$ couplings. This effective Lagrangian is appropriate for parameterizing corrections to neutral current processes; an analysis of corrections to charged-current processes requires a different set of four-fermion operators.

Assuming $\varepsilon_{\alpha\beta} = 0$ for $\alpha \neq \beta$ we need consider only the terms $\varepsilon_{\mu\mu}^{f*}$ ($* = V, A, L, R$). If we rewrite Eq. (1.1) as

$$\begin{aligned}
\mathcal{L} &= -\sqrt{2}G_F \left[\bar{\nu}\gamma_\mu P_L \nu \right] \left[g_V^{\nu f} \bar{f}\gamma^\mu f - g_A^{\nu f} \bar{f}\gamma^\mu \gamma_5 f \right] \\
&= -2\sqrt{2}G_F \left[\bar{\nu}\gamma_\mu P_L \nu \right] \left[g_L^{\nu f} \bar{f}\gamma^\mu P_L f + g_R^{\nu f} \bar{f}\gamma^\mu P_R f \right],
\end{aligned} \tag{4.20}$$

where

$$\begin{aligned}
g_V^{\nu f} &= 2g_L^\nu g_V^f = \rho \left(I_3^f - 2Q^f \sin^2 \theta_W \right), \\
g_A^{\nu f} &= 2g_L^\nu g_A^f = \rho \left(I_3^f \right), \\
g_L^{\nu f} &= 2g_L^\nu g_L^f = \rho \left(I_3^f - Q^f \sin^2 \theta_W \right), \\
g_R^{\nu f} &= 2g_L^\nu g_R^f = \rho \left(-Q^f \sin^2 \theta_W \right),
\end{aligned} \tag{4.21}$$

then we see that adding Eq. (4.19) to the SM Lagrangian will simply shift the effective couplings:

$$\begin{aligned}
g_V^{\nu f} &\longrightarrow \tilde{g}_V^{\nu f} = g_V^{\nu f} + \varepsilon_{\mu\mu}^{fV}, \\
g_A^{\nu f} &\longrightarrow \tilde{g}_A^{\nu f} = g_A^{\nu f} + \varepsilon_{\mu\mu}^{fA}, \\
g_L^{\nu f} &\longrightarrow \tilde{g}_L^{\nu f} = g_L^{\nu f} + \varepsilon_{\mu\mu}^{fL}, \\
g_R^{\nu f} &\longrightarrow \tilde{g}_R^{\nu f} = g_R^{\nu f} + \varepsilon_{\mu\mu}^{fR}.
\end{aligned} \tag{4.22}$$

Consequently, errors on the $g_P^{\nu f}$'s translate directly into errors on the $\varepsilon_{\mu\mu}^{fP}$'s, $P = V, A$ or $P = L, R$.

Neutrino-lepton NSI

The world average value for neutrino-electron effective couplings, dominated by CHARM II, is

$$\begin{aligned}
g_V^{\nu e} &= -0.040 \pm 0.015, \\
g_A^{\nu e} &= -0.507 \pm 0.014, \\
\text{Corr}(g_V^{\nu e}, g_A^{\nu e}) &= -0.05.
\end{aligned} \tag{4.23}$$

The current 1σ bounds from CHARM II, Eq. (4.23) translates to $|\varepsilon_{\mu\mu}^{eP}| < 0.01$, ($P = L, R$) with a correlation of 0.07 [69]. At the current precision goals, NuSOnG's $\nu_\mu e$ and $\bar{\nu}_\mu e$ will significantly reduce the uncertainties on these NSI's, to

$$\begin{aligned}
|\varepsilon_{\mu\mu}^{eV}| &< 0.0036, \\
|\varepsilon_{\mu\mu}^{eA}| &< 0.0019, \\
\text{Corr}(\varepsilon_{\mu\mu}^{eV}, \varepsilon_{\mu\mu}^{eA}) &= -0.57,
\end{aligned} \tag{4.24}$$

or in terms of the chiral couplings,

$$\begin{aligned}
|\varepsilon_{\mu\mu}^{eL}| &< 0.0015, \\
|\varepsilon_{\mu\mu}^{eR}| &< 0.0025, \\
\text{Corr}(\varepsilon_{\mu\mu}^{eL}, \varepsilon_{\mu\mu}^{eR}) &= 0.64.
\end{aligned} \tag{4.25}$$

Neutrino-Quark NSI

We next consider the $f = u, d$ case. The change in the parameters g_L^2 and g_R^2 due to the NSI's is

$$\Delta g_L^2 = 2g_L^{\nu u} \varepsilon_{\mu\mu}^{uL} + 2g_L^{\nu d} \varepsilon_{\mu\mu}^{dL}$$

$$\begin{aligned}
&\approx +0.69 \varepsilon_{\mu\mu}^{uL} - 0.85 \varepsilon_{\mu\mu}^{dL} , \\
\Delta g_R^2 &= 2g_R^{\nu u} \varepsilon_{\mu\mu}^{uR} + 2g_R^{\nu d} \varepsilon_{\mu\mu}^{dR} \\
&\approx -0.31 \varepsilon_{\mu\mu}^{uR} + 0.15 \varepsilon_{\mu\mu}^{dR} ,
\end{aligned} \tag{4.26}$$

so only these linear combinations are constrained. The bounds from NuTeV (rescaled to 1σ bounds from ref. [69]) are:

$$\begin{aligned}
\varepsilon_{\mu\mu}^{uL} &= -0.0053 \pm 0.0020 , \\
\varepsilon_{\mu\mu}^{dL} &= +0.0043 \pm 0.0016 , \\
|\varepsilon_{\mu\mu}^{uR}| &< 0.0035 , \\
|\varepsilon_{\mu\mu}^{dR}| &< 0.0073 .
\end{aligned} \tag{4.27}$$

These bounds are obtained by setting only one of the parameters be non-zero at a time. If NuSO_nG reduces the errors on the NuTeV measurement of g_L^2 and g_R^2 by a factor of 2, the 1σ bounds on the NSI parameters are similarly reduced:

$$\begin{aligned}
|\varepsilon_{\mu\mu}^{uL}| &< 0.001 , \\
|\varepsilon_{\mu\mu}^{dL}| &< 0.0008 , \\
|\varepsilon_{\mu\mu}^{uR}| &< 0.002 , \\
|\varepsilon_{\mu\mu}^{dR}| &< 0.004 .
\end{aligned} \tag{4.28}$$

We note that neutrino-quark scattering will also be sensitive to NSIs which correct CC interactions. These interactions are not included in Eq. (4.19). If they are important, as is the case in some of the scenarios we treat later, a new analysis is necessary and the bounds above cannot be used. This is to be contrasted to the neutrino-lepton case, discussed in the previous subsection.

4.2.3 Neutrissimos, Neutrino Mixing and Gauge Couplings

In those classes of models which include moderately heavy electroweak gauge singlet (“neutrissimo”) states, with masses above 45 GeV, the mixing of the $SU(2)_L$ -active neutrinos and the sterile states may lead to a suppression of the neutrino-gauge couplings. The resulting pattern of modified interactions is distinct from those of the previous section since they will also induce correlated shifts to the charged-current coupling. For example, Ref. [5] presents models with one sterile state per active neutrino flavor and intergenerational mixing among neutrinos. In these models the flavor eigenstates are linear combinations of mass eigenstates, and those mass eigenstates too heavy to be produced in final states result in an effective suppression of the neutrino-gauge boson coupling. This suppression may be flavor-dependent depending on the structure of the neutrino mixing matrix. If the mass matrix contains Majorana terms, such models permit both lepton flavor violation and lepton universality violation.

Neutrinos couple to the W and the Z through interactions described by:

$$\mathcal{L} = \frac{g}{\sqrt{2}} W_\mu^- \bar{\ell}_L \gamma^\mu \nu_{\ell L} + \frac{g}{\sqrt{2}} W_\mu^+ \bar{\nu}_{\ell L} \gamma^\mu \ell_L + \frac{e}{2s_W c_W} Z_\mu \bar{\nu}_{\ell L} \gamma^\mu \nu_{\ell L} , \tag{4.29}$$

where $\ell = e, \mu, \tau$. If the neutrinos mix with gauge singlet states so that the $SU(2)_L$ interaction eigenstate is a superposition of mass eigenstates $\nu_{\ell, \text{light}}$ and $\nu_{\ell, \text{heavy}}$

$$\nu_{\ell L} = \nu_{\ell, \text{light}} \cos \theta_\ell + \nu_{\ell, \text{heavy}} \sin \theta_\ell , \tag{4.30}$$

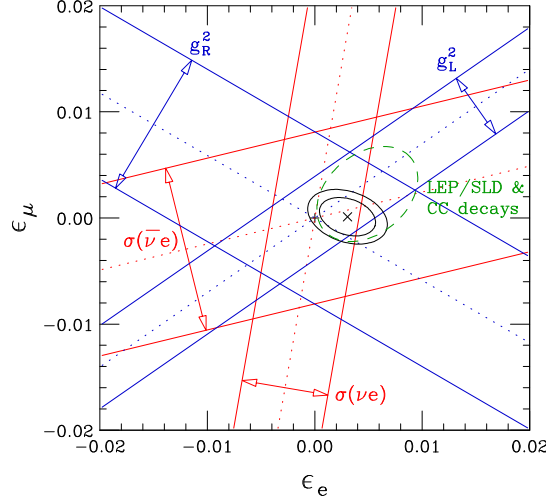


Figure 4.2: Potential constraint on ϵ_e and ϵ_μ from NuSONG (see Eq. (4.33)). This is a two-dimensional projection of a 4 parameter fit with S , T , ϵ_e and ϵ_μ . The green ellipse is the 90% CL contour of a fit to all the charge current particle decay data + LEP/SLD.

then the interaction of the light states is given by

$$\begin{aligned} \mathcal{L} = & \left(\frac{g}{\sqrt{2}} W_\mu^- \bar{\ell}_L \gamma^\mu \nu_{\ell, \text{light}} + \frac{g}{\sqrt{2}} W_\mu^+ \bar{\nu}_{\ell, \text{light}} \gamma^\mu \ell_L \right) \cos \theta_\ell \\ & + \left(\frac{e}{2s_W c_W} Z_\mu \bar{\nu}_{\ell, \text{light}} \gamma^\mu \nu_{\ell, \text{light}} \right) \cos^2 \theta_\ell . \end{aligned} \quad (4.31)$$

Defining

$$\epsilon_\ell \equiv 1 - \cos^2 \theta_\ell \quad (4.32)$$

the shift in the Lagrangian due to this mixing is

$$\delta \mathcal{L} = - \left(\frac{g}{\sqrt{2}} W_\mu^- \bar{\ell}_L \gamma^\mu \nu_\ell + \frac{g}{\sqrt{2}} W_\mu^+ \bar{\nu}_\ell \gamma^\mu \ell_L \right) \frac{\epsilon_\ell}{2} - \left(\frac{e}{2s_W c_W} Z_\mu \bar{\nu}_\ell \gamma^\mu \nu_\ell \right) \epsilon_\ell , \quad (4.33)$$

where we have dropped the subscript “light” from the neutrino fields.

Lepton universality data from W decays and from charged current π , τ and K decays [4] constraint differences $\epsilon_{\ell_i} - \epsilon_{\ell_j}$. LEP/SLD and other precision electroweak data will impose additional constraints on ϵ_ℓ in combination with the oblique parameters, as will NuSONG. A fit to all the charge current decay data and LEP/SLD with S , T , ϵ_e and ϵ_μ yields

$$\begin{aligned} S &= -0.05 \pm 0.11 , \\ T &= -0.44 \pm 0.28 , \\ \epsilon_e &= 0.0049 \pm 0.0022 , \\ \epsilon_\mu &= 0.0023 \pm 0.0021 . \end{aligned} \quad (4.34)$$

The correlations are shown in table 4.1.

	S	T	ϵ_e	ϵ_μ
S	1.00	0.53	-0.09	-0.09
T		1.00	-0.73	-0.71
ϵ_e			1.00	0.33
ϵ_μ				1.00

Table 4.1: Correlation among the fit parameters in a fit to charged current decay and LEP/SLD data.

If we now included hypothetical data from NuSOng, assuming NuSOng achieves its precision goals and measures central values consistent with the Standard Model, we see the constraints on ϵ_μ and ϵ_e are substantially improved. In this case, the fit yields

$$\begin{aligned}
S &= 0.00 \pm 0.10, \\
T &= -0.11 \pm 0.12, \\
\epsilon_e &= 0.0030 \pm 0.0017, \\
\epsilon_\mu &= 0.0001 \pm 0.0012.
\end{aligned}
\tag{4.35}$$

with correlations given in Table 4.2.

	S	T	ϵ_e	ϵ_μ
S	1.00	0.51	0.15	0.39
T		1.00	-0.58	0.09
ϵ_e			1.00	-0.29
ϵ_μ				1.00

Table 4.2: Correlation among the fit parameters in a fit to charge current decay, LEP/SLD, and possible NuSOng data.

Fig. 4.2 shows the two dimensional cross section in the ϵ_e - ϵ_μ plane of the four dimensional fit. The likelihood contours are 2D projections. Though not obvious from the figure, it is NuSOng's improved measurement of g_L^2 which contributes the most to strengthening the bounds on the ϵ_ℓ .

In models of this class lepton flavor violating decays such as $\mu \rightarrow e\gamma$ impose additional constraints on products $\epsilon_{\ell_i}\epsilon_{\ell_j}$. For example, the strong constraint from $\mu \rightarrow e\gamma$ implies $\epsilon_e\epsilon_\mu \approx 0$. This type of model has been proposed as a solution to the NuTeV anomaly. If we take only one of ϵ_e or ϵ_μ to be nonzero (to respect the constraint from $\mu \rightarrow e\gamma$), the NuTeV value of g_L^2 is accommodated in the fit by best-fit values of ϵ that are large and positive and best-fit values of T are large and negative (consistent with a heavy Higgs).

4.2.4 Sensitivity in the Case of Specific Theoretical Models

We next consider the constraints imposed by the proposed NuSOng measurements on explicit models of beyond the SM physics. An explicit model provides relations among effective operators which give stronger and sometimes better-motivated constraints on new physics than is obtained from bounds obtained by considering effective operators one by one, but at the expense of the generality of the conclusions. Many models can be analyzed using the effective Lagrangian of Eq. (4.19), but others introduce new operators and must be treated individually. The list of models considered is not exhaustive, but rather illustrates the new physics reach of NuSOng.

Generation distinguishing Z'

The existence of the Z' 's which distinguish among generations can affect neutrino scattering. These will be probed by NuSONG at the TeV scale [18, 19, 20, 72, 73, 74]. Few models of this class, namely gauged $B - 3L_\mu$ and gauged $L_\mu - L_\tau$, were at one time suggested as possible explanations of the NuTeV anomaly [17], however, we have shown in Chapter 2 that they cannot serve this purpose. Nevertheless, they remain interesting examples to consider.

- In the gauged $B - 3L_\mu$ the Z' modifies $\nu_\mu N$ DIS. The exchange of the Z' between the ν_μ and the quarks induces operators with coefficients

$$\begin{aligned}\varepsilon_{\mu\mu}^{uL} &= \varepsilon_{\mu\mu}^{uR} = \varepsilon_{\mu\mu}^{dL} = \varepsilon_{\mu\mu}^{dR} \\ &= -\frac{1}{2\sqrt{2}G_F} \frac{g_{Z'}^2}{M_{Z'}^2} \equiv \varepsilon_{B-3L_\mu},\end{aligned}\quad (4.36)$$

which shift g_L^2 and g_R^2 by

$$\Delta g_L^2 = \Delta g_R^2 = -\frac{2s_W^2}{3} \varepsilon_{B-3L_\mu}.\quad (4.37)$$

It should be noted that since ε_{B-3L_μ} is negative, this shows that both g_L^2 and g_R^2 will be shifted positive. This, in fact, excludes gauged $B - 3L_\mu$ as an explanation of the NuTeV anomaly. With this said, a NuSONG measurement of g_L^2 and g_R^2 that improves on NuTeV errors by a factor of 2 yields a 2σ bound

$$\frac{M_{Z'}}{g_{Z'}} > 2.2 \text{ TeV}.\quad (4.38)$$

which is comparable and complementary to the existing bound from D0 of 1.9 TeV (see Eq. (36) in Ref. [9]), and thus interesting to consider.

- As another example, consider gauged $L_e - L_\mu$. The Z' in such a model will affect $\nu_\mu e$ and $\bar{\nu}_\mu e$ ES through a direct exchange of the Z' between the neutrino and the electron. The effective Lagrangian of the Z' exchange interaction is

$$\mathcal{L}_{L_e-L_\mu} = +\frac{g_{Z'}^2}{M_{Z'}^2} (\bar{\nu}_{\mu L} \gamma_\sigma \nu_{\mu L}) (\bar{e} \gamma^\sigma e).\quad (4.39)$$

Comparison with Eq. (4.19) tells us that effectively, we have the following NSI's:

$$\varepsilon_{\mu\mu}^{eV} = -\frac{1}{\sqrt{2}G_F} \frac{g_{Z'}^2}{M_{Z'}^2}, \quad \varepsilon_{\mu\mu}^{eA} = 0.\quad (4.40)$$

Taking into account the large correlation in Eq. (4.24), the 1σ bound on $\varepsilon_{\mu\mu}^{eV}$ when $\varepsilon_{\mu\mu}^{eA} = 0$ is

$$|\varepsilon_{\mu\mu}^{eV}| < 0.0030.\quad (4.41)$$

This translates into the 95% (2σ) bound given by

$$\frac{M_{Z'}}{g_{Z'}} > 3.2 \text{ TeV}.\quad (4.42)$$

The existing bound for this ratio from LEP/LEP2 is 4.1 TeV [9] so NuSONG will not be able to improve this particular bound.

Extended Higgs Models

In the Zee [75] and Babu-Zee [76] models, an isosinglet scalar h^+ with hypercharge $Y = +1$ is introduced, which couples to left-handed lepton doublets as

$$\mathcal{L}_h = \lambda_{ab} (\ell_{aL}^T C i\sigma_2 \ell_{bL}) h^+ + h.c. = \lambda_{ab} (\overline{\ell_{aL}^c} i\sigma_2 \ell_{bL}) h^+ + h.c. , \quad (4.43)$$

where (ab) are flavor indices: $a, b = e, \mu, \tau$. The hypercharge assignment prohibits the h^\pm fields from having a similar interaction with the quarks. Due to $SU(2)$ gauge invariance, the couplings λ_{ab} are antisymmetric: $\lambda_{ab} = -\lambda_{ba}$. This interaction is analogous to the R-parity violating $\hat{L}\hat{L}\hat{E}$ coupling with h^\pm playing the role of the slepton.

Expanding Eq. (4.43), we obtain

$$\mathcal{L} = 2 [\lambda_{e\mu} (\overline{\nu_{eL}^c} \mu_L - \overline{\nu_{\mu L}^c} e_L) + \lambda_{e\tau} (\overline{\nu_{eL}^c} \tau_L - \overline{\nu_{\tau L}^c} e_L) + \lambda_{\mu\tau} (\overline{\nu_{\mu L}^c} \tau_L - \overline{\nu_{\tau L}^c} \mu_L)] h^+ + h.c. \quad (4.44)$$

The only terms relevant for NuSOng is

$$-2\lambda_{e\mu} (\overline{\nu_{\mu L}^c} e_L) h^+ + h.c. \quad (4.45)$$

The exchange of an h induces the following interaction:

$$\mathcal{L}_{\text{Babu/Zee}} = +\frac{4|\lambda_{e\mu}|^2}{M_h^2} (\overline{\nu_{\mu L}^c} e_L) (\overline{e_L} \nu_\mu^c) = +\frac{2|\lambda_{e\mu}|^2}{M_h^2} (\overline{\nu_{\mu L}} \gamma_\sigma \nu_{\mu L}) (\overline{e_L} \gamma^\sigma e_L) , \quad (4.46)$$

which leads to

$$\varepsilon_{\mu\mu}^{eL} = -\frac{1}{\sqrt{2}G_F} \frac{|\lambda_{e\mu}|^2}{M_h^2} , \quad \varepsilon_{\mu\mu}^{eR} = 0 . \quad (4.47)$$

Again, taking into account the large correlation seen in Eq. (4.25), the 1σ bound on $\varepsilon_{\mu\mu}^{eL}$ when $\varepsilon_{\mu\mu}^{eR} = 0$ is

$$|\varepsilon_{\mu\mu}^{eL}| < 0.0011 , \quad (4.48)$$

which translates into the 2σ (95%) bound given by:

$$\frac{M_h}{|\lambda_{e\mu}|} > 5.2 \text{ TeV} , \quad (4.49)$$

which is competitive with the current bound from τ -decay of 5.4 TeV.

R-parity Violating SUSY

Assuming the particle content of the Minimal Supersymmetric Standard Model (MSSM), the most general R-parity violating superpotential (involving only tri-linear couplings) has the form [77]

$$W_{\mathcal{R}} = \frac{1}{2} \lambda_{ijk} \hat{L}_i \hat{L}_j \hat{E}_k + \lambda'_{ijk} \hat{L}_i \hat{Q}_j \hat{D}_k + \frac{1}{2} \lambda''_{ijk} \hat{U}_i \hat{D}_j \hat{D}_k , \quad (4.50)$$

where \hat{L}_i , \hat{E}_i , \hat{Q}_i , \hat{D}_i , and \hat{U}_i are the left-handed MSSM superfields defined in the usual fashion, and the subscripts $i, j, k = 1, 2, 3$ are the generation indices. (Note, however, that in some references, such as Ref. [78], the isospin singlet superfields \hat{E}_i , \hat{D}_i , and \hat{U}_i are defined to be right-handed, so

the corresponding left-handed fields in Eq. (4.50) appear with a superscript c indicating charge-conjugation.) $SU(2)_L$ gauge invariance requires the couplings λ_{ijk} to be antisymmetric in the first two indices:

$$\lambda_{ijk} = -\lambda_{jik} , \quad (4.51)$$

whereas $SU(3)$ gauge invariance requires the couplings λ''_{ijk} to be antisymmetric in the latter two:

$$\lambda''_{ijk} = -\lambda''_{ikj} . \quad (4.52)$$

These conditions reduce the number of R-parity violating couplings in Eq. (4.50) to 45 (9 λ_{ijk} , 27 λ'_{ijk} , and 9 λ''_{ijk}). The purely baryonic operator $\hat{U}_i \hat{D}_j \hat{D}_k$ is irrelevant to our discussion on NuSOng so we will not consider the λ''_{ijk} couplings further. We also neglect possible bilinear R-parity violating couplings which have the effect of mixing the neutrinos with the neutral higgsino.

- The $\hat{L}\hat{L}\hat{E}$ part of the R-parity violating Lagrangian, Eq. (4.50), expressed in terms of the component fields is

$$\mathcal{L}_{LLE} = \lambda_{ijk} [\tilde{\nu}_{iL} \overline{e_{kR}} e_{jL} + \tilde{e}_{jL} \overline{e_{kR}} \nu_{iL} + \tilde{e}_{kR}^* \overline{\nu_{iL}} e_{jL}] + h.c. \quad (4.53)$$

The second and third terms of this Lagrangian, together with their hermitian conjugates, contribute to $\nu_\mu e$ ES at NuSOng. Since λ_{ijk} is antisymmetric under $i \leftrightarrow j$, it follows that $i \neq j$. The exchange of sleptons induce the following interaction:

$$\begin{aligned} \mathcal{L}_{LLE} &= + \sum_{k=1}^3 \frac{|\lambda_{21k}|^2}{M_{\tilde{e}_{kR}}^2} (\overline{\nu_{\mu L}}^c e_L) (\overline{e_L} \nu_{\mu L}^c) + \sum_{j=1,3} \frac{|\lambda_{2j1}|^2}{M_{\tilde{e}_{jL}}^2} (\overline{\nu_{\mu L}} e_R) (\overline{e_R} \nu_{\mu L}) \\ &= + \sum_{k=1}^3 \frac{|\lambda_{21k}|^2}{2M_{\tilde{e}_{kR}}^2} (\overline{\nu_{\mu L}} \gamma_\sigma \nu_{\mu L}) (\overline{e_L} \gamma^\sigma e_L) - \sum_{j=1,3} \frac{|\lambda_{2j1}|^2}{2M_{\tilde{e}_{jL}}^2} (\overline{\nu_{\mu L}} \gamma_\sigma \nu_{\mu L}) (\overline{e_R} \gamma^\sigma e_R) , \end{aligned} \quad (4.54)$$

Therefore,

$$\varepsilon_{\mu\mu}^{eL} = -\frac{1}{4\sqrt{2}G_F} \sum_{k=1}^3 \frac{|\lambda_{21k}|^2}{M_{\tilde{e}_{kR}}^2} , \quad \varepsilon_{\mu\mu}^{eR} = +\frac{1}{4\sqrt{2}G_F} \sum_{j=1,3} \frac{|\lambda_{2j1}|^2}{M_{\tilde{e}_{jL}}^2} . \quad (4.55)$$

There are four different couplings involved in these expressions, namely: λ_{211} , λ_{212} , λ_{213} , and λ_{231} . If we look at the contribution of each coupling separately, we find

$$\begin{aligned} \varepsilon_{\mu\mu}^{eL} &= -\frac{1}{4\sqrt{2}G_F} \frac{|\lambda_{211}|^2}{M_{\tilde{e}_{1R}}^2} , & \varepsilon_{\mu\mu}^{eR} &= +\frac{1}{4\sqrt{2}G_F} \frac{|\lambda_{211}|^2}{M_{\tilde{e}_{1L}}^2} , \\ \varepsilon_{\mu\mu}^{eL} &= -\frac{1}{4\sqrt{2}G_F} \frac{|\lambda_{212}|^2}{M_{\tilde{e}_{2R}}^2} , & \varepsilon_{\mu\mu}^{eR} &= 0 , \\ \varepsilon_{\mu\mu}^{eL} &= -\frac{1}{4\sqrt{2}G_F} \frac{|\lambda_{213}|^2}{M_{\tilde{e}_{3R}}^2} , & \varepsilon_{\mu\mu}^{eR} &= 0 , \\ \varepsilon_{\mu\mu}^{eL} &= 0 , & \varepsilon_{\mu\mu}^{eR} &= +\frac{1}{4\sqrt{2}G_F} \frac{|\lambda_{231}|^2}{M_{\tilde{e}_{3L}}^2} . \end{aligned} \quad (4.56)$$

Coupling	95% NuSOng bound	current 95% bound
$ \lambda_{121} $	0.03	0.05 (V_{ud})
$ \lambda_{122} $	0.04	0.05 (V_{ud})
$ \lambda_{123} $	0.04	0.05 (V_{ud})
$ \lambda_{231} $	0.05	0.07 (τ decay)
$ \lambda'_{211} $	0.05	0.06 (π decay)
$ \lambda'_{212} $	0.06	0.06 (π decay)
$ \lambda'_{213} $	0.06	0.06 (π decay)
$ \lambda'_{221} $	0.07	0.21 (D meson decay)
$ \lambda'_{231} $	0.07	0.45 ($Z \rightarrow \mu^+ \mu^-$)

Table 4.3: Potential bounds on the R-parity violating LLE (top) and LQD (bottom) couplings from NuSOng, assuming that only one coupling is non-zero at a time for each set. All squark and slepton masses are set to 100 GeV. To obtain limits for different masses, rescale by $(\frac{M}{100 \text{ GeV}})$. Current bounds are from Ref. [78].

If either $\varepsilon_{\mu\mu}^{eL}$ or $\varepsilon_{\mu\mu}^{eR}$ is restricted to zero, the bound on the other will be

$$\begin{aligned} \varepsilon_{\mu\mu}^{eL} &< 0.0011, & \text{if } \varepsilon_{\mu\mu}^{eR} &= 0, \\ \varepsilon_{\mu\mu}^{eR} &< 0.0019, & \text{if } \varepsilon_{\mu\mu}^{eL} &= 0. \end{aligned} \quad (4.57)$$

These bounds on the epsilons, as well as that obtained in Eq. (4.25), can be converted into bounds on the mass to coupling constant ratios using Eq. (4.56). However, in the case of R-parity violation, it is customary to fix the sparticle masses to 100 GeV and express the bound as a bound on the coupling constants. This is due to the fact that if the sparticles exist, they will be discovered through non-R-parity-violating interactions and their masses will be measured/constrained independently. As an example, consider the λ_{211} coupling. Both $\varepsilon_{\mu\mu}^{eL}$ and $\varepsilon_{\mu\mu}^{eR}$ depend on the value of this coupling as apparent from the first line of Eq. (4.56). If we set the masses of the left handed and right handed selectrons equal to each other then the right hand sides of the equations on the first line of Eq. (4.56) will depend on only one parameter, mass-to-coupling ratio of the selectron. Using the potential NuSOng bounds on the values of $\varepsilon_{\mu\mu}^{eL}$ and $\varepsilon_{\mu\mu}^{eR}$ given by Eq. (4.25) and performing one parameter fit we obtain the following bound on the mass-to-coupling ratio for the selectrons:

$$\frac{M_{\tilde{e}_1}}{|\lambda_{211}|} > 3.3 \text{ TeV}, \quad (4.58)$$

where $M_{\tilde{e}_1}$ is the mass of the right and left handed selectrons. Setting $M_{\tilde{e}_1} = 100 \text{ GeV}$ we obtain the following bound on the value of $|\lambda_{211}|$

$$|\lambda_{211}| < 0.03. \quad (4.59)$$

The bounds on the other couplings can be obtained in a similar fashion and the results are tabulated in Table 4.3. They can be compared to current bounds Ref. [78]. NuSOng improves all of these bounds.

- The $\hat{L}\hat{Q}\hat{D}$ part of the R-parity violating Lagrangian expressed in terms of the component fields is

$$\mathcal{L}_{LQD} = \lambda'_{ijk} \left[\tilde{\nu}_{iL} \overline{d_{kR}} d_{jL} + \tilde{d}_{jL} \overline{d_{kR}} \nu_{iL} + \tilde{d}_{kR}^* \overline{\nu_{iL}^c} d_{jL} \right]$$

$$- \left(\tilde{e}_{iL} \overline{d_{kR}} u_{jL} + \tilde{u}_{jL} \overline{d_{kR}} e_{iL} + \tilde{d}_{kR}^* \overline{e_{iL}} u_{jL} \right) \Big] + h.c. \quad (4.60)$$

The second and third terms of this Lagrangian, together with their hermitian conjugates, contribute to NC $\nu_\mu N$ DIS at NuSOnG. In addition, the third and sixth terms contribute to CC $\nu_\mu N$ DIS through an s -channel sdown. The induced effective interactions are:

$$\begin{aligned} \mathcal{L}_{\text{LQD}} &= \sum_{j=1}^3 \frac{|\lambda'_{2j1}|^2}{M_{\tilde{d}_{jL}}^2} (\overline{d_R} \nu_{\mu L}) (\overline{\nu_{\mu L}} d_R) + \sum_{k=1}^3 \frac{|\lambda'_{21k}|^2}{M_{\tilde{d}_{kR}}^2} (\overline{\nu_{\mu L}^c} d_L) (\overline{d_L} \nu_{\mu L}^c) \\ &\quad - \sum_{k=1}^3 \frac{|\lambda'_{21k}|^2}{M_{\tilde{d}_{kR}}^2} \left[(\overline{\nu_{\mu L}^c} d_L) (\overline{u_L} \mu^c) + h.c. \right] \\ &= - \sum_{j=1}^3 \frac{|\lambda'_{2j1}|^2}{2M_{\tilde{d}_{jL}}^2} (\overline{\nu_{\mu L}} \gamma_\sigma \nu_{\mu L}) (\overline{d_R} \gamma^\sigma d_R) + \sum_{k=1}^3 \frac{|\lambda'_{21k}|^2}{2M_{\tilde{d}_{kR}}^2} (\overline{\nu_{\mu L}} \gamma_\sigma \nu_{\mu L}) (\overline{d_L} \gamma^\sigma d_L) \\ &\quad - \sum_{k=1}^3 \frac{|\lambda'_{21k}|^2}{2M_{\tilde{d}_{kR}}^2} \left[(\overline{\mu_L} \gamma_\sigma \nu_{\mu L}) (\overline{u_L} \gamma^\sigma d_L) + h.c. \right]. \end{aligned} \quad (4.61)$$

The NSI parameters are

$$\begin{aligned} \varepsilon_{\mu\mu}^{dL} &= -\frac{1}{4\sqrt{2}G_F} \sum_{k=1}^3 \frac{|\lambda'_{21k}|^2}{M_{\tilde{d}_{kR}}^2}, \\ \varepsilon_{\mu\mu}^{dR} &= -\frac{1}{4\sqrt{2}G_F} \sum_{j=1}^3 \frac{|\lambda'_{2j1}|^2}{M_{\tilde{d}_{jL}}^2}, \\ \varepsilon_c &= +\frac{1}{4\sqrt{2}G_F} \sum_{k=1}^3 \frac{|\lambda'_{21k}|^2}{M_{\tilde{d}_{kR}}^2} = -\varepsilon_{\mu\mu}^{dL}, \end{aligned} \quad (4.62)$$

where we have introduced the parameter ε_c to account for the non-standard charged current coupling:

$$-2\sqrt{2}G_F \varepsilon_c \left[(\overline{\mu_L} \gamma_\sigma \nu_{\mu L}) (\overline{u_L} \gamma^\sigma d_L) + h.c. \right]. \quad (4.63)$$

There are five couplings contributing to the ε 's, namely λ'_{211} , λ'_{212} , λ'_{213} , λ'_{221} , and λ'_{231} . If we write out their contributions separately, we find

$$\begin{aligned} \varepsilon_{\mu\mu}^{dL} &= -\frac{1}{4\sqrt{2}G_F} \frac{|\lambda'_{211}|^2}{M_{\tilde{d}_{1R}}^2}, & \varepsilon_{\mu\mu}^{dR} &= -\frac{1}{4\sqrt{2}G_F} \frac{|\lambda'_{211}|^2}{M_{\tilde{d}_{1L}}^2}, \\ \varepsilon_{\mu\mu}^{dL} &= -\frac{1}{4\sqrt{2}G_F} \frac{|\lambda'_{212}|^2}{M_{\tilde{d}_{2R}}^2}, & \varepsilon_{\mu\mu}^{dR} &= 0, \\ \varepsilon_{\mu\mu}^{dL} &= -\frac{1}{4\sqrt{2}G_F} \frac{|\lambda'_{213}|^2}{M_{\tilde{d}_{3R}}^2}, & \varepsilon_{\mu\mu}^{dR} &= 0, \\ \varepsilon_{\mu\mu}^{dL} &= 0, & \varepsilon_{\mu\mu}^{dR} &= -\frac{1}{4\sqrt{2}G_F} \frac{|\lambda'_{221}|^2}{M_{\tilde{d}_{2L}}^2}, \\ \varepsilon_{\mu\mu}^{dL} &= 0, & \varepsilon_{\mu\mu}^{dR} &= -\frac{1}{4\sqrt{2}G_F} \frac{|\lambda'_{231}|^2}{M_{\tilde{d}_{3L}}^2}. \end{aligned} \quad (4.64)$$

The shifts in g_L^2 and g_R^2 are:

$$\begin{aligned}\delta g_L^2 &= 2(g_L^{\nu d} + g_L^2)\varepsilon_{\mu\mu}^{dL}, \\ \delta g_R^2 &= 2g_R^2\varepsilon_{\mu\mu}^{dL} + 2g_R^{\nu d}\varepsilon_{\mu\mu}^{dR}.\end{aligned}\quad (4.65)$$

If either $\varepsilon_{\mu\mu}^{dL}$ or $\varepsilon_{\mu\mu}^{dR}$ is restricted to zero, the bound on the other will be

$$\begin{aligned}|\varepsilon_{\mu\mu}^{dL}| &< 0.0027, & \text{if } \varepsilon_{\mu\mu}^{dR} = 0, \\ |\varepsilon_{\mu\mu}^{dR}| &< 0.0039, & \text{if } \varepsilon_{\mu\mu}^{dL} = 0.\end{aligned}\quad (4.66)$$

We can convert these bounds on the epsilons into bounds on the couplings in the same way as we did before for the LLE case². The potential 2σ bounds on the R-parity violating LQD couplings are shown in Table 4.3. These bounds are presented for masses of 100 GeV. To obtain limits for different masses, one simply rescales by $(\frac{M}{100\text{GeV}})$. We see that NuSOnG's measurements are competitive with π decay bounds, and improves the current bounds on the 221 and 231 couplings by factors of 3 and 5, respectively.

Generation Non-Diagonal Leptoquarks

We reviewed leptoquarks in Chapter 2 and the leptoquark Lagrangian is given by Eq. (2.102). Leptoquarks effects can be seen at NuSOnG through $\nu_\mu N$ DIS. The interactions that contribute to $\nu_\mu N$ DIS are those with indices $(ij) = (12)$. Note that the ν_μ -electron cross-section, which is also going to be measured by NuSOnG, will not be affected by the leptoquarks because the scattering process does not involve quarks. This can be used to distinguish between different explanations of the NuTeV anomaly.

Since leptoquark exchange can interfere with both W and Z exchange processes, we cannot use the limits on NSI's given by Eq. (4.25) as is. In the following, we calculate the shifts in g_L^2 and g_R^2 induced by the exchange of these leptoquarks.

- S_1 :

S_1^0 contributes to both NC and CC $\nu_\mu N$ DIS. The contribution of the g_{1R}^{12} coupling of S_1^0 to the CC process is suppressed, however, since it requires a chirality flip to interfere with the SM process of W exchange in the t -channel. The effective interactions induced by S_1 are therefore:

$$\begin{aligned}\mathcal{L}_{S_1} &= +\frac{|g_{1L}^{12}|^2}{M_{S_1}^2}(\bar{d}_L^c\nu_{\mu L})(\bar{\nu}_{\mu L}d_L^c) - \frac{|g_{1L}^{12}|^2}{M_{S_1}^2}\left[(\bar{\mu}_L u_L^c)(\bar{d}_L^c\nu_{\mu L}) + h.c.\right] \\ &= +\frac{|g_{1L}^{12}|^2}{2M_{S_1}^2}(\bar{\nu}_{\mu L}\gamma_\sigma\nu_{\mu L})(\bar{d}_L\gamma^\sigma d_L) - \frac{|g_{1L}^{12}|^2}{2M_{S_1}^2}\left[(\bar{\mu}_L\gamma_\sigma\nu_{\mu L})(\bar{u}_L\gamma^\sigma d_L) + h.c.\right].\end{aligned}\quad (4.67)$$

The effective NSI's are:

$$\varepsilon_{\mu\mu}^{dL} = -\varepsilon_c = -\frac{1}{4\sqrt{2}G_F}\frac{|g_{1L}^{12}|^2}{M_{S_1}^2}, \quad \varepsilon_{\mu\mu}^{dR} = \varepsilon_{\mu\mu}^{uL} = \varepsilon_{\mu\mu}^{uR} = 0.\quad (4.68)$$

The shifts in g_L^2 and g_R^2 are

$$\delta g_L^2 = 2(g_L^{\nu d} + g_L^2)\varepsilon_{\mu\mu}^{dL},$$

²See the discussion following Eq. (4.57)

$$\delta g_R^2 = 2g_R^2 \varepsilon_{\mu\mu}^{dL}. \quad (4.69)$$

The bounds of Eq. (4.16) lead to

$$|\varepsilon_{\mu\mu}^{dL}| < 0.0027, \quad (4.70)$$

which translates to the 95% bound of

$$|g_{1L}^{12}|^2 < 0.0036 \left(\frac{M_{S_1}}{100 \text{ GeV}} \right)^2, \quad (4.71)$$

or

$$\frac{M_{S_1}}{|g_{1L}^{12}|} > 1.7 \text{ TeV}. \quad (4.72)$$

- \vec{S}_3 :

S_3^0 , and S_3^- contribute to NC $\nu_\mu N$ DIS in the s -channel. S_3^0 also contribute to CC $\nu_\mu N$ DIS. The effective interactions induced by \vec{S}_3 are therefore:

$$\begin{aligned} \mathcal{L}_{S_3} &= + \frac{|g_{3L}^{12}|^2}{M_{S_3^0}^2} (\bar{d}_L^c \nu_{\mu L}) (\nu_{\mu L} d_L^c) + 2 \frac{|g_{3L}^{12}|^2}{M_{S_3^-}^2} (\bar{u}_L^c \nu_{\mu L}) (\nu_{\mu L} u_L^c) \\ &\quad + \frac{|g_{3L}^{12}|^2}{M_{S_3^0}^2} \left[(\bar{\mu}_L u_L^c) (\bar{d}_L^c \nu_{\mu L}) + h.c. \right] \\ &= + \frac{|g_{3L}^{12}|^2}{2M_{S_3^0}^2} (\bar{\nu}_{\mu L} \gamma_\sigma \nu_{\mu L}) (\bar{d}_L \gamma^\sigma d_L) + \frac{|g_{3L}^{12}|^2}{M_{S_3^-}^2} (\bar{\nu}_{\mu L} \gamma_\sigma \nu_{\mu L}) (\bar{u}_L \gamma^\sigma u_L) \\ &\quad + \frac{|g_{3L}^{12}|^2}{2M_{S_3^0}^2} \left[(\bar{\mu}_L \gamma_\sigma \nu_{\mu L}) (\bar{u}_L \gamma^\sigma d_L) + h.c. \right], \end{aligned} \quad (4.73)$$

The effective NSI's are:

$$\begin{aligned} \varepsilon_{\mu\mu}^{uL} &= -\frac{1}{2\sqrt{2}G_F} \frac{|g_{3L}^{12}|^2}{M_{S_3^-}^2}, & \varepsilon_{\mu\mu}^{uR} &= 0, \\ \varepsilon_c = \varepsilon_{\mu\mu}^{dL} &= -\frac{1}{4\sqrt{2}G_F} \frac{|g_{3L}^{12}|^2}{M_{S_3^0}^2}, & \varepsilon_{\mu\mu}^{dR} &= 0, \end{aligned} \quad (4.74)$$

and the shifts in g_L^2 and g_R^2 are

$$\begin{aligned} \delta g_L^2 &= 2(g_L^{\nu d} - g_L^2) \varepsilon_{\mu\mu}^{dL} + 2g_L^{\nu u} \varepsilon_{\mu\mu}^{uL}, \\ \delta g_R^2 &= -2g_R^2 \varepsilon_{\mu\mu}^{dL}. \end{aligned} \quad (4.75)$$

If we assume degeneracy of the masses of leptoquarks in the same iso-multiplet, $M_{S_3^0} = M_{S_3^-} \equiv M_{S_3}$, then

$$\varepsilon_{\mu\mu}^{uL} = 2\varepsilon_{\mu\mu}^{dL} = -\frac{1}{2\sqrt{2}G_F} \frac{|g_{3L}^{12}|^2}{M_{S_3}^2}, \quad , \quad (4.76)$$

and

$$\delta g_L^2 = 2(g_L^{\nu d} - g_L^2 + 2g_L^{\nu u}) \varepsilon_{\mu\mu}^{dL},$$

$$\delta g_R^2 = -2g_R^2 \varepsilon_{\mu\mu}^{dL}. \quad (4.77)$$

The bounds in Eq. (4.16) then lead to the bound

$$|\varepsilon_{\mu\mu}^{dL}| < 0.0077, \quad (4.78)$$

which translates to the 95% bound of

$$|g_{3L}^{12}|^2 < 0.010 \left(\frac{M_{S_3}}{100 \text{ GeV}} \right)^2, \quad (4.79)$$

or

$$\frac{M_{S_3}}{|g_{3L}^{12}|} > 1.0 \text{ TeV}. \quad (4.80)$$

- S_2 .

S_2 contributes to both NC and CC processes, but the CC process is suppressed. The contribution to the NC process is

$$\begin{aligned} \mathcal{L}_{S_2} &= \frac{|h_{2L}^{12}|^2}{M_{S_2^-}^2} (\bar{\nu}_{\mu L} u_R) (\bar{u}_R \nu_{\mu L}) \\ &= -\frac{|h_{2L}^{12}|^2}{2M_{S_2^-}^2} (\bar{\nu}_{\mu L} \gamma_\sigma \nu_{\mu L}) (\bar{u}_R \gamma^\sigma u_R). \end{aligned} \quad (4.81)$$

Therefore,

$$\varepsilon_{\mu\mu}^{uR} = +\frac{1}{2\sqrt{2}G_F} \frac{|h_{2L}^{12}|^2}{M_{S_2^-}^2}, \quad (4.82)$$

and all other ε 's are zero. The shifts in g_L^2 and g_R^2 are

$$\delta g_L^2 = 0, \quad \delta g_R^2 = 2g_R^{\nu u} \varepsilon_{\mu\mu}^{uR}, \quad (4.83)$$

leading to the constraint

$$|\varepsilon_{\mu\mu}^{uR}| < 0.0019, \quad (4.84)$$

which at 2σ translates to

$$|h_{2L}^{12}|^2 < 0.0013 \left(\frac{M_{S_2^-}}{100 \text{ GeV}} \right)^2, \quad (4.85)$$

or

$$\frac{M_{S_2^-}}{|h_{2L}^{12}|} > 2.8 \text{ TeV}. \quad (4.86)$$

- \tilde{S}_2 :

The contribution of \tilde{S}_2^- to the NC process is

$$\mathcal{L}_{\tilde{S}_2} = \frac{|\tilde{h}_{2L}^{12}|^2}{M_{\tilde{S}_2^-}^2} (\bar{\nu}_{\mu L} d_R) (\bar{d}_R \nu_{\mu L})$$

$$= -\frac{|\tilde{h}_{2L}^{12}|^2}{2M_{\tilde{S}_2^-}^2} (\overline{\nu_{\mu L}} \gamma_\sigma \nu_{\mu L}) (\overline{d_R} \gamma^\sigma d_R) . \quad (4.87)$$

Therefore,

$$\varepsilon_{\mu\mu}^{dR} = +\frac{1}{2\sqrt{2}G_F} \frac{|\tilde{h}_{2L}^{12}|^2}{M_{\tilde{S}_2^-}^2} , \quad (4.88)$$

and all other ε 's are zero. The shifts in g_L^2 and g_R^2 are

$$\delta g_L^2 = 0 , \quad \delta g_R^2 = 2g_R^{\nu d} \varepsilon_{\mu\mu}^{dR} , \quad (4.89)$$

leading to the constraint

$$|\varepsilon_{\mu\mu}^{dR}| < 0.0039 , \quad (4.90)$$

which at 2σ translates to

$$|\tilde{h}_{2L}^{12}|^2 < 0.0026 \left(\frac{M_{\tilde{S}_2^-}}{100 \text{ GeV}} \right)^2 . \quad (4.91)$$

or

$$\frac{M_{\tilde{S}_2^-}}{|\tilde{h}_{2L}^{12}|} > 2.0 \text{ TeV} , \quad (4.92)$$

- V_1 :

V_1 exchange leads to the effective interaction given by (after a Fierz transformation):

$$\mathcal{L}_{V_1} = -\frac{|h_{1L}^{12}|^2}{M_{V_1}^2} (\overline{\nu_{\mu L}} \gamma_\sigma \nu_{\mu L}) (\overline{u_L} \gamma^\sigma u_L) - \frac{|h_{1L}^{12}|^2}{M_{V_1}^2} \left[(\overline{\mu_L} \gamma_\sigma \nu_{\mu L}) (\overline{u_L} \gamma^\sigma d_L) + h.c. \right] . \quad (4.93)$$

Therefore,

$$\varepsilon_{\mu\mu}^{uL} = \varepsilon_c = +\frac{1}{2\sqrt{2}G_F} \frac{|h_{1L}^{12}|^2}{M_{V_1}^2} , \quad (4.94)$$

and g_L^2 and g_R^2 are shifted by

$$\begin{aligned} \delta g_L^2 &= 2(g_L^{\nu u} - g_L^2) \varepsilon_{\mu\mu}^{uL} , \\ \delta g_R^2 &= -2g_R^2 \varepsilon_{\mu\mu}^{uL} , \end{aligned} \quad (4.95)$$

leading to the constraint

$$|\varepsilon_{\mu\mu}^{uL}| < 0.0060 , \quad (4.96)$$

which at 2σ gives

$$|h_{1L}^{12}|^2 < 0.0040 \left(\frac{M_{V_1}}{100 \text{ GeV}} \right)^2 , \quad (4.97)$$

or

$$\frac{M_{V_1}}{|h_{1L}^{12}|} > 1.6 \text{ TeV} . \quad (4.98)$$

- \vec{V}_3 :

The exchange of \vec{V}_3 leads to the following effective interactions (after a Fierz transformation):

$$\begin{aligned} \mathcal{L}_{V_3} = & -\frac{|h_{3L}^{12}|^2}{M_{V_3^0}^2} (\bar{\nu}_{\mu L} \gamma_\sigma \nu_{\mu L}) (\bar{u}_L \gamma^\sigma u_L) - 2 \frac{|h_{3L}^{12}|^2}{M_{V_3^-}^2} (\bar{\nu}_{\mu L} \gamma_\sigma \nu_{\mu L}) (\bar{d}_L \gamma^\sigma d_L) \\ & + \frac{|h_{3L}^{12}|^2}{M_{V_3^0}^2} \left[(\bar{\mu}_L \gamma_\sigma \nu_{\mu L}) (\bar{u}_L \gamma^\sigma d_L) + h.c. \right]. \end{aligned} \quad (4.99)$$

Therefore,

$$\varepsilon_{\mu\mu}^{uL} = -\varepsilon_c = +\frac{1}{2\sqrt{2}G_F} \frac{|h_{3L}^{12}|^2}{M_{V_3^0}^2}, \quad \varepsilon_{\mu\mu}^{dL} = +\frac{1}{\sqrt{2}G_F} \frac{|h_{3L}^{12}|^2}{M_{V_3^-}^2}, \quad (4.100)$$

with the other ε 's zero. The shifts in g_L^2 and g_R^2 are

$$\begin{aligned} \delta g_L^2 &= 2(g_L^{\nu u} + g_L^2) \varepsilon_{\mu\mu}^{uL} + 2g_L^{\nu d} \varepsilon_{\mu\mu}^{dL}, \\ \delta g_R^2 &= 2g_R^2 \varepsilon_{\mu\mu}^{uL}. \end{aligned} \quad (4.101)$$

Assuming degeneracy of the masses, $M_{V_3^0} = M_{V_3^-} \equiv M_{V_3}$, we have

$$\varepsilon_{\mu\mu}^{dL} = 2\varepsilon_{\mu\mu}^{uL} = +\frac{1}{\sqrt{2}G_F} \frac{|h_{3L}^{12}|^2}{M_{V_3}^2}, \quad (4.102)$$

and

$$\begin{aligned} \delta g_L^2 &= 2(g_L^{\nu u} + g_L^2 + 2g_L^{\nu d}) \varepsilon_{\mu\mu}^{uL}, \\ \delta g_R^2 &= 2g_R^2 \varepsilon_{\mu\mu}^{uL}, \end{aligned} \quad (4.103)$$

leading to the constraint

$$|\varepsilon_{\mu\mu}^{uL}| < 0.0017, \quad (4.104)$$

which at 2σ gives

$$|h_{3L}^{12}|^2 < 0.0011 \left(\frac{M_{V_3}}{100 \text{ GeV}} \right)^2, \quad (4.105)$$

or

$$\frac{M_{V_3}}{|h_{3L}^{12}|} > 3.0 \text{ TeV}. \quad (4.106)$$

- V_2 :

The exchange of the V_2 can affect both NC and CC processes, but the CC process is suppressed, so we will only consider the NC process. The effective interaction is

$$\mathcal{L}_{V_2} = -\frac{|g_{2L}^{12}|^2}{M_{V_2^-}^2} (\bar{\nu}_{\mu L} \gamma_\sigma d_R^c) (\bar{d}_R^c \gamma^\sigma \nu_{\mu L}) = +\frac{|g_{2L}^{12}|^2}{M_{V_2^-}^2} (\bar{\nu}_{\mu L} \gamma_\sigma \nu_{\mu L}) (\bar{d}_R \gamma^\sigma d_R). \quad (4.107)$$

Therefore,

$$\varepsilon_{\mu\mu}^{dR} = -\frac{1}{2\sqrt{2}G_F} \frac{|g_{2L}^{12}|^2}{M_{V_2^-}^2}, \quad (4.108)$$

with all other ε 's equal to zero. The shifts in δg_L^2 and δg_R^2 are

$$\delta g_L^2 = 0, \quad \delta g_R^2 = 2g_R^{\nu d} \varepsilon_{\mu\mu}^{dR}, \quad (4.109)$$

leading to the constraint

$$|\varepsilon_{\mu\mu}^{dR}| < 0.0039, \quad (4.110)$$

which at 2σ translates to

$$|g_{2L}^{12}|^2 < 0.0026 \left(\frac{M_{V_2^-}}{100 \text{ GeV}} \right), \quad (4.111)$$

or

$$\frac{M_{V_2^-}}{|g_{2L}^{12}|} > 2.0 \text{ TeV}. \quad (4.112)$$

- \tilde{V}_2 :

The exchange of \tilde{V}_2 leads to the effective interaction

$$\mathcal{L}_{\tilde{V}_2} = -\frac{|\tilde{g}_{2L}^{12}|^2}{M_{\tilde{V}_2^-}^2} (\bar{\nu}_{\mu L} \gamma_\sigma u_R^c) (\bar{u}_R^c \gamma^\sigma \nu_{\mu L}) = +\frac{|\tilde{g}_{2L}^{12}|^2}{M_{\tilde{V}_2^-}^2} (\bar{\nu}_{\mu L} \gamma_\sigma \nu_{\mu L}) (\bar{u}_R \gamma^\sigma u_R). \quad (4.113)$$

Therefore,

$$\varepsilon_{\mu\mu}^{uR} = -\frac{1}{2\sqrt{2}G_F} \frac{|\tilde{g}_{2L}^{12}|^2}{M_{\tilde{V}_2^-}^2}, \quad (4.114)$$

with all other ε 's equal to zero. The shifts in δg_L^2 and δg_R^2 are

$$\delta g_L^2 = 0, \quad \delta g_R^2 = 2g_R^{\nu u} \varepsilon_{\mu\mu}^{uR}, \quad (4.115)$$

leading to the constraint

$$|\varepsilon_{\mu\mu}^{uR}| < 0.0019, \quad (4.116)$$

which at 2σ translates to

$$|\tilde{g}_{2L}^{12}|^2 < 0.0013 \left(\frac{M_{\tilde{V}_2^-}}{100 \text{ GeV}} \right)^2, \quad (4.117)$$

or

$$\frac{M_{\tilde{V}_2^-}}{|\tilde{g}_{2L}^{12}|} > 2.8 \text{ TeV}. \quad (4.118)$$

Assuming degenerate masses within each iso-multiplet, the shifts in g_L^2 and g_R^2 can be written generically as

$$\begin{aligned} \delta g_L^2 &= C_L \frac{|\lambda_{LQ}^{12}|^2 / M_{LQ}^2}{g^2 / M_W^2} = \frac{C_L}{4\sqrt{2}G_F} \frac{|\lambda_{LQ}^{12}|^2}{M_{LQ}^2}, \\ \delta g_R^2 &= C_R \frac{|\lambda_{LQ}^{12}|^2 / M_{LQ}^2}{g^2 / M_W^2} = \frac{C_R}{4\sqrt{2}G_F} \frac{|\lambda_{LQ}^{12}|^2}{M_{LQ}^2}, \end{aligned} \quad (4.119)$$

where λ_{LQ}^{12} denotes the $(ij) = (12)$ coupling of the leptoquark and M_{LQ} is its mass. C_L , and C_R are constants that depend on the type leptoquark. In table 4.4 we list what they are, and in figure 4.3 we plot the dependence of δg_L^2 and δg_R^2 on the ratio $|\lambda_{LQ}|^2/M_{LQ}^2$. Table 4.4 also lists the projected NuSOng bounds on the coupling constants. Existing bounds on S_1 , \vec{S}_3 , V_1 , and \vec{V}_3 couplings from $R_\pi = B(\pi \rightarrow e\nu)/B(\pi \rightarrow \mu\nu)$ are already much stronger, but could be circumvented for \vec{S}_3 and \vec{V}_3 if the masses within the multiplet are allowed to be non-degenerate.

LQ	C_L	C_R	$ \lambda_{LQ}^{12} ^2$	NuSOng 95% bound	95% bound from R_π
S_1	$s^2 \left(\frac{4}{3} - \frac{10}{9} s^2 \right)$	$-\frac{10}{9} s^4$	$ g_{1L}^{12} ^2$	0.0036	0.0037
\vec{S}_3	$+\frac{10}{9} s^4$	$+\frac{10}{9} s^4$	$ g_{3L}^{12} ^2$	0.010	0.0008
S_2	0	$-\frac{8}{3} s^2$	$ h_{2L}^{12} ^2$	0.0013	N/A
\vec{S}_2	0	$+\frac{4}{3} s^2$	$ h_{2L}^{12} ^2$	0.0026	N/A
V_1	$s^2 \left(\frac{4}{3} - \frac{20}{9} s^2 \right)$	$-\frac{20}{9} s^4$	$ h_{1L}^{12} ^2$	0.0040	0.0018
\vec{V}_3	$-4s^2 \left(1 - \frac{5}{9} s^2 \right)$	$+\frac{20}{9} s^4$	$ h_{3L}^{12} ^2$	0.0011	0.0004
V_2	0	$-\frac{4}{3} s^2$	$ g_{2L}^{12} ^2$	0.0026	N/A
\vec{V}_2	0	$+\frac{8}{3} s^2$	$ \tilde{g}_{2L}^{12} ^2$	0.0013	N/A

Table 4.4: Potential and existing 95% bounds on the leptoquark couplings squared when the leptoquark masses are set to 100 GeV. To obtain the limits for different leptoquark masses, multiply by $(M_{LQ}/100 \text{ GeV})^2$. Existing bounds on the S_1 , \vec{S}_3 , V_1 , and \vec{V}_3 couplings from $R_\pi = B(\pi \rightarrow e\nu)/B(\pi \rightarrow \mu\nu)$ are also shown.

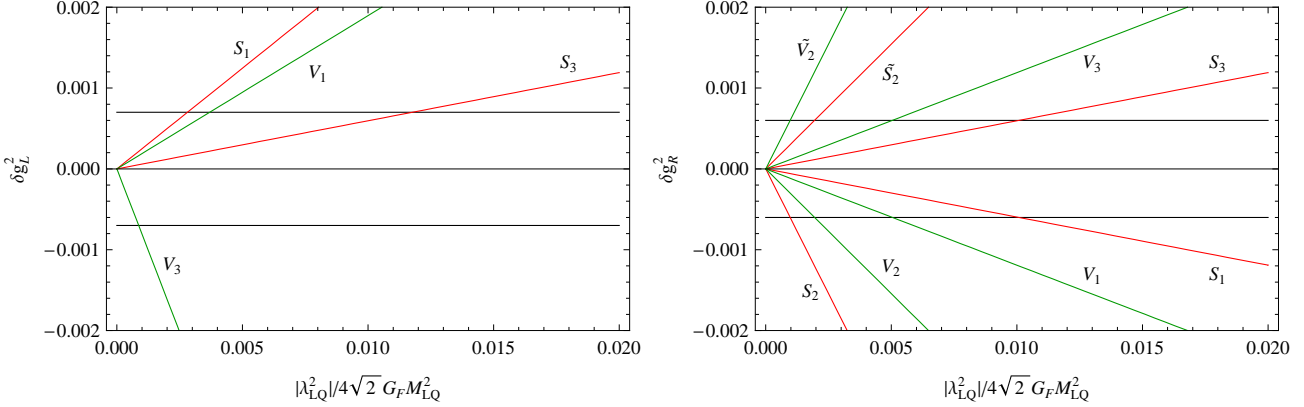


Figure 4.3: Shifts in g_L^2 and g_R^2 due to leptoquarks. Horizontal lines indicate the projected 1σ limits of NuSOng.

4.2.5 A New NuSOng Anomaly? $g_R^2 \neq (g_R^2)_{SM}$

Table 4.4 does not provide bounds on the leptoquarks S_2 , \vec{S}_2 , V_2 , and \vec{V}_2 from R_π since their exchange do not interfere with the W exchange process. Current bounds on these leptoquarks are fairly weak [29]. Furthermore, their presence can affect the value of g_R^2 , but not the value of g_L^2 , as is evident from the values of C_L and C_R listed in Table 4.4 and Fig. 4.3. Therefore, we can envision a scenario, given that a concrete model that makes it possible exists, in which NuSOng finds that g_R^2 is shifted away from its SM value, while g_L^2 is not. The mass to coupling ratios required to produce significant shifts in g_R^2 are listed in Table 4.5. If a deviation as large as 3σ is observed, the

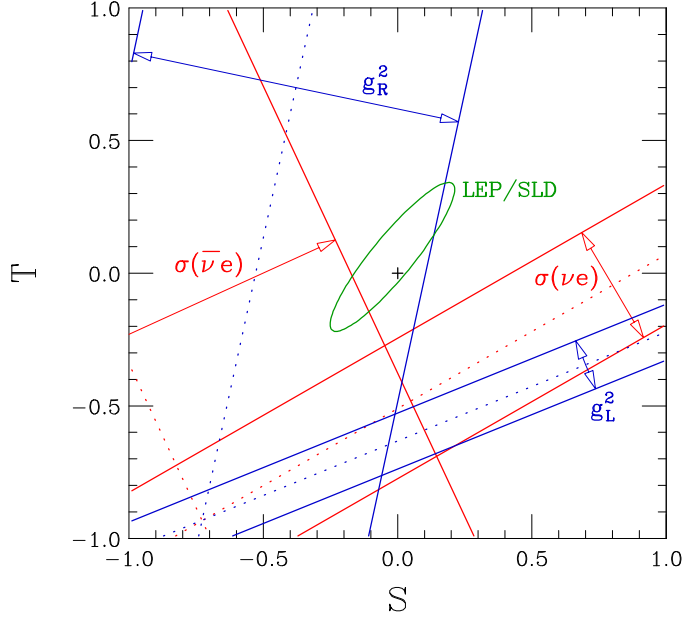


Figure 4.4: Expected S - T plot if a 6σ deviation is seen in g_L^2 which is due to a non-zero gauge suppression parameter ϵ_μ . All four observables g_L^2 , g_R^2 , $\sigma(\nu_\mu e)$, and $\sigma(\bar{\nu}_\mu e)$ are shifted away from their SM values. Unfortunately, the expected errors in g_R^2 and $\sigma(\bar{\nu}_\mu e)$ are too large for this shift to be seen. Seeing the shift in $\sigma(\nu_\mu e)$ may also be difficult.

1σ band on the ST plot for g_R^2 will be so displaced from the origin (*i.e.* the SM) that it will be off screen at the scale shown in Figs. 4.4 through 4.6.

deviation from SM	S_2	\tilde{S}_2	V_2	\tilde{V}_2
$+6\sigma$	N/A	1.1 TeV	N/A	1.6 TeV
$+3\sigma$	N/A	1.6 TeV	N/A	2.3 TeV
-3σ	2.3 TeV	N/A	1.6 TeV	N/A
-6σ	1.6 TeV	N/A	1.1 TeV	N/A
2σ NuTeV bound	>2.5 TeV	>1.3 TeV	>1.7 TeV	>1.8 TeV

Table 4.5: The values of $M_{LQ}/|\lambda_{LQ}^{12}|$ required for the leptoquarks S_2 , \tilde{S}_2 , V_2 , \tilde{V}_2 to shift the value of g_R^2 by $\pm 3\sigma$ and $\pm 6\sigma$. For comparison, the 2σ lower bound from NuTeV is also listed, though the reanalysis could change the bounds significantly. The NuTeV bounds are asymmetric for positive and negative shifts in g_R^2 due to the fact that the NuTeV central value is about 0.6σ above the SM value.

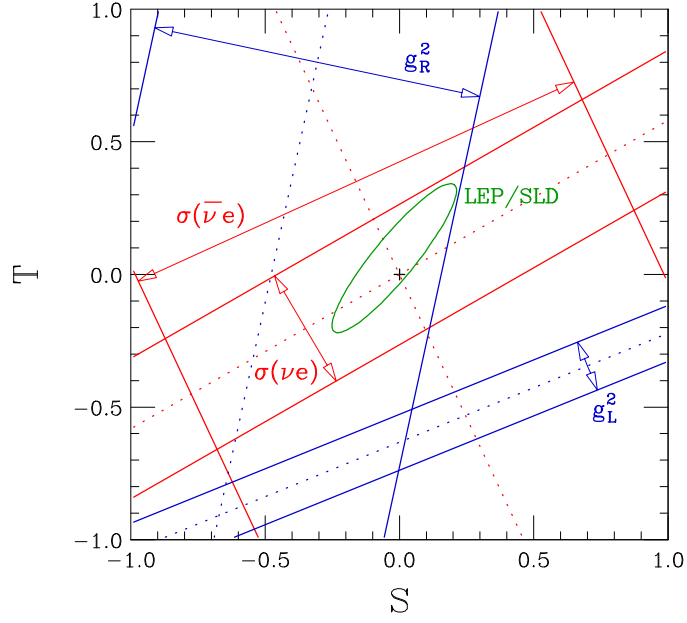


Figure 4.5: Expected S - T plot if a 6σ deviation is seen in g_L^2 which is due to a non-zero gauge suppression parameter ϵ_e . The $\nu_\mu N$ DIS observables g_L^2 and g_R^2 will be shifted away from their SM values, but not the $\nu_\mu e$ ES observables $\sigma(\nu_\mu e)$ and $\sigma(\bar{\nu}_\mu e)$. However, the expected error in g_R^2 is too large for this shift to be seen.

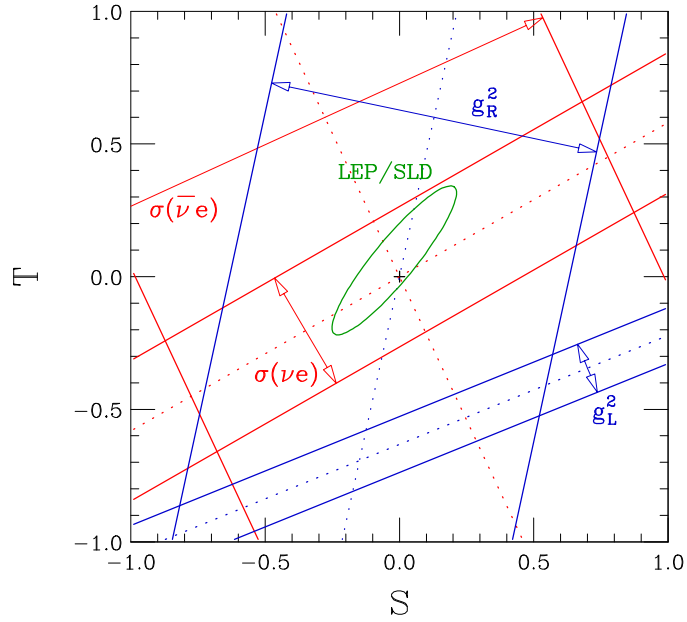


Figure 4.6: Expected S - T plot if a 6σ deviation is seen in g_L^2 which is due to triplet leptoquarks with large mass splitting. Only g_L^2 is shifted from its SM value.

Chapter 5

Fermilab→Hyper-Kamiokande experiment

The Long Baseline (LBL) neutrino oscillation experiments are also sensitive to the physics beyond the SM through matter effects and will be complementary to the LHC. Thus, in this chapter we give an example of a LBL experiment which can be performed in the future and discuss what we can learn about possible extensions of the SM which this experiment will be able to probe.

5.1 Introduction

When considering matter effects on neutrino oscillation, it is customary to consider only the W -exchange interaction of the ν_e with the electrons in matter. However, if new interactions beyond the Standard Model (SM) that distinguish among the three generations of neutrinos exist, they can lead to extra matter effects via radiative corrections to the $Z\nu\nu$ vertex, which effectively violate neutral current universality, or via the direct exchange of new particles between the neutrinos and matter particles [79].

Many models of physics beyond the SM introduce interactions which distinguish among generations: gauged $L_\alpha - L_\beta$ [18, 19] and gauged $B - \alpha L_e - \beta L_\mu - \gamma L_\tau$ [72, 73, 74, 80] models introduce Z 's and Higgs sectors which distinguish among the three generations of leptons; topcolor assisted technicolor treats the third generation differently from the first two to explain the large top mass [81, 82]; R-parity violating couplings in supersymmetric models couple fermions/sfermions from different generations [77, 78, 83].

The effective Hamiltonian that governs neutrino oscillation in the presence of neutral-current lepton universality violation, or new physics that couples to the different generations differently, is given by [10]

$$H = \tilde{U} \begin{bmatrix} \lambda_1 & 0 & 0 \\ 0 & \lambda_2 & 0 \\ 0 & 0 & \lambda_3 \end{bmatrix} \tilde{U}^\dagger = U \begin{bmatrix} 0 & 0 & 0 \\ 0 & \delta m_{21}^2 & 0 \\ 0 & 0 & \delta m_{31}^2 \end{bmatrix} U^\dagger + \begin{bmatrix} a & 0 & 0 \\ 0 & 0 & 0 \\ 0 & 0 & 0 \end{bmatrix} + \begin{bmatrix} b_e & 0 & 0 \\ 0 & b_\mu & 0 \\ 0 & 0 & b_\tau \end{bmatrix}. \quad (5.1)$$

In this expression, U is the MNS matrix [84],

$$a = 2EV_{CC}, \quad V_{CC} = \sqrt{2}G_F N_e = N_e \frac{g^2}{4M_W^2}, \quad (5.2)$$

is the usual matter effect due to W -exchange between ν_e and the electrons [85], and b_e, b_μ, b_τ are the extra matter effects which we assume to be flavor diagonal and non-equal. The matter effect terms in this Hamiltonian can always be written as

$$\begin{aligned} & \begin{bmatrix} a & 0 & 0 \\ 0 & 0 & 0 \\ 0 & 0 & 0 \end{bmatrix} + \begin{bmatrix} b_e & 0 & 0 \\ 0 & b_\mu & 0 \\ 0 & 0 & b_\tau \end{bmatrix} \\ &= \begin{bmatrix} \left(a + b_e - \frac{b_\mu + b_\tau}{2}\right) & 0 & 0 \\ 0 & \left(\frac{b_\mu - b_\tau}{2}\right) & 0 \\ 0 & 0 & -\left(\frac{b_\mu - b_\tau}{2}\right) \end{bmatrix} + \left(\frac{b_\mu + b_\tau}{2}\right) \begin{bmatrix} 1 & 0 & 0 \\ 0 & 1 & 0 \\ 0 & 0 & 1 \end{bmatrix}. \end{aligned} \quad (5.3)$$

The unit matrix term does not contribute to neutrino oscillation so it can be dropped. We define the parameter ξ as

$$\frac{b_\tau - b_\mu}{a} = \xi. \quad (5.4)$$

Then, the effective Hamiltonian can be written as

$$H = \tilde{U} \begin{bmatrix} \lambda_1 & 0 & 0 \\ 0 & \lambda_2 & 0 \\ 0 & 0 & \lambda_3 \end{bmatrix} \tilde{U}^\dagger = U \begin{bmatrix} 0 & 0 & 0 \\ 0 & \delta m_{21}^2 & 0 \\ 0 & 0 & \delta m_{31}^2 \end{bmatrix} U^\dagger + a \begin{bmatrix} 1 & 0 & 0 \\ 0 & -\xi/2 & 0 \\ 0 & 0 & +\xi/2 \end{bmatrix}, \quad (5.5)$$

where we have absorbed the extra b -terms in the $(1, 1)$ element into a .

The extra ξ -dependent contribution in Eq. (5.5) can manifest itself when $a > |\delta m_{31}^2|$ (*i.e.* $E \gtrsim 10$ GeV for typical matter densities in the Earth) in the ν_μ and $\bar{\nu}_\mu$ survival probabilities as [10]

$$\begin{aligned} P(\nu_\mu \rightarrow \nu_\mu) &\approx 1 - \sin^2 \left(2\theta_{23} - \frac{a\xi}{\delta m_{31}^2} \right) \sin^2 \frac{\Delta}{2}, \\ P(\bar{\nu}_\mu \rightarrow \bar{\nu}_\mu) &\approx 1 - \sin^2 \left(2\theta_{23} + \frac{a\xi}{\delta m_{31}^2} \right) \sin^2 \frac{\Delta}{2}, \end{aligned} \quad (5.6)$$

where

$$\Delta \approx \Delta_{31} c_{13}^2 - \Delta_{21} c_{12}^2, \quad \Delta_{ij} = \frac{\delta m_{ij}^2}{2E} L, \quad c_{ij} = \cos \theta_{ij}, \quad (5.7)$$

and the CP violating phase δ has been set to zero. As is evident from these expressions, the small shift due to ξ will be invisible if the value of $\sin^2 2\theta_{23}$ is too close to one. However, if the value of $\sin^2 2\theta_{23}$ is as low as $\sin^2 2\theta_{23} = 0.92$ (the current 90% lower bound [86]), and if ξ is as large as $\xi = 0.025$ (the central value from CHARM/CHARM II [87]), then the shift in the survival probability at the first oscillation dip can be as large as $\sim 40\%$. If the Fermilab-NUMI beam in its high-energy mode [88] were aimed at a declination angle of 46° toward the planned Hyper-Kamiokande detector [89] in Kamioka, Japan (baseline 9120 km), such a shift would be visible after just one year of data taking, assuming a Mega-ton fiducial volume and 100% efficiency. The absence of any shift after 5 years of data taking would constrain ξ to [10]

$$|\xi| \leq \xi_0 \equiv 0.005, \quad (5.8)$$

at the 99% confidence level.

In this chapter, we look at how this potential limit on ξ would translate into constraints on new physics, in particular, on the couplings and masses of new particles. As mentioned above, the models must be those that distinguish among different generations. We consider the following four classes of models:

1. Models with a generation distinguishing Z' boson. This class includes gauged $L_e - L_\mu$, gauged $L_e - L_\tau$, gauged $B - \alpha L_e - \beta L_\mu - \gamma L_\tau$, and topcolor assisted technicolor.
2. Models with leptoquarks (scalar and vector). This class includes various Grand Unification Theory (GUT) models and extended technicolor (ETC).
3. The Supersymmetric Standard Model with R-parity violation.
4. Extended Higgs models. This class includes the Babu model, the Zee model, and various models with triplet Higgs, as well as the generation distinguishing Z' models listed above.

These classes will be discussed one by one in sections 5.2 through 5.5. The constraints on these models will be compared with existing ones from LEP/SLD, the Tevatron, and other low energy experiments, and with those expected from direct searches for the new particles at the LHC.

5.2 Models with an extra Z' boson

Z' generically refers to any electrically neutral gauge boson corresponding to a flavor-diagonal generator of some new gauge group. Here, we are interested in models in which the Z' couples differently to different generations. The models we will consider are (A) gauged $L_e - L_\mu$ and $L_e - L_\tau$, (B) gauged $B - \alpha L_e - \beta L_\mu - \gamma L_\tau$, with $\alpha + \beta + \gamma = 3$, and (C) topcolor assisted technicolor.

5.2.1 Gauged $L_e - L_\mu$ and $L_e - L_\tau$

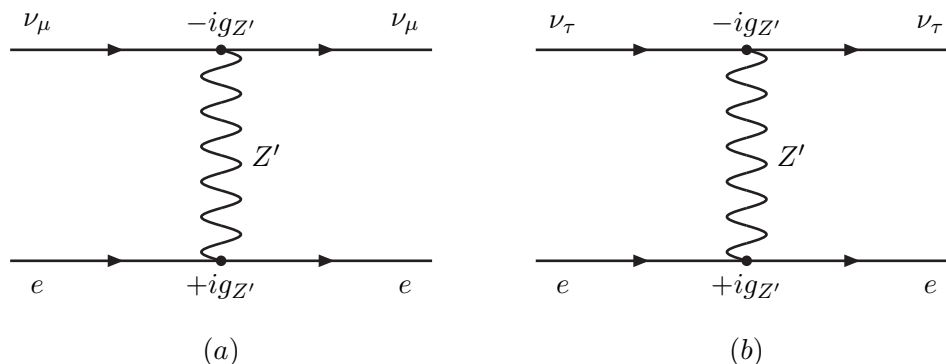


Figure 5.1: Diagrams that contribute to neutrino oscillation matter effects in (a) the gauged $L_e - L_\mu$ model, and (b) the gauged $L_e - L_\tau$ model.

In Ref. [18, 19], it was pointed out that the charges $L_e - L_\mu$, $L_e - L_\tau$, and $L_\mu - L_\tau$ are anomaly free within the particle content of the Standard Model, and therefore can be gauged. Models with

these symmetries are recently receiving renewed attention in attempts to explain the large mixing angles observed in the neutrino sector [20]. Of these, gauged $L_e - L_\mu$ and $L_e - L_\tau$ affect neutrino oscillation in matter. These models necessarily possess a Higgs sector which also distinguishes among different lepton generations [90], but we will only consider the effect of the extra gauge boson in this section and relegate the effect of the Higgs sector to a more generic discussion in section 5.5.

The interaction Lagrangian for gauged $L_e - L_\ell$ ($\ell = \mu$ or τ) is given by

$$\mathcal{L} = g_{Z'} \left(\bar{e}\gamma^\mu e - \bar{\ell}\gamma^\mu \ell + \bar{\nu}_{eL}\gamma^\mu \nu_{eL} - \bar{\nu}_{\ell L}\gamma^\mu \nu_{\ell L} \right) Z'_\mu . \quad (5.9)$$

The diagrams that affect neutrino propagation in matter are shown in Fig. 5.1. (The exchange of the Z' between the ν_e and the electrons do not lead to new matter effects.) The forward scattering amplitude of the left-handed neutrino $\nu_{\ell L}$ ($\ell = \mu, \tau$) is

$$i\mathcal{M} = (ig_{Z'})(-ig_{Z'}) \langle \nu_{\ell L} | \bar{\nu}_{\ell L}\gamma^\mu \nu_{\ell L} | \nu_{\ell L} \rangle \left(\frac{ig_{\mu\nu}}{M_{Z'}^2} \right) \langle e | \bar{e}\gamma^\nu e | e \rangle . \quad (5.10)$$

The electrons in matter are non-relativistic, so only the time-like components of the currents need to be considered. Replacing $\langle e | \bar{e}\gamma^0 e | e \rangle = \langle e | e^\dagger e | e \rangle$ with N_e , the number density of electrons in matter, and $\langle \nu_{\ell L} | \bar{\nu}_{\ell L}\gamma^0 \nu_{\ell L} | \nu_{\ell L} \rangle = \langle \nu_{\ell L} | \nu_{\ell L}^\dagger \nu_{\ell L} | \nu_{\ell L} \rangle$ with $\phi_{\nu_\ell}^\dagger \phi_{\nu_\ell}$, where ϕ_{ν_ℓ} is the wave function of the left-handed neutrino $\nu_{\ell L}$, we obtain

$$i\mathcal{M} = i \frac{g_{Z'}^2}{M_{Z'}^2} (\phi_{\nu_\ell}^\dagger \phi_{\nu_\ell}) N_e \equiv -iV_{\nu_\ell} (\phi_{\nu_\ell}^\dagger \phi_{\nu_\ell}) . \quad (5.11)$$

Therefore, the effective potential felt by the neutrinos as they traverse matter can be identified as

$$V_{\nu_\ell} = -\frac{g_{Z'}^2}{M_{Z'}^2} N_e . \quad (5.12)$$

The effective ξ 's for the $L_e - L_\mu$ and $L_e - L_\tau$ cases are

$$\begin{aligned} \xi_{L_e - L_\mu} &= -\frac{V_{\nu_\mu}}{V_{CC}} = +4 \frac{(g_{Z'}^2/M_{Z'}^2)}{(g^2/M_W^2)} = +\frac{1}{\sqrt{2}G_F} \left(\frac{g_{Z'}}{M_{Z'}} \right)^2 , \\ \xi_{L_e - L_\tau} &= +\frac{V_{\nu_\tau}}{V_{CC}} = -4 \frac{(g_{Z'}^2/M_{Z'}^2)}{(g^2/M_W^2)} = -\frac{1}{\sqrt{2}G_F} \left(\frac{g_{Z'}}{M_{Z'}} \right)^2 . \end{aligned} \quad (5.13)$$

Ignoring potential contributions from the Higgs sector, a bound on ξ of $|\xi| \leq \xi_0 = 0.005$ from Eq. (5.8) translates into:

$$\frac{M_{Z'}}{g_{Z'}} \geq \sqrt{\frac{1}{\sqrt{2}G_F \xi_0}} \approx 3500 \text{ GeV} , \quad (5.14)$$

for both the $L_e - L_\mu$ and $L_e - L_\tau$ cases.

The Z' in gauged $L_e - L_\ell$ ($\ell = \mu, \tau$) cannot be sought for at the LHC since they only couple to leptons. However, they can be produced in e^+e^- collisions and subsequently decay into e^+e^- or $\ell^+\ell^-$ pairs, and stringent constraints already exist from LEP/LEP2. The exchange of the Z' induces the

	Λ_- (TeV) from $e^+e^- \rightarrow e^+e^-$	Λ_+ (TeV) from $e^+e^- \rightarrow \mu^+\mu^-$	Λ_+ (TeV) from $e^+e^- \rightarrow \tau^+\tau^-$	Reference
L3	10.1	14.4	7.6	[91]
OPAL	10.6	12.7	8.6	[92]
DELPHI	13.9	12.2	15.8	[93]
ALEPH	12.5	10.5	12.8	[94]

Table 5.1: The 95% confidence level lower bounds on the compositeness scale Λ^\pm (TeV) from leptonic LEP/LEP2 data. Dividing by $\sqrt{4\pi}$ converts these limits to those on $(M_{Z'}/g_{Z'})$.

following effective four-fermion interactions, relevant to e^+e^- colliders, among the charged leptons at energies far below the Z' mass:

$$\mathcal{L} = -\frac{g_{Z'}^2}{2M_{Z'}^2} (\bar{e}\gamma_\mu e) (\bar{e}\gamma^\mu e) + \frac{g_{Z'}^2}{M_{Z'}^2} (\bar{e}\gamma_\mu e) (\bar{\ell}\gamma^\mu \ell) . \quad (5.15)$$

The LEP collaborations fit their data to

$$\mathcal{L} = -\frac{4\pi}{2\Lambda_-^2} (\bar{e}\gamma_\mu e) (\bar{e}\gamma^\mu e) + \frac{4\pi}{\Lambda_+^2} (\bar{e}\gamma_\mu e) (\bar{\ell}\gamma^\mu \ell) , \quad (5.16)$$

with the 95% confidence limits on Λ_\pm shown in Table 5.1. The strongest constraint for the $L_e - L_\mu$ case comes from the $e^+e^- \rightarrow \mu^+\mu^-$ channel of L3, which translates to

$$\frac{M_{Z'}}{g_{Z'}} \geq 4.1 \text{ TeV} , \quad (5.17)$$

while that for the $L_e - L_\tau$ case comes from the $e^+e^- \rightarrow \tau^+\tau^-$ channel of DELPHI, which translates to

$$\frac{M_{Z'}}{g_{Z'}} \geq 4.5 \text{ TeV} . \quad (5.18)$$

Though these are the 95% confidence limits while that given in Eq. (5.14) is the 99% limit, it is clear that the bound on ξ will not lead to any improvement of already existing bounds from LEP/LEP2.

5.2.2 Gauged $B - (\alpha L_e + \beta L_\mu + \gamma L_\tau)$

In Refs. [72, 73, 74, 80], extensions of the SM gauge group to $SU(3)_C \times SU(2)_L \times U(1)_Y \times U(1)_X$ with $X = B - (\alpha L_e + \beta L_\mu + \gamma L_\tau)$ were considered. Again, the motivation was to explain the observed pattern of neutrino masses and mixings. The cases $(\alpha, \beta, \gamma) = (0, 0, 3)$, $(3, 0, 0)$, and $(0, \frac{3}{2}, \frac{3}{2})$ were considered, respectively, in Refs. [72], [73], and [74]. In all cases, the condition

$$\alpha + \beta + \gamma = 3 \quad (5.19)$$

is required for anomaly cancellation within the SM plus right-handed neutrinos¹. When $\alpha \neq \beta \neq \gamma$, the $U(1)_X$ gauge boson, *i.e.* the Z' , couples to the three lepton generations differently, and can lead to extra neutrino oscillation matter effects. As in the gauged $L_e - L_\ell$ case, the Higgs sectors of these

¹Only the right-handed neutrinos with non-zero X charge need to be included for anomaly cancellation.

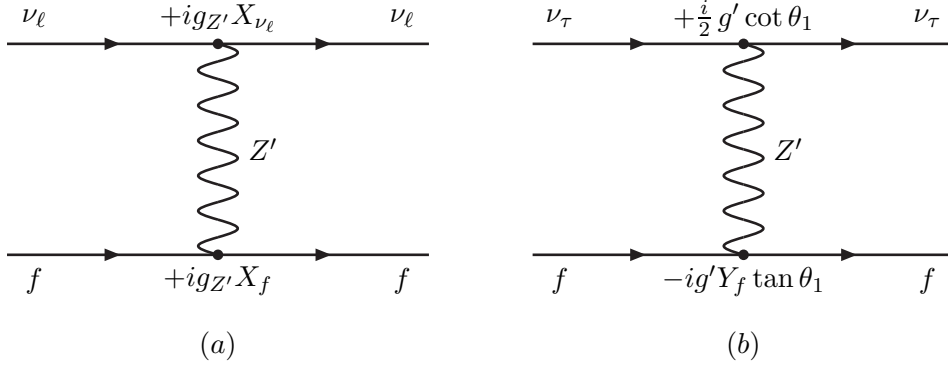


Figure 5.2: Diagrams that contribute to neutrino oscillation matter effects in (a) the gauged $X = B - \alpha L_e - \beta L_\mu - \gamma L_\tau$ model, $\ell = \{e, \mu, \tau\}$, $f = \{u, d, e\}$, and (b) topcolor assisted technicolor, $f = \{u_L, u_R, d_L, d_R, e_L, e_R\}$.

models also necessarily distinguish among the lepton generations, but we relegate the discussion of their effects to section 5.5.

For generic values of (α, β, γ) , the Z' couples to the quarks and leptons as

$$\mathcal{L}_{Z'} = g_{Z'} J_X^\mu Z'_\mu, \quad (5.20)$$

where

$$\begin{aligned} J_X^\mu &= \sum_f X_f (\bar{f} \gamma^\mu f) \\ &= \frac{1}{3} \sum_q (\bar{q} \gamma^\mu q) - \alpha (\bar{e} \gamma^\mu e + \bar{\nu}_e \gamma^\mu \nu_e) - \beta (\bar{\mu} \gamma^\mu \mu + \bar{\nu}_\mu \gamma^\mu \nu_\mu) - \gamma (\bar{\tau} \gamma^\mu \tau + \bar{\nu}_\tau \gamma^\mu \nu_\tau). \end{aligned} \quad (5.21)$$

The forward scattering amplitude of the left-handed neutrino $\nu_{\ell L}$ ($\ell = e, \mu, \tau$) on matter fermion F ($F = p, n, e$) due to Z' -exchange (*cf.* Fig. 5.2a) is

$$i\mathcal{M}_F = (+ig_{Z'} X_{\nu_\ell})(+ig_{Z'}) \langle \nu_{\ell L} | \bar{\nu}_\ell \gamma^\mu \nu_\ell | \nu_{\ell L} \rangle \left(\frac{ig_{\mu\nu}}{M_{Z'}^2} \right) \langle F | J_X^\nu | F \rangle. \quad (5.22)$$

Again, we can assume that the matter fermions are non-relativistic, so that only the time-like components of the currents need be considered. Then, we can make the replacements

$$\begin{aligned} \langle e | J_X^0 | e \rangle &= -\alpha \langle e | e^\dagger e | e \rangle \rightarrow -\alpha N_e, \\ \langle p | J_X^0 | p \rangle &= \frac{1}{3} \langle p | (u^\dagger u + d^\dagger d) | p \rangle \rightarrow \frac{1}{3} (2N_p + N_p) = N_p, \\ \langle n | J_X^0 | n \rangle &= \frac{1}{3} \langle n | (u^\dagger u + d^\dagger d) | n \rangle \rightarrow \frac{1}{3} (N_n + 2N_n) = N_n, \end{aligned} \quad (5.23)$$

and

$$\langle \nu_{\ell L} | \bar{\nu}_\ell \gamma^0 \nu_\ell | \nu_{\ell L} \rangle = \langle \nu_{\ell L} | (\nu_{\ell L}^\dagger \nu_{\ell L} + \nu_{\ell R}^\dagger \nu_{\ell R}) | \nu_{\ell L} \rangle = \langle \nu_{\ell L} | \nu_{\ell L}^\dagger \nu_{\ell L} | \nu_{\ell L} \rangle \rightarrow \phi_{\nu_\ell}^\dagger \phi_{\nu_\ell}, \quad (5.24)$$

which gives us

$$i\mathcal{M}_F = -iX_{\nu_\ell} \frac{g_{Z'}^2}{M_{Z'}^2} (\phi_{\nu_\ell}^\dagger \phi_{\nu_\ell}) (X_F N_F), \quad (5.25)$$

where we have defined $X_p = X_n = 1$. Summing over $F = p, n, e$, we find:

$$\begin{aligned} i\mathcal{M} &= i \sum_{F=p,n,e} \mathcal{M}_F \\ &= -iX_{\nu_\ell} \frac{g_{Z'}^2}{M_{Z'}^2} (\phi_{\nu_\ell}^\dagger \phi_{\nu_\ell}) (N_p + N_n - \alpha N_e) = -iV_{\nu_\ell} (\phi_{\nu_\ell}^\dagger \phi_{\nu_\ell}), \end{aligned} \quad (5.26)$$

where

$$V_{\nu_\ell} \equiv +X_{\nu_\ell} \frac{g_{Z'}^2}{M_{Z'}^2} (N_n + N_p - \alpha N_e) \quad (5.27)$$

can be identified as the effective potential experienced by the left-handed neutrino $\nu_{\ell L}$ as it travels through matter. Since the Earth is electrically neutral and is mostly composed of lighter elements, we can make the approximation $N_n \approx N_p = N_e \equiv N$, in which case

$$V_{\nu_\ell} \approx -X_{\nu_\ell} \frac{g_{Z'}^2}{M_{Z'}^2} (\alpha - 2)N. \quad (5.28)$$

The effective ξ is then

$$\xi_{(\alpha,\beta,\gamma)} = \frac{V_{\nu_\tau} - V_{\nu_\mu}}{V_{CC}} = -4(\alpha - 2)(\beta - \gamma) \frac{(g_{Z'}/M_{Z'})^2}{(g/M_W)^2}. \quad (5.29)$$

When $\alpha = 2$, the contribution of the matter electrons is canceled by those of the matter nucleons and $\xi_{(2,\beta,\gamma)}$ vanishes, regardless of the values of β and γ . When $\beta = \gamma$, the matter effects on ν_μ and ν_τ will be the same, again resulting in $\xi_{(\alpha,\beta,\beta)} = 0$, regardless of the value of α .

In Fig. 5.3, we plot the dependence of $\xi_{Z'}$ on the Z' mass for selected values of $g_{Z'}$ for the case $\alpha = \beta = 0$, $\gamma = 3$, namely, the Z' couples to $B - 3L_\tau$. In this case

$$\xi_{(0,0,3)} = -24 \frac{(g_{Z'}/M_{Z'})^2}{(g/M_W)^2} = -\frac{6}{\sqrt{2}G_F} \left(\frac{g_{Z'}}{M_{Z'}} \right)^2. \quad (5.30)$$

Ignoring the possible contribution of the Higgs sector, a bound on ξ of $|\xi| \leq \xi_0 = 0.005$ from Eq. (5.8) translates into:

$$\frac{M_{Z'}}{g_{Z'}} \geq \sqrt{\frac{6}{\sqrt{2}G_F \xi_0}} \approx 8500 \text{ GeV}. \quad (5.31)$$

More generically, the bound on the Z' mass is

$$\frac{M_{Z'}}{g_{Z'}} \geq \sqrt{\frac{|(\alpha - 2)(\beta - \gamma)|}{\sqrt{2}G_F \xi_0}} \approx \sqrt{|(\alpha - 2)(\beta - \gamma)|} \times (3500 \text{ GeV}). \quad (5.32)$$

This bound is plotted in Fig. 5.4 as a function of β for three different values of $g_{Z'}$, and two different values of α . The value of γ is fixed by the anomaly cancellation condition, Eq. (5.19), to $\gamma = 3 - \alpha - \beta$. The region of the $(\beta, M_{Z'})$ parameter space below each curve will be excluded.

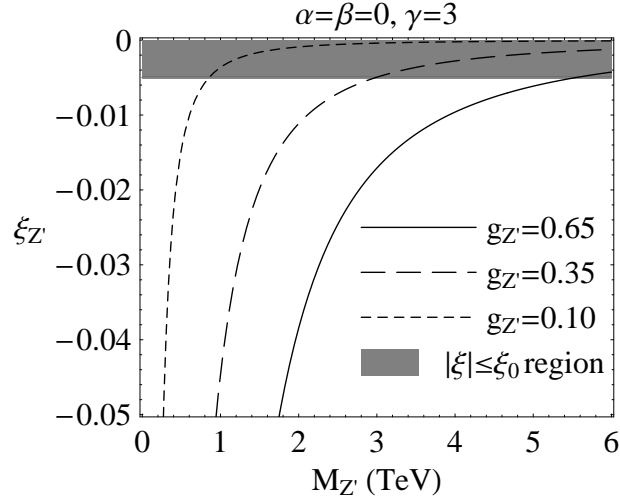


Figure 5.3: $\xi_{Z'}$ dependence on the Z' mass for the special case $\alpha = \beta = 0, \gamma = 3$.

(α, β, γ)	$g_{Z'}$	2σ (95%) limit from LEP/SLD [80]	95% limit from CDF [95]/D0 [37]	limit from $ \xi \leq \xi_0$ (99%)
$(0, 0, 3)$	0.65	580 GeV	~ 1 TeV	5500 GeV
	0.35	220 GeV	~ 0.6 TeV	3000 GeV
$(0, \frac{3}{2}, \frac{3}{2})$	0.65	500 GeV	880 GeV	—
	0.35	—	470 GeV	—

Table 5.2: Current and possible lower bounds on the Z' mass in gauged $B - \alpha L_3 - \beta L_\mu - \gamma L_\tau$ models.

Let us now look at existing bounds. We limit our attention to the $\alpha = 0$ case, i.e. the Z' couples to $B - \beta L_\mu - \gamma L_\tau$, with $\beta + \gamma = 3$. In this case, the Z' can be produced in $p\bar{p}$ collisions and subsequently decay into $\mu^+\mu^-$ or $\tau^+\tau^-$ pairs. The exchange of the Z' in this case leads to the following four-fermion interactions, relevant to $p\bar{p}$ colliders, between the charged leptons and the light quarks at energies way below the Z' mass:

$$\mathcal{L} = +\frac{\beta g_{Z'}^2}{3M_{Z'}^2} (\bar{u}\gamma^\mu u + \bar{d}\gamma^\mu d) (\bar{\mu}\gamma_\mu \mu) + \frac{\gamma g_{Z'}^2}{3M_{Z'}^2} (\bar{u}\gamma^\mu u + \bar{d}\gamma^\mu d) (\bar{\tau}\gamma_\mu \tau) . \quad (5.33)$$

D0 has searched for the contact interaction

$$\mathcal{L} = +\frac{4\pi}{\Lambda_+^2} (\bar{u}\gamma^\mu u + \bar{d}\gamma^\mu d) (\bar{\mu}\gamma_\mu \mu) \quad (5.34)$$

in its dimuon production data [37] and has set a 95% confidence level limit of

$$\Lambda_+ \geq 6.88 \text{ TeV} . \quad (5.35)$$

This translates into

$$\frac{M_{Z'}}{g_{Z'}} \geq \sqrt{|\beta|} \times (1.1 \text{ TeV}) . \quad (5.36)$$

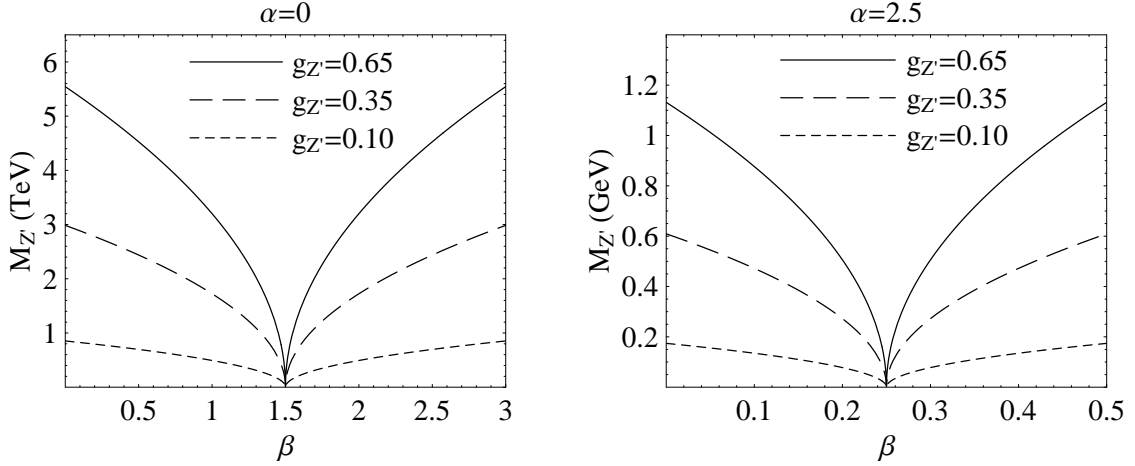


Figure 5.4: Lower bounds on Z' mass.

CDF has searched for the production of a Z' followed by its decay into $\tau^+\tau^-$ pairs [95] and has set a 95% confidence level lower bound of

$$M_{Z'} \geq 400 \text{ GeV} \quad (5.37)$$

for a sequential Z' (i.e. a Z' with the exact same couplings to the fermions as the SM Z). Rescaling to account for the difference in couplings, we estimate

$$\frac{M_{Z'}}{g_{Z'}} \gtrsim \sqrt{|\gamma|} \times (1 \text{ TeV}) . \quad (5.38)$$

Limits on this model also exist from a global analysis of loop effects in LEP/SLD data [80], but they are weaker than the direct search limits from the Tevatron. In Table 5.2, we compare the bounds from LEP/SLD, CDF/D0, and the potential bounds from a measurement of ξ for two choices of (α, β, γ) , and two choices for the value of $g_{Z'}$. For the $(\alpha, \beta, \gamma) = (0, 0, 3)$ case, we can expect a significant improvement over current bounds.

The sensitivity of the LHC to Z' s has been analyzed assuming Z' decay into e^+e^- or $\mu^+\mu^-$ pairs, or 2 jets [41]. For a sequential Z' , the LHC is sensitive to masses as heavy as 5 TeV with 100 fb^{-1} of integrated luminosity. The Z' of the $(\alpha, \beta, \gamma) = (0, 0, 3)$ model, however, decays mostly into $\tau^+\tau^-$, which will not provide as clean a signal as decays into the lighter charged lepton pairs. Ref. [96] estimates that if $g_{Z'} \sim g' \approx 0.35$, then the LHC reach will be up to about 1 TeV with 100 fb^{-1} . If this estimate is correct, the potential bound on $M_{Z'}$ from neutrino oscillation may be better than that from the LHC. A complete detector analysis may show that the actual reach of the LHC is somewhat higher, but even then we can expect the neutrino oscillation bound to be competitive with the LHC bound for the $(0, 0, 3)$ model.

5.2.3 Topcolor Assisted Technicolor

Another example of a model with a Z' which distinguishes among different generations is topcolor assisted technicolor [81, 82]. Models of this class are hybrids of topcolor and technicolor: the

	$SU(3)_s$	$SU(3)_w$	$U(1)_s$	$U(1)_w$	$SU(2)_L$
$(t, b)_L$	3	1	$\frac{1}{6}$	0	2
$(t, b)_R$	3	1	$\left(\frac{2}{3}, -\frac{1}{3}\right)$	0	1
$(\nu_\tau, \tau^-)_L$	1	1	$-\frac{1}{2}$	0	2
τ_R^-	1	1	-1	0	1
$(c, s)_L, (u, d)_L$	1	3	0	$\frac{1}{6}$	2
$(c, s)_R, (u, d)_R$	1	3	0	$\left(\frac{2}{3}, -\frac{1}{3}\right)$	1
$(\nu_\mu, \mu^-)_L, (\nu_e, e^-)_L$	1	1	0	$-\frac{1}{2}$	2
μ_R^-, e_R^-	1	1	0	-1	1

Table 5.3: Charge assignments of the ordinary fermions. The $U(1)$ charges are equal to the SM hypercharges normalized to $Q_{em} = I_3 + Y$.

topcolor interactions generate the large top-mass (and a fraction of the W and Z masses), while the technicolor interactions generate (the majority of) the W and Z masses. The models include a Z' in the topcolor sector, the interactions of which helps the top to condense, but prevents the bottom from doing so also. To extract the interactions of this Z' relevant to our discussion, we need to look at the model in some detail.

Though there are several different versions of topcolor assisted technicolor, we consider here the simplest in which the quarks and leptons transform under the gauge group

$$SU(3)_s \times SU(3)_w \times U(1)_s \times U(1)_w \times SU(2)_L \quad (5.39)$$

with coupling constants g_{3s} , g_{3w} , g_{1s} , g_{1w} , and g . It is assumed that $g_{3s} \gg g_{3w}$ and $g_{1s} \gg g_{1w}$. $SU(2)_L$ is the usual weak-isospin gauge group of the SM with coupling constant g . The charge assignments of the three generation of ordinary fermions under these gauge groups are given in Table 5.3. Note that each generation must transform non-trivially under only one of the $SU(3)$'s and one of the $U(1)$'s, and that those charges are the same as that of the SM color, and hypercharge Y (normalized to $Q_{em} = I_3 + Y$). This ensures anomaly cancellation.

At scale $\Lambda \sim 1$ TeV, technicolor, which is included in the model to generate the W and Z masses, is assumed to become strong and generate a condensate (of something which is left unspecified) which breaks the two $SU(3)$'s and the two $U(1)$'s to their diagonal subgroups:

$$SU(3)_s \times SU(3)_w \rightarrow SU(3)_c, \quad U(1)_s \times U(1)_w \rightarrow U(1)_Y, \quad (5.40)$$

which we identify with the usual SM color and hypercharge groups. The massless unbroken $SU(3)$ gauge bosons (the gluons G_μ^a) and the massive broken $SU(3)$ gauge bosons (the so called *colorons* C_μ^a) are related to the original $SU(3)_s \times SU(3)_w$ gauge fields $X_{s\mu}^a$ and $X_{w\mu}^a$ by

$$\begin{aligned} C_\mu &= X_{s\mu} \cos \theta_3 - X_{w\mu} \sin \theta_3 \\ G_\mu &= X_{s\mu} \sin \theta_3 + X_{w\mu} \cos \theta_3 \end{aligned} \quad (5.41)$$

where we have suppressed the color indices, and

$$\tan \theta_3 = \frac{g_{3w}}{g_{3s}}. \quad (5.42)$$

The currents to which the gluons and colorons couple to are:

$$g_{3s}J_{3s}^\mu X_{s\mu} + g_{3w}J_{3w}^\mu X_{w\mu} = g_3 (\cot \theta_3 J_{3s}^\mu - \tan \theta_3 J_{3w}^\mu) C_\mu + g_3 (J_{3s}^\mu + J_{3w}^\mu) G_\mu , \quad (5.43)$$

where

$$\frac{1}{g_3^2} = \frac{1}{g_{3s}^2} + \frac{1}{g_{3w}^2} . \quad (5.44)$$

Since the quarks carry only one of the $SU(3)$ charges, we can identify

$$J_3^\mu = J_{3s}^\mu + J_{3w}^\mu \quad (5.45)$$

as the QCD color current, and g_3 as the QCD coupling constant.

Similarly, the massless unbroken $U(1)$ gauge boson B_μ and the massive broken $U(1)$ gauge boson Z'_μ are related to the original $U(1)_s \times U(1)_w$ gauge fields $Y_{s\mu}$ and $Y_{w\mu}$ by

$$\begin{aligned} Z'_\mu &= Y_{s\mu} \cos \theta_1 - Y_{w\mu} \sin \theta_1 \\ B_\mu &= Y_{s\mu} \sin \theta_1 + Y_{w\mu} \cos \theta_1 \end{aligned} \quad (5.46)$$

where

$$\tan \theta_1 = \frac{g_{1w}}{g_{1s}} . \quad (5.47)$$

The currents to which the B_μ and Z'_μ couple to are:

$$g_{1s}J_{1s}^\mu Y_{s\mu} + g_{1w}J_{1w}^\mu Y_{w\mu} = g_1 (\cot \theta_1 J_{1s}^\mu - \tan \theta_1 J_{1w}^\mu) Z'_\mu + g_1 (J_{1s}^\mu + J_{1w}^\mu) B_\mu , \quad (5.48)$$

where

$$\frac{1}{g_1^2} = \frac{1}{g_{1s}^2} + \frac{1}{g_{1w}^2} . \quad (5.49)$$

Again, since the fermions carry only one of the $U(1)$ charges, we can identify

$$J_1^\mu = J_{1s}^\mu + J_{1w}^\mu \quad (5.50)$$

as the SM hypercharge current, and g_1 as the SM hypercharge coupling constant g' . Note that the interactions of the colorons and the Z' with the third generation fermions are strong, while their interactions with the first and second generation fermions are weak. This results in the formation of a top-condensate which accounts for the large mass of the top quark.²

Therefore, the interaction of the Z' in this model with the quarks and leptons is given by

$$\mathcal{L} = g' (\cot \theta_1 J_{1s}^\mu - \tan \theta_1 J_{1w}^\mu) Z'_\mu , \quad (5.51)$$

where g' is the SM hypercharge coupling, and

$$\begin{aligned} J_{1s}^\mu &= \frac{1}{6} (\bar{t}_L \gamma^\mu t_L + \bar{b}_L \gamma^\mu b_L) + \frac{2}{3} \bar{t}_R \gamma^\mu t_R - \frac{1}{3} \bar{b}_R \gamma^\mu b_R - \frac{1}{2} (\bar{\tau}_L \gamma^\mu \tau_L + \bar{\nu}_{\tau L} \gamma^\mu \nu_{\tau L}) - \bar{\tau}_R \gamma^\mu \tau_R , \\ J_{1w}^\mu &= \frac{1}{6} (\bar{c}_L \gamma^\mu c_L + \bar{s}_L \gamma^\mu s_L) + \frac{2}{3} \bar{c}_R \gamma^\mu c_R - \frac{1}{3} \bar{s}_R \gamma^\mu s_R - \frac{1}{2} (\bar{\mu}_L \gamma^\mu \mu_L + \bar{\nu}_{\mu L} \gamma^\mu \nu_{\mu L}) - \bar{\mu}_R \gamma^\mu \mu_R \\ &\quad + \frac{1}{6} (\bar{u}_L \gamma^\mu u_L + \bar{d}_L \gamma^\mu d_L) + \frac{2}{3} \bar{u}_R \gamma^\mu u_R - \frac{1}{3} \bar{d}_R \gamma^\mu d_R - \frac{1}{2} (\bar{e}_L \gamma^\mu e_L + \bar{\nu}_{e L} \gamma^\mu \nu_{e L}) - \bar{e}_R \gamma^\mu e_R . \end{aligned}$$

²The Z' -exchange interaction in the $t\bar{t}$ channel is attractive, but that in the $b\bar{b}$ channel is repulsive. This repulsion is assumed to be strong enough to counter the attraction due to the colorons and prevent the bottom from condensing.

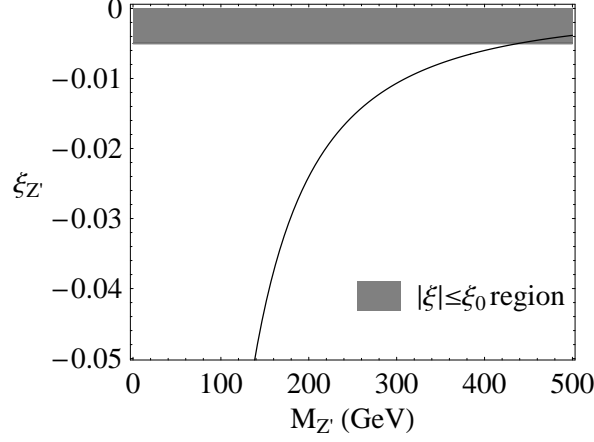


Figure 5.5: ξ_{TT} dependence on the Z' mass in the top color assisted technicolor model.

(5.52)

The exchange of the Z' leads to the current-current interaction

$$\frac{1}{2} (\cot \theta_1 J_{1s} - \tan \theta_1 J_{1w}) (\cot \theta_1 J_{1s} - \tan \theta_1 J_{1w}) , \quad (5.53)$$

the $J_{1s}J_{1s}$ part of which does not contribute to neutrino oscillations on the Earth, while the $J_{1w}J_{1w}$ part is suppressed relative to the $J_{1w}J_{1s}$ part by a factor of $\tan^2 \theta_1 \ll 1$. Therefore, we only need to consider the $J_{1s}J_{1w}$ interaction which only affects the propagation of $\nu_{\tau L}$ (*cf.* Fig. 5.2b). The forward scattering amplitude of $\nu_{\tau L}$ against fermion $F = p, n, e$ is given by

$$\begin{aligned} i\mathcal{M} &= (-ig' \cot \theta_1)(+ig' \tan \theta_1) \langle \nu_{\tau L} | \left(-\frac{1}{2} \bar{\nu}_\tau \gamma^\mu P_L \nu_\tau \right) | \nu_{\tau L} \rangle \frac{ig_{\mu\nu}}{M_{Z'}^2} \\ &\quad \times \langle F | \left[\bar{u} \gamma^\nu \left(\frac{1}{6} P_L + \frac{2}{3} P_R \right) u + \bar{d} \gamma^\nu \left(\frac{1}{6} P_L - \frac{1}{3} P_R \right) d + \bar{e} \gamma^\nu \left(-\frac{1}{2} P_L - P_R \right) e \right] | F \rangle \\ &\rightarrow -\frac{ig'^2}{2M_{Z'}^2} (\phi_{\nu_\tau}^\dagger \phi_{\nu_\tau}) \left[\frac{1}{2} \left(\frac{1}{6} + \frac{2}{3} \right) (2N_p + N_n) + \frac{1}{2} \left(\frac{1}{6} - \frac{1}{3} \right) (N_p + 2N_n) + \frac{1}{2} \left(-\frac{1}{2} - 1 \right) N_e \right] \\ &= -\frac{ig'^2}{2M_{Z'}^2} (\phi_{\nu_\tau}^\dagger \phi_{\nu_\tau}) \left(\frac{3}{4} N_p + \frac{1}{4} N_n - \frac{3}{4} N_e \right) \\ &= -\frac{ig'^2}{8M_{Z'}^2} (\phi_{\nu_\tau}^\dagger \phi_{\nu_\tau}) N_n \\ &\approx -i \left(\frac{g'^2}{M_{Z'}^2} \right) \frac{N}{8} (\phi_{\nu_\tau}^\dagger \phi_{\nu_\tau}) = -i V_{\nu_\tau} (\phi_{\nu_\tau}^\dagger \phi_{\nu_\tau}) . \end{aligned} \quad (5.54)$$

Note that the angle θ_1 has vanished from this expression and the only unknown parameter here is the Z' mass.

The effective potentials felt by the different neutrino flavors are

$$V_{\nu_e} = V_{\nu_\mu} = 0 , \quad V_{\nu_\tau} = +\frac{N}{8} \frac{g'^2}{M_{Z'}^2} , \quad (5.55)$$

and the effective ξ is

$$\xi_{TT} = \frac{V_{\nu\tau} - V_{\nu\mu}}{V_{CC}} = \frac{1}{2} \frac{(g'/M_{Z'})^2}{(g/M_W)^2} = \frac{1}{2} \tan^2 \theta_W \frac{M_W^2}{M_{Z'}^2} = \frac{1}{2} \sin^2 \theta_W \frac{M_Z^2}{M_{Z'}^2}. \quad (5.56)$$

The dependence of ξ_{TT} on the Z' mass is shown in Fig. 5.5. The limit $|\xi_{TT}| \leq \xi_0 = 0.005$ in this case translates to:

$$M_{Z'} \geq M_Z \sqrt{\frac{\sin^2 \theta_W}{2\xi_0}} \approx 440 \text{ GeV}. \quad (5.57)$$

This potential limit from the measurement of ξ is much weaker than what is already available from precision electroweak data [82], or from the direct search for $p\bar{p} \rightarrow Z'X \rightarrow \tau^+\tau^-X$ at CDF mentioned earlier [95].

5.3 Generation Non-Diagonal Leptoquarks

The review of the leptoquarks was presented in Chapter 2. Since the leptoquarks must distinguish among different generation fermions to contribute to neutrino oscillation matter effects, the leptoquark Lagrangian is given by Eq. (2.102). The interactions that contribute to neutrino oscillation matter effects are those with indices $(ij) = (12)$ and $(ij) = (13)$.

In the following, we calculate the effective value of ξ induced by the exchange of these leptoquarks. The leptoquark fields are naturally grouped into pairs from the way they couple to the quarks and leptons: (S_1, \vec{S}_3) , (S_2, \vec{S}_2) , (V_2, \vec{V}_2) , and (V_1, \vec{V}_3) . We treat each of these pairs in turn, and then discuss the potential bounds on the leptoquark couplings and masses.

5.3.1 S_1 and \vec{S}_3 leptoquarks

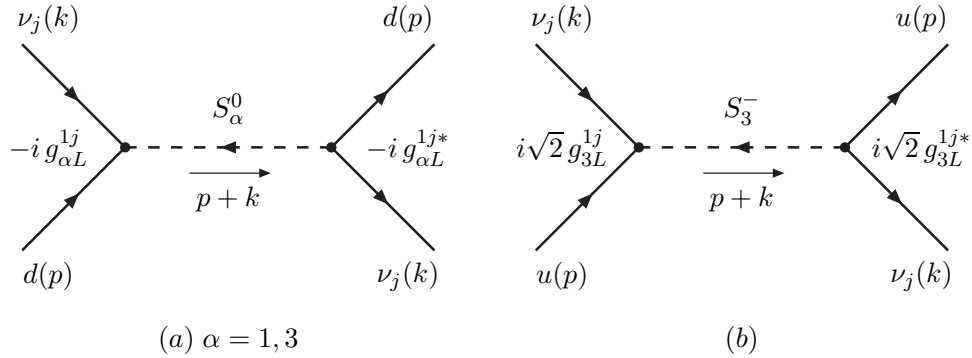


Figure 5.6: Diagrams contributing to neutrino oscillation matter effects from the exchange of (a) S_1^0 or the isospin 0 component of \vec{S}_3 , and (b) the isospin -1 component of \vec{S}_3 . The EM charge $Q_{em} = I_3 + Y$ for S_1^0 and S_3^0 are $+\frac{1}{3}$, while that for S_3^- is $-\frac{2}{3}$.

The $(ij) = (12)$ and (13) interactions of the leptoquarks S_1 and \vec{S}_3 are, respectively,

$$\mathcal{L} = -g_{1L}^{12}(\bar{d}_L^c \nu_{\mu L})S_1 - g_{1L}^{13}(\bar{d}_L^c \nu_{\tau L})S_1 + h.c., \quad (5.58)$$

and

$$\mathcal{L} = g_{3L}^{12} \left[-(\bar{d}_L^c \nu_{\mu L}) S_3^0 + \sqrt{2}(\bar{u}_L^c \nu_{\mu L}) S_3^- \right] + g_{3L}^{13} \left[-(\bar{d}_L^c \nu_{\tau L}) S_3^0 + \sqrt{2}(\bar{u}_L^c \nu_{\tau L}) S_3^- \right] + h.c. \quad (5.59)$$

The interactions described by Eqs. (5.58) and (5.59) can be written in a common general form as

$$\mathcal{L} = \lambda (\bar{q}^c P_L \nu) S + \lambda^* (\bar{\nu} P_R q^c) \bar{S}, \quad (5.60)$$

where $q = u$ or d . The Feynman diagrams contributing to neutrino oscillation matter effects are shown in Fig. 5.6. At momenta much smaller than the mass of the leptoquark, the corresponding matrix element is

$$i\mathcal{M} = (-i)^2 |\lambda|^2 \langle \nu, q | (\bar{\nu} P_R q^c) \left(\frac{-i}{M_S^2} \right) (\bar{q}^c P_L \nu) | \nu, q \rangle. \quad (5.61)$$

Using the Fierz rearrangement

$$(\bar{\nu} P_R q^c) (\bar{q}^c P_L \nu) = -\frac{1}{2} (\bar{\nu} \gamma^\mu P_L \nu) (\bar{q}^c \gamma_\mu P_R q^c) = +\frac{1}{2} (\bar{\nu} \gamma^\mu P_L \nu) (\bar{q} \gamma_\mu P_L q), \quad (5.62)$$

we obtain

$$i\mathcal{M} = \frac{i|\lambda|^2}{2M_S^2} \langle \nu | \bar{\nu} \gamma^\mu P_L \nu | \nu \rangle \langle q | \bar{q} \gamma_\mu P_L q | q \rangle \rightarrow i \frac{|\lambda|^2}{4M_S^2} N_q (\phi_\nu^\dagger \phi_\nu) = -iV_\nu (\phi_\nu^\dagger \phi_\nu), \quad (5.63)$$

where

$$V_\nu \equiv -\frac{N_q |\lambda|^2}{4 M_S^2}. \quad (5.64)$$

Applying this expression to the S_1 case, the effective potential for the neutrino of generation number j is:

$$V_{\nu_j} = -\frac{N_d |g_{1L}^{1j}|^2}{4 M_{S_1}^2} = -\frac{(N_p + 2N_n) |g_{1L}^{1j}|^2}{4 M_{S_1}^2} \approx -\frac{3N |g_{1L}^{1j}|^2}{4 M_{S_1}^2}, \quad (5.65)$$

The effective ξ is then

$$\xi_{S_1} = \frac{V_{\nu_3} - V_{\nu_2}}{V_{CC}} = +3 \frac{(|g_{1L}^{12}|^2 - |g_{1L}^{13}|^2)/M_{S_1}^2}{g^2/M_W^2}. \quad (5.66)$$

For the \vec{S}_3 case, the effective potential is

$$\begin{aligned} V_{\nu_j} &= -\frac{N_d |g_{3L}^{1j}|^2}{4 M_{S_3^0}^2} - \frac{N_u |g_{3L}^{1j}|^2}{2 M_{S_3^-}^2} \\ &= -|g_{3L}^{1j}|^2 \left[\frac{(N_p + 2N_n)}{4M_{S_3^0}^2} - \frac{(2N_p + N_n)}{2M_{S_3^-}^2} \right] \\ &\approx -\frac{3N}{4} |g_{3L}^{1j}|^2 \left(\frac{1}{M_{S_3^0}^2} + \frac{2}{M_{S_3^-}^2} \right), \end{aligned} \quad (5.67)$$

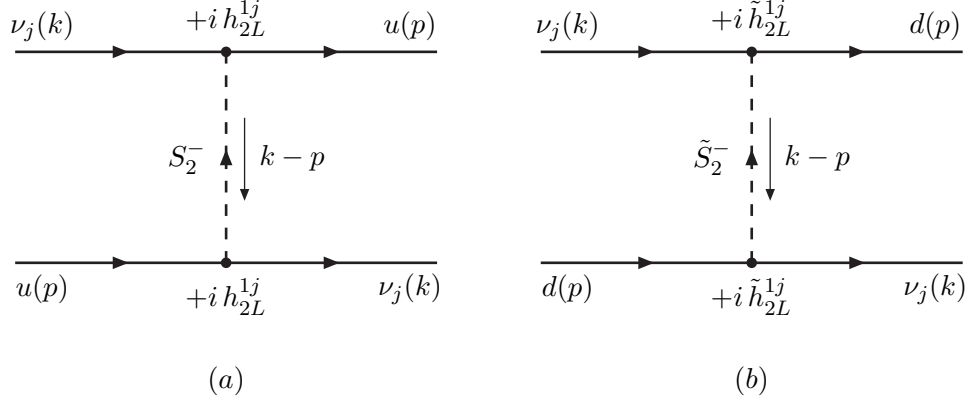


Figure 5.7: Diagrams contributing to neutrino oscillation matter effects from the exchange of (a) S_2^- , and (b) \tilde{S}_2^- . The EM charge $Q_{em} = I_3 + Y$ for S_2^- is $+\frac{2}{3}$, while that for \tilde{S}_2^- is $-\frac{1}{3}$.

and the effective ξ is

$$\xi_{\tilde{S}_3} = \frac{V_{\nu_3} - V_{\nu_2}}{V_{CC}} = +3 \frac{|g_{3L}^{12}|^2 - |g_{3L}^{13}|^2}{g^2/M_W^2} \left(\frac{1}{M_{S_3^0}^2} + \frac{2}{M_{S_3^-}^2} \right). \quad (5.68)$$

In the case of degenerate mass, $M_{S_3^0} = M_{S_3^-} \equiv M_{S_3}$, we have

$$\xi_{\tilde{S}_3} = +9 \frac{(|g_{3L}^{12}|^2 - |g_{3L}^{13}|^2)/M_{S_3}^2}{g^2/M_W^2}. \quad (5.69)$$

5.3.2 S_2 and \tilde{S}_2 leptoquarks

The relevant interactions are

$$\mathcal{L} = h_{2L}^{12} (\bar{u}_R \nu_{\mu L}) S_2^- + h_{2L}^{13} (\bar{u}_R \nu_{\tau L}) S_2^- + h.c. \quad (5.70)$$

for S_2^- and

$$\mathcal{L} = \tilde{h}_{2L}^{12} (\bar{d}_R \nu_{\mu L}) \tilde{S}_2^- + \tilde{h}_{2L}^{13} (\bar{d}_R \nu_{\tau L}) \tilde{S}_2^- + h.c. \quad (5.71)$$

for \tilde{S}_2^- leptoquarks. Both (5.70) and (5.71) can be written in a common general form as

$$\mathcal{L} = \lambda (\bar{q} P_L \nu) S + \lambda^* (\bar{\nu} P_R q) \bar{S}, \quad (5.72)$$

where $q = u$ or d . The Feynman diagram contributing to neutrino oscillation matter effects is shown in Fig. 5.7a. For momenta much smaller than the mass of the leptoquark, the corresponding matrix element is

$$i\mathcal{M} = (-i)^2 |\lambda|^2 \langle \nu, q | (\bar{\nu} P_R q) \left(\frac{-i}{M_S^2} \right) (\bar{q} P_L \nu) | \nu, q \rangle. \quad (5.73)$$

Using the Fierz identity given in Eq. (5.62) again, we obtain

$$i\mathcal{M} = -i \frac{|\lambda|^2}{2M_S^2} \langle \nu | \bar{\nu} \gamma^\mu P_L \nu | \nu \rangle \langle q | \bar{q} \gamma_\mu P_R q | q \rangle \rightarrow -i \frac{|\lambda|^2}{4M_S^2} N_q (\phi_\nu^\dagger \phi_\nu) = -i V_\nu (\phi_\nu^\dagger \phi_\nu), \quad (5.74)$$

where

$$V_\nu = +\frac{N_q |\lambda|^2}{4 M_S^2}. \quad (5.75)$$

Applying this expression to the S_2^- case, the effective potential for the neutrino of generation number j is

$$V_{\nu_j} = +\frac{N_u |h_{2L}^{1j}|^2}{4 M_{S_2^-}^2} = +\frac{(2N_p + N_n) |h_{2L}^{1j}|^2}{4 M_{S_2^-}^2} \approx +\frac{3N |h_{2L}^{1j}|^2}{4 M_{S_2^-}^2}, \quad (5.76)$$

and the effective ξ is

$$\xi_{S_2^-} = \frac{V_{\nu_3} - V_{\nu_2}}{V_{CC}} = -3 \frac{(|h_{2L}^{12}|^2 - |h_{2L}^{13}|^2)/M_{S_2^-}^2}{g^2/M_W^2}. \quad (5.77)$$

The effective potential for the \tilde{S}_2^- case is

$$V_{\nu_j} = +\frac{N_d |\tilde{h}_{2L}^{1j}|^2}{4 M_{\tilde{S}_2^-}^2} = +\frac{(N_p + 2N_n) |\tilde{h}_{2L}^{1j}|^2}{4 M_{\tilde{S}_2^-}^2} \approx +\frac{3N |\tilde{h}_{2L}^{1j}|^2}{4 M_{\tilde{S}_2^-}^2}, \quad (5.78)$$

and the effective ξ is

$$\xi_{\tilde{S}_2^-} = \frac{V_{\nu_3} - V_{\nu_2}}{V_{CC}} = -3 \frac{(|\tilde{h}_{2L}^{12}|^2 - |\tilde{h}_{2L}^{13}|^2)/M_{\tilde{S}_2^-}^2}{g^2/M_W^2}. \quad (5.79)$$

5.3.3 V_2 and \tilde{V}_2

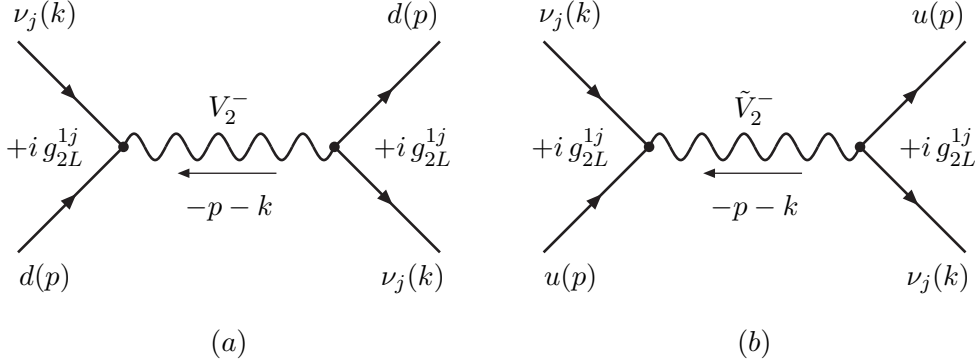


Figure 5.8: Diagrams contributing to neutrino oscillation matter effects from the exchange of (a) V_2^- , and (b) \tilde{V}_2^- . The EM charge $Q_{em} = I_3 + Y$ for V_2^- is $+\frac{1}{3}$, while that for \tilde{V}_2^- is $-\frac{2}{3}$.

The relevant interactions for V_2^- are

$$\mathcal{L} = g_{2L}^{12} (\bar{d}_R^c \gamma^\mu \nu_{\mu L}) V_{2\mu}^- + g_{2L}^{13} (\bar{d}_R^c \gamma^\mu \nu_{\tau L}) V_{2\mu}^- + h.c. \quad (5.80)$$

and those for \tilde{V}_2^- are

$$\mathcal{L} = \tilde{g}_{2L}^{12} (\bar{u}_R^c \gamma^\mu \nu_{\mu L}) \tilde{V}_{2\mu}^- + \tilde{g}_{2L}^{13} (\bar{u}_R^c \gamma^\mu \nu_{\tau L}) \tilde{V}_{2\mu}^- + h.c. \quad (5.81)$$

Both (5.80) and (5.81) can be written in a common general form as

$$\mathcal{L} = \lambda (\bar{q}^c \gamma^\mu P_L \nu) V_\mu + \lambda^* (\bar{\nu} \gamma^\mu P_L q^c) \bar{V}_\mu . \quad (5.82)$$

The Feynman diagrams contributing to neutrino oscillation matter effects are shown in Fig. 5.8. For momenta much smaller than the mass of the leptoquark the corresponding matrix element is

$$i\mathcal{M} = (-i)^2 |\lambda|^2 \langle \nu, q | (\bar{\nu} \gamma^\mu P_L q^c) \left(\frac{i}{M_V^2} \right) (\bar{q}^c \gamma_\mu P_L \nu) | \nu, q \rangle . \quad (5.83)$$

Using the Fierz rearrangement

$$(\bar{\nu} \gamma^\mu P_L q^c) (\bar{q}^c \gamma_\mu P_L \nu) = (\bar{\nu} \gamma^\mu P_L \nu) (\bar{q}^c \gamma_\mu P_L q^c) = -(\bar{\nu} \gamma^\mu P_L \nu) (\bar{q} \gamma_\mu P_R q) , \quad (5.84)$$

we obtain

$$i\mathcal{M} = i \frac{|\lambda|^2}{M_V^2} \langle \nu | \bar{\nu} \gamma^\mu P_L \nu | \nu \rangle \langle q | \bar{q} \gamma_\mu P_R q | q \rangle \rightarrow i \frac{|\lambda|^2}{2M_V^2} N_q (\phi_\nu^\dagger \phi_\nu) = -i V_\nu (\phi_\nu^\dagger \phi_\nu) , \quad (5.85)$$

where

$$V_\nu \equiv -\frac{N_q |\lambda|^2}{2 M_V^2} . \quad (5.86)$$

Applying this to the V_2^- case, the effective potential for the neutrino of generation number j is

$$V_{\nu_j} = -\frac{N_d |g_{2L}^{1j}|^2}{2 M_{V_2^-}^2} = -\frac{(N_p + 2N_n) |g_{2L}^{1j}|^2}{2 M_{V_2^-}^2} \approx -\frac{3N |g_{2L}^{1j}|^2}{2 M_{V_2^-}^2} . \quad (5.87)$$

The effective ξ is

$$\xi_{V_2^-} = \frac{V_{\nu_3} - V_{\nu_2}}{V_{CC}} = +6 \frac{(|g_{2L}^{12}|^2 - |g_{2L}^{13}|^2) / M_{V_2^-}^2}{g^2 / M_W^2} . \quad (5.88)$$

The effective potential for the \tilde{V}_2^- case is

$$V_{\nu_j} = -\frac{N_u |\tilde{g}_{2L}^{1j}|^2}{2 M_{\tilde{V}_2^-}^2} = -\frac{(2N_p + N_n) |\tilde{g}_{2L}^{1j}|^2}{2 M_{\tilde{V}_2^-}^2} \approx -\frac{N_u |\tilde{g}_{2L}^{1j}|^2}{2 M_{\tilde{V}_2^-}^2} . \quad (5.89)$$

The effective ξ is

$$\xi_{\tilde{V}_2^-} = \frac{V_{\nu_3} - V_{\nu_2}}{V_{CC}} = +6 \frac{(|\tilde{g}_{2L}^{12}|^2 - |\tilde{g}_{2L}^{13}|^2) / M_{\tilde{V}_2^-}^2}{g^2 / M_W^2} . \quad (5.90)$$

5.3.4 V_1 and \vec{V}_3 leptoquarks

The relevant interactions for V_1 are

$$\mathcal{L} = h_{1L}^{12} (\bar{u}_L \gamma^\mu \nu_{\mu L}) V_{1\mu} + h_{1L}^{13} (\bar{u}_L \gamma^\mu \nu_{\tau L}) V_{1\mu} + h.c. \quad (5.91)$$

and those for \vec{V}_3 are

$$\mathcal{L} = h_{3L}^{12} \left[(\bar{u}_L \gamma^\mu \nu_{\mu L}) V_{3\mu}^0 + \sqrt{2} (\bar{d}_L \gamma^\mu \nu_{\mu L}) V_{3\mu}^- \right]$$

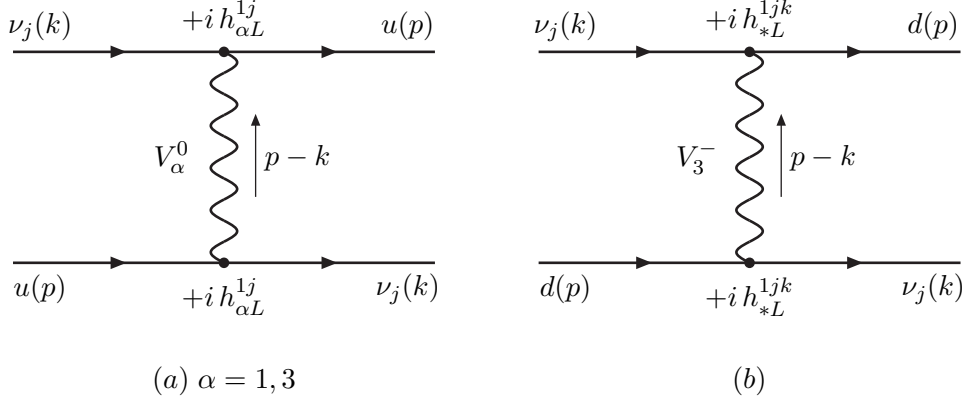


Figure 5.9: Diagrams contributing to neutrino oscillation matter effects from the exchange of (a) V_1^0 or the isospin 0 component of \vec{V}_3 , and (b) the isospin -1 component of \vec{V}_3 . The EM charges $Q_{em} = I_3 + Y$ for V_1^0 and V_3^0 are $+\frac{2}{3}$, while that for V_3^- is $-\frac{1}{3}$.

$$+h_{3L}^{13} \left[(\bar{u}_L \gamma^\mu \nu_{\tau L}) V_{3\mu}^0 + \sqrt{2} (\bar{d}_L \gamma^\mu \nu_{\tau L}) V_{3\mu}^- \right] + h.c. \quad (5.92)$$

The interactions described by Eqs. (5.91) and (5.92) can be written in a common general form as

$$\mathcal{L} = \lambda (\bar{q} \gamma^\mu P_L \nu) V + \lambda^* (\bar{\nu} \gamma^\mu P_L q) \bar{V} . \quad (5.93)$$

The Feynman diagrams contributing to neutrino oscillation matter effects are shown in Fig. 5.9. For momenta much smaller than the mass of the leptoquark the corresponding matrix element is

$$i\mathcal{M} = (-i)^2 |\lambda|^2 \langle \nu, q | (\bar{\nu} \gamma^\mu P_L q) \left(\frac{i}{M_V^2} \right) (\bar{q} \gamma_\mu P_L \nu) | \nu, q \rangle . \quad (5.94)$$

Using the Fierz identity given in Eq. (5.84) again, we find

$$i\mathcal{M} = -i \frac{|\lambda|^2}{M_V^2} \langle \nu | \bar{\nu} \gamma^\mu P_L \nu | \nu \rangle \langle q | \bar{q} \gamma_\mu P_L q | q \rangle \rightarrow -i \frac{|\lambda|^2}{2M_V^2} N_q (\phi_\nu^\dagger \phi_\nu) = -i V_\nu (\phi_\nu^\dagger \phi_\nu) , \quad (5.95)$$

where

$$V_\nu \equiv + \frac{N_q |\lambda|^2}{2 M_V^2} . \quad (5.96)$$

Applying this result to the V_1 case, effective potential is

$$V_{\nu_j} = + \frac{N_u |h_{1L}^{1j}|^2}{2 (M_{V_1})^2} = + \frac{(2N_p + N_n) |h_{1L}^{1j}|^2}{2 (M_{V_1})^2} \approx + \frac{3N |h_{1L}^{1j}|^2}{2 (M_{V_1})^2} . \quad (5.97)$$

The effective ξ is

$$\xi_{V_1} = \frac{V_{\nu_3} - V_{\nu_2}}{V_{CC}} = -6 \frac{(|h_{1L}^{12}|^2 - |h_{1L}^{13}|^2) / M_{V_1}^2}{g^2 / M_W^2} . \quad (5.98)$$

LQ	C_{LQ}	$\delta\lambda_{LQ}^2$	upper bound from $ \xi \leq \xi_0$	current bounds from Ref. [30]
S_1	+3	$ g_{1L}^{12} ^2 - g_{1L}^{13} ^2$	1.1×10^{-3}	$(g_{1L}^{12})^2 \leq 3.7 \times 10^{-3}$ (R_π) $(g_{1L}^{13})^2 \leq 0.7$ ($\tau \rightarrow \pi\nu$)
\vec{S}_3	+9	$ g_{3L}^{12} ^2 - g_{3L}^{13} ^2$	3.7×10^{-4}	$(g_{3L}^{12})^2 \leq 8 \times 10^{-4}$ (R_π) $(g_{3L}^{13})^2 \leq 0.7$ ($\tau \rightarrow \pi\nu$)
S_2	-3	$ h_{2L}^{12} ^2 - h_{2L}^{13} ^2$	1.1×10^{-3}	$(h_{2L}^{12})^2 \leq 1$ ($\mu N \rightarrow \mu X$)
\vec{S}_2	-3	$ \tilde{h}_{2L}^{12} ^2 - \tilde{h}_{2L}^{13} ^2$	1.1×10^{-3}	$(\tilde{h}_{2L}^{12})^2 \leq 2$ ($\mu N \rightarrow \mu X$)
V_2	+6	$ g_{2L}^{12} ^2 - g_{2L}^{13} ^2$	5.5×10^{-4}	$(g_{2L}^{12})^2 \leq 1$ ($\mu N \rightarrow \mu X$)
\vec{V}_2	+6	$ \tilde{g}_{2L}^{12} ^2 - \tilde{g}_{2L}^{13} ^2$	5.5×10^{-4}	$(\tilde{g}_{2L}^{12})^2 \leq 5$ ($\mu N \rightarrow \mu X$)
V_1	-6	$ h_{1L}^{12} ^2 - h_{1L}^{13} ^2$	5.5×10^{-4}	$(h_{1L}^{12})^2 \leq 1.8 \times 10^{-3}$ (R_π) $(h_{1L}^{13})^2 \leq 0.1$ ($D \rightarrow \mu\nu$)
\vec{V}_3	-18	$ h_{3L}^{12} ^2 - h_{3L}^{13} ^2$	1.8×10^{-4}	$(h_{3L}^{12})^2 \leq 4 \times 10^{-4}$ (R_π) $(h_{3L}^{13})^2 \leq 0.1$ ($D \rightarrow \mu\nu$)

Table 5.4: Constraints on the leptoquark couplings with all the leptoquark masses set to 100 GeV. To obtain the bounds for a different leptoquark mass M_{LQ} , simply rescale these numbers with the factor $(M_{LQ}/100 \text{ GeV})^2$.

The effective potential for the \vec{V}_3 case is

$$\begin{aligned}
V_{\nu_j} &= +\frac{N_u}{2} \frac{|h_{3L}^{1j}|^2}{M_{V_3^0}^2} + N_d \frac{|h_{3L}^{1j}|^2}{M_{V_3^-}^2} \\
&= +|h_{3L}^{1j}|^2 \left[\frac{(2N_p + N_n)}{2M_{V_3^0}^2} + \frac{(N_p + 2N_n)}{M_{V_3^-}^2} \right] \\
&\approx +\frac{3N}{2} |h_{3L}^{1j}|^2 \left(\frac{1}{M_{V_3^0}^2} + \frac{2}{M_{V_3^-}^2} \right). \tag{5.99}
\end{aligned}$$

The effective ξ is

$$\xi_{\vec{V}_3} = \frac{V_{\nu_3} - V_{\nu_2}}{V_{CC}} = -6 \frac{|h_{3L}^{12}|^2 - |h_{3L}^{13}|^2}{g^2/M_W^2} \left(\frac{1}{M_{V_3^0}^2} + \frac{2}{M_{V_3^-}^2} \right). \tag{5.100}$$

In the case of degenerate mass, $M_{V_3^0} = M_{V_3^-} \equiv M_{V_3}$, we have

$$\xi_{\vec{V}_3} = -18 \frac{(|h_{3L}^{12}|^2 - |h_{3L}^{13}|^2)/M_{V_3}^2}{g^2/M_W^2}. \tag{5.101}$$

5.3.5 Constraints on the Leptoquark Couplings and Masses

Assuming³ a common mass for leptoquarks in the same $SU(2)_L$ weak-isospin multiplet, the effective ξ due to the exchange of any particular type of leptoquark can be written in the form

$$\xi_{LQ} = C_{LQ} \frac{\delta\lambda_{LQ}^2/M_{LQ}^2}{g^2/M_W^2} = \frac{C_{LQ}}{4\sqrt{2}G_F} \left(\frac{\delta\lambda_{LQ}^2}{M_{LQ}^2} \right). \tag{5.102}$$

³The consideration given in this section overlaps to some extent with the consideration of section 2.4.1.

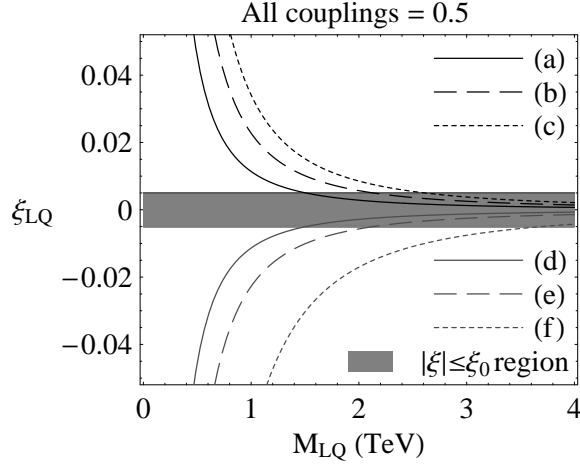


Figure 5.10: ξ_{LQ} dependence on the leptoquark mass for $\sqrt{\Delta\lambda_{LQ}^2} = 0.5$. (a) S_1 ; (b) V_2, \tilde{V}_2 ; (c) \vec{S}_3 ; (d) S_2, \tilde{S}_2 ; (e) V_1 ; (f) \vec{V}_3 .

Process	(ij)	LQ	Assumptions	95% CL bound	Reference
$p\bar{p} \rightarrow LQ \bar{L}\bar{Q} X \rightarrow (j\nu)(j\nu)X$	(**)	S	$\beta = 0^{(a)}$	117 GeV	CDF [31]
$p\bar{p} \rightarrow LQ \bar{L}\bar{Q} X \rightarrow (j\nu)(j\nu)X$	(**)	S	$\beta = 0$	135 GeV	D0 [32]
$p\bar{p} \rightarrow LQ \bar{L}\bar{Q} X \rightarrow (j\mu)(j\mu)X$	(*2)	S	$\beta = 0.5$	208 GeV	CDF [33]
$p\bar{p} \rightarrow LQ \bar{L}\bar{Q} X \rightarrow (j\mu)(j\nu)X$					
$p\bar{p} \rightarrow LQ \bar{L}\bar{Q} X \rightarrow (j\mu)(j\mu)X$	(*2)	S	$\beta = 0.5$	204 GeV	D0 [34]
$p\bar{p} \rightarrow LQ \bar{L}\bar{Q} X \rightarrow (j\mu)(j\nu)X$					
$p\bar{p} \rightarrow LQ \mu X \rightarrow (j\mu)\mu X$	(*2)	S	$\beta = 0.5, \lambda = 1^{(b)}$	226 GeV ^(c)	D0 [35]
$p\bar{p} \rightarrow LQ \bar{L}\bar{Q} X \rightarrow (j\tau)(j\tau)X$	(*3)	V	minimal coupling [97]	251 GeV	CDF [98]

Table 5.5: Direct search limits on the Leptoquark mass from the Tevatron. ^(a) β is the assumed branching fraction $B(LQ \rightarrow q\ell) = 1 - B(LQ \rightarrow q\nu)$, and ^(b) λ is the Yukawa coupling of the Leptoquark with the quark-lepton pair. ^(c)Combined bound with the pair production data.

Here, C_{LQ} is a constant prefactor, and $\delta\lambda_{LQ}^2$ represents

$$\delta\lambda_{LQ}^2 = |\lambda_{LQ}^{12}|^2 - |\lambda_{LQ}^{13}|^2, \quad (5.103)$$

where λ_{LQ}^{ij} is a generic coupling constant. The values of C_{LQ} and $\delta\lambda_{LQ}^2$ for the different types of leptoquark are listed in the first two columns of Table 5.4. In Fig. 5.10, we show how ξ_{LQ} depend on the leptoquark mass M_{LQ} for the choice $\sqrt{\delta\lambda_{LQ}^2} = 0.5$, where we have assumed $\delta\lambda_{LQ}^2 > 0$. To obtain the picture for the case when $\delta\lambda_{LQ}^2 < 0$, the vertical axis of the graph should be flipped. The constraint $|\xi_{LQ}| \leq \xi_0$ translates into:

$$M_{LQ} \geq M_W \sqrt{\frac{|\delta\lambda_{LQ}^2|}{g^2}} \sqrt{\frac{|C_{LQ}|}{\xi_0}} = \sqrt{\frac{|C_{LQ}||\delta\lambda_{LQ}^2|}{4\sqrt{2}G_F \xi_0}} \approx \sqrt{|C_{LQ}||\delta\lambda_{LQ}^2|} \times (1700 \text{ GeV}). \quad (5.104)$$

The resulting bounds are shown in Fig. 5.11, where the regions of the $(M_{LQ}, \sqrt{|\delta\lambda_{LQ}^2|})$ parameter space below each of the lines will be excluded. One can also fix the leptoquark mass and obtain

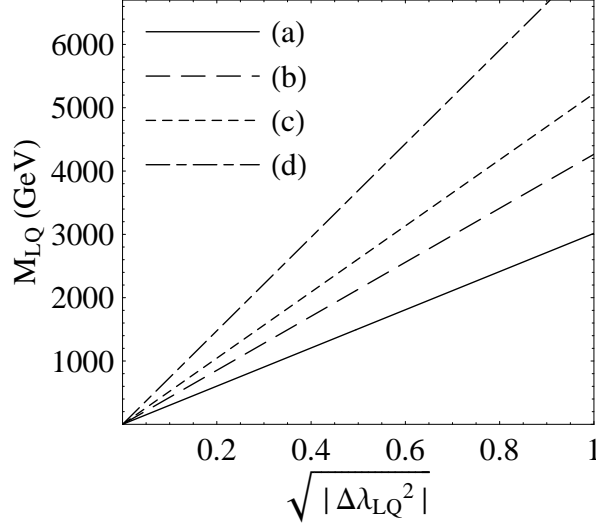


Figure 5.11: Lower bounds on the leptoquark masses. (a) S_1, S_2, \tilde{S}_2 ; (b) V_1, V_2, \tilde{V}_2 ; (c) \tilde{S}_3 ; (d) \tilde{V}_3 .

upper bounds on the leptoquark couplings:

$$|\delta\lambda_{LQ}^2| \leq \left(\frac{4\sqrt{2}G_F \xi_0}{|C_{LQ}|} \right) M_{LQ}^2 = \frac{3.3 \times 10^{-3}}{|C_{LQ}|} \left(\frac{M_{LQ}}{100 \text{ GeV}} \right)^2. \quad (5.105)$$

The values when $M_{LQ} = 100 \text{ GeV}$ are listed in the third column of Table 5.4. The bounds for a different choice of leptoquark mass M_{LQ} can be obtained by multiplying by a factor of $(M_{LQ}/100\text{GeV})^2$. This result can be compared with various indirect bounds from rare processes which are listed in the last column of Table 5.4⁴. As can be seen, the limits from $|\xi| \leq \xi_0$ can significantly improve existing bounds.

Limits on leptoquark masses from direct searches at the Tevatron are listed in Table 5.5. Bounds from LEP and LEP II are weaker due to their smaller center of mass energies. Since neutrino oscillation is only sensitive to leptoquarks with $(ij) = (12)$ and/or $(ij) = (13)$ couplings, we only quote limits which apply to leptoquarks with *only* those particular couplings, that is, leptoquarks that decay into a first generation quark, and either a second or third generation lepton. Though it is usually stated in collider analyses that leptoquarks are assumed to decay into a quark-lepton pair of one particular generation, it is often the case that the jets coming from the quarks are not flavor tagged. Analyses that look for the leptoquark in the quark-neutrino decay channel are of course blind to the flavor of the neutrino. Therefore, the bounds listed apply to leptoquarks with generation non-diagonal couplings also.

As can be seen from Table 5.5, the mass bounds from the Tevatron are typically around 200 GeV and are mostly independent of the leptoquark-quark-lepton coupling λ . This independence is due to the dominance of the strong interaction processes, $q\bar{q}$ annihilation and gluon fusion, in the leptoquark pair-production cross sections, and the fact that heavy leptoquarks decay without a displaced vertex even for very small values of λ : the decay widths of scalar and vector leptoquarks

⁴We updated the limits of Ref. [30] extracted from the measured value of R_π .

with leptoquark-quark-lepton coupling λ are given by $\lambda^2 M_{LQ}/16\pi$ and $\lambda^2 M_{LQ}/24\pi$, respectively, which correspond to lifetimes of $O(10^{-21})$ seconds for $M_{LQ} = O(10^2)$ GeV, and $\lambda = O(10^{-2})$. In contrast, the potential bound on M_{LQ} from neutrino oscillation, Eq. (5.104), depends on the coupling $\sqrt{|C_{LQ}||\delta\lambda_{LQ}^2|}$, but can be expected to be stronger than the existing ones for $\sqrt{|C_{LQ}||\delta\lambda_{LQ}^2|}$ as small as 0.1.

Bounds on leptoquarks with $(ij) = (12)$ couplings can also be obtained from bounds on contact interactions of the form

$$\mathcal{L} = \pm \frac{4\pi}{(\Lambda_{q\mu}^\pm)^2} (\bar{q}\gamma^\mu P_X q) (\bar{\mu}\gamma_\mu P_L \mu) , \quad (5.106)$$

where $X = L$ or R , and $q = u$ or d . For instance, at energies much lower than the leptoquark mass, the exchange of the S_1 leptoquark leads to the interaction

$$\mathcal{L}_{S_1} = + \frac{|g_{1L}^{12}|^2}{2M_{S_1}^2} (\bar{u}\gamma^\mu P_L u) (\bar{\mu}\gamma_\mu P_L \mu) . \quad (5.107)$$

The remaining cases are listed in Table 5.6. The 95% CL lower bounds on the $\Lambda_{q\ell}^\pm$'s from CDF can be found in Ref. [36], and the cases relevant to our discussion are listed in Table 5.7. These bounds translate into bounds on the leptoquark masses and couplings listed in Table 5.6. Clearly, the potential bounds from $|\xi| < \xi_0$, also listed in Table 5.6, are much stronger. It should be noted, though, that the results of Ref. [36] are from Tevatron Run I, and we can expect the Run II results to improve these bounds. Indeed, Ref. [37] from D0 analyzes the Run II data for contact interactions of the form

$$\mathcal{L} = \pm \frac{4\pi}{(\Lambda^\pm)^2} (\bar{u}\gamma^\mu P_X u + \bar{d}\gamma^\mu P_X d) (\bar{\mu}\gamma_\mu P_L \mu) , \quad X = L \text{ or } R , \quad (5.108)$$

and places 95% CL lower bounds on the Λ^\pm 's in the $4 \sim 7$ TeV range. While these are not exactly the interactions induced by leptoquarks, we can nevertheless expect that the bounds on the $\Lambda_{q\mu}^\pm$'s will be in a similar range, and thereby conclude that the Run II data will roughly double the lower bounds from Run I. Even then, Table 5.6 indicates that the potential bounds from $|\xi| < \xi_0$ will be much stronger.

The prospects for leptoquark discovery at the LHC are discussed in Refs. [41, 42]. At the LHC, leptoquarks can be pair-produced via gluon fusion and quark-antiquark annihilation, or singly-produced with an accompanying lepton via quark-gluon fusion. The pair-production cross section is dominated by gluon fusion, which does not involve the leptoquark-quark-lepton coupling λ , and is therefore independent of the details assumed for the leptoquark interactions. Once produced, each leptoquark will decay into a lepton plus jet, regardless of whether the coupling is generation diagonal or not. The leptoquark width in this decay depends on λ , but it is too narrow compared to the calorimeter resolution for the λ -dependence to be of relevance in the analyses. Therefore, though the analyses of Refs. [41, 42] assume specific values of λ and generation diagonal couplings, we expect their conclusions to apply equally well to different λ -values and generation non-diagonal cases: for $\beta = B(LQ \rightarrow q\ell) = 0.5$, the expected sensitivity is up to $M_{LQ} \approx 1$ TeV with 30^{-1} fb of data [42]. Again, in contrast, the the potential bound from neutrino oscillation, Eq. (5.104), depends on the coupling $\sqrt{|C_{LQ}||\delta\lambda_{LQ}^2|}$. If $\sqrt{|C_{LQ}||\delta\lambda_{LQ}^2|} = O(1)$, then Eq. (5.104) will be competitive with the expected LHC bound.

LQ	Induced Interaction	CDF 95% CL [36]	$ \xi < \xi_0$
S_1	$+\frac{ g_{1L}^{12} ^2}{2M_{S_1}^2} (\bar{u}\gamma^\mu P_L u) (\bar{\mu}\gamma_\mu P_L \mu)$	$\frac{M_{S_1}}{ g_{1L}^{12} } \geq 0.68 \text{ TeV}$	$\frac{M_{S_1}}{\sqrt{\delta g_{1L}^2}} \geq 3.0 \text{ TeV}$
S_2	$-\frac{ h_{2L}^{12} ^2}{2M_{S_2}^2} (\bar{u}\gamma^\mu P_R u) (\bar{\mu}\gamma_\mu P_L \mu)$	$\frac{M_{S_2}}{ h_{2L}^{12} } \geq 0.72 \text{ TeV}$	$\frac{M_{S_2}}{\sqrt{\delta h_{2L}^2}} \geq 3.0 \text{ TeV}$
\tilde{S}_2	$-\frac{ \tilde{h}_{2L}^{12} ^2}{2M_{\tilde{S}_2}^2} (\bar{d}\gamma^\mu P_R d) (\bar{\mu}\gamma_\mu P_L \mu)$	$\frac{M_{\tilde{S}_2}}{ \tilde{h}_{2L}^{12} } \geq 0.38 \text{ TeV}$	$\frac{M_{\tilde{S}_2}}{\sqrt{\delta \tilde{h}_{2L}^2}} \geq 3.0 \text{ TeV}$
S_3	$+\frac{ g_{3L}^{12} ^2}{2M_{S_3}^2} (\bar{u}\gamma^\mu P_L u + 2\bar{d}\gamma^\mu P_L d) (\bar{\mu}\gamma_\mu P_L \mu)$	—	$\frac{M_{S_3}}{\sqrt{\delta g_{3L}^2}} \geq 5.2 \text{ TeV}$
V_1	$-\frac{ h_{1L}^{12} ^2}{M_{V_1}^2} (\bar{d}\gamma^\mu P_L d) (\bar{\mu}\gamma_\mu P_L \mu)$	$\frac{M_{V_1}}{ h_{1L}^{12} } \geq 0.48 \text{ TeV}$	$\frac{M_{V_1}}{\sqrt{\delta h_{1L}^2}} \geq 4.3 \text{ TeV}$
V_2	$+\frac{ g_{2L}^{12} ^2}{M_{V_2}^2} (\bar{d}\gamma^\mu P_R d) (\bar{\mu}\gamma_\mu P_L \mu)$	$\frac{M_{V_2}}{ g_{2L}^{12} } \geq 0.56 \text{ TeV}$	$\frac{M_{V_2}}{\sqrt{\delta g_{2L}^2}} \geq 4.3 \text{ TeV}$
\tilde{V}_2	$+\frac{ \tilde{g}_{2L}^{12} ^2}{M_{\tilde{V}_2}^2} (\bar{u}\gamma^\mu P_R u) (\bar{\mu}\gamma_\mu P_L \mu)$	$\frac{M_{\tilde{V}_2}}{ \tilde{g}_{2L}^{12} } \geq 0.85 \text{ TeV}$	$\frac{M_{\tilde{V}_2}}{\sqrt{\delta \tilde{g}_{2L}^2}} \geq 4.3 \text{ TeV}$
V_3	$-\frac{ h_{3L}^{12} ^2}{M_{V_1}^2} (2\bar{u}\gamma^\mu P_L u + \bar{d}\gamma^\mu P_L d) (\bar{\mu}\gamma_\mu P_L \mu)$	—	$\frac{M_{V_3}}{\sqrt{\delta h_{3L}^2}} \geq 7.4 \text{ TeV}$

Table 5.6: The quark-muon interactions induced by leptoquark exchange, and the bounds from CDF [36] compared with potential bounds from neutrino oscillations. Only the couplings that also contribute to neutrino oscillation are listed. Analysis of the Tevatron Run II data is expected to improve the CDF bound by a factor of two.

$(q\mu)$ chirality	$\Lambda_{u\mu}^+$ (TeV)	$\Lambda_{u\mu}^-$ (TeV)	$\Lambda_{d\mu}^+$ (TeV)	$\Lambda_{d\mu}^-$ (TeV)
(LL)	3.4	4.1	2.3	1.7
(RL)	3.0	3.6	2.0	1.9

Table 5.7: The 95% CL lower bound on the compositeness scale from CDF [36]. Results from D0 [37] do not provide limits for cases where the muons couple to only u or d , but we expect the bounds to be in the range $4 \sim 7$ TeV.

5.4 SUSY Standard Model with R-parity Violation

Let us next consider contributions from R-parity violating couplings. Assuming the particle content of the Minimal Supersymmetric Standard Model (MSSM), the most general R-parity violating superpotential (involving only tri-linear couplings) has the form [77]

$$W_{\mathcal{R}} = \frac{1}{2} \lambda_{ijk} \hat{L}_i \hat{L}_j \hat{E}_k + \lambda'_{ijk} \hat{L}_i \hat{Q}_j \hat{D}_k + \frac{1}{2} \lambda''_{ijk} \hat{U}_i \hat{D}_j \hat{D}_k, \quad (5.109)$$

where \hat{L}_i , \hat{E}_i , \hat{Q}_i , \hat{D}_i , and \hat{U}_i are the left-handed MSSM superfields defined in the usual fashion, and the subscripts $i, j, k = 1, 2, 3$ are the generation indices. (Note, however, that in some references, such as Ref. [78], the isospin singlet superfields \hat{E}_i , \hat{D}_i , and \hat{U}_i are defined to be right-handed, so the corresponding left-handed fields in Eq. (5.109) appear with a superscript c indicating charge-conjugation.) $SU(2)_L$ gauge invariance requires the couplings λ_{ijk} to be antisymmetric in the first two indices:

$$\lambda_{ijk} = -\lambda_{jik}, \quad (5.110)$$

whereas $SU(3)$ gauge invariance requires the couplings λ''_{ijk} to be antisymmetric in the latter two:

$$\lambda''_{ijk} = -\lambda''_{ikj}. \quad (5.111)$$

These conditions reduce the number of R-parity violating couplings in Eq. (5.109) to 45 (9 λ_{ijk} , 27 λ'_{ijk} , and 9 λ''_{ijk}). The purely baryonic operator $\hat{U}_i \hat{D}_j \hat{D}_k$ is irrelevant to our discussion on neutrino oscillation so we will not consider the λ''_{ijk} couplings further. We also neglect possible bilinear R-parity violating couplings which have the effect of mixing the neutrinos with the neutral higgsino; their effect on neutrino oscillation has been discussed extensively by many authors [78, 99, 100].

5.4.1 $\hat{L}\hat{L}\hat{E}$ couplings

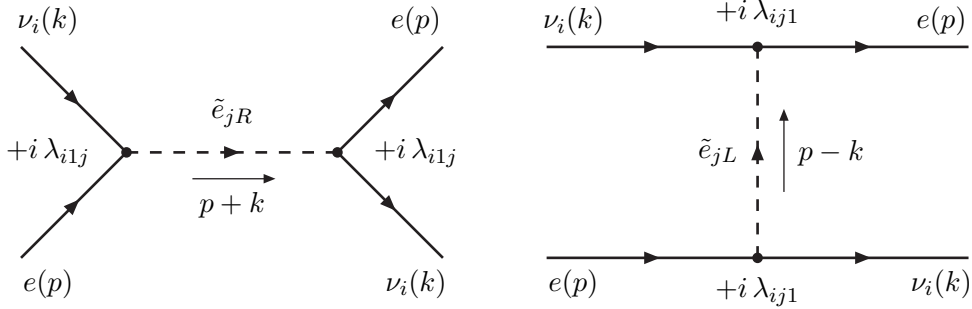


Figure 5.12: LLE interactions that contribute to neutrino oscillation matter effects..

The $\hat{L}\hat{L}\hat{E}$ part of the R-parity violating Lagrangian, Eq. (5.109), expressed in terms of the component fields is

$$\mathcal{L}_{LLE} = \lambda_{ijk} [\tilde{\nu}_{iL} \overline{e_{kR}} e_{jL} + \tilde{e}_{jL} \overline{e_{kR}} \nu_{iL} + \tilde{e}_{kR}^* \overline{\nu_{iL}} e_{jL}] + h.c. \quad (5.112)$$

The second and third terms of this Lagrangian, together with their hermitian conjugates, contribute to neutrino oscillation matter effects. The corresponding Feynman diagrams are shown in Fig 5.12. Since λ_{ijk} is antisymmetric under $i \leftrightarrow j$, it follows that $i \neq j$. Calculations similar to those for the scalar leptoquarks yield

$$V_{\tilde{e}}(\nu_i) = \frac{N_e}{4} \left(\sum_{j \neq i} \frac{|\lambda_{ij1}|^2}{M_{\tilde{e}_{jL}}^2} - \sum_j \frac{|\lambda_{i1j}|^2}{M_{\tilde{e}_{jR}}^2} \right), \quad (5.113)$$

or if we write everything out explicitly:

$$\begin{aligned} V_{\tilde{e}}(\nu_2) &= \frac{N_e}{4} \left(\frac{|\lambda_{211}|^2}{M_{\tilde{e}_{1L}}^2} + \frac{|\lambda_{231}|^2}{M_{\tilde{e}_{3L}}^2} - \frac{|\lambda_{211}|^2}{M_{\tilde{e}_{1R}}^2} - \frac{|\lambda_{212}|^2}{M_{\tilde{e}_{2R}}^2} - \frac{|\lambda_{213}|^2}{M_{\tilde{e}_{3R}}^2} \right), \\ V_{\tilde{e}}(\nu_3) &= \frac{N_e}{4} \left(\frac{|\lambda_{311}|^2}{M_{\tilde{e}_{1L}}^2} + \frac{|\lambda_{321}|^2}{M_{\tilde{e}_{2L}}^2} - \frac{|\lambda_{311}|^2}{M_{\tilde{e}_{1R}}^2} - \frac{|\lambda_{312}|^2}{M_{\tilde{e}_{2R}}^2} - \frac{|\lambda_{313}|^2}{M_{\tilde{e}_{3R}}^2} \right). \end{aligned} \quad (5.114)$$

The effective ξ is

$$\begin{aligned} \xi_{\tilde{e}} &= \frac{V_{\tilde{e}}(\nu_3) - V_{\tilde{e}}(\nu_2)}{V_{CC}} \\ &= \frac{1}{g^2/M_W^2} \left(- \sum_{j=1,3} \frac{|\lambda_{2j1}|^2}{M_{\tilde{e}_{jL}}^2} - \sum_{j=1,2} \frac{|\lambda_{3j1}|^2}{M_{\tilde{e}_{jL}}^2} + \sum_{j=1}^3 \frac{|\lambda_{21j}|^2 - |\lambda_{31j}|^2}{M_{\tilde{e}_{jR}}^2} \right) \end{aligned}$$

$$\begin{aligned}
&= \frac{1}{g^2/M_W^2} \left[(|\lambda_{211}|^2 - |\lambda_{311}|^2) \left(\frac{1}{M_{\tilde{e}_{1R}}^2} - \frac{1}{M_{\tilde{e}_{1L}}^2} \right) \right. \\
&\quad \left. + |\lambda_{231}|^2 \left(\frac{1}{M_{\tilde{e}_{2L}}^2} - \frac{1}{M_{\tilde{e}_{3L}}^2} \right) + \frac{|\lambda_{212}|^2 - |\lambda_{312}|^2}{M_{\tilde{e}_{2R}}^2} + \frac{|\lambda_{213}|^2 - |\lambda_{313}|^2}{M_{\tilde{e}_{3R}}^2} \right]. \quad (5.115)
\end{aligned}$$

For degenerate s-electron masses $M_{\tilde{e}_{jL}} = M_{\tilde{e}_{jR}} \equiv M_{\tilde{e}_j}$, we have

$$\xi_{\tilde{e}} = \frac{1}{g^2/M_W^2} \left(\frac{|\lambda_{231}|^2 + |\lambda_{122}|^2 - |\lambda_{132}|^2}{M_{\tilde{e}_2}^2} - \frac{|\lambda_{231}|^2 - |\lambda_{123}|^2 + |\lambda_{133}|^2}{M_{\tilde{e}_3}^2} \right), \quad (5.116)$$

where we have used $\lambda_{ijk} = -\lambda_{jik}$ to reorder the indices.

5.4.2 $\hat{L}\hat{Q}\hat{D}$ couplings

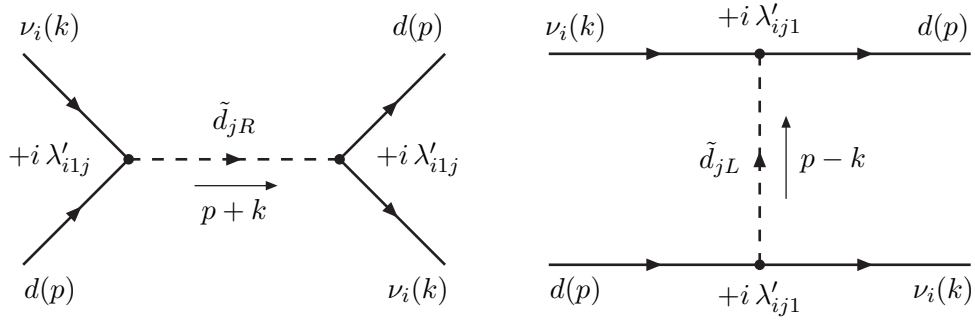


Figure 5.13: LQD interactions that contribute to neutrino oscillation matter effects..

The $\hat{L}\hat{Q}\hat{D}$ part of the R-parity violating Lagrangian expressed in terms of the component fields is

$$\begin{aligned}
\mathcal{L}_{LQD} &= \lambda'_{ijk} \left[\tilde{\nu}_{iL} \bar{d}_{kR} d_{jL} + \tilde{d}_{jL} \bar{d}_{kR} \nu_{iL} + \tilde{d}_{kR}^* \bar{\nu}_{iL}^c d_{jL} \right. \\
&\quad \left. - \left(\tilde{e}_{iL} \bar{d}_{kR} u_{jL} + \tilde{u}_{jL} \bar{d}_{kR} e_{iL} + \tilde{d}_{kR}^* \bar{e}_{iL}^c u_{jL} \right) \right] + h.c. \quad (5.117)
\end{aligned}$$

The second and third terms of this Lagrangian, together with their hermitian conjugates, contribute to neutrino oscillation matter effects. The corresponding Feynman diagrams are shown in Fig 5.13. Calculations similar to those for the scalar leptoquarks lead to the following effective potential for neutrino flavor ν_i :

$$V_{\tilde{d}}(\nu_i) = \sum_{j=1}^3 \frac{N_p + 2N_n}{4} \left(\frac{|\lambda'_{ij1}|^2}{M_{\tilde{d}_{jL}}^2} - \frac{|\lambda'_{ij1}|^2}{M_{\tilde{d}_{jR}}^2} \right) \approx \sum_{j=1}^3 \frac{3N}{4} \left(\frac{|\lambda'_{ij1}|^2}{M_{\tilde{d}_{jL}}^2} - \frac{|\lambda'_{ij1}|^2}{M_{\tilde{d}_{jR}}^2} \right). \quad (5.118)$$

The effective ξ is

$$\xi_{\tilde{d}} = \frac{V_{\tilde{d}}(\nu_3) - V_{\tilde{d}}(\nu_2)}{V_{CC}}$$

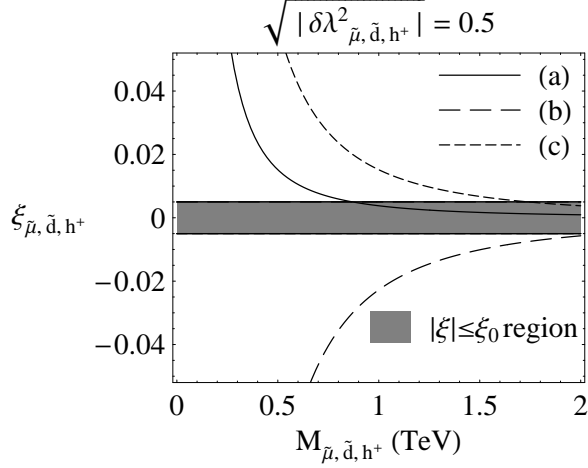


Figure 5.14: Dependence of $\xi_{\tilde{\mu}, \tilde{d}, h^\pm}$ on the smuon, sdown, and h^\pm masses for $\sqrt{|\delta\lambda_{\tilde{\mu}, \tilde{d}, h^\pm}^2|} = 0.5$ in the (a) $\hat{L}\hat{L}\hat{E}$ R-parity violating interaction; (b) $\hat{L}\hat{Q}\hat{D}$ R-parity violating interaction; and (c) the Zee/Babu-Zee models.

$$= -3 \sum_{j=1}^3 \frac{\left(|\lambda'_{2j1}|^2 - |\lambda'_{3j1}|^2 \right) / M_{\tilde{d}_{jL}}^2 - \left(|\lambda'_{21j}|^2 - |\lambda'_{31j}|^2 \right) / M_{\tilde{d}_{jR}}^2}{g^2 / M_W^2}. \quad (5.119)$$

For degenerate d -squark masses $M_{\tilde{d}_{jL}} = M_{\tilde{d}_{jR}} \equiv M_{\tilde{d}_j}$, we have

$$\xi_{\tilde{d}} = -3 \sum_{j=1}^3 \frac{\left(|\lambda'_{2j1}|^2 - |\lambda'_{3j1}|^2 + |\lambda'_{21j}|^2 - |\lambda'_{31j}|^2 \right) / M_{\tilde{d}_j}^2}{g^2 / M_W^2}. \quad (5.120)$$

5.4.3 Constraints on the R-parity Violating Couplings and Squark/Slepton Masses

To illustrate our result for R-parity violating interactions, we simplify the analysis by assuming that only the λ_{122} and λ_{132} couplings are non-zero for the $\hat{L}\hat{L}\hat{E}$ case, and only the λ'_{211} and λ'_{311} couplings are non-zero for the $\hat{L}\hat{Q}\hat{D}$ case. Under these assumptions, only the smuon, $\tilde{e}_2 = \tilde{\mu}$, contributes in the first case, and only the sdown, $\tilde{d}_1 = \tilde{d}$, contributes in the latter. The corresponding ξ 's are

$$\begin{aligned} \xi_{\tilde{\mu}} &= + \frac{\delta\lambda_{\tilde{\mu}}^2 / M_{\tilde{\mu}}^2}{(g/M_W)^2} = + \frac{1}{4\sqrt{2}G_F} \left(\frac{\delta\lambda_{\tilde{\mu}}^2}{M_{\tilde{\mu}}^2} \right), \\ \xi_{\tilde{d}} &= -6 \frac{\delta\lambda_{\tilde{d}}^2 / M_{\tilde{d}}^2}{(g/M_W)^2} = - \frac{6}{4\sqrt{2}G_F} \left(\frac{\delta\lambda_{\tilde{d}}^2}{M_{\tilde{d}}^2} \right), \end{aligned} \quad (5.121)$$

where

$$\begin{aligned} \delta\lambda_{\tilde{\mu}}^2 &\equiv |\lambda_{122}|^2 - |\lambda_{132}|^2, \\ \delta\lambda_{\tilde{d}}^2 &\equiv |\lambda'_{211}|^2 - |\lambda'_{311}|^2. \end{aligned} \quad (5.122)$$

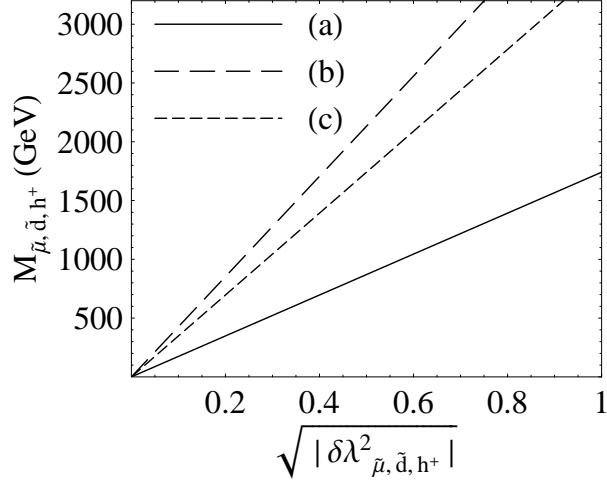


Figure 5.15: Lower bounds on (a) the smuon mass in the $\hat{L}\hat{L}\hat{E}$ R-parity violating interaction model, (b) the sdown mass in the $\hat{L}\hat{Q}\hat{D}$ R-parity violating interaction model, and (c) the h^\pm mass in the Zee/Babu-Zee models, respectively.

Fig. 5.14 shows how $\xi_{\tilde{\mu}}$ and $\xi_{\tilde{d}}$ depend on masses of the smuon and the sdown for a specific choice of couplings: $\sqrt{\delta\lambda_{\tilde{\mu}}^2} = \sqrt{\delta\lambda_{\tilde{d}}^2} = 0.5$ (we have assumed $\delta\lambda_{\tilde{d}}^2$ and $\delta\lambda_{\tilde{\mu}}^2$ to be positive). The bound $|\xi| \leq \xi_0 = 0.005$ translates into:

$$\begin{aligned}
 M_{\tilde{\mu}} &\geq \sqrt{|\delta\lambda_{\tilde{\mu}}^2|} \sqrt{\frac{1}{4\sqrt{2}G_F\xi_0}} \approx \sqrt{|\delta\lambda_{\tilde{\mu}}^2|} \times (1700 \text{ GeV}) , \\
 M_{\tilde{d}} &\geq \sqrt{|\delta\lambda_{\tilde{d}}^2|} \sqrt{\frac{6}{4\sqrt{2}G_F\xi_0}} \approx \sqrt{|\delta\lambda_{\tilde{d}}^2|} \times (4300 \text{ GeV}) .
 \end{aligned} \tag{5.123}$$

The resulting graphs for the lower mass bounds are shown in Fig. 5.15. The regions of the $(M_{\tilde{\mu}}, \sqrt{|\delta\lambda_{\tilde{\mu}}^2|})$ and $(M_{\tilde{d}}, \sqrt{|\delta\lambda_{\tilde{d}}^2|})$ parameter spaces below each of the lines are excluded. One can also fix the smuon and sdown masses and obtain upper bounds on the R-parity violating couplings:

$$\begin{aligned}
 \sqrt{|\delta\lambda_{\tilde{\mu}}^2|} &\leq \sqrt{4\sqrt{2}G_F\xi_0} M_{\tilde{\mu}} = (0.057) \left(\frac{M_{\tilde{\mu}}}{100 \text{ GeV}} \right) , \\
 \sqrt{|\delta\lambda_{\tilde{d}}^2|} &\leq \sqrt{\frac{4\sqrt{2}G_F\xi_0}{6}} M_{\tilde{d}} = (0.023) \left(\frac{M_{\tilde{d}}}{100 \text{ GeV}} \right) .
 \end{aligned} \tag{5.124}$$

These relations are actually more useful than Eq. (5.123) since if the smuon and sdown exist, their masses will be measured/constrained by searches for their pair-production at the LHC, independently of the size of possible R-parity violating couplings.

Current bounds on R-parity violating couplings come from a variety of sources [78, 83]. The current indirect bounds of the four couplings under consideration from low-energy experiments are listed in Table 5.8. Comparison with Eq. (5.124) shows that the bounds on λ_{122} and λ_{132} are already

Coupling	Current 2σ Bound	Observable/Process
$ \lambda_{122} $	$0.05 \left(\frac{M_{\tilde{\mu}_R}}{100 \text{ GeV}} \right)$	V_{ud} from nuclear β decay/muon decay
$ \lambda_{132} $	$0.07 \left(\frac{M_{\tilde{\mu}_R}}{100 \text{ GeV}} \right)$	$R_\tau = \frac{\Gamma(\tau^- \rightarrow e^- \bar{\nu}_e \nu_\tau)}{\Gamma(\tau^- \rightarrow \mu^- \bar{\nu}_\mu \nu_\tau)}$
$ \lambda_{122} \lambda_{132}^* $	$(2.2 \times 10^{-3}) \left(\frac{M_{\tilde{\nu}_R}}{100 \text{ GeV}} \right)^2$	$\tau \rightarrow 3\mu$
$ \lambda'_{211} $	$0.06 \left(\frac{M_{\tilde{d}_R}}{100 \text{ GeV}} \right)$	$R_\pi = \frac{\Gamma(\pi^- \rightarrow e^- \bar{\nu}_e)}{\Gamma(\pi^- \rightarrow \mu^- \bar{\nu}_\mu)}$
$ \lambda'_{311} $	$0.12 \left(\frac{M_{\tilde{d}_R}}{100 \text{ GeV}} \right)$	$R_{\tau\pi} = \frac{\Gamma(\tau^- \rightarrow \pi^- \nu_\tau)}{\Gamma(\pi^- \rightarrow \mu^- \nu_\mu)}$

Table 5.8: Current 2σ bounds on R-parity violating couplings from Ref. [78]. These bounds assume that each coupling is non-zero only one at a time.

fairly tight, and neutrino oscillation will do little to improve them. On the other hand, the bounds on λ'_{211} and λ'_{311} can potentially be improved by factors of roughly 2.5 and 5, respectively.

Bounds on R-parity violating couplings from ep and $p\bar{p}$ colliders come from searches for s -channel resonant production of sparticles. The bounds from the ep collider HERA necessarily involve the couplings λ'_{1jk} since the squark must couple to the first generation lepton (electron or positron) [101, 102, 103, 104] so we will not discuss them here. The bound from the Tevatron comes from the analysis of D0 which looked for the R-parity violating processes $d\bar{u} \rightarrow \tilde{\mu}$ or $d\bar{d} \rightarrow \tilde{\nu}_\mu$, which occur if $\lambda'_{211} \neq 0$, followed by the decay of the slepton via the R-parity conserving processes $\tilde{\mu} \rightarrow \tilde{\chi}_{1,2,3,4}^0 \mu$ or $\tilde{\nu}_\mu \rightarrow \tilde{\chi}_{1,2}^\pm \mu$ [105]. The neutralinos and charginos produced in these processes cascade decay down to the $\tilde{\chi}_1^0$ (the assumed lightest supersymmetric particle, or LSP) which decays via a virtual smuon, muon-sneutrino, or squark through the R-parity violating λ'_{211} coupling again into a muon and two jets, giving 2 muons in the final state. The bound on the value of λ'_{211} from this analysis depends in a complicated manner on all the masses of the particles involved in the processes. If one uses a minimal supergravity (mSUGRA) framework [106] with $\tan\beta = 5$, $\mu < 0$, and $A_0 = 0$, then the 95% bound is $\lambda'_{211} \leq 0.1$ assuming $M_{\tilde{\mu}} = 363 \text{ GeV}$ [105]. A similar bound would result from Eq. (5.124) if $M_{\tilde{d}} = 460 \text{ GeV}$. However, since squarks are generically much heavier than sleptons [106], the existing D0 bound is effectively stronger than the potential bound from $|\xi| \leq \xi_0$.

5.5 Extended Higgs Models

Most models, including the Standard Model (SM) and its various extensions, possess Higgs sectors which distinguish among the different generation fermions. The models discussed in section 5.2 are necessarily so, and so are the Zee [75] and Babu-Zee [76] models of neutrino mass, as well as various triplet Higgs models [107]. As representative cases, we consider the effect of the singlet Higgs in the Zee and Babu-Zee models, and that of a triplet Higgs with hypercharge $Y = +1$ ($Q_{em} = I_3 + Y$).

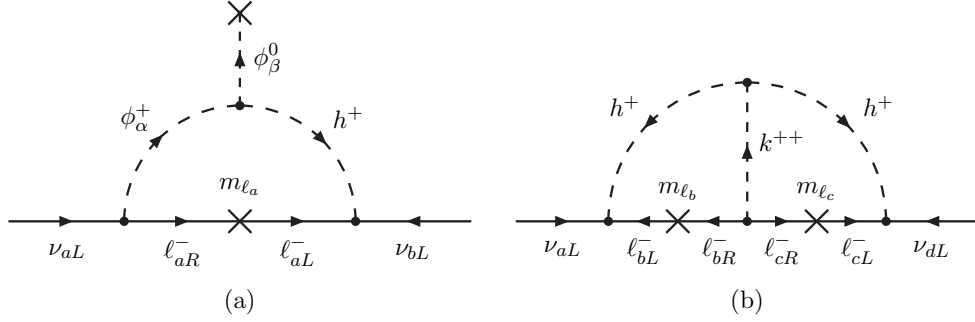


Figure 5.16: Diagrams which generate the Majorana masses and mixings of the neutrino in the (a) Zee [75] and (b) Babu-Zee [76] models.

5.5.1 Singlet Higgs in the Zee and Babu-Zee Models

In the Zee [75] and Babu-Zee [76] models, an isosinglet scalar h^+ with hypercharge $Y = +1$ is introduced, which couples to left-handed lepton doublets as

$$\mathcal{L}_h = \lambda_{ab} (\ell_{aL}^\top C i\sigma_2 \ell_{bL}) h^+ + h.c. = \lambda_{ab} (\overline{\ell_{aL}^c} i\sigma_2 \ell_{bL}) h^+ + h.c. , \quad (5.125)$$

where (ab) are flavor indices: $a, b = e, \mu, \tau$. The hypercharge assignment prohibits the h^\pm fields from having a similar interaction with the quarks. Due to $SU(2)$ gauge invariance, the couplings λ_{ab} are antisymmetric: $\lambda_{ab} = -\lambda_{ba}$. This interaction is analogous to the R-parity violating $\hat{L}\hat{L}\hat{E}$ coupling with h^\pm playing the role of the slepton.

In the Zee model [75], in addition to the h^\pm , two or more $SU(2)$ doublets ϕ_α ($\alpha = 1, 2, \dots$) with hypercharge $Y = -\frac{1}{2}$ are introduced which couple to the h^\pm via

$$\mathcal{L}_{\phi\phi h} = M_{\alpha\beta} (\phi_\alpha^\top i\tau_2 \phi_\beta) h^+ + h.c. , \quad (5.126)$$

and to the fermions in the usual fashion. The couplings $M_{\alpha\beta}$ are antisymmetric, just like λ_{ab} , which necessitates the introduction of more than one doublet. In this model, Majorana masses and mixings of the neutrinos are generated at one-loop as shown in Fig. 5.16a. The extra doublets can also contribute to neutrino oscillation depending on their Yukawa couplings to the leptons, but we will assume that their effect is negligible compared to that of the h^\pm .

In the Babu-Zee model [76], in addition to the h^\pm , another isosinglet scalar k^{++} with hypercharge $Y = +2$ is introduced which couples to the right-handed leptons and h^\pm via

$$\mathcal{L}_k = \lambda'_{ab} (\overline{e_{aR}^c} e_{bR}) k^{++} - M h^+ h^+ k^{--} + h.c. , \quad (5.127)$$

where $\lambda'_{ab} = \lambda'_{ba}$. In this model, Majorana masses and mixings of the neutrinos are generated at the two-loop level as shown in Fig. 5.16b. In this case, the extra scalar, k , does not contribute to neutrino oscillation.

Expanding Eq. (5.125), we obtain

$$\mathcal{L} = 2 [\lambda_{e\mu} (\overline{\nu_{eL}^c} \mu_L - \overline{\nu_{\mu L}^c} e_L) + \lambda_{e\tau} (\overline{\nu_{eL}^c} \tau_L - \overline{\nu_{\tau L}^c} e_L) + \lambda_{\mu\tau} (\overline{\nu_{\mu L}^c} \tau_L - \overline{\nu_{\tau L}^c} \mu_L)] h^+ + h.c. \quad (5.128)$$

Keeping only the terms that are relevant for neutrino oscillation matter effects, we have

$$-2 (\lambda_{e\mu} \overline{\nu_{\mu L}^c} e_L + \lambda_{e\tau} \overline{\nu_{\tau L}^c} e_L) h^+ + h.c. \quad (5.129)$$

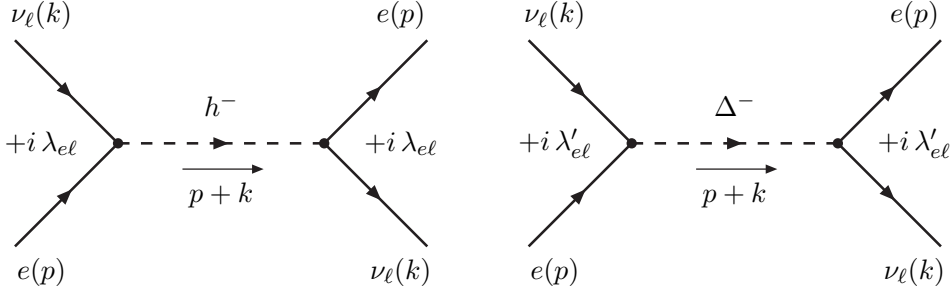


Figure 5.17: Contribution to neutrino oscillation matter effects from a singly-charged Higgs in the Zee, Babu-Zee, and $Y = 1$ Triplet Higgs models.

The corresponding Feynman diagram is shown in Fig. 5.17.

Calculations similar to those for the S_1 leptoquark yield

$$V_{\nu_\mu} = -N \frac{|\lambda_{e\mu}|^2}{M_h^2}, \quad V_{\nu_\tau} = -N \frac{|\lambda_{e\tau}|^2}{M_h^2}, \quad (5.130)$$

and

$$\xi_h = \frac{V_{\nu_\tau} - V_{\nu_\mu}}{V_{CC}} = 4 \frac{(|\lambda_{e\mu}|^2 - |\lambda_{e\tau}|^2)/M_h^2}{(g/M_W)^2} = +\frac{1}{\sqrt{2}G_F} \left(\frac{\delta\lambda_h^2}{M_h^2} \right), \quad (5.131)$$

where we have defined $\delta\lambda_h^2 \equiv |\lambda_{e\mu}|^2 - |\lambda_{e\tau}|^2$. The dependence of ξ_h on the h^\pm mass is plotted in Fig. 5.14 for the case $\sqrt{\delta\lambda_h^2} = 0.5$, where we have assumed $\delta\lambda_h^2 > 0$. The bound $|\xi| \leq \xi_0 = 0.005$ translates into

$$\left| \frac{\delta\lambda_h^2}{M_h^2} \right| \leq \sqrt{2}G_F \xi_0 = (8.2 \times 10^{-8}) \text{ GeV}^{-2}, \quad (5.132)$$

or

$$M_h \geq \sqrt{\frac{|\delta\lambda_h^2|}{\sqrt{2}G_F \xi_0}} \approx \sqrt{|\delta\lambda_h^2|} \times (3500 \text{ GeV}). \quad (5.133)$$

This result is represented graphically in Fig. 5.15. The region of the $(M_h, \sqrt{|\delta\lambda_h^2|})$ parameter space below the constructed line would be excluded.

A constraint on the exact same combination of the couplings and mass of the h^\pm as above exists from τ decay data: The measured value of the $\tau^- \rightarrow \nu_\tau e^- \bar{\nu}_e$ branching fraction imposes the constraint [108]

$$\left| \frac{\delta\lambda_h^2}{M_h^2} \right| \leq (3.4 \times 10^{-8}) \text{ GeV}^{-2}, \quad (5.134)$$

which is clearly stronger than Eq. (5.132).

5.5.2 Triplet Higgs with $Y = +1$

We denote the components of an isotriplet Higgs with hypercharge $Y = +1$ as

$$\begin{bmatrix} \Delta^{++} \\ \Delta^+ \\ \Delta^0 \end{bmatrix}. \quad (5.135)$$

It is customary to write this in 2×2 matrix form:

$$\Delta \equiv \frac{1}{\sqrt{2}} \left[\Delta^0 \left(\frac{\sigma_1 - i\sigma_2}{\sqrt{2}} \right) + \Delta^+ \sigma_3 + \Delta^{++} \left(\frac{\sigma_1 + i\sigma_2}{\sqrt{2}} \right) \right] = \begin{bmatrix} \Delta^+/\sqrt{2} & \Delta^{++} \\ \Delta^0 & -\Delta^+/\sqrt{2} \end{bmatrix}. \quad (5.136)$$

The coupling of Δ to the leptons is then

$$\mathcal{L}_\Delta = \sqrt{2} \lambda'_{ab} (\ell_{aL}^\top C i\sigma_2 \Delta \ell_{bL}) + h.c. = \sqrt{2} \lambda'_{ab} (\overline{\ell_{aL}^c} i\sigma_2 \Delta \ell_{bL}) + h.c. \quad (5.137)$$

This time, the couplings are symmetric in the flavor indices $\lambda'_{ab} = \lambda'_{ba}$, and the factor of $\sqrt{2}$ is thrown in for latter convenience. Expanding out, we find

$$\mathcal{L}_\Delta = \lambda'_{ab} \left[\sqrt{2} (\overline{\nu_{aL}^c} \nu_{bL}) \Delta^0 - (\overline{\nu_{aL}^c} e_{bL} + \overline{e_{aL}^c} \nu_{bL}) \Delta^+ - \sqrt{2} (\overline{e_{aL}^c} e_{bL}) \Delta^{++} \right] + h.c. \quad (5.138)$$

and the terms relevant to neutrino oscillation in matter are:

$$-2 \left(\lambda'_{ee} \overline{\nu_{eL}^c} e_L + \lambda'_{e\mu} \overline{\nu_{\mu L}^c} e_L + \lambda'_{e\tau} \overline{\nu_{\tau L}^c} e_L \right) \Delta^+ + h.c. \quad (5.139)$$

Of these, the λ'_{ee} term does not affect ξ , while the other terms are precisely the same as those listed in Eq. (5.129). So without further calculations, we can conclude that all the results of the previous subsection apply in this case also.

This page left blank intentionally.

Chapter 6

Summary

We have considered several neutrino experiments and analyzed the constraints they can impose on various models of new physics. In the last chapter we summarize our results.

6.1 NuTeV

We considered several explanations of the NuTeV anomaly suggested in the literature: gauged $L_\mu - L_\tau$, gauged $B - 3L_\mu$, and S_1 , \vec{S}_3 , V_1 , and \vec{V}_3 leptoquark models. We found that the $L_\mu - L_\tau$ model cannot explain NuTeV and be consistent with the most recent LEP data at the same time. The $B - 3L_\mu$ model cannot explain the NuTeV anomaly at all because in this model the value of g_L^2 is *larger* than the SM prediction while NuTeV observed the *suppression* of this parameter with respect to its SM value. The same can be said of the S_1 , V_1 leptoquark models, and the $SU(2)$ triplet \vec{S}_3 leptoquark model with degenerate masses. In all these models g_L^2 acquires a positive rather than a negative shift with respect to its SM value. The mass-degenerate \vec{V}_3 leptoquark shifts the value of g_L^2 in the negative direction. However, the size of the shift needed to explain the NuTeV anomaly requires the value of the mass-to-coupling ratio which is incompatible with the measured value of R_π .

However, we found that the \vec{S}_3 and \vec{V}_3 leptoquark models with the mass-non-degenerate components of the $SU(2)$ triplet are capable of explaining the NuTeV anomaly. In these models, the parameter g_L^2 acquires a negative shift and the size of this shift can be adjusted to the value needed to explain NuTeV without contradicting experimental data.

6.2 Neutrissimo Lifetime

Neutrissimo models presented in Chapter 3 were also suggested as potential candidates for explaining the NuTeV anomaly [5, 6]. The models of this type are still phenomenologically viable and predict the existence of the mostly-right-handed heavy Majorana neutrino states, called neutrissimos, which have their masses in a few TeV range. The values of the masses suggest that these particles can be produced at the LHC energies. Thus, in Chapter 3, we addressed the question of whether or not these states can actually be observed at the LHC. We calculated the mass spectrum, decay widths and lifetimes of the neutrissimos that appear in the model proposed by Okamura et al. in Ref. [5]. We mapped the parameter space of the Okamura model to the interior of a unit circle,

and represented the results of our calculations as density-contour plots over it. We showed that for the phenomenologically viable region of the model's parameter space, the neutrissimos have masses of a few TeV, and are short-lived with the typical lifetimes from 10^{-26} to 10^{-24} seconds. Assuming that the particles are non-relativistic, the maximum distance they can travel from their production points before decay is in the range of 10^{-17} to 10^{-15} meters. Therefore, if produced at colliders they will decay inside the detector. At the same time, the decay widths are very small comparing to the masses. The typical width-to-mass ratio is in the range of 0.1 to 3 percent. Therefore, the invariant mass spectrum of the decay products can be expected to show a very narrow peak.

Since the neutrissimo is a Majorana particle, the signature of its production at the LHC would involve lepton number violation, e.g., the production of like-sign leptons. Our analysis showed that if the neutrissimo mass is smaller than around 150 GeV than it can be seen at the LHC. If it is heavier than 150 GeV that the number of expected events is too small to lead to an observable event rate. This suggests that we should also try to look for the signatures of these particles in some other experiments involving neutrinos. One such experiment, called NuSOng, was considered by us in Chapter 4.

6.3 NuSOng

NuSOng is an experiment which can search for new physics from keV through TeV energy scales. This thesis has focused mainly on the Terascale physics which can be accessed through this new high statistics neutrino scattering experiment.

We considered several models of new physics which NuSOng will be able to constrain. The models we considered are: the neutrissimo models, generation distinguishing Z' models, such as gauged $B - 3L_\mu$ and gauged $L_e - L_\mu$ models, extended Higgs models, R -parity violating SUSY models and various types of generation non-diagonal leptoquarks.

We found that NuSOng's improved measurement of g_L^2 would substantially improve the constraints on ϵ_μ and ϵ_e , the parameters which deviation from unity would signal a violation of the lepton universality. The deviation of these parameters from unity is an intrinsic feature of the neutrissimo models, considered in chapter 3. Thus, if NuSOng does not see the signature of the neutrissimos it would be able to put constraints on this type of new physics models or, conversely, if the neutrissimos exist NuSOng would see the suppression of the number of the neutral current events in the quark-neutrino scattering with respect to the number predicted by the SM¹.

We saw that the NuSOng potential lower bound on the mass-to-coupling ratio of the Z' appearing in the gauged $B - 3L_\mu$ model is comparable and complementary to the existing bound from D0. On the other hand, the NuSOng lower bound on the mass-to-coupling ratio of the Z' of the $L_e - L_\mu$ model is found to be weaker than the existing bound from LEP/LEP2 measurements, so NuSOng will not be able to improve this particular bound.

The R -parity violating interactions that NuSOng is able to constrain come from the $\hat{L}\hat{L}\hat{E}$ and $\hat{L}\hat{Q}\hat{D}$ parts of the R -parity violating MSSM Lagrangian. In the $\hat{L}\hat{L}\hat{E}$ case the NuSOng potential bounds on the couplings are slightly better than currently existing bounds. In the $\hat{L}\hat{Q}\hat{D}$ case the NuSOng potential bounds on the couplings are either competitive with currently existing bounds or by a factor of 3 or 5 stronger. The result of our analysis is summarized in Table 4.3 of Chapter 4.

¹This would be exactly the same as the anomaly observed by the NuTeV experiment.

Model	Stronger than existing bounds?	Competitive with LHC?
Gauged $L_e - L_\mu$ and $L_e - L_\tau$	No	—
Gauged $B - 3L_\tau$	Yes	Yes
Topcolor Assisted Technicolor	No	—
Leptoquarks	Yes	Yes*
R-parity violation	No	—
Zee, Babu-Zee, Triplet Higgs	No	—

Table 6.1: The result of our survey. The potential bound from the Fermilab→Hyper-Kamiokande experiment is compared with existing bounds, and the expected bounds from the LHC. If the existing bound is already stronger, no comparison with the LHC bound is made. *The leptoquark bound will be competitive with the LHC, provided that $\sqrt{|C_{LQ}||\delta\lambda_{LQ}^2|} = O(1)$.

We also considered several types of leptoquarks which can affect the result of the NuSONG experiment. We found that existing bounds on S_1 , \vec{S}_3 , V_1 , and \vec{V}_3 leptoquark couplings from $R_\pi = B(\pi \rightarrow e\nu)/B(\pi \rightarrow \mu\nu)$ are already much stronger than potential bounds from NuSONG. However, these bounds can be circumvented for \vec{S}_3 and \vec{V}_3 if the masses within the multiplets are allowed to be non-degenerate.

For S_2 , \tilde{S}_2 , V_2 , and \tilde{V}_2 leptoquarks the existing bounds are fairly weak and NuSONG is able to significantly improve them. If any of these particles exist, NuSONG could see the shift in the value of g_R^2 , but not in the value of g_L^2 . This would be opposite to what was observed by NuTeV.

6.4 Fermilab→Hyper-Kamiokande

We also surveyed the potential constraints on various models of new physics which could be obtained from a hypothetical Fermilab→Hyper-Kamiokande, or similar type of experiment. We saw that the experiment of this type will be able to place constraints on the couplings and masses of new particles that are exchanged between the neutrinos and matter fermions.

Table 6.1 summarizes our result. Of the models surveyed, the potential bound on gauged $B - 3L_\tau$ can be expected to be stronger than the expected bound from the LHC. Bounds on generation non-diagonal leptoquarks can be competitive if $\sqrt{|C_{LQ}||\delta\lambda_{LQ}^2|} = O(1)$. For these cases, neutrino oscillation can be used as an independent check in the event that such new physics is discovered at the LHC.

All the other models are already well constrained by existing experiments, either indirectly by low-energy precision measurements, or by direct searches at colliders. Generically, the couplings and masses of new particles that couple only to leptons are well constrained by lepton universality, while their contribution to neutrino oscillation tend to be suppressed since they only interact with the electrons in matter. This tends to render the existing bound stronger than the potential bound from the Fermilab→Hyper-Kamiokande experiment.

Topcolor assisted technicolor, and R-parity violating LQD couplings involve interactions with the quarks in matter, but they too belong to the list of already well-constrained models. For the Z' in topcolor assisted technicolor, the proton and electron contributions to neutrino oscillation cancel, just as for the Standard Model Z , and the coupling is also fixed to a small value, which results in a weak bound from the Fermilab→Hyper-Kamiokande experiment. For the LQD coupling,

restriction to minimal supergravity provided an extra constraint which strengthened the existing bound.

The fact that only a limited number of models (at least among those we surveyed) can be well constrained by the Fermilab→Hyper-Kamiokande experiment means, conversely, that if a non-zero effect² is observed in neutrino oscillation, the list of possible new physics that could lead to such an effect is also limited. This could, in principle, help distinguish among possible new physics which have the same type of signature (*e.g.* a leptoquark which may, or may not be generation diagonal) at the LHC.

6.5 Future prospects

In addition to the projects presented in this thesis, I have calculated CP asymmetries in the neutrino and MSSM chargino decays to see if they can explain the matter-antimatter asymmetry of the universe, and am also working on producing a list of possible interpretations of the W decay anomaly. In the immediate future, I plan to continue analyzing data coming from different elementary particle experiments, especially those involving neutrinos: Borexino, MiniBooNE, LENS, NuSOnG, just to name a few, and paying very close attention to the news from the LHC.

In the long term, I plan to continue doing my research in high energy physics. More data will be available as time passes and more experiments will be performed. For example, the International Linear Collider (ILC), if built, will provide us with another excellent opportunity to probe physics beyond the SM. And I strongly believe that no matter how many secrets of Nature we reveal in the future, there will always be things which puzzle us, things which are yet to be discovered, analyzed, and explained.

²Non-zero ξ in our notation.

Appendix A

Ratios of the neutral to charged current events

In this Appendix, I will give a somewhat simplified version of the derivation of Eqs. (2.1)-(2.2). The derivation is based on the materials of the lecture presented by Prof. Takeuchi at the 1991 Nagoya Spring School on Dynamical Symmetry Breaking [109].

The amplitudes for the neutral current processes $\nu_\mu(k)u(p) \rightarrow \nu_\mu(k')u(p')$ and $\bar{\nu}_\mu(k)u(p) \rightarrow \bar{\nu}_\mu(k')u(p')$, where p, p', k, k' are the momenta of the particles, are given by:

$$\mathcal{M}_{\nu u \rightarrow \nu u} = \frac{G_F}{\sqrt{2}} \rho \left[\bar{u}(k') \gamma_\mu (1 - \gamma_5) u(k) \right] \left[\bar{u}(p') \{ g_L^u \gamma^\mu (1 - \gamma_5) + g_R^u \gamma^\mu (1 + \gamma_5) \} u(p) \right] \quad (\text{A.1})$$

$$\mathcal{M}_{\bar{\nu} u \rightarrow \bar{\nu} u} = \frac{G_F}{\sqrt{2}} \rho \left[\bar{v}(k) \gamma_\mu (1 - \gamma_5) v(k') \right] \left[\bar{u}(p') \{ g_L^u \gamma^\mu (1 - \gamma_5) + g_R^u \gamma^\mu (1 + \gamma_5) \} u(p) \right] \quad (\text{A.2})$$

Neglecting the u -quark mass, we find

$$|\mathcal{M}_{\nu u \rightarrow \nu u}|^2 = 128 G_F^2 \rho^2 \left[(g_L^u)^2 (p \cdot k)^2 + (g_R^u)^2 (p \cdot k')^2 \right], \quad (\text{A.3})$$

$$|\mathcal{M}_{\bar{\nu} u \rightarrow \bar{\nu} u}|^2 = 128 G_F^2 \rho^2 \left[(g_L^u)^2 (p \cdot k')^2 + (g_R^u)^2 (p \cdot k)^2 \right]. \quad (\text{A.4})$$

Similarly,

$$|\mathcal{M}_{\nu d \rightarrow \nu d}|^2 = 128 G_F^2 \rho^2 \left[(g_L^d)^2 (p \cdot k)^2 + (g_R^d)^2 (p \cdot k')^2 \right], \quad (\text{A.5})$$

$$|\mathcal{M}_{\bar{\nu} d \rightarrow \bar{\nu} d}|^2 = 128 G_F^2 \rho^2 \left[(g_L^d)^2 (p \cdot k')^2 + (g_R^d)^2 (p \cdot k)^2 \right]. \quad (\text{A.6})$$

On the other hand, the amplitudes for the charged current processes $\nu_\mu(k)d(p) \rightarrow \mu^-(k')u(p')$ and $\bar{\nu}_\mu(k)u(p) \rightarrow \mu^+(k')d(p')$ are given by

$$\mathcal{M}_{\nu d \rightarrow \mu^- u} = \frac{G_F}{\sqrt{2}} \left[\bar{u}(k') \gamma_\mu (1 - \gamma_5) u(k) \right] \left[\bar{u}(p') \gamma^\mu (1 - \gamma_5) u(p) \right], \quad (\text{A.7})$$

$$\mathcal{M}_{\bar{\nu} u \rightarrow \mu^+ d} = \frac{G_F}{\sqrt{2}} \left[\bar{v}(k) \gamma_\mu (1 - \gamma_5) v(k') \right] \left[\bar{u}(p') \gamma^\mu (1 - \gamma_5) u(p) \right], \quad (\text{A.8})$$

from which we find

$$|\mathcal{M}_{\nu d \rightarrow \mu^- u}|^2 = 128 G_F^2 (p \cdot k)^2, \quad (\text{A.9})$$

$$|\mathcal{M}_{\bar{\nu} u \rightarrow \mu^+ d}|^2 = 128 G_F^2 (p \cdot k')^2. \quad (\text{A.10})$$

If we denote the probability of finding a u -quark with momentum p inside the target as $f_u(p)$, and the same for the d -quark as $f_d(p)$, then the contributions to the deep inelastic cross sections from the scattering between ν_μ or $\bar{\nu}_\mu$ with momentum k and quarks with momentum p would be:

$$\begin{aligned} d\sigma(\nu_\mu N \rightarrow \nu_\mu X) &\propto \rho^2 [(g_L^u)^2 (p \cdot k)^2 + (g_R^u)^2 (p \cdot k')^2] f_u(p) dp \\ &+ \rho^2 [(g_L^d)^2 (p \cdot k)^2 + (g_R^d)^2 (p \cdot k')^2] f_d(p) dp, \end{aligned} \quad (\text{A.11})$$

$$\begin{aligned} d\sigma(\bar{\nu}_\mu N \rightarrow \bar{\nu}_\mu X) &\propto \rho^2 [(g_L^u)^2 (p \cdot k')^2 + (g_R^u)^2 (p \cdot k)^2] f_u(p) dp \\ &+ \rho^2 [(g_L^d)^2 (p \cdot k')^2 + (g_R^d)^2 (p \cdot k)^2] f_d(p) dp, \end{aligned} \quad (\text{A.12})$$

$$d\sigma(\nu_\mu N \rightarrow \mu^- X) \propto (p \cdot k)^2 f_d(p) dp, \quad (\text{A.13})$$

$$d\sigma(\bar{\nu}_\mu N \rightarrow \mu^+ X) \propto (p \cdot k')^2 f_u(p) dp. \quad (\text{A.14})$$

When the target is an isoscalar, it will contain the same number of u -quarks and d -quarks. Therefore, we can expect

$$f_u(p) = f_d(p) \equiv f(p).$$

Then,

$$d\sigma(\nu_\mu N \rightarrow \nu_\mu X) \propto g_L^2 (p \cdot k)^2 f(p) dp + g_R^2 (p \cdot k')^2 f(p) dp, \quad (\text{A.15})$$

$$d\sigma(\bar{\nu}_\mu N \rightarrow \bar{\nu}_\mu X) \propto g_L^2 (p \cdot k')^2 f(p) dp + g_R^2 (p \cdot k)^2 f(p) dp, \quad (\text{A.16})$$

$$d\sigma(\nu_\mu N \rightarrow \mu^- X) \propto (p \cdot k)^2 f(p) dp, \quad (\text{A.17})$$

$$d\sigma(\bar{\nu}_\mu N \rightarrow \mu^+ X) \propto (p \cdot k')^2 f(p) dp, \quad (\text{A.18})$$

where

$$g_L^2 = \rho^2 [(g_L^u)^2 + (g_L^d)^2], \quad (\text{A.19})$$

$$g_R^2 = \rho^2 [(g_R^u)^2 + (g_R^d)^2]. \quad (\text{A.20})$$

Eqs. (A.15)-(A.18) imply

$$\sigma(\nu_\mu N \rightarrow \nu_\mu X) = g_L^2 \sigma(\nu_\mu N \rightarrow \mu^- X) + g_R^2 \sigma(\bar{\nu}_\mu N \rightarrow \mu^+ X), \quad (\text{A.21})$$

$$\sigma(\bar{\nu}_\mu N \rightarrow \bar{\nu}_\mu X) = g_L^2 \sigma(\bar{\nu}_\mu N \rightarrow \mu^+ X) + g_R^2 \sigma(\nu_\mu N \rightarrow \mu^- X), \quad (\text{A.22})$$

or

$$R_\nu = g_L^2 + r g_R^2, \quad (\text{A.23})$$

$$R_{\bar{\nu}} = g_L^2 + \frac{g_R^2}{r}. \quad (\text{A.24})$$

This page left blank intentionally.

Appendix B

Calculation of the W vertex corrections in the $L_\mu - L_\tau$ model

In this Appendix we show how we calculate radiative corrections to the W vertex in the $L_\mu - L_\tau$ model. The corresponding Feynman diagram is shown in Fig. B.1. We consider only the situation when W^- decays into the anti-neutrino and charged lepton of the second generation. For ν_τ and τ in the final state the consideration and the final result are exactly the same.

B.1 Matrix element

The relevant terms of the interaction Lagrangian are

$$\mathcal{L}_1(x) = \frac{g}{\sqrt{2}} \bar{\mu}(x) \gamma^\mu P_L \nu_\mu(x) W_\mu(x), \quad (\text{B.1})$$

$$\mathcal{L}_2(y) = g_X \bar{\mu}(y) \gamma^\nu \mu(y) X_\nu(y), \quad (\text{B.2})$$

$$\mathcal{L}_3(z) = g_X \bar{\nu}_\mu(z) \gamma^\gamma P_L \nu_\mu(z) X_\gamma(z). \quad (\text{B.3})$$

Applying Feynman rules to this process we obtain the expression for the amplitude

$$iM = \frac{gg_X^2}{\sqrt{2}} \cdot \bar{u}(p_2) \Gamma^\mu P_L v(p_1) \varepsilon_\mu(p_3), \quad (\text{B.4})$$

where

$$\Gamma^\mu = \int \frac{d^d q}{(2\pi)^d} \gamma^\nu \frac{\not{q} + \not{p}_3}{(q + p_3)^2 + i\epsilon} \gamma^\mu \frac{\not{q}}{q^2 + i\epsilon} \gamma^\nu \frac{1}{(q + p_1)^2 - M_X^2 + i\epsilon}. \quad (\text{B.5})$$

The 4-momentum assignment is shown in Fig. B.1. d is the space-time dimension. Introducing

$$A^{\mu'\mu\nu'} \equiv \gamma^\nu \gamma^{\mu'} \gamma^\mu \gamma^{\nu'} \gamma_\nu = -2\gamma^{\nu'} \gamma^\mu \gamma^{\mu'} + (4 - d)\gamma^{\mu'} \gamma^\mu \gamma^{\nu'}, \quad (\text{B.6})$$

we can write

$$\Gamma^\mu = \int \frac{d^d q}{(2\pi)^d} \frac{A^{\mu'\mu\nu'} (q + p_3)_\mu q_\nu}{q^2 (q + p_3)^2 [(q + p_1)^2 - M_X^2]}. \quad (\text{B.7})$$

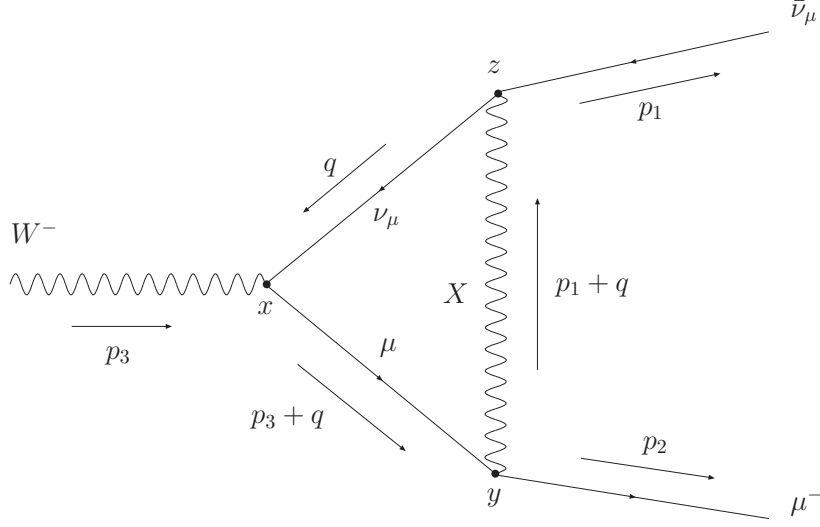


Figure B.1: Correction to the W vertex due to the X exchange between the final state leptons.

Using Feynman's formula

$$\frac{1}{q^2(q+p_3)^2[(q+p_1)^2 - M_X^2]} = \int_0^1 dx dy dz \delta(x+y+z-1) \cdot \frac{2}{D^3}, \quad (\text{B.8})$$

where

$$D = xq^2 + y(q+p_3)^2 + z[(q+p_1) - M_X^2], \quad (\text{B.9})$$

we write

$$\Gamma^\mu = 2 \int_0^1 dx dy dz \delta(x+y+z-1) \cdot A^{\mu'\mu\nu'} B_{\mu'\nu'}, \quad (\text{B.10})$$

where

$$B_{\mu'\nu'} = \int \frac{d^d q}{(2\pi)^d} \cdot \frac{(q+p_3)_{\mu'} q_{\nu'}}{D^3}. \quad (\text{B.11})$$

Next, we can expand D as

$$D = q^2(x+y+z) + 2(q, yp_3 + zp_1) + yM_W^2 - zM_X^2 = l^2 - \Delta, \quad (\text{B.12})$$

where¹

$$l^\mu = q^\mu + yp_3^\mu + zp_1^\mu, \quad (\text{B.13})$$

$$\Delta = M_W^2(y^2 - y + yz + z\delta), \quad (\text{B.14})$$

$$\delta \equiv \frac{M_X^2}{M_W^2}. \quad (\text{B.15})$$

¹We used $2(p_1, p_3) = 2(p_1, p_2) = M_W^2$.

$B^{\mu\nu}$ becomes

$$B^{\mu\nu} = \int \frac{d^d l}{(2\pi)^4} \cdot \frac{(l^\mu - yp_3^\mu - zp_1^\mu + p_3^\mu)(l^\nu - yp_3^\nu - zp_1^\nu)}{(l^2 - \Delta)^3}. \quad (\text{B.16})$$

Only even powers of l^μ give non-zero contributions. Thus,

$$B^{\mu\nu} = \int \frac{d^d l}{(2\pi)^4} \cdot \frac{l^\mu l^\nu + (yp_3^\mu + zp_1^\mu)(yp_3^\nu + zp_1^\nu) - p_3^\mu(yp_3^\nu + zp_1^\nu)}{(l^2 - \Delta)^3}. \quad (\text{B.17})$$

Symmetry of the integral allows us to replace

$$l^\mu l^\nu \rightarrow \frac{1}{d} \cdot l^2 \cdot g^{\mu\nu}.$$

We can simplify the expression for Γ^μ making use of Dirac equations:

$$\bar{u}(p_2) \not{p}_2 = 0, \quad \not{p}_1 v(p_1) = 0. \quad (\text{B.18})$$

In order to do that we have to commute all \not{p}_2 's to the left-most and all \not{p}_1 's to the right-most positions. We also make use of the identity

$$\gamma^\mu \gamma^\nu \gamma_\mu = -(d-2)\gamma^\nu. \quad (\text{B.19})$$

The independent of l^2 part of the numerator Eq. (B.17) is

$$\begin{aligned} & (yp_{3\mu} + zp_{1\mu})(yp_{3\nu} + zp_{1\nu}) - p_{3\mu}(yp_{3\nu} + zp_{1\nu}) = [(y-1)(p_{1\mu} + p_{2\mu}) + zp_{1\mu}][y(p_{1\nu} + p_{2\nu}) + zp_{1\nu}] \\ & = [p_{1\mu}(y+z-1) + (y-1)p_{2\mu}][(y+z)p_{1\nu} + yp_{2\nu}] = p_{1\mu}p_{1\nu}(y+z-1)(y+z) + y(y-1)p_{2\mu}p_{2\nu} \\ & + p_{1\mu}p_{2\nu}y(y+z-1) + (y-1)(y+z)p_{2\mu}p_{1\nu}. \end{aligned}$$

The contribution of the first two term in the expression above vanishes when we take into account Dirac equations (B.18). Thus,

$$\begin{aligned} A^{\mu'\mu\nu'} B_{\mu'\nu'} &= \int \frac{d^d l}{(2\pi)^d} [-2\gamma^{\nu'} \gamma^\mu \gamma^{\mu'} + (4-d)\gamma^{\mu'} \gamma^\mu \gamma^{\nu'}] \\ & \times \frac{g_{\mu'\nu'} l^2/d + p_{1\mu'} p_{2\nu'} y(y+z-1) + p_{1\nu'} p_{2\mu'} (y-1)(y+z)}{(l^2 - \Delta)^3} \\ &= \int \frac{d^d l}{(2\pi)^d} \frac{1}{(l^2 - \Delta)^3} \left\{ \frac{l^2}{d} [2(d-2)\gamma^\mu - (4-d)(d-2)\gamma^\mu] \right. \\ & \left. + (4-d)y(y+z-1) \not{p}_1 \gamma^\mu \not{p}_2 - 2 \not{p}_1 \gamma^\mu \not{p}_2 (y-1)(y+z) \right\} \\ &= \int \frac{d^d l}{(2\pi)^d} \frac{\gamma^\mu l^2 (d-2)^2/d + [(4-d)y(y+z-1) - 2(y-1)(y+z)] \not{p}_1 \gamma^\mu \not{p}_2}{(l^2 - \Delta)^3}. \end{aligned}$$

The second term in the numerator of the expression above gives a finite contribution to the total integral. It does not need to be regularized by dimensional regularization, so we take $d = 4$ for this term. Then

$$A^{\mu'\mu\nu'} B_{\mu'\nu'} = \int \frac{d^d l}{(2\pi)^d} \frac{\gamma^\mu r l^2 + 2(1-y)(y+z) \not{p}_1 \gamma^\mu \not{p}_2}{(l^2 - \Delta)^3},$$

where we introduced

$$r = (d-2)^2/d. \quad (\text{B.20})$$

In $\not{p}_1 \gamma^\mu \not{p}_2$ we can either commute \not{p}_1 to the right or \not{p}_2 to the left.

$$\gamma^\alpha \gamma^\mu \gamma^\beta = \gamma^\alpha (2g^{\mu\beta} - \gamma^\beta \gamma^\mu) = 2g^{\mu\beta} \gamma^\alpha - \gamma^\alpha \gamma^\beta \gamma^\mu.$$

The first term in the expression above gives zero acting on $v(p_1)$. The second term is

$$- (2g^{\alpha\beta} - \gamma^\beta \gamma^\alpha) \gamma^\mu.$$

And again the second term in the parenthesis gives zero acting on $\bar{u}(p_2)$. Thus

$$\gamma^\alpha \gamma^\mu \gamma^\beta \rightarrow -2g^{\alpha\beta} \gamma^\mu,$$

or

$$\not{p}_1 \gamma^\mu \not{p}_2 \rightarrow -2(p_1, p_2) \gamma^\mu = -M_W^2 \gamma^\mu.$$

Putting all together we find that

$$\Gamma^\mu = 2 \int_0^1 dx dy dz \delta(x+y+z-1) \int \frac{d^d l}{(2\pi)^d} \cdot \frac{r l^2 - 2(1-y)(y+z) M_W^2}{(l^2 - \Delta)^3} \cdot \gamma^\mu \equiv iF \gamma^\mu, \quad (\text{B.21})$$

where

$$F = -2i \int_0^1 dx dy dz \delta(x+y+z-1) \int \frac{d^d l}{(2\pi)^d} \cdot \frac{r l^2 - 2(1-y)(y+z) M_W^2}{(l^2 - \Delta)^3}. \quad (\text{B.22})$$

The expressions for the matrix element (B.4) and its conjugated become

$$iM = \frac{igg_X^2}{\sqrt{2}} \bar{u}(p_2) F \gamma^\mu P_L v(p_1) \varepsilon_\mu(p_3), \quad (\text{B.23})$$

$$-iM^\dagger = -\frac{igg_X^2}{\sqrt{2}} \bar{v}(p_1) F^* \gamma^\nu P_L u(p_2) \varepsilon_\nu^*(p_3). \quad (\text{B.24})$$

B.2 $\Delta\Gamma/\Gamma$

We also have to consider the tree level process shown in Fig. B.2. The tree-level matrix element M_t can be obtained by considering the part of the interaction Lagrangian given by Eq. (B.1). Applying standard Feynman rules we find that

$$iM_t = i \frac{g}{\sqrt{2}} \bar{u}(p_2) \gamma^\mu P_L v(p_1) \varepsilon_\mu(p_3), \quad (\text{B.25})$$

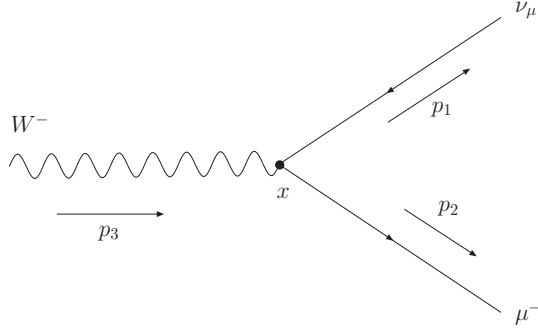


Figure B.2: The tree level W vertex.

and

$$-iM_t^\dagger = -i\frac{g}{\sqrt{2}}\bar{v}(p_1)\gamma^\mu P_L u(p_2)\varepsilon_\mu(p_3). \quad (\text{B.26})$$

The 4-momentum assignment is clear from Fig. B.2. The matrix element M for the vertex correction due to the X exchange was calculated in the previous section and given by Eq. (B.23). The total matrix element is $M_{\text{tot}} = M_t + M$. Squaring it and summing over the spins of the final state particles we obtain to the leading order:

$$|\overline{M_{\text{tot}}}|^2 = |\overline{M_t}|^2 + \overline{M_t^\dagger M_t} + \overline{M M_t^\dagger}. \quad (\text{B.27})$$

We denote $\Delta\Gamma$ the correction to the W vertex due to the X exchange and Γ is the tree level W decay width². For two-body decay processes the phase space factor is just a constant which cancels in the ratio $\Delta\Gamma/\Gamma$, so we do not have to worry about it. Up to the irrelevant constant factor

$$\Gamma \sim |\overline{M_t}|^2, \quad \Delta\Gamma \sim \overline{M_t^\dagger M_t} + \overline{M M_t^\dagger}, \quad (\text{B.28})$$

and

$$\frac{\Delta\Gamma}{\Gamma} = \frac{\overline{M_t^\dagger M_t} + \overline{M M_t^\dagger}}{|\overline{M_t}|^2}. \quad (\text{B.29})$$

Calculation of $|\overline{M_t}|^2$

Let us calculate $|\overline{M_t}|^2$ first. The tree level matrix element and its conjugated are given by Eqs. (B.25) and (B.26).

$$\begin{aligned} |\overline{M_t}|^2 &= \frac{g^2}{2} \text{Tr}(\not{p}_1 \gamma^\nu P_L \not{p}_2 \gamma^\mu P_L) \sum_{\text{pol's}} \varepsilon_\mu(p_3) \varepsilon_\nu^*(p_3) \\ &= \frac{g^2}{2} \text{Tr}(\gamma^{\mu_1} \gamma^\nu \gamma_{\mu_2} \gamma^\mu P_L) p_{1\mu_1} p_{2\mu_2} \left(-g_{\mu\nu} + \frac{p_{3\mu} p_{3\nu}}{M_W^2} \right), \end{aligned}$$

because

$$\sum_{\text{pol's}} \varepsilon_\mu(p_3) \varepsilon_\nu^*(p_3) = -g_{\mu\nu} + \frac{p_{3\mu} p_{3\nu}}{M_W^2}. \quad (\text{B.30})$$

²It should not be confused with the Γ we used in the previous section. From now on Γ is the tree level W decay width.

We know that

$$\text{Tr}(\gamma^{\mu_1}\gamma^{\nu}\gamma^{\mu_2}\gamma^{\mu}) = 4(g^{\mu_1\nu}g^{\mu_2\mu} - g^{\mu_1\mu_2}g^{\mu\nu} + g^{\mu_1\mu}g^{\mu_2\nu}), \quad (\text{B.31})$$

$$\text{Tr}(\gamma^{\mu_1}\gamma^{\nu}\gamma^{\mu_2}\gamma^{\mu}\gamma_5) = -4i\epsilon^{\mu_1\nu\mu_2\mu}. \quad (\text{B.32})$$

$\epsilon^{\mu_1\nu\mu_2\mu}$ term does not contribute to the final result because it is contracted with the symmetric tensor given by the right-hand side of Eq. (B.30). So, we do not have to worry about it. Thus,

$$\begin{aligned} |\overline{M}_t|^2 &= g^2 \left[p_1^\nu p_2^\mu - (p_1, p_2)g^{\mu\nu} + p_1^\mu p_2^\nu \right] \left(-g_{\mu\nu} + \frac{p_{3\mu}p_{3\nu}}{M_W^2} \right) \\ &= -g^2 \left\{ (p_1, p_2) - 4(p_1, p_2) + (p_1, p_2) - \frac{1}{M_W^2} [2(p_2, p_3)(p_1, p_3) - (p_1, p_2)p_3^2] \right\} \\ &= g^2(p_1, p_2) + \frac{2g^2}{M_W^2}(p_1, p_3)(p_2, p_3). \end{aligned}$$

Using the conservation of the total 4-momentum and taking $p_1^2 = p_2^2 = 0$ we find

$$\begin{aligned} (p_1, p_3) &= (p_1, p_1 + p_2) = p_1^2 + (p_1, p_2) = (p_1, p_2), \\ (p_2, p_3) &= (p_2, p_1 + p_2) = p_2^2 + (p_1, p_2) = (p_1, p_2). \end{aligned}$$

To find (p_1, p_2) we consider

$$p_3^2 = M_W^2 = (p_1 + p_2)^2 = p_1^2 + p_2^2 + 2(p_1, p_2).$$

Therefore,

$$(p_1, p_2) = \frac{M_W^2}{2}. \quad (\text{B.33})$$

The square of the matrix element becomes

$$|\overline{M}_t|^2 = g^2(p_1, p_2) \left[1 + 2\frac{(p_1, p_2)}{M_W^2} \right],$$

or, using Eq. (B.33), we can rewrite it as

$$|\overline{M}_t|^2 = g^2 M_W^2. \quad (\text{B.34})$$

Calculation of $\frac{\Delta\Gamma}{\Gamma}$

The matrix elements M and M_t are given by Eqs. (B.23) and (B.25), respectively. It is not difficult to see that the calculation of $M^\dagger M_t + M M_t^\dagger$ are very similar to the calculation of $|\overline{M}_t|^2$. We can immediately write down the result

$$\overline{M^\dagger M_t} = g^2 g_X^2 F M_W^2, \quad (\text{B.35})$$

$$\overline{M M_t^\dagger} = g^2 g_X^2 F^* M_W^2, \quad (\text{B.36})$$

and

$$\overline{M^\dagger M_t} + \overline{M M_t^\dagger} = |\overline{M_t}|^2 g_X^2 2 \operatorname{Re} F.$$

Finally,

$$\frac{\Delta \Gamma}{\Gamma} = g_X^2 2 \operatorname{Re} F. \quad (\text{B.37})$$

Therefore, we need to calculate $\operatorname{Re} F$.

B.3 Calculation of the real part of F

The expression for F is given by Eq. (B.22). We can rewrite it as follows.

$$F = -2i \int_0^1 dx dy dz \delta(x + y + z - 1) [I_1 - I_2 \cdot M_W^2 2(1 - y)(y + z)], \quad (\text{B.38})$$

where

$$I_1 = \int \frac{d^d l}{(2\pi)^d} \cdot \frac{r l^2}{(l^2 - \Delta)^3}, \quad (\text{B.39})$$

$$I_2 = \int \frac{d^d l}{(2\pi)^d} \cdot \frac{1}{(l^2 - \Delta)^3}, \quad (\text{B.40})$$

$$r = \frac{(d - 2)^2}{d}. \quad (\text{B.41})$$

Using standard formulas we get³

$$I_2 = \frac{(-1)^3 i}{(4\pi)^{d/2}} \cdot \frac{\Gamma(3 - 2)}{\Gamma(3)} \cdot \left(\frac{1}{\Delta}\right)^{3-2} = -\frac{i}{(4\pi)^2} \cdot \frac{\Gamma(1)}{\Gamma(3)} \cdot \frac{1}{\Delta}.$$

Taking into account that $\Gamma(1) = 0! = 1$ and $\Gamma(3) = 2! = 2$ we obtain

$$I_2 = -\frac{i}{2(4\pi)^2} \cdot \frac{1}{\Delta}. \quad (\text{B.42})$$

Similarly,

$$I_1 = \frac{(-1)^2 i}{(4\pi)^{d/2}} \cdot \frac{d}{2r} \frac{\Gamma(3 - 1 - \frac{d}{2})}{\Gamma(3)} \cdot \left(\frac{1}{\Delta}\right)^{2-\frac{d}{2}} = i \frac{d}{4} \cdot \frac{\Gamma(2 - \frac{d}{2})}{(4\pi)^{d/2}} \cdot \left(\frac{1}{\Delta}\right)^{2-\frac{d}{2}} \cdot \frac{(d - 2)^2}{d}. \quad (\text{B.43})$$

Introducing a small parameter ϵ satisfying $d = 4 - 2\epsilon$ we find that

$$2 - \frac{d}{2} = 2 - (2 - \epsilon) = \epsilon,$$

and

$$(d - 2)^2 = (2 - 2\epsilon)^2 = 4(1 - \epsilon)^2 \approx 4(1 - 2\epsilon).$$

³ Γ 's in the expressions for the integrals I_1 and I_2 stand for Gamma-functions, not the decay width.

Therefore

$$I_1 = \frac{i}{(4\pi)^2} \cdot \Gamma(\epsilon)(4\pi)^\epsilon \Delta^{-\epsilon}(1-2\epsilon). \quad (\text{B.44})$$

Using standard expansion formulas

$$\Gamma(\epsilon) \approx \frac{1}{\epsilon} - \gamma + O(\epsilon), \quad (\text{B.45})$$

$$(4\pi)^\epsilon = e^{\epsilon \ln 4\pi} \approx 1 + \epsilon \ln 4\pi + O(\epsilon), \quad (\text{B.46})$$

$$\Delta^{-\epsilon} = e^{-\epsilon \ln \Delta} \approx 1 - \epsilon \ln \Delta + O(\epsilon), \quad (\text{B.47})$$

we find

$$I_1 = \frac{i}{(4\pi)^2} \left[\frac{1}{\epsilon} + \ln 4\pi - \ln \frac{\Delta}{\mu^2} - 2 - \gamma + O(\epsilon) \right], \quad (\text{B.48})$$

where we introduced a mass scale parameter μ . The final answer must be independent of this parameter.

The expression for F becomes

$$F = \frac{2}{(4\pi)^2} \int_0^1 dx dy dz \delta(x+y+z-1) \left[\frac{1}{\epsilon} + \ln 4\pi - \ln \frac{\Delta}{\mu^2} - 2 - \gamma + \frac{(1-y)(y+z)}{\Delta} \cdot M_W^2 \right]. \quad (\text{B.49})$$

Recall that $\Delta = M_W^2(y^2 - y + yz + z\delta)$, where $\delta = M_X^2/M_W^2$. Introducing integrals

$$\begin{aligned} G_1 &\equiv \int_0^1 dx dy dz \delta(x+y+z-1) \frac{(1-y)(y+z)}{y^2 - y(1-z) + z\delta} \\ &= \int_0^1 dy \int_0^{1-y} dz \frac{(1-y)(y+z)}{y^2 - y(1-z) + z\delta}, \end{aligned} \quad (\text{B.50})$$

$$G_2 \equiv \int_0^1 dy \int_0^{1-y} dz \ln \frac{\Delta}{M_W^2} = \int_0^1 dy \int_0^{1-y} dz \ln(y^2 - y + yz + z\delta) \quad (\text{B.51})$$

$$= \int_0^1 dy \int_0^{1-y} dz \ln[(y+\delta)z - y(1-y)], \quad (\text{B.52})$$

and calculating

$$\int dx dy dz \delta(x+y+z-1) = \int_0^1 dy \int_0^{1-y} dz = \int_0^1 dy(1-y) = \frac{1}{2}, \quad (\text{B.53})$$

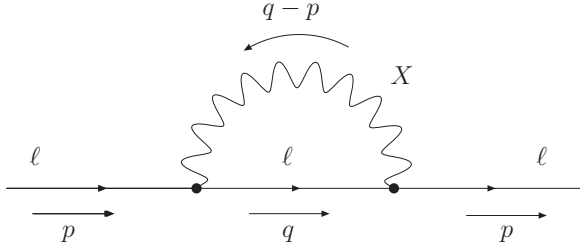


Figure B.3: The X contribution to the self-energy.

we rewrite our expression for F as

$$2F = \frac{1}{4\pi^2} \left\{ \frac{1}{2} \left[\frac{1}{\epsilon} - \gamma - 2 + \ln 4\pi \right] - \frac{1}{2} \ln \frac{M_W^2}{\mu^2} + G_1 - G_2 \right\} \quad (\text{B.54})$$

We will not present here the details of calculations of the two dimensional integrals G_1 and G_2 . The calculations are straightforward, though, a bit tedious. The result is

$$G_1 - G_2 = 1 - \delta - (\delta + 2) \ln \delta - (1 + \delta)^2 \left[\text{Li}_2 \left(\frac{\delta}{1 + \delta} \right) + \frac{1}{2} \ln^2 \delta - \frac{\pi^2}{6} \right], \quad (\text{B.55})$$

where Li_2 is the Spence function defined in the main text by Eq. (2.34). Introducing parameter E defined as

$$E \equiv \frac{1}{\epsilon} - \gamma + \ln 4\pi, \quad (\text{B.56})$$

we obtain the following expression for the real part of F :

$$\text{Re } F = \frac{1}{16\pi^2} \left\{ E - 2 - \ln \frac{M_W^2}{\mu^2} - 2 \left[1 + \delta + (\delta + 2) \ln \delta + (1 + \delta)^2 \left(\text{Li}_2 \left(\frac{\delta}{1 + \delta} \right) + \frac{1}{2} \ln^2 \delta - \frac{\pi^2}{6} \right) \right] \right\}. \quad (\text{B.57})$$

B.4 Contribution from the renormalization of the wave functions

Note that our Eq. (B.57) for $\text{Re } F$ contains a part which blows up in the limit $\epsilon \rightarrow 0$. To make it finite we need to take into account contribution from the renormalization of the wave functions of the final state fermions. In order to do that we need to calculate the X contribution to the fermion self-energy. The corresponding Feynman diagram and our 4-momentum assignment are shown in Fig. B.3.

The Lagrangian is

$$\mathcal{L} = g_X \cdot (\bar{\ell} \gamma^\nu \ell) \cdot X_\nu, \quad (\text{B.58})$$

where $\ell = \{\mu, \nu_\mu\}$. The contribution of the X to the fermion self-energy is

$$-i\Sigma(\not{p}) = (ig_X)^2 \int \frac{d^d q}{(2\pi)^d} \cdot \gamma^\mu \cdot \frac{i \not{q}}{q^2 + i\epsilon} \cdot \gamma^\nu \cdot \frac{ig_{\mu\nu}}{(q-p)^2 - M_X^2 + i\epsilon}$$

Using Eq. (B.19) we can rewrite it as

$$-i\Sigma(\not{p}) = g_X^2 (d-2) \gamma^\mu B_\mu, \quad (\text{B.59})$$

where

$$B_\mu = \int \frac{d^d q}{(2\pi)^d} \cdot \frac{q_\mu}{q^2[(q-p)^2 - M_X^2]} . \quad (\text{B.60})$$

Feynman's formula

$$\frac{1}{AB} = \int_0^1 dx \frac{1}{xA + (1-x)B} \quad (\text{B.61})$$

applied to B_μ gives

$$B_\mu = \int_0^1 dx \int \frac{d^d q}{(2\pi)^d} \cdot \frac{q_\mu}{D} , \quad (\text{B.62})$$

where (remember that $p^2 = 0$)

$$D = (1-x)q^2 + x[q^2 - 2(q,p) - M_X^2] = l^2 - \Delta , \quad \Delta \equiv xM_X^2 .$$

Thus

$$B_\mu = \int_0^1 dx \cdot xp_\mu \int \frac{d^d q}{(2\pi)^d} \cdot \frac{1}{(l^2 - \Delta)^2} , \quad (\text{B.63})$$

and $-i\Sigma(\not{p})$ becomes

$$-i\Sigma(\not{p}) = g_X^2(d-2) \not{p} \int_0^1 dx \cdot x \int \frac{d^d q}{(2\pi)^d} \cdot \frac{1}{(l^2 - \Delta)^2} . \quad (\text{B.64})$$

We can use the following formula to perform d -dimensional integration

$$\int \frac{d^d q}{(2\pi)^d} \cdot \frac{1}{(l^2 - \Delta)^2} = \frac{(-1)^2 i}{(4\pi)^{d/2}} \cdot \frac{\Gamma(2 - \frac{d}{2})}{\Gamma(2)} \left(\frac{1}{\Delta}\right)^{2 - \frac{d}{2}} = \frac{i}{(4\pi)^2} \cdot (4\pi)^\epsilon \cdot \Gamma(\epsilon) \cdot \Delta^{-\epsilon} . \quad (\text{B.65})$$

Expanding ϵ dependent terms to the leading order in ϵ and performing one-dimensional integration over x we obtain

$$\Sigma(\not{p}) = -\frac{g_X^2}{16\pi^2} \cdot \not{p} \cdot \left[E - \ln \frac{M_W^2}{\mu^2} - \ln \delta - \frac{1}{2} \right] , \quad (\text{B.66})$$

where E is defined by Eq. (B.56).

B.5 Putting all together

The self-energy corrections change the propagator of the external fermion. For massless fermions the propagator becomes

$$i \frac{Z_2}{\not{p}} ,$$

where

$$Z_2 = 1 + \frac{d}{d\not{p}} \Sigma(\not{p}) \equiv 1 + \delta Z_2 . \quad (\text{B.67})$$

The square of the matrix element acquires an extra contribution which is equal to

$$iM_t (iM_t \delta Z_2)^\dagger + (iM_t \delta Z_2) (iM_t)^\dagger = |M_t|^2 \cdot 2 \operatorname{Re} \delta Z_2 ,$$

where M_t is the tree level matrix element calculated above. The expression for $\Delta\Gamma/\Gamma$ becomes

$$\frac{\Delta\Gamma}{\Gamma} = g_X^2 \cdot 2 \operatorname{Re}(F + \delta Z_2) . \quad (\text{B.68})$$

Thus, putting all together we find that

$$\frac{\Delta\Gamma}{\Gamma} = -\frac{g_X^2}{4\pi^2} \cdot \left\{ \frac{7}{4} + \delta + \left(\delta + \frac{3}{2} \right) \ln \delta + (1 + \delta)^2 \left[\operatorname{Li}_2 \left(\frac{\delta}{1 + \delta} \right) + \frac{1}{2} \ln^2 \delta - \frac{\pi^2}{6} \right] \right\} . \quad (\text{B.69})$$

This page left blank intentionally.

Appendix C

Minimum χ^2 fit in the $L_\mu - L_\tau$ model

In this Appendix we explain how we made the minimum χ^2 fit in the $L_\mu - L_\tau$ model the result of which we used in section 2.2.5.

The values of the ρ parameter and $\sin^2 \theta_W \equiv s^2$ are shifted by the SM correction and by the corrections specific to the $L_\mu - L_\tau$ model. We denote the SM corrections to the tree level values of the ρ parameter and s^2 by $\delta\rho_{\text{SM}}$ and δs_{SM}^2 , respectively. We also denote the corresponding $L_\mu - L_\tau$ model corrections to ρ and s^2 by $\delta\rho$ and δs^2 .

The effective Z couplings are¹

$$e : \quad g_V^e = \sqrt{\rho} \left(-\frac{1}{2} + 2s_*^2 \right), \quad g_A^e = \sqrt{\rho} \left(-\frac{1}{2} \right), \quad (\text{C.1})$$

$$\mu : \quad g_V^\mu = \sqrt{\rho} \left(-\frac{1}{2} + 2s_*^2 \right) (1 + \delta_V) + \delta_M, \quad g_A^\mu = \sqrt{\rho} \left(-\frac{1}{2} \right) (1 + \delta_V), \quad (\text{C.2})$$

$$\tau : \quad g_V^\tau = \sqrt{\rho} \left(-\frac{1}{2} + 2s_*^2 \right) (1 + \delta_V) - \delta_M, \quad g_A^\tau = \sqrt{\rho} \left(-\frac{1}{2} \right) (1 + \delta_V) \quad (\text{C.3})$$

for charged leptons and

$$\nu_e : \quad g_V^{\nu_e} = \sqrt{\rho} \left(+\frac{1}{2} \right), \quad g_A^{\nu_e} = \sqrt{\rho} \left(+\frac{1}{2} \right), \quad (\text{C.4})$$

$$\nu_\mu : \quad g_V^{\nu_\mu} = \sqrt{\rho} \cdot \left(+\frac{1}{2} \right) \cdot (1 + \delta_V) + \frac{\delta_M}{2}, \quad g_A^{\nu_\mu} = \sqrt{\rho} \cdot \left(+\frac{1}{2} \right) \cdot (1 + \delta_V) + \frac{\delta_M}{2}, \quad (\text{C.5})$$

$$\nu_\tau : \quad g_V^{\nu_\tau} = \sqrt{\rho} \cdot \left(+\frac{1}{2} \right) \cdot (1 + \delta_V) - \frac{\delta_M}{2}, \quad g_A^{\nu_\tau} = \sqrt{\rho} \cdot \left(+\frac{1}{2} \right) \cdot (1 + \delta_V) - \frac{\delta_M}{2}. \quad (\text{C.6})$$

s_*^2 is the corrected value of the $\sin^2 \theta_W$. The $\sqrt{\rho}$ and s_*^2 are

$$\sqrt{\rho} = \sqrt{1 + \delta\rho_{\text{SM}} + \delta\rho} \approx 1 + \frac{1}{2}\delta\rho_{\text{SM}} + \frac{1}{2}\delta\rho, \quad (\text{C.7})$$

$$s_*^2 = s^2 + \delta s_{\text{SM}}^2 + \delta s^2. \quad (\text{C.8})$$

¹See Eqs. (2.50) through (2.55).

The result of plugging these expressions in Eq. (C.1) should be equal to the experimentally measured value of g_V^e :

$$\begin{aligned}
[g_V^e]_{\text{exp}} &= \left(1 + \frac{1}{2}\delta\rho_{\text{SM}} + \frac{1}{2}\delta\rho\right) \left(-\frac{1}{2} + 2s^2 + 2\delta s_{\text{SM}}^2 + 2\delta s^2\right) \\
&= \left(-\frac{1}{2} + 2s^2\right) \left(1 + \frac{2\delta s_{\text{SM}}^2}{-\frac{1}{2} + 2s^2}\right) \left(1 + \frac{1}{2}\delta\rho_{\text{SM}}\right) \left(1 + \frac{1}{2}\delta\rho + \frac{2\delta s^2}{-\frac{1}{2} + 2s^2}\right) \\
&= [g_V^e]_{\text{ZF}} \left(1 + \frac{1}{2}\delta\rho + \frac{2\delta s^2}{-\frac{1}{2} + 2s^2}\right),
\end{aligned}$$

where

$$[g_V^e]_{\text{ZF}} \equiv \left(-\frac{1}{2} + 2s^2\right) \left(1 + \frac{1}{2}\delta\rho_{\text{SM}} + \frac{2\delta s_{\text{SM}}^2}{-\frac{1}{2} + 2s^2}\right)$$

is the SM prediction for g_V^e which includes one-loop corrections. We calculate the values of $[g_V^e]_{\text{ZF}}$ using the ZFITTER program package. We can do analogous calculations for the effective couplings of the other charged leptons. The result is

$$[g_V^e]_{\text{exp}} = [g_V^e]_{\text{ZF}} \left(1 + \frac{1}{2}\delta\rho + \frac{2\delta s^2}{-\frac{1}{2} + 2s^2}\right), \quad (\text{C.9})$$

$$[g_A^e]_{\text{exp}} = [g_A^e]_{\text{ZF}} \left(1 + \frac{1}{2}\delta\rho\right), \quad (\text{C.10})$$

$$[g_V^\mu]_{\text{exp}} = [g_V^\mu]_{\text{ZF}} \left(1 + \frac{1}{2}\delta\rho + \frac{2\delta s^2}{-\frac{1}{2} + 2s^2} + \frac{\delta_M}{-\frac{1}{2} + 2s^2} + \delta_V\right), \quad (\text{C.11})$$

$$[g_A^\mu]_{\text{exp}} = [g_A^\mu]_{\text{ZF}} \left(1 + \frac{1}{2}\delta\rho + \delta_V\right), \quad (\text{C.12})$$

$$[g_V^\tau]_{\text{exp}} = [g_V^\tau]_{\text{ZF}} \left(1 + \frac{1}{2}\delta\rho + \frac{2\delta s^2}{-\frac{1}{2} + 2s^2} - \frac{\delta_M}{-\frac{1}{2} + 2s^2} + \delta_V\right), \quad (\text{C.13})$$

$$[g_A^\tau]_{\text{exp}} = [g_A^\tau]_{\text{ZF}} \left(1 + \frac{1}{2}\delta\rho + \delta_V\right), \quad (\text{C.14})$$

Now, let us consider the effective couplings for the neutrinos. The LEP collaboration extracted the value of $g_A^\nu = g_V^\nu$ from the measurement of the Z invisible width. So, g_A^ν is actually the *average*

value of the effective neutrino couplings given by Eqs. (C.4)-(C.6). The value of this parameter is cited in Table 2.2 of section 2.2.5. Thus, using Eqs. (C.4)-(C.6) we find

$$[g_A^\nu]_{\text{exp}} = [g_V^\nu]_{\text{exp}} = \sqrt{\rho} \left(+\frac{1}{2} \right) \cdot \frac{1}{3} (3 + 2\delta_V).$$

Expanding the $\sqrt{\rho}$ as in Eq. (C.7) and factoring out the SM contribution we obtain

$$[g_A^\nu]_{\text{exp}} = [g_A^\nu]_{\text{ZF}} \left(1 + \frac{1}{2}\rho + \frac{2}{3}\delta_V \right). \quad (\text{C.15})$$

Now we have everything at hand to construct the χ^2 function. First of all, we introduce the vector:

$$X^T = (x_1, x_2, x_3, x_4, x_5, x_6, x_7), \quad (\text{C.16})$$

where

$$x_i = \frac{x_i^{\text{th}} - x_i^{\text{exp}}}{\sigma_i}, \quad i = 1, \dots, 7. \quad (\text{C.17})$$

x_i^{th} are given by the functions of δs^2 , $\delta\rho$, δ_V , and δ_M appearing on the right-hand sides of Eqs. (C.9)-(C.15) and x_i^{exp} are the central values of the effective couplings appearing on the left-hand sides of these equations. σ_j are the standard deviations of the experimental values². We are treating x_i^{th} as true values.

The χ^2 function is

$$\chi^2 = -\frac{1}{2} \cdot X^T A X, \quad (\text{C.18})$$

where A is the matrix which can be found from the following relationship

$$\langle x_i \cdot x_j \rangle = \text{Cov}(x_i^{\text{exp}}, x_j^{\text{exp}}) / (\sigma_i \sigma_j) = r_{ij} = (A^{-1})_{ij}. \quad (\text{C.19})$$

r_{ij} are the correlation coefficients. They can be found in Table 2.2. The matrix A is found to be

$$A = \begin{pmatrix} 3.3484 & 2.3177 & -0.8600 & -0.6544 & 0.2527 & -0.2924 & -0.0730 \\ 2.3177 & 2.6293 & -0.4817 & -0.3691 & 0.1719 & -0.1696 & -0.0359 \\ -0.8600 & -0.4817 & 1.5104 & -0.2757 & -0.0278 & 0.4706 & -0.0273 \\ -0.6544 & -0.3691 & -0.2757 & 1.3015 & -0.0321 & -0.0869 & 0.1035 \\ 0.2527 & 0.1719 & -0.0278 & -0.0321 & 1.0316 & 0.0899 & 0.0144 \\ -0.2924 & -0.1696 & 0.4706 & -0.0869 & 0.0899 & 1.1571 & -0.0164 \\ -0.0730 & -0.0359 & -0.0273 & 0.1035 & 0.0144 & -0.0164 & 1.0091 \end{pmatrix}. \quad (\text{C.20})$$

The values of δs^2 , $\delta\rho$, δ_V , and δ_M minimizing the χ^2 function are listed in the second column of Table 2.1.

To find the standard deviations and correlation coefficients we need to reinterpret the constructed χ^2 in terms of new variables ($\xi_i - \xi_i^0$), $i = 1, \dots, 4$, where

$$\xi_1 = \delta s^2, \quad \xi_2 = \delta\rho, \quad \xi_3 = \delta_V, \quad \xi_4 = \delta_V, \quad (\text{C.21})$$

²The central values, standard deviations, and correlation coefficients are listed in Table 2.2. Our assignment for indices i and j can also be seen from the table.

and ξ_i^0 are the central values listed in the second column of Table 2.1. In terms of these new variable the χ^2 becomes

$$\chi^2 = -\frac{1}{2} \cdot \sum_{i=1}^4 \sum_{j=1}^4 (\xi_i - \xi_i^0) b_{ij} (\xi_j - \xi_j^0). \quad (\text{C.22})$$

Matrix B is

$$B = \begin{pmatrix} 2.38852 \times 10^7 & -550217. & -122638. & -1.44191 \times 10^6 \\ -550217. & 980177. & 515371. & -22792.3 \\ -122638. & 515371. & 2.71172 \times 10^6 & -89745.8 \\ -1.44191 \times 10^6 & -22792.3 & -89745.8 & 1.21361 \times 10^6 \end{pmatrix}. \quad (\text{C.23})$$

Inverse of this matrix is the variance-covariance matrix for δs^2 , $\delta\rho$, δ_V , and δ_M :

$$B^{-1} = \begin{pmatrix} 0.45809 \cdot 10^{-7} & 0.27716 \cdot 10^{-7} & -0.13807 \cdot 10^{-8} & 0.54845 \cdot 10^{-7} \\ 0.27716 \cdot 10^{-7} & 0.11503 \cdot 10^{-5} & -0.21609 \cdot 10^{-6} & 0.38554 \cdot 10^{-7} \\ -0.13807 \cdot 10^{-8} & -0.21609 \cdot 10^{-6} & 0.41059 \cdot 10^{-6} & 0.24664 \cdot 10^{-7} \\ 0.54845 \cdot 10^{-7} & 0.38554 \cdot 10^{-7} & 0.24664 \cdot 10^{-7} & 0.89170 \cdot 10^{-6} \end{pmatrix}, \quad (\text{C.24})$$

and the correlation matrix is

$$Corr = \begin{pmatrix} 1 & 0.12074 & -0.01007 & 0.27136 \\ 0.12074 & 1 & -0.31443 & 0.03807 \\ -0.01007 & -0.31443 & 1 & 0.04076 \\ 0.27136 & 0.03807 & 0.04076 & 1 \end{pmatrix}. \quad (\text{C.25})$$

Thus, the central values of δs^2 , $\delta\rho$, δ_V , and δ_M and the corresponding standard deviations are given in Table 2.1, and the correlation coefficients are listed in Eq. (C.25). The combination has a χ^2/dof of 5.10/3.

Appendix D

Calculation of the neutrissimo lifetime

In this Appendix we calculate the 2-body decay widths of the neutrissimo for all three decay channels: $N \rightarrow n + Z$, $N \rightarrow l + W$, $N \rightarrow n + h$.

D.1 $N_i \rightarrow n_j + Z$

Only the first term of the Lagrangian given by Eq. (3.28) is relevant for these processes. This term is

$$\mathcal{L} = \frac{g}{2 \cos \theta_W} [\bar{n}_j (A_{ji} \gamma^\mu P_L - (A^{ji})^* \gamma^\mu P_R) N_i] Z_\mu. \quad (\text{D.1})$$

We find it convenient to introduce the following notation:

$$a^{ji} \equiv \frac{g}{2 \cos \theta_W} (A^{ji})^* \quad (\text{D.2})$$

Then, the interaction Lagrangian becomes

$$\mathcal{L} = \bar{n} (a^* \gamma^\mu P_L - a \gamma^\mu P_R) N Z_\mu, \quad (\text{D.3})$$

where we dropped indices i and j . We will reintroduce them at the final stage of our calculations.

Feynman diagram corresponding to the process in question is the third diagram in Fig. 3.4. The matrix element and its conjugated are

$$iM = ia^* \epsilon_\mu(k) \bar{u}_n(q) \gamma^\mu P_L u_N(p) - ia \epsilon_\mu(k) \bar{u}_n(q) \gamma^\mu P_R u_N(p), \quad (\text{D.4})$$

$$-iM^\dagger = -ia \epsilon_\nu^*(k) \bar{u}_N(p) \gamma^\nu P_L u_n(q) + ia^* \epsilon_\nu^*(k) \bar{u}_N(p) \gamma^\nu P_R u_n(q), \quad (\text{D.5})$$

where p , q , and k are momenta of N , n , and Z , respectively. Squaring the matrix element and summing over spins and polarizations of the final state particles we obtain

$$\begin{aligned} |\bar{M}|^2 &\equiv \sum_{\text{spins, pol's}} MM^\dagger = |a|^2 \left(\sum_{\text{pol's}} \epsilon_\mu(k) \epsilon_\nu^*(k) \right) \sum_{\text{spins}} \{ \text{Tr} [\bar{u}_n(q) \gamma^\mu P_L u_N(p) \bar{u}_N(p) \gamma^\nu P_L u_n(q)] \\ &- \text{Tr} [\bar{u}_n(q) \gamma^\mu P_R u_N(p) \bar{u}_N(p) \gamma^\nu P_L u_n(q)] + \text{Tr} [\bar{u}_n(q) \gamma^\mu P_R u_N(p) \bar{u}_N(p) \gamma^\nu P_R u_n(q)] \\ &- \text{Tr} [\bar{u}_n(q) \gamma^\mu P_L u_N(p) \bar{u}_N(p) \gamma^\nu P_R u_n(q)] \}. \end{aligned} \quad (\text{D.6})$$

Now let us make use of the following relationships:

$$\sum_{\text{spins}} u_N(p) \bar{u}_N(p) = \not{p} + M, \quad (\text{D.7})$$

$$\sum_{\text{spins}} u_n(q) \bar{u}_n(q) = \not{q}, \quad (\text{D.8})$$

$$\sum_{\text{pol's}} \epsilon_\mu(k) \epsilon_\nu^*(k) = -g_{\mu\nu} + \frac{k_\mu k_\nu}{M_Z^2}, \quad (\text{D.9})$$

where M and M_Z are the neutrino and Z boson masses, respectively¹. The masses of the light neutrinos n are negligibly small.

Now we can write

$$\begin{aligned} \text{Tr} [\bar{u}_n(q) \gamma^\mu P_{R,L} u_N(p) \bar{u}_N(p) \gamma^\nu P_{L,R} u_n(q)] &= \text{Tr} [\not{q} \gamma^\mu P_{R,L} (\not{p} + M) \gamma^\nu P_{L,R}] \\ &= \text{Tr} [P_{L,R} \not{q} \gamma^\mu P_{R,L} (\not{p} + M) \gamma^\nu] = \text{Tr} [\not{q} \gamma^\mu P_{L,R} P_{R,L} (\not{p} + M) \gamma^\nu] = 0. \end{aligned} \quad (\text{D.10})$$

Thus, we see that the second and the third terms in Eq. (D.6) are equal to zero.

$$\begin{aligned} |\bar{M}|^2 &= |a|^2 \text{Tr} \left[\not{q} \gamma^\mu P_L (\not{p} + M) \gamma^\nu P_L + \not{q} \gamma^\mu P_R (\not{p} + M) \gamma^\nu P_R \right] \left(\frac{k_\mu k_\nu}{M_Z^2} - g_{\mu\nu} \right) \\ &= |a|^2 \left(\frac{k_\mu k_\nu}{M_Z^2} - g_{\mu\nu} \right) \text{Tr} [\not{q} \gamma^\mu \not{p} \gamma^\nu], \end{aligned} \quad (\text{D.11})$$

because $P_L + P_R = I$.

$$|\bar{M}|^2 = |a|^2 \left(\frac{k_\mu k_\nu}{M_Z^2} - g_{\mu\nu} \right) q_\alpha p_\beta \text{Tr} (\gamma^\alpha \gamma^\mu \gamma^\beta \gamma^\nu). \quad (\text{D.12})$$

$$\text{Tr} (\gamma^\alpha \gamma^\mu \gamma^\beta \gamma^\nu) = 4 (g^{\alpha\mu} g^{\beta\nu} - g^{\alpha\beta} g^{\mu\nu} + g^{\alpha\nu} g^{\beta\mu}). \quad (\text{D.13})$$

$$\begin{aligned} |\bar{M}|^2 &= |a|^2 \left(\frac{k_\mu k_\nu}{M_Z^2} - g_{\mu\nu} \right) 4 (q^\mu p^\nu - (p, q) g^{\mu\nu} + q^\nu p^\mu) \\ &= 4|a|^2 \left[\frac{(k, q)(k, p) - (p, q)k^2 + (k, q)(k, p)}{M_Z^2} - (p, q) + 4(p, q) - (p, q) \right], \end{aligned} \quad (\text{D.14})$$

where we used $g^{\mu\nu} g_{\mu\nu} = 4$.

$$\begin{aligned} |\bar{M}|^2 &= 4|a|^2 \left[\frac{2(k, q)(k, p) - (p, q)M_Z^2}{M_Z^2} + 2(p, q) \right] \\ &= 4|a|^2 \frac{2(k, q)(k, p) + (p, q)M_Z^2}{M_Z^2}. \end{aligned} \quad (\text{D.15})$$

¹The neutrino mass M should not be confused with our notation for the matrix element. We hope that the distinction between them is self-obvious.

Let us now find the scalar products in the expression above. Note that

$$p^2 = M^2 = (q + k)^2 = q^2 + k^2 + 2(k, q) = M_Z^2 + 2(k, q).$$

Therefore,

$$(k, q) = \frac{M^2 - M_Z^2}{2}. \quad (\text{D.16})$$

Using the conservation of the total momentum we can write

$$(p, q) = (q + k, q) = q^2 + (k, q).$$

This means that

$$(p, q) = \frac{M^2 - M_Z^2}{2}. \quad (\text{D.17})$$

Similarly,

$$(k, p) = (k, p + k) = (k, q) + k^2 = \frac{M^2 - M_Z^2}{2} + M_Z^2 = \frac{M^2 + M_Z^2}{2}.$$

Using these results we can rewrite Eq. (D.15) as follows.

$$|\bar{M}|^2 = 4|a|^2 \frac{M^2 - M_Z^2}{2M_Z^2} (M^2 + 2M_Z^2),$$

or, finally,

$$|\bar{M}|^2 = 2|a|^2 \frac{M^4}{M_Z^2} \left(1 - \frac{M_Z^2}{M^2}\right) \left(1 + 2\frac{M_Z^2}{M^2}\right). \quad (\text{D.18})$$

D.2 $N_i \rightarrow \ell_j^\mp + W^\pm$

Only the second and the third terms of the Lagrangian given by Eq. (3.28) are relevant for these processes. They are

$$\mathcal{L} = \frac{g}{\sqrt{2}} (\bar{\ell}_j B^{ji} \gamma^\mu P_L N_i) W_\mu^- - \frac{g}{\sqrt{2}} (\bar{\ell}_j^c (B^{ji})^* \gamma^\mu P_R N_i) W_\mu^+. \quad (\text{D.19})$$

Recall that

$$\bar{\ell} = \int \frac{d^3 \vec{k}}{(2\pi)^3 2E_{\vec{k}}} \sum_s [b_s^\dagger(k) \bar{u}_s(k) e^{ikx} + d_s(k) \bar{v}_s(k) e^{-ikx}], \quad (\text{D.20})$$

$$\bar{\ell}^c = \int \frac{d^3 \vec{k}}{(2\pi)^3 2E_{\vec{k}}} \sum_s [b_s(k) \bar{v}_s(k) e^{-ikx} + d_s^\dagger(k) \bar{u}_s(k) e^{ikx}]. \quad (\text{D.21})$$

We find it convenient to introduce the following notation:

$$b^{ji} \equiv \frac{g}{\sqrt{2}} B^{ji}. \quad (\text{D.22})$$

- Let us consider the process $N_i \rightarrow \ell^+ + W^-$ generated by the second term of the Lagrangian (D.19). The corresponding Feynman diagram is the second diagram in Fig. 3.4. The Lagrangian is

$$\mathcal{L} = -b^* (\bar{\ell}^c \gamma^\mu P_R N) W_\mu^+. \quad (\text{D.23})$$

where we dropped the indices i and j . We will reinstate them in the very end of our calculations.

The matrix element and its conjugated are

$$iM = -ib^* \epsilon_\mu(k) \bar{u}_l(q) \gamma^\mu P_R u_N(p), \quad (\text{D.24})$$

$$-iM^\dagger = ib \epsilon_\nu^*(k) \bar{u}_N(p) \gamma^\nu P_R u_l(q), \quad (\text{D.25})$$

where p , q , and k are momenta of the neutrino, lepton, and W boson, respectively.

$$|\bar{M}|^2 = |b|^2 \left(\frac{k_\mu k_\nu}{M_Z^2} - g_{\mu\nu} \right) \text{Tr} [\not{q} \gamma^\mu P_R (\not{p} + M) \gamma^\nu P_R]. \quad (\text{D.26})$$

Note that

$$q_\alpha p_\beta \text{Tr} (\gamma^\alpha \gamma^\mu \gamma^\beta \gamma^\nu \gamma_5) \sim q_\alpha p_\beta \epsilon^{\alpha\mu\beta\nu}. \quad (\text{D.27})$$

The antisymmetric tensor is contracted with the symmetric tensor $(k_\mu k_\nu)/M_Z^2 - g_{\mu\nu}$. The resulting combination is obviously zero. Thus, we only have to consider

$$|\bar{M}|^2 = \frac{|b|^2}{2} \left(\frac{k_\mu k_\nu}{M_Z^2} - g_{\mu\nu} \right) q_\alpha p_\beta \text{Tr} (\gamma^\alpha \gamma^\mu \gamma^\beta \gamma^\nu) = 2|b|^2 \left(\frac{k_\mu k_\nu}{M_Z^2} - g_{\mu\nu} \right) (q^\mu p^\nu - (p, q) g^{\mu\nu} + q^\nu p^\mu), \quad (\text{D.28})$$

where we make use of Eq. (D.13). But we already calculated a similar combination in part D.1. Thus, we can easily write down the result which is

$$|\bar{M}|^2 = |b|^2 \frac{M^4}{M_W^2} \left(1 - \frac{M_W^2}{M^2} \right) \left(1 + 2 \frac{M_W^2}{M^2} \right). \quad (\text{D.29})$$

- The process $N_i \rightarrow \ell^- + W^+$ generated by the first term of the Lagrangian (D.19) corresponds to the first Feynman diagram in Fig. 3.4. The Lagrangian is

$$\mathcal{L} = b (\bar{\ell} \gamma^\mu P_L N) W_\mu^-. \quad (\text{D.30})$$

It is not difficult to see that in this case calculations are exactly the same as in the $N_i \rightarrow \ell^+ + W^-$ case. We will not repeat them here. It should be clear that the final result for $|\bar{M}|^2$ is given by the same Eq. (D.29).

D.3 $N_i \rightarrow n_j + h$

Only the last term of the Lagrangian given by Eq. (3.28) is relevant for this process. It is

$$\mathcal{L} = -\bar{n}_j \left[C^{ji} h P_L + \left(C^{ji} \tilde{h} P_R \right)^* \right] N_i. \quad (\text{D.31})$$

The corresponding Feynman diagram is the last diagram shown in Fig. 3.4. Dropping indices i and j , we find that the matrix element for this process and its conjugated are

$$iM = -i\bar{u}_n(q) (CP_L + C^*P_R) u_N(p), \quad (\text{D.32})$$

$$-iM^\dagger = i\bar{u}_N(p) (C^*P_L + CP_R) u_n(q). \quad (\text{D.33})$$

Therefore,

$$\begin{aligned} |\bar{M}|^2 &= \text{Tr}[(\not{p} + M)(C^*P_R + CP_L) \not{q}(CP_L + C^*P_R)] \\ &= |C|^2 \{ \text{Tr}[(\not{p} + M) \not{q}P_L] + \text{Tr}[(\not{p} + M) \not{q}P_R] \} = |C|^2 \text{Tr}(\not{p} \not{q}) \end{aligned} \quad (\text{D.34})$$

$$= 4|C|^2(p, q). \quad (\text{D.35})$$

Using the conservation of the total 4-momentum we can write

$$(p, q) = \frac{M^2 - m_h^2}{2}, \quad (\text{D.36})$$

which is analogous to the result given by Eq. (D.17). Thus, finally, we can rewrite the expression for the square of the matrix element as

$$|\bar{M}|^2 = 2|C|^2(M^2 - m_h^2). \quad (\text{D.37})$$

D.4 Integration over the phase space

Now we need to calculate phase space factors associated with the processes we have just considered. We consider a general case when N with the 4-momentum p decays into a two-particle state. One particle in the final state is assumed to be massive with the 4-momentum k and the other is assumed to be massless and with the 4-momentum q . The final formula will be applicable to all processes we considered above.

The differential decay width is

$$d\Gamma = \frac{1}{2s+1} \frac{1}{2E} |\bar{M}|^2 (2\pi)^4 \delta^4(p - q - k) \frac{d^3\vec{q}}{2E_1(2\pi)^3} \frac{d^3\vec{k}}{2E_2(2\pi)^3}, \quad (\text{D.38})$$

where $s = 1/2$ is the spin of the neutrino, E , E_1 , and E_2 and the energies of the neutrino, massless and massive particles, respectively. At the rest frame of the neutrino $E = M$. Thus,

$$d\Gamma = \frac{1}{2} \cdot \frac{|\bar{M}|^2}{2M} \cdot \frac{1}{4(2\pi)^2} \cdot \delta^4(p - q - k) \cdot \frac{d^3\vec{q}}{E_1} \cdot \frac{d^3\vec{k}}{E_2}. \quad (\text{D.39})$$

Now we have to integrate over all possible \vec{q} and \vec{k} . In order to do that let us consider

$$D \equiv \int \delta^4(p - q - k) \cdot \frac{d^3\vec{q}}{E_1} \cdot \frac{d^3\vec{k}}{E_2} = \int \delta(M - E_1 - E_2) \cdot \frac{d^3\vec{q}}{E_1 E_2}. \quad (\text{D.40})$$

Note that

$$d^3\vec{q} = |\vec{q}|^2 d|\vec{q}| d\Omega, \quad (\text{D.41})$$

where $d\Omega$ is the element of the solid angle. By examining Eqs. (D.18), (D.29), and (D.37) we can easily convince ourselves that $|\bar{M}|^2$'s do not have any angular dependence in the case we are interested in. Thus, the solid angle part can be integrated out giving us an extra factor of 4π .

At the rest frame of the neutrissimo $\vec{q} + \vec{k} = 0$ which means that $|\vec{q}| = |\vec{k}|$. Then

$$E_1^2 - |\vec{q}|^2 = 0, \quad E_2 - |\vec{q}|^2 = m^2,$$

where $m = \{M_Z, M_W, m_h\}$ depending on the decay channel. Differentiating these equations we get

$$2E_1 dE_1 = 2E_2 dE_2 = 2|\vec{q}| d|\vec{q}|,$$

or

$$dE_1 = \frac{|\vec{q}| d|\vec{q}|}{E_1}, \quad dE_2 = \frac{|\vec{q}| d|\vec{q}|}{E_2}.$$

Therefore,

$$d(E_1 + E_2) = \left(\frac{1}{E_1} + \frac{1}{E_2} \right) |\vec{q}| d|\vec{q}| = \frac{E_1 + E_2}{E_1 E_2} |\vec{q}| d|\vec{q}|.$$

This means that

$$d|\vec{q}| = \frac{E_1 E_2}{E_1 + E_2} \cdot \frac{d(E_1 + E_2)}{|\vec{q}|}. \quad (\text{D.42})$$

We will see below that $|\vec{q}|$ is a constant. Thus, we can write

$$D = 4\pi \int \delta[M - (E_1 + E_2)] \cdot \frac{|\vec{q}|^2}{E_1 E_2} \cdot \frac{E_1 E_2}{E_1 + E_2} \cdot \frac{d(E_1 + E_2)}{|\vec{q}|},$$

or

$$D = \frac{4\pi |\vec{q}|}{M}. \quad (\text{D.43})$$

Now we can calculate the total decay width.

$$\Gamma = \int d\Gamma = \frac{1}{2} \cdot \frac{1}{2M} |\bar{M}|^2 \frac{1}{(2\pi)^2} \frac{1}{4} D = \frac{|\bar{M}|^2}{16M} \frac{1}{4\pi^2} \frac{4\pi |\vec{q}|}{M},$$

or

$$\Gamma = \frac{|\bar{M}|^2}{16\pi M^2} |\vec{q}|. \quad (\text{D.44})$$

What is $|\vec{q}|$? Using the conservation of the total 4-momentum we find that

$$(p, q) = \frac{M^2 - m^2}{2},$$

which is analogous to the result given by Eq. (D.17). On the other hand, at the rest frame of the neutrissimo

$$(p, q) = ME_1 = M|\vec{q}|,$$

where we used $E_1^2 - |\vec{q}|^2 = 0$. Thus,

$$|\vec{q}| = \frac{M}{2} \left(1 - \frac{m^2}{M^2} \right). \quad (\text{D.45})$$

The total decay width becomes

$$\Gamma = \frac{|\bar{M}|^2}{32\pi M} \cdot \left(1 - \frac{m^2}{M^2}\right). \quad (\text{D.46})$$

Now we can put our results together. Using our formulas for $|\bar{M}|^2$'s given by Eqs. (D.18), (D.29), and (D.37) and Eq. (D.46) we find the expressions for the decay widths

$$\begin{aligned} \Gamma(N \rightarrow nZ) &= \frac{|a|^2}{16\pi} \cdot \frac{M^3}{M_Z^2} \cdot \left(1 - \frac{M_Z^2}{M^2}\right)^2 \left(1 + 2\frac{M_Z^2}{M^2}\right), \\ \Gamma(N \rightarrow \ell^+W^-) = \Gamma(N \rightarrow \ell^-W^+) &= \frac{|b|^2}{32\pi} \cdot \frac{M^3}{M_W^2} \cdot \left(1 - \frac{M_W^2}{M^2}\right)^2 \cdot \left(1 + 2\frac{M_W^2}{M^2}\right), \\ \Gamma(N \rightarrow nh) &= \frac{|C|^2}{16\pi} \cdot M \left(1 - \frac{m_h^2}{M^2}\right)^2. \end{aligned} \quad (\text{D.47})$$

Recall that

$$a = \frac{g}{2 \cos \theta_W} A^*, \quad b = \frac{g}{\sqrt{2}} B.$$

Therefore,

$$\begin{aligned} \Gamma(N \rightarrow nZ) &= \frac{g^2 |A|^2}{64\pi \cos^2 \theta_W} \cdot \frac{M^3}{M_Z^2} \cdot \left(1 - \frac{M_Z^2}{M^2}\right)^2 \left(1 + 2\frac{M_Z^2}{M^2}\right), \\ \Gamma(N \rightarrow \ell^+W^-) = \Gamma(N \rightarrow \ell^-W^+) &= \frac{g^2 |B|^2}{64\pi} \cdot \frac{M^3}{M_W^2} \cdot \left(1 - \frac{M_W^2}{M^2}\right)^2 \cdot \left(1 + 2\frac{M_W^2}{M^2}\right), \\ \Gamma(N \rightarrow nh) &= \frac{|C|^2}{16\pi} \cdot M \left(1 - \frac{m_h^2}{M^2}\right)^2. \end{aligned} \quad (\text{D.48})$$

Now, making use of the well-known relationships

$$\cos \theta_W = \frac{M_W}{M_Z}, \quad g^2 = \sqrt{2} G_F \cdot 4M_W^2,$$

and reinstating the indices i and j we obtain the expressions for the decay widths given by Eq. (3.31).

This page left blank intentionally.

Appendix E

Errors on the effective couplings in the NuSOnG analysis

In this Appendix we show how measurements of $\sigma(\nu_\mu e)$ and $\sigma(\bar{\nu}_\mu e)$ translate into constraints on $g_V^{\nu e}$ and $g_A^{\nu e}$. From Eq. (4.6), we find

$$\begin{aligned}\frac{\delta\sigma_{\nu_\mu e}}{\sigma_{\nu_\mu e}} &= \frac{2g_V^{\nu e} + g_A^{\nu e}}{(g_V^{\nu e})^2 + g_V^{\nu e}g_A^{\nu e} + (g_A^{\nu e})^2} \delta g_V^{\nu e} + \frac{g_V^{\nu e} + 2g_A^{\nu e}}{(g_V^{\nu e})^2 + g_V^{\nu e}g_A^{\nu e} + (g_A^{\nu e})^2} \delta g_A^{\nu e}, \\ \frac{\delta\sigma_{\bar{\nu}_\mu e}}{\sigma_{\bar{\nu}_\mu e}} &= \frac{2g_V^{\nu e} - g_A^{\nu e}}{(g_V^{\nu e})^2 - g_V^{\nu e}g_A^{\nu e} + (g_A^{\nu e})^2} \delta g_V^{\nu e} - \frac{g_V^{\nu e} - 2g_A^{\nu e}}{(g_V^{\nu e})^2 - g_V^{\nu e}g_A^{\nu e} + (g_A^{\nu e})^2} \delta g_A^{\nu e}.\end{aligned}\quad (\text{E.1})$$

To simplify the notation, let us make the replacements $g_V^{\nu e} \rightarrow V$, and $g_A^{\nu e} \rightarrow A$. Then,

$$\begin{aligned}\frac{\delta\sigma_{\nu_\mu e}}{\sigma_{\nu_\mu e}} &= \left(\frac{2V + A}{V^2 + VA + A^2} \right) \delta V + \left(\frac{V + 2A}{V^2 + VA + A^2} \right) \delta A, \\ \frac{\delta\sigma_{\bar{\nu}_\mu e}}{\sigma_{\bar{\nu}_\mu e}} &= \left(\frac{2V - A}{V^2 - VA + A^2} \right) \delta V - \left(\frac{V - 2A}{V^2 - VA + A^2} \right) \delta A.\end{aligned}\quad (\text{E.2})$$

Inverting this relation, we find

$$\begin{aligned}\delta V &= \frac{(V^2 + VA + A^2)(V - 2A)}{4(V^2 - A^2)} \frac{\delta\sigma_{\nu_\mu e}}{\sigma_{\nu_\mu e}} + \frac{(V^2 - VA + A^2)(V + 2A)}{4(V^2 - A^2)} \frac{\delta\sigma_{\bar{\nu}_\mu e}}{\sigma_{\bar{\nu}_\mu e}}, \\ \delta A &= \frac{(V^2 + VA + A^2)(2V - A)}{4(V^2 - A^2)} \frac{\delta\sigma_{\nu_\mu e}}{\sigma_{\nu_\mu e}} - \frac{(V^2 - VA + A^2)(2V + A)}{4(V^2 - A^2)} \frac{\delta\sigma_{\bar{\nu}_\mu e}}{\sigma_{\bar{\nu}_\mu e}}.\end{aligned}\quad (\text{E.3})$$

To simplify the notation further, let us write the fractional errors of $\sigma_{\nu_\mu e}$ and $\sigma_{\bar{\nu}_\mu e}$ as $\epsilon_{\nu e}$ and $\epsilon_{\bar{\nu} e}$, respectively. Assuming that the measurements of $\sigma_{\nu_\mu e}$ and $\sigma_{\bar{\nu}_\mu e}$ are uncorrelated (for the sake of simplicity), we find

$$\begin{aligned}\langle \delta V \delta V \rangle &= \frac{(V^2 + VA + A^2)^2 (V - 2A)^2}{16(V^2 - A^2)^2} \epsilon_{\nu e}^2 + \frac{(V^2 - VA + A^2)^2 (V + 2A)^2}{16(V^2 - A^2)^2} \epsilon_{\bar{\nu} e}^2, \\ \langle \delta A \delta A \rangle &= \frac{(V^2 + VA + A^2)^2 (2V - A)^2}{16(V^2 - A^2)^2} \epsilon_{\nu e}^2 + \frac{(V^2 - VA + A^2)^2 (2V + A)^2}{16(V^2 - A^2)^2} \epsilon_{\bar{\nu} e}^2, \\ \langle \delta V \delta A \rangle &= \frac{(V^2 + VA + A^2)^2 (V - 2A)(2V - A)}{16(V^2 - A^2)^2} \epsilon_{\nu e}^2\end{aligned}$$

$$-\frac{(V^2 - VA + A^2)^2(V + 2A)(2V + A)}{16(V^2 - A^2)^2}\epsilon_{\bar{\nu}e}^2. \quad (\text{E.4})$$

Therefore, the errors of V and A are

$$\begin{aligned} \Delta V &= \sqrt{\frac{(V^2 + VA + A^2)^2(V - 2A)^2}{16(V^2 - A^2)^2}\epsilon_{\nu e}^2 + \frac{(V^2 - VA + A^2)^2(V + 2A)^2}{16(V^2 - A^2)^2}\epsilon_{\bar{\nu}e}^2}, \\ \Delta A &= \sqrt{\frac{(V^2 + VA + A^2)^2(2V - A)^2}{16(V^2 - A^2)^2}\epsilon_{\nu e}^2 + \frac{(V^2 - VA + A^2)^2(2V + A)^2}{16(V^2 - A^2)^2}\epsilon_{\bar{\nu}e}^2}, \end{aligned} \quad (\text{E.5})$$

and the correlation coefficient between them is

$$\begin{aligned} \text{Corr}(V, A) &= \frac{1}{16(V^2 - A^2)^2\Delta V \Delta A} \left[(V^2 + VA + A^2)^2(V - 2A)(2V - A)\epsilon_{\nu e}^2 \right. \\ &\quad \left. - (V^2 - VA + A^2)^2(V + 2A)(2V + A)\epsilon_{\bar{\nu}e}^2 \right] \end{aligned} \quad (\text{E.6})$$

Bibliography

- [1] [NuTeV Collaboration] G. P. Zeller *et al.*, Phys. Rev. Lett. **88**, 091802 (2002) [Erratum-ibid. **90**, 239902 (2003)] [arXiv:hep-ex/0110059]; Phys. Rev. D **65**, 111103 (2002) [Erratum-ibid. D **67**, 119902 (2003)] [arXiv:hep-ex/0203004]; arXiv:hep-ex/0207052; K. S. McFarland *et al.*, arXiv:hep-ex/0205080.
- [2] [ALEPH Collaboration], arXiv:hep-ex/0212036.
- [3] J. Alcaraz *et al.* [ALEPH Collaboration], arXiv:hep-ex/0612034.
- [4] W. Loinaz, N. Okamura, S. Rayyan, T. Takeuchi and L. C. R. Wijewardhana, Phys. Rev. D **70**, 113004 (2004) [arXiv:hep-ph/0403306].
- [5] W. Loinaz, N. Okamura, S. Rayyan, T. Takeuchi and L. C. R. Wijewardhana, Phys. Rev. D **68**, 073001 (2003) [arXiv:hep-ph/0304004].
- [6] W. Loinaz, N. Okamura, T. Takeuchi and L. C. R. Wijewardhana, Phys. Rev. D **67**, 073012 (2003) [arXiv:hep-ph/0210193]; T. Takeuchi, arXiv:hep-ph/0209109.
- [7] A. Pronin and T. Takeuchi, arXiv:hep-ph/0607030.
- [8] T. Adams *et al.*, arXiv:0803.0354 [hep-ph].
- [9] M. Honda, Y. Kao, N. Okamura, A. Pronin and T. Takeuchi, arXiv:0707.4545 [hep-ph].
- [10] M. Honda, N. Okamura and T. Takeuchi, arXiv:hep-ph/0603268; M. Honda, Y. Kao, N. Okamura and T. Takeuchi, arXiv:hep-ph/0602115; M. Honda, Y. Kao, N. Okamura, A. Pronin and T. Takeuchi, arXiv:hep-ph/0610281; M. Honda, Y. Kao, N. Okamura, A. Pronin and T. Takeuchi, arXiv:0704.0369 [hep-ph].
- [11] C. H. Llewellyn Smith, Nucl. Phys. B **228**, 205 (1983).
- [12] M. S. Chanowitz, Phys. Rev. D **66**, 073002 (2002) [arXiv:hep-ph/0207123].
- [13] [LEP Collaboration], arXiv:hep-ex/0312023.
- [14] B. A. Dobrescu and R. K. Ellis, Phys. Rev. D **69**, 114014 (2004) [arXiv:hep-ph/0310154].
- [15] K. P. O. Diener, S. Dittmaier and W. Hollik, Phys. Rev. D **69**, 073005 (2004) [arXiv:hep-ph/0310364].
- [16] P. Gambino, Int. J. Mod. Phys. A **19**, 808 (2004) [arXiv:hep-ph/0311257].

- [17] S. Davidson, S. Forte, P. Gambino, N. Rius and A. Strumia, JHEP **0202**, 037 (2002) [hep-ph/0112302];
S. Davidson, J. Phys. G **29**, 2001 (2003) [arXiv:hep-ph/0209316];
P. Gambino, arXiv:hep-ph/0211009.
- [18] X. G. He, G. C. Joshi, H. Lew and R. R. Volkas, Phys. Rev. D **43**, 22 (1991).
- [19] X. G. He, G. C. Joshi, H. Lew and R. R. Volkas, Phys. Rev. D **44**, 2118 (1991).
- [20] S. Baek, N. G. Deshpande, X. G. He and P. Ko, Phys. Rev. D **64**, 055006 (2001) [arXiv:hep-ph/0104141];
S. Choubey and W. Rodejohann, Eur. Phys. J. C **40**, 259 (2005) [arXiv:hep-ph/0411190];
W. Rodejohann and M. A. Schmidt, Phys. Atom. Nucl. **69**, 1833 (2006) [arXiv:hep-ph/0507300];
B. Adhikary, Phys. Rev. D **74**, 033002 (2006) [arXiv:hep-ph/0604009];
T. Ota and W. Rodejohann, Phys. Lett. B **639**, 322 (2006) [arXiv:hep-ph/0605231];
E. J. Chun and K. Turzyski, arXiv:hep-ph/0703070;
See also Ref. [21].
- [21] E. Ma and D. P. Roy, Phys. Rev. D **65**, 075021 (2002).
- [22] E. Ma, D. P. Roy and S. Roy, Phys. Lett. B **525**, 101 (2002) [arXiv:hep-ph/0110146].
- [23] D. Buskulic *et al.* [ALEPH Collaboration], Z. Phys. C **66**, 3 (1995).
- [24] C. D. Carone and H. Murayama, Phys. Rev. Lett. **74**, 3122 (1995) [arXiv:hep-ph/9411256].
- [25] W. M. Yao *et al.* [Particle Data Group], J. Phys. G **33**, 1 (2006).
- [26] [ALEPH Collaboration], Phys. Rept. **427**, 257 (2006) [arXiv:hep-ex/0509008].
- [27] D. Y. Bardin, P. Christova, M. Jack, L. Kalinovskaya, A. Olchevski, S. Riemann and T. Riemann, Comput. Phys. Commun. **133**, 229 (2001) [arXiv:hep-ph/9908433].
- [28] W. Buchmüller, R. Rückl and D. Wyler, Phys. Lett. B **191**, 442 (1987) [Erratum-ibid. B **448**, 320 (1999)];
J. Blumlein and R. Ruckl, Phys. Lett. B **304**, 337 (1993);
M. Tanabashi, in the Review of Particle Properties [25].
- [29] S. Davidson, D. C. Bailey and B. A. Campbell, Z. Phys. C **61**, 613 (1994) [arXiv:hep-ph/9309310].
- [30] E. Gabrielli, Phys. Rev. D **62**, 055009 (2000) [arXiv:hep-ph/9911539].
- [31] D. Acosta *et al.* [CDF Collaboration], Phys. Rev. D **71**, 112001 (2005) [Erratum-ibid. D **71**, 119901 (2005)] [arXiv:hep-ex/0410076].
- [32] V. M. Abazov *et al.* [D0 Collaboration], Phys. Lett. B **640**, 230 (2006) [arXiv:hep-ex/0607009].
- [33] A. Abulencia *et al.* [CDF Collaboration], Phys. Rev. D **73**, 051102 (2006) [arXiv:hep-ex/0512055].

- [34] V. M. Abazov *et al.* [D0 Collaboration], Phys. Lett. B **636**, 183 (2006) [arXiv:hep-ex/0601047].
- [35] V. M. Abazov *et al.* [D0 Collaboration], Phys. Lett. B **647**, 74 (2007) [arXiv:hep-ex/0612012].
- [36] F. Abe *et al.* [CDF Collaboration], Phys. Rev. Lett. **79**, 2198 (1997).
- [37] N. P. Xuan, fermilab-thesis-2005-40, UMI-31-66510.
- [38] O. U. Shanker, Nucl. Phys. B **206**, 253 (1982).
- [39] O. U. Shanker, Nucl. Phys. B **204**, 375 (1982).
- [40] M. Finkemeier, Phys. Lett. B **387**, 391 (1996) [arXiv:hep-ph/9505434].
- [41] ATLAS detector and physics performance. Technical design report. Vol. 2, CERN-LHCC-99-15, ATLAS-TDR-15;
CMS physics : Technical Design Report v.2 : Physics performance, CERN-LHCC-2006-021, CMS-TDR-008-2.
- [42] V. A. Mitsou, N. C. Benekos, I. Panagoulas and T. D. Papadopoulou, Czech. J. Phys. **55**, B659 (2005) [arXiv:hep-ph/0411189].
- [43] T. Yanagida, in *Proceedings of the Workshop on Unified Theory and Baryon Number in the Universe*, ed. O. Sawada and A. Sugamoto (KEK, report 79-18, 1979), p.95; M. Gell-Mann, P. Ramond and S. Slansky, in *Supergravity*, ed. P. van Nieuwenhuizen and D. Z. Freedman (North-Holland, Amsterdam, 1979), p315; R. N. Mohapatra and G. Senjanović, Phys. Rev. Lett. **44**, 912 (1980).
- [44] L. N. Chang, D. Ng and J. N. Ng, Phys. Rev. D **50**, 4589 (1994) [arXiv:hep-ph/9402259].
- [45] C. D. Carone and H. Murayama, Phys. Lett. B **392**, 403 (1997) [arXiv:hep-ph/9610383].
- [46] N. Arkani-Hamed, L. J. Hall, H. Murayama, D. R. Smith and N. Weiner, Phys. Rev. D **64**, 115011 (2001) [arXiv:hep-ph/0006312].
- [47] E. Ma, Phys. Rev. Lett. **86**, 2502 (2001) [arXiv:hep-ph/0011121].
- [48] S. M. Bilenky:1998dt:1998dt:1998dt, C. Giunti and W. Grimus, Prog. Part. Nucl. Phys. **43**, 1 (1999) [arXiv:hep-ph/9812360].
- [49] J. C. Pati and A. Salam, Phys. Rev. D **8**, 1240 (1973).
- [50] A. Denner, H. Eck, O. Hahn and J. Kublbeck, Nucl. Phys. B **387**, 467 (1992).
- [51] A. Djouadi, Z. Phys. C **63**, 317 (1994) [arXiv:hep-ph/9308339].
- [52] J. A. Aguilar-Saavedra, Int. J. Mod. Phys. C **8**, 147 (1997) [arXiv:hep-ph/9607313].
- [53] P. Achard *et al.* [L3 Collaboration], Phys. Lett. B **517**, 67 (2001) [arXiv:hep-ex/0107014].
- [54] D. A. Dicus, D. D. Karatas and P. Roy, Phys. Rev. D **44**, 2033 (1991).
- [55] The NuSONG Expression of Interest is available from the Fermilab Directorate or at <http://www-nusong.fnal.gov>

- [56] A. Datta, M. Guchait and A. Pilaftsis, Phys. Rev. D **50**, 3195 (1994) [arXiv:hep-ph/9311257].
- [57] F. M. L. Almeida, Y. D. A. Coutinho, J. A. Martins Simoes and M. A. B. do Vale, Phys. Rev. D **62**, 075004 (2000) [arXiv:hep-ph/0002024].
- [58] O. Panella, M. Cannoni, C. Carimalo and Y. N. Srivastava, Phys. Rev. D **65**, 035005 (2002) [arXiv:hep-ph/0107308].
- [59] T. Han and B. Zhang, Phys. Rev. Lett. **97**, 171804 (2006) [arXiv:hep-ph/0604064].
- [60] F. del Aguila, J. A. Aguilar-Saavedra and R. Pittau, J. Phys. Conf. Ser. **53**, 506 (2006) [arXiv:hep-ph/0606198].
- [61] O. Adriani *et al.* [L3 Collaboration], Phys. Lett. B **295**, 371 (1992);
P. Achard *et al.* [L3 Collaboration], Phys. Lett. B **517**, 67 (2001) [arXiv:hep-ex/0107014].
- [62] T. H. Ho, C. R. Ching and Z. J. Tao, Phys. Rev. D **42**, 2265 (1990).
- [63] A. Datta, M. Guchait and D. P. Roy, Phys. Rev. D **47**, 961 (1993) [arXiv:hep-ph/9208228].
- [64] ATLAS: Detector and physics performance technical design report, Volume 2, section 21.6.2
“Search for right-handed Majorana neutrinos”, CERN-LHCC-99-15 (May 25, 1999).
Available from the CERN LHC website at
<http://atlas.web.cern.ch/Atlas/GROUPS/PHYSICS/TDR/access.html>
- [65] Z. Berezhiani, R. S. Raghavan and A. Rossi, Nucl. Phys. B **638**, 62 (2002) [arXiv:hep-ph/0111138].
- [66] M. E. Peskin and T. Takeuchi, Phys. Rev. D **46**, 381 (1992).
- [67] M. E. Peskin and T. Takeuchi, Phys. Rev. Lett. **65**, 964 (1990).
- [68] M. E. Peskin and J. D. Wells, Phys. Rev. D **64**, 093003 (2001) [arXiv:hep-ph/0101342].
- [69] A. Bandyopadhyay *et al.* [ISS Physics Working Group], arXiv:0710.4947 [hep-ph].
- [70] S. Davidson, C. Pena-Garay, N. Rius and A. Santamaria, JHEP **0303**, 011 (2003) [arXiv:hep-ph/0302093].
- [71] R. N. Mohapatra *et al.*, Rept. Prog. Phys. **70**, 1757 (2007) [arXiv:hep-ph/0510213].
- [72] E. Ma, Phys. Lett. B **433**, 74 (1998) [arXiv:hep-ph/9709474];
E. Ma and U. Sarkar, Phys. Lett. B **439**, 95 (1998) [arXiv:hep-ph/9807307];
P. B. Pal and U. Sarkar, Phys. Lett. B **573**, 147 (2003) [arXiv:hep-ph/0306088].
- [73] E. Ma, D. P. Roy and U. Sarkar, Phys. Lett. B **444**, 391 (1998) [arXiv:hep-ph/9810309].
- [74] E. Ma and D. P. Roy, Phys. Rev. D **59**, 097702 (1999); [arXiv:hep-ph/9811266].
- [75] A. Zee, Phys. Lett. B **93**, 389 (1980) [Erratum-ibid. B **95**, 461 (1980)].
- [76] K. S. Babu, Phys. Lett. B **203**, 132 (1988);
A. Zee, Nucl. Phys. B **264**, 99 (1986).

- [77] L. J. Hall and M. Suzuki, Nucl. Phys. B **231**, 419 (1984);
H. E. Haber and G. L. Kane, Phys. Rept. **117**, 75 (1985);
M. Nowakowski and A. Pilaftsis, Nucl. Phys. B **461**, 19 (1996) [arXiv:hep-ph/9508271];
See also [106].
- [78] R. Barbier *et al.*, Phys. Rept. **420**, 1 (2005) [arXiv:hep-ph/0406039].
- [79] A. Zee, Phys. Lett. B **161**, 141 (1985);
M. Fukugita and T. Yanagida, Phys. Lett. B **206**, 93 (1988).
- [80] L. N. Chang, O. Lebedev, W. Loinaz, and T. Takeuchi, Phys. Rev. D **63**, 074013 (2001) [arXiv:hep-ph/0010118].
- [81] C. T. Hill, Phys. Lett. B **345**, 483 (1995) [arXiv:hep-ph/9411426];
R. S. Chivukula, B. A. Dobrescu and J. Terning, Phys. Lett. B **353**, 289 (1995) [arXiv:hep-ph/9503203];
K. D. Lane and E. Eichten, Phys. Lett. B **352**, 382 (1995) [arXiv:hep-ph/9503433];
G. Buchalla, G. Burdman, C. T. Hill, and D. Kominis, Phys. Rev. D **53**, 5185 (1996) [arXiv:hep-ph/9510376];
K. D. Lane, Phys. Rev. D **54**, 2204 (1996) [arXiv:hep-ph/9602221];
K. D. Lane, Phys. Lett. B **433**, 96 (1998) [arXiv:hep-ph/9805254];
W. Loinaz and T. Takeuchi, Phys. Rev. D **60**, 115008 (1999) [arXiv:hep-ph/9903362].
- [82] D. Kominis, Phys. Lett. B **358**, 312 (1995) [arXiv:hep-ph/9506305];
R. S. Chivukula and J. Terning, Phys. Lett. B **385**, 209 (1996) [arXiv:hep-ph/9606233];
Y. Su, G. F. Bonini and K. D. Lane, Phys. Rev. Lett. **79**, 4075 (1997) [arXiv:hep-ph/9706267];
W. Loinaz and T. Takeuchi, Phys. Rev. D **60**, 015005 (1999) [arXiv:hep-ph/9812377];
G. Burdman, K. D. Lane and T. Rador, Phys. Lett. B **514**, 41 (2001) [arXiv:hep-ph/0012073].
- [83] O. Lebedev, W. Loinaz and T. Takeuchi, Phys. Rev. D **61**, 115005 (2000) [arXiv:hep-ph/9910435];
O. Lebedev, W. Loinaz and T. Takeuchi, Phys. Rev. D **62**, 015003 (2000) [arXiv:hep-ph/9911479].
- [84] Z. Maki, M. Nakagawa and S. Sakata, Prog. Theor. Phys. **28**, 870 (1962).
- [85] L. Wolfenstein, Phys. Rev. D **17**, 2369 (1978);
R. R. Lewis, Phys. Rev. D **21**, 663 (1980);
V. D. Barger, K. Whisnant, S. Pakvasa and R. J. N. Phillips, Phys. Rev. D **22**, 2718 (1980);
S. P. Mikheyev and A. Yu. Smirnov, Yad. Fiz. **42**, 1441 (1985), [Sov. J. Nucl. Phys. **42**, 913 (1986)];
S. P. Mikheyev and A. Yu. Smirnov, Nuovo Cimento **C9**, 17 (1986).
- [86] Y. Ashie *et al.* [Super-Kamiokande Collaboration], Phys. Rev. D **71**, 112005 (2005) [arXiv:hep-ex/0501064].
- [87] J. Dorenbosch *et al.* [CHARM Collaboration], Phys. Lett. B **180**, 303 (1986);
P. Vilain *et al.* [CHARM-II Collaboration], Phys. Lett. B **320**, 203 (1994).
- [88] NUMI Technical Design Handbook,
available at http://www-numi.fnal.gov/numwork/tdh/tdh_index.html

- [89] Y. Itow *et al.*, arXiv:hep-ex/0106019;
updated version available at <http://neutrino.kek.jp/jhfnu/>.
- [90] R. Foot, Mod. Phys. Lett. A **20**, 3035 (2005) [arXiv:hep-ph/0505154].
- [91] M. Acciarri *et al.* [L3 Collaboration], Phys. Lett. B **489**, 81 (2000) [arXiv:hep-ex/0005028].
- [92] G. Abbiendi *et al.* [OPAL Collaboration], Eur. Phys. J. C **33**, 173 (2004) [arXiv:hep-ex/0309053].
- [93] J. Abdallah *et al.* [DELPHI Collaboration], Eur. Phys. J. C **45**, 589 (2006) [arXiv:hep-ex/0512012].
- [94] S. Schael *et al.* [ALEPH Collaboration], Eur. Phys. J. C **49**, 411 (2007) [arXiv:hep-ex/0609051].
- [95] D. Acosta *et al.* [CDF Collaboration], Phys. Rev. Lett. **95**, 131801 (2005) [arXiv:hep-ex/0506034].
- [96] E. Ma and D. P. Roy, Phys. Rev. D **58**, 095005 (1998) [arXiv:hep-ph/9806210].
- [97] J. Blumlein, E. Boos and A. Kryukov, Z. Phys. C **76**, 137 (1997) [arXiv:hep-ph/9610408].
- [98] CDF note 8309, “Search for Third Generation Vector Leptoquarks in Run II”,
http://www-cdf.fnal.gov/physics/exotic/r2a/20070308.3genvlq/vlq3_public_page_files/lq3_cdfpubnote.ps.
- [99] C. S. Aulakh and R. N. Mohapatra, Phys. Lett. B **119**, 136 (1982);
L. J. Hall and M. Suzuki, Nucl. Phys. B **231**, 419 (1984);
I. H. Lee, Nucl. Phys. B **246**, 120 (1984);
J. R. Ellis, G. Gelmini, C. Jarlskog, G. G. Ross and J. W. F. Valle, Phys. Lett. B **150**, 142 (1985);
G. G. Ross and J. W. F. Valle, Phys. Lett. B **151**, 375 (1985);
S. Dawson, Nucl. Phys. B **261**, 297 (1985);
V. D. Barger, G. F. Giudice and T. Han, Phys. Rev. D **40**, 2987 (1989).
- [100] R. Hempfling, Nucl. Phys. B **478**, 3 (1996) [arXiv:hep-ph/9511288];
A. G. Akeroyd, M. A. Diaz, J. Ferrandis, M. A. Garcia-Jareno and J. W. F. Valle, Nucl. Phys. B **529**, 3 (1998) [arXiv:hep-ph/9707395];
E. J. Chun, S. K. Kang, C. W. Kim and U. W. Lee, Nucl. Phys. B **544**, 89 (1999) [arXiv:hep-ph/9807327];
E. J. Chun and J. S. Lee, Phys. Rev. D **60**, 075006 (1999) [arXiv:hep-ph/9811201];
D. E. Kaplan and A. E. Nelson, JHEP **0001**, 033 (2000) [arXiv:hep-ph/9901254];
J. C. Romao, M. A. Diaz, M. Hirsch, W. Porod and J. W. F. Valle, Phys. Rev. D **61**, 071703(R) (2000) [arXiv:hep-ph/9907499];
F. Takayama and M. Yamaguchi, Phys. Lett. B **476**, 116 (2000) [arXiv:hep-ph/9910320];
M. Hirsch, M. A. Diaz, W. Porod, J. C. Romao and J. W. F. Valle, Phys. Rev. D **62**, 113008 (2000) [Erratum-ibid. D **65**, 119901 (2002)] [arXiv:hep-ph/0004115];
M. A. Diaz, M. Hirsch, W. Porod, J. C. Romao and J. W. F. Valle, Phys. Rev. D **68**, 013009 (2003) [Erratum-ibid. D **71**, 059904 (2005)] [arXiv:hep-ph/0302021];
E. J. Chun, D. W. Jung, S. K. Kang and J. D. Park, Phys. Rev. D **66**, 073003 (2002) [arXiv:hep-ph/0206030];

- E. J. Chun, D. W. Jung and J. D. Park, Phys. Lett. B **557**, 233 (2003) [arXiv:hep-ph/0211310];
D. W. Jung, S. K. Kang, J. D. Park and E. J. Chun, JHEP **0408**, 017 (2004) [arXiv:hep-ph/0407106].
- [101] S. Chekanov *et al.* [ZEUS Collaboration], Phys. Rev. D **68**, 052004 (2003) [arXiv:hep-ex/0304008].
- [102] S. Chekanov *et al.* [ZEUS Collaboration], Eur. Phys. J. C **44**, 463 (2005) [arXiv:hep-ex/0501070].
- [103] C. Adloff *et al.* [H1 Collaboration], Phys. Lett. B **568**, 35 (2003) [arXiv:hep-ex/0305015].
- [104] A. Aktas *et al.* [H1 Collaboration], Eur. Phys. J. C **36**, 425 (2004) [arXiv:hep-ex/0403027].
- [105] V. M. Abazov *et al.* [D0 Collaboration], Phys. Rev. Lett. **97**, 111801 (2006) [arXiv:hep-ex/0605010].
- [106] S. P. Martin, arXiv:hep-ph/9709356.
- [107] J. F. Gunion and C. Hays, in E. Accomando *et al.*, “Workshop on CP studies and non-standard Higgs physics,” arXiv:hep-ph/0608079, chapter 13, pages 497-526;
A. G. Akeroyd and M. Aoki, Phys. Rev. D **72**, 035011 (2005) [arXiv:hep-ph/0506176].
- [108] K. S. Babu and C. Macesanu, Phys. Rev. D **67**, 073010 (2003) [arXiv:hep-ph/0212058].
- [109] T. Takeuchi, presented at the 1991 Nagoya Spring School on Dynamical Symmetry Breaking, Nakatsugawa, Japan, 1991, SLAC-PUB-5619 (<http://www.slac.stanford.edu/pubs/slacpubs/5000/slac-pub-5619.html>).